frontiers | Research Topics

Bioactive materials and musculoskeletal disease

Edited by
Jun Lin, Nader Parvin, Ganjun Feng and Yusheng Li

Published in
Frontiers in Bioengineering and Biotechnology
Frontiers in Materials

ISSN 1664-8714
ISBN 978-2-83251-773-4
DOI 10.3389/978-2-83251-773-4

About Frontiers

Frontiers is more than just an open access publisher of scholarly articles: it is a pioneering approach to the world of academia, radically improving the way scholarly research is managed. The grand vision of Frontiers is a world where all people have an equal opportunity to seek, share and generate knowledge. Frontiers provides immediate and permanent online open access to all its publications, but this alone is not enough to realize our grand goals.

Frontiers journal series

The Frontiers journal series is a multi-tier and interdisciplinary set of open-access, online journals, promising a paradigm shift from the current review, selection and dissemination processes in academic publishing. All Frontiers journals are driven by researchers for researchers; therefore, they constitute a service to the scholarly community. At the same time, the *Frontiers journal series* operates on a revolutionary invention, the tiered publishing system, initially addressing specific communities of scholars, and gradually climbing up to broader public understanding, thus serving the interests of the lay society, too.

Dedication to quality

Each Frontiers article is a landmark of the highest quality, thanks to genuinely collaborative interactions between authors and review editors, who include some of the world's best academicians. Research must be certified by peers before entering a stream of knowledge that may eventually reach the public - and shape society; therefore, Frontiers only applies the most rigorous and unbiased reviews. Frontiers revolutionizes research publishing by freely delivering the most outstanding research, evaluated with no bias from both the academic and social point of view. By applying the most advanced information technologies, Frontiers is catapulting scholarly publishing into a new generation.

What are Frontiers Research Topics?

Frontiers Research Topics are very popular trademarks of the *Frontiers journals series*: they are collections of at least ten articles, all centered on a particular subject. With their unique mix of varied contributions from Original Research to Review Articles, Frontiers Research Topics unify the most influential researchers, the latest key findings and historical advances in a hot research area.

Find out more on how to host your own Frontiers Research Topic or contribute to one as an author by contacting the Frontiers editorial office: frontiersin.org/about/contact

Bioactive materials and musculoskeletal disease

Topic editors

Jun Lin — First Affiliated Hospital of Soochow University, China
Nader Parvin — Amirkabir University of Technology, Iran
Ganjun Feng — Sichuan University, China
Yusheng Li — Central South University, China

Citation

Lin, J., Parvin, N., Feng, G., Li, Y., eds. (2023). *Bioactive materials and musculoskeletal disease*. Lausanne: Frontiers Media SA.
doi: 10.3389/978-2-83251-773-4

Table of contents

frontiers | Frontiers in Bioengineering and Biotechnology

TYPE Editorial
PUBLISHED 13 February 2023
DOI 10.3389/fbioe.2023.1153019

OPEN ACCESS

EDITED AND REVIEWED BY
Mingqiang Li,
Third Affiliated Hospital of Sun Yat-sen University, China

*CORRESPONDENCE
Ganjun Feng,
gjfenghx@163.com

SPECIALTY SECTION
This article was submitted to Biomaterials, a section of the journal Frontiers in Bioengineering and Biotechnology

RECEIVED 28 January 2023
ACCEPTED 07 February 2023
PUBLISHED 13 February 2023

CITATION
Huang Y and Feng G (2023), Editorial: Biomaterial advances in intervertebral disc degeneration.
Front. Bioeng. Biotechnol. 11:1153019.
doi: 10.3389/fbioe.2023.1153019

Editorial: Biomaterial advances in intervertebral disc degeneration

Yong Huang and Ganjun Feng*

Department of Orthopedic Surgery and Orthopedic Research Institute, West China Hospital, Sichuan University, Chengdu, Sichuan, China

KEYWORDS

biomaterial, tissue engineering, drug delivery system, hydrogels, intervertebral disc degeneration

Editorial on the Research Topic
Biomaterial advances in intervertebral disc degeneration

Neck and back pain are ubiquitous in modern society, leading to serious lifelong disability and placing an enormous socioeconomic burden on the global healthcare system. Although the etiology of neck and back pain is multifaceted and still incompletely understood, intervertebral disc degeneration (IDD) is considered to be the most significant contributor. The current treatments for IDD, including medication, surgery, and others, are limited to symptomatic relief but fail to restore the structure and homeostasis of the intervertebral disc. The failure leads to the steady deterioration of compromised discs and undesirable consequences, such as recrudescence or adjacent vertebral disease. Tissue-engineered approaches hold great promise for the treatment of IDD. Gullbrand et al. designed and manufactured a disc-like angle ply structure (DAPS), which has distinct components that mimic the structure of the native disc. The long-term integration and mechanical function of engineered DAPS *in vivo*, even in large animal models have been successfully tested (Gullbrand et al., 2018). After that, Sloan et al. demonstrated that combined nucleus pulposus augmentation using hyaluronic acid injection and annulus fibrosus repair using photo cross-linked collagen patch restore nucleus pulposus hydration, heal annulus fibrosus defects and maintain native torsional and compressive stiffness up to 6 weeks after discectomy injury in a large animal model. These studies move this approach a step towards translational feasibility (Sloan et al., 2020).

Given the indispensable role of biomaterials in tissue engineering for IDD, we prepared this Research Topic to summarize the progress in this field. The harsh microenvironment of IDD is not suitable for disc regeneration. Therefore, various therapeutic agents, including small molecular, growth factor, exosome, and nucleic acids-based drugs are employed to reduce the inflammatory response, promote extracellular matrix synthesis, and direct cell differentiation to create a good regenerative microenvironment. Traditional drug delivery such as systemic administration or *via in situ* injection has low drug availability and high off-target toxicity. Liu et al. have systematically demonstrated that biomaterials-based nano-drug delivery systems have improved treatment results of therapeutic agents for IDD because of their good biodegradability, biocompatibility, precise targeted specific drug delivery, prolonged drug release time, and enhanced drug efficacy (Liu et al., 2023). Except for drug delivery, a good cell carrier is critical for tissue regeneration. The microsphere is a class of three-dimensional spherical structures with an average particle size of 1–1000 μm that could be used in cell carrying and biomedical substance delivery. Guo et al. recently reviewed the use of various microspheres for disc regeneration and clearly demonstrated that the high

encapsulation rate and excellent slow-release properties conferred by the porous structure, coupled with good surface adhesion for cell immigration, have led to the gradual emergence of microspheres as the carrier of choice in the field of tissue engineering (Guo et al., 2022). In order to achieve long-term delivery and avoid leakage-associated complications, stimulus-responsive composite hydrogels have been employed. Gao et al. have highlighted the critical role of stimulus-responsive composite hydrogels in disc regenerative medicine with controllable mechanical properties and the ability to achieve liquid-solid phase transition under certain conditions (Gao et al., 2022).

In conclusion, we believe that the studies and reviews on this Research Topic provide new insight into the choice of biomaterials for engineering solutions for intervertebral disc regeneration. We hope to achieve a perfect regenerative repair of the intervertebral disc with the help of emerging material development as soon as possible.

Author contributions

YH drafted the manuscript. GF critically revised the manuscript.

Funding

The authors acknowledge the funding support from the National Natural Science Foundation of China (No. 82072434, 82272546), the Sichuan Science and Technology Program (2021YFS0218).

Conflict of interest

The authors declare that the research was conducted in the absence of any commercial or financial relationships that could be construed as a potential conflict of interest.

Publisher's note

All claims expressed in this article are solely those of the authors and do not necessarily represent those of their affiliated organizations, or those of the publisher, the editors and the reviewers. Any product that may be evaluated in this article, or claim that may be made by its manufacturer, is not guaranteed or endorsed by the publisher.

References

Gao, X. D., Zhang, X. B., Zhang, R. H., Yu, D. C., Chen, X. Y., Hu, Y. C., et al. (2022). Aggressive strategies for regenerating intervertebral discs: Stimulus-responsive composite hydrogels from single to multiscale delivery systems. *J. Mater Chem. B* 10 (30), 5696–5722. doi:10.1039/d2tb01066f

Gullbrand, S. E., Ashinsky, B. G., Bonnevie, E. D., Kim, D. H., Engiles, J. B., Smith, L. J., et al. (2018). Long-term mechanical function and integration of an implanted tissue-engineered intervertebral disc. *Sci. Transl. Med.* 10 (468), eaau0670. doi:10.1126/scitranslmed.aau0670

Guo, T., Zhang, X., Hu, Y., Lin, M., Zhang, R., Chen, X., et al. (2022). New hope for treating intervertebral disc degeneration: Microsphere-based delivery system. *Front. Bioeng. Biotechnol.* 10, 933901. doi:10.3389/fbioe.2022.933901

Liu, W., Ma, Z., Wang, Y., and Yang, J. (2023). Multiple nano-drug delivery systems for intervertebral disc degeneration: Current status and future perspectives. *Bioact. Mater* 23, 274–299. doi:10.1016/j.bioactmat.2022.11.006

Sloan, S. R., Jr., Wipplinger, C., Kirnaz, S., Navarro-Ramirez, R., Schmidt, F., McCloskey, D., et al. (2020). Combined nucleus pulposus augmentation and annulus fibrosus repair prevents acute intervertebral disc degeneration after discectomy. *Sci. Transl. Med.* 12 (534), eaay2380. doi:10.1126/scitranslmed.aay2380

frontiers in Bioengineering and Biotechnology

ORIGINAL RESEARCH
published: 13 December 2021
doi: 10.3389/fbioe.2021.796602

Triggering Drug Release and Thermal-Disrupting Interface Induced Mitigation of Composite Photothermal Hydrogel Treating Infectious Wounds

Long Hua[1,2,3‡], Hu Qian[1], Ting Lei[1], Wenbin Liu[1], Xi He[1], Yihe Hu[1,2†‡] and Pengfei Lei[1,2†*]*

[1]Department of Orthopedics, The First Affiliated Hospital, Medical College of Zhejiang University, Hangzhou, China, [2]Department of Orthopedics, Xiangya Hospital Central South University, Hunan Engineering Research Center of Biomedical Metal and Ceramic Implants, Changsha, China, [3]The Sixth Affiliated Hospital, Xinjiang Medical University, Urumqi, China

Introduction: With the development of photothermal technology, the appearance of composite photothermal hydrogels has increased the selectivity of treating infectious skin defects. However, how to design composite photothermal hydrogel with better antibacterial performance, reduce the resistance rate of bacteria, and the damage rate of normal tissue still needs further study.

Methods: The Prussian blue and tannic acid were loaded on polyacrylamide hydrogels. Characterization of DLS, Zeta potential, UV absorption spectrum, hydrogel swelling rate, scanning electronic microscopic, drug release profile, photothermal properties, *in vitro* cytocompatibility, and antibacterial properties. Experiments were measured by skin defect repair, antibacterial detection, and histological staining experiments.

Results: The polyacrylamide hydrogel with photothermal effect and controllable release of tannic acid was successfully prepared. The hydrogel has strong light transmittance and adhesion, and the swelling rate can reach 600%, which improves the self-cleaning ability. SEM results showed the porous structure of hydrogels, promoting cell growth. Through photothermal switches, the composite hydrogel represented adjustable and controllable drug release ability. Combined with the synergistic antibacterial effect of tannic acid, this further enhanced the antibacterial ability and reduced the probability of antibiotic resistance. The *in vitro* and *in vivo* experiments showed the hydrogel had good biocompatibility and excellent antibacterial properties, which could promote the repair of infectious skin defects in SD rats.

Conclusion: We fabricated a hydrogel with a triggering drug release rate, alleviating heat damage, transparent morphology, mechanical stability, strong adhesion, good biocompatibility, and synergistic antibacterial ability, which presents new treatment options for infectious skin defect repair.

Keywords: triggering drug release, thermal-disrupting interface induced mitigation, tannic acid, Prussian blue, photothermal hydrogel

OPEN ACCESS

Edited by:
Jun Lin,
First Affiliated Hospital of Soochow University, China

Reviewed by:
Zheng Guo,
Tangdu Hospital, China
Yi-Chen Ethan Li,
Feng Chia University, Taiwan

***Correspondence:**
Yihe Hu
csuhuyihe@163.com
Pengfei Lei
pengfeilei@csu.edu.cn

[†]These authors have contributed equally to this work

[‡]ORCID:
Long Hua,
orcid.org/0000-0002-4581-6826;
Yihe Hu,
orcid.org/0000-0002-5161-0429

Specialty section:
This article was submitted to Biomaterials, a section of the journal Frontiers in Bioengineering and Biotechnology

Received: *17 October 2021*
Accepted: *09 November 2021*
Published: *13 December 2021*

Citation:
Hua L, Qian H, Lei T, Liu W, He X, Hu Y and Lei P (2021) Triggering Drug Release and Thermal-Disrupting Interface Induced Mitigation of Composite Photothermal Hydrogel Treating Infectious Wounds. Front. Bioeng. Biotechnol. 9:796602. doi: 10.3389/fbioe.2021.796602

INTRODUCTION

Globally, one-third of all deaths are caused by infections (Li et al., 2018). Among them, the treatment of infectious skin defects due to acute injuries, burns, and chronic diseases such as diabetes remains a challenge (Ning et al., 2014; Zheng et al., 2018). Traditional treatments involve the use of drugs such as antibiotics. However, increasing drug resistance has reduced the effectiveness of this kind of treatment to near useless (Dai et al., 2017). At the same time, the loss of skin tissue reduces the ability to form a barrier against bacteria, which can exacerbate the infection (Mao et al., 2018). Therefore, there is an urgent need for a new treatment strategy to improve the current severe situation of inadequate treatment options.

With the development of photothermal technology, more and more photothermal nanomaterials have been used in the treatment of infectious skin defects because of their good photothermal conversion and bactericidal properties. Among them, metallic and nonmetallic nanoparticles are included such as Ag-based (Cao et al., 2020), Au-based (Ngo-Duc et al., 2020), Cu-based (Yu et al., 2020), and graphene-based NPs (Zhang et al., 2019). However, the application of these materials has been hindered due to their biotoxicity and instability, as well as the high temperature generated at the interface of biological tissues, which can cause damage to normal tissues (Hu et al., 2020). Therefore, the research and development of a composite material with low biotoxicity and good biocompatibility, which has excellent bactericidal performance and can reduce bacterial resistance to protect normal tissues, is still a goal pursued by scholars (Zhou et al., 2016).

The excellent stability and biocompatibility of metal-organic frameworks have been widely reported (Li et al., 2019). Among them, Prussian blue has been widely studied because of its simple synthesis method, strong structural stability, good biocompatibility, photothermal properties, and strong sterilization efficiency (Wang et al., 2018; Borzenkov et al., 2019; Cai et al., 2019; Li et al., 2019; Luo et al., 2019; Han et al., 2020; Mukherjee et al., 2020; Sharma et al., 2020) Maaoui et al. (2016). reported for the first time that Prussian blue nanoparticles could effectively kill *MRSA* and *E. coli* through the photothermal effect. Other literature reported that Prussian blue could kill *E. coli* 100% within 5 min through the photothermal effect. However, due to its high photothermal conversion rate, Prussian blue may increase the risk of damage to normal tissue (Jiang et al., 2018). Tannic acid is a polyphenolic compound, which is the active ingredient extracted from gallnut (Ninan et al., 2016; Yan et al., 2019; Liu et al., 2020). It has been reported in the literature that it has antibacterial, antioxidant, antiviral, and other activities. Tannic acid also has the function of inhibiting bacterial quorum sensing (QS) and preventing the formation of bacterial biofilms (Liu et al., 2020). However, tannic acid has limited antimicrobial ability against Gram-negative bacteria *E. coli*, which limits its application (Sahiner et al., 2016). Polyacrylamide has good biocompatibility and non-toxicity and is often used in drug delivery and skin repair research (Xue et al., 2019). Its 3D hydrogel network provides a moist environment for cells, promotes permeability of oxygen and water molecules, and protects against microbial invasion (Gan et al., 2018). Its good mechanical properties are characterized by strong stress and flexibility, so it is often possible to construct hydrogels with good properties without chemical modification (Chen et al., 2018; Fang et al., 2019). The electrostatic, hydrogen bonding, and hydrophobic interactions of the groups in hydrogel make it have the characteristics of strong viscosity, which can enhance the skin adhesion ability of the hydrogel (Xue et al., 2019; Hao et al., 2020). In addition, with the increase of water, the adhesion decreases, making the hydrogel easy to peel off (Ning et al., 2014). Therefore, the construction of polyacrylamide composite hydrogel loaded with Prussian blue nanoparticles and tannic acid is expected to improve its antibacterial performance and tissue repair ability while reducing the side effects of the material through synergistic effect.

In this study, polyacrylamide composite photothermal hydrogel containing Prussian blue nanoparticles and tannic acid was prepared by precipitation method and immersion method. We fabricate composite hydrogel, which has antimicrobial ability, skin repair ability, triggering drug release (TDR), and thermal-disrupting interface induced mitigation (TRIM) alleviating heat damage. In this paper, the physical and chemical characterization, *in vivo* and *in vitro* biocompatibility, anti-infection ability, and tissue repair ability of the composite photothermal hydrogel were detected and analyzed. The scientific hypothesis that this composite photothermal hydrogel has good biocompatibility and antibacterial ability to promote skin repair is put forward (**Figure 1**). There are no reports of the use of Prussian blue nanoparticles combined with tannic acid-loaded polyacrylamide composite photothermal hydrogel for the treatment of infectious skin defects.

RESULTS AND DISCUSSION

Physical Characterization of Composite Photothermal Hydrogel

In this study, TA-PB@PAAm hydrogel was successfully fabricated (**Figure 2A**). TA-PB@PAAm hydrogel presented a blue transparent peptone-like appearance, which was mainly due to the doping of Prussian blue nanoparticles. As the content of Prussian blue increased, the color of the hydrogel deepened. The hydrogel has a strong adhesion effect, which may be caused by electrostatic, hydrogen bonding, and hydrophobic interactions. According to the SEM test results (**Figure 2B**), TA-PB@PAAm hydrogel presented a uniformly distributed porous structure, and its pore size distribution was about 1 μm. SEM characterization of PB nanoparticles showed that they presented a cubic structure with a diameter of about 50 nm (**Figure 2C**).

The absorption peaks of PB, PB@PAAm, and TA-PB@PAAm were detected by UV-Spectrum, and it was found that their absorption peaks were 700 nm (**Figure 2D**). The particle size of PB, PB@PAAm hydrogel precursor solution, and TA-PB@PAAm hydrogel precursor solution were detected. The Zeta potential of PB, TA, TA + PB, PAAm hydrogel precursor

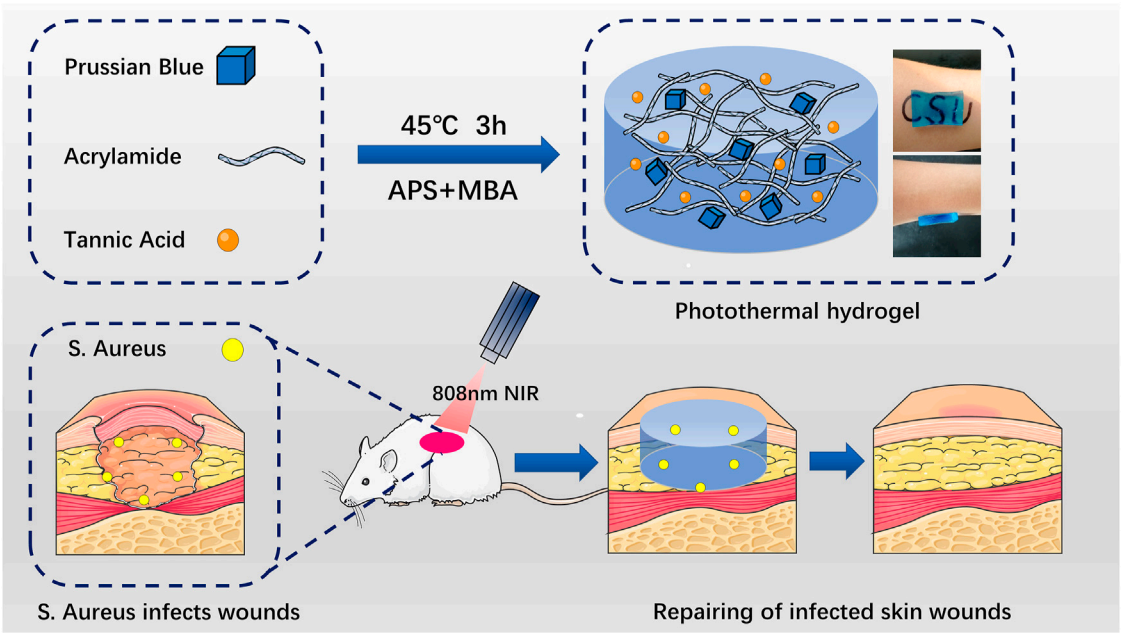

FIGURE 1 | Schematic diagram of Prussian blue nanoparticles and tannic acid drug particles loaded on acrylamide hydrogel for the elimination of bacteria and promotion of skin repair through the synergistic photothermal and antibacterial action of the drugs. APS: ammonium persulfate. MBA: 4-sulfanylbutanimidamide.

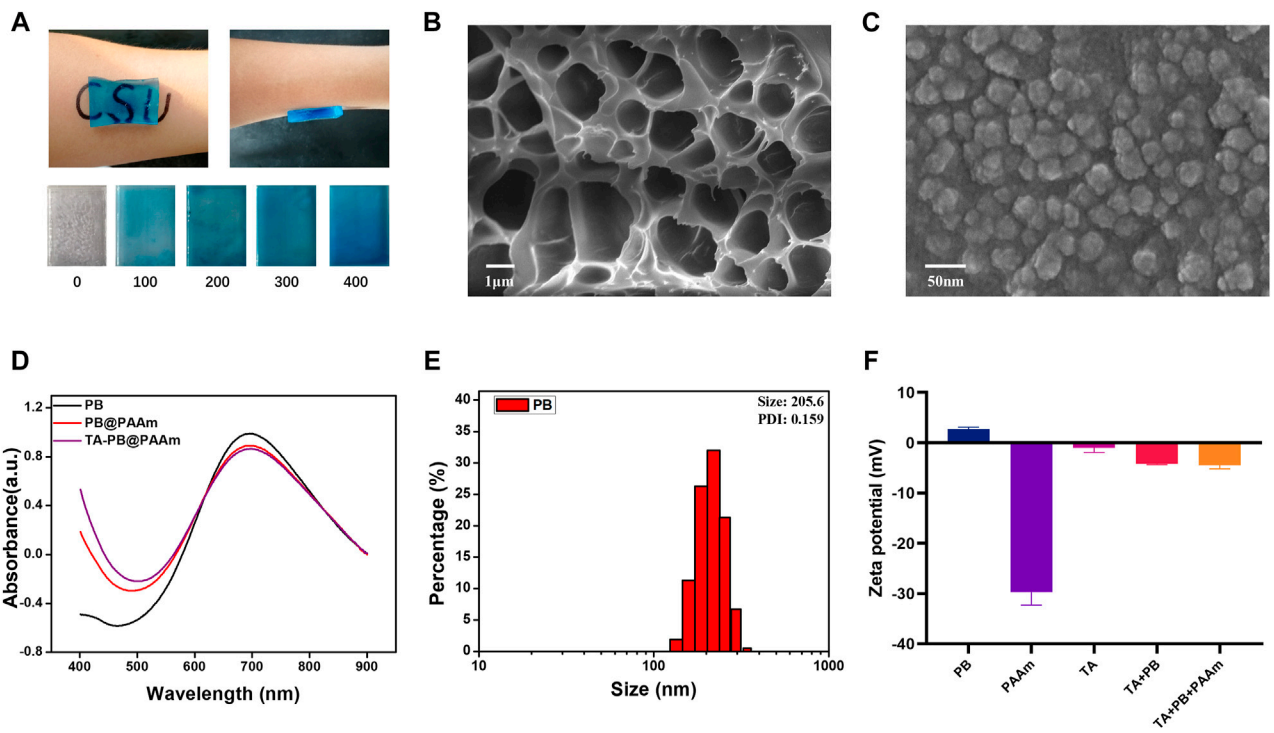

FIGURE 2 | Physical and chemical characterization of hydrogel composites. **(A)** Appearance of the materials, which are prepared with different concentrations of Prussian blue and the adsorption properties (unit = ug/ml). **(B)** Porous structure of formed composite photothermal hydrogels. **(C)** SEM microscopic morphology of Prussian blue nanoparticles. **(D)** UV absorption spectra of PB, PB@PAAm and TA-PB@PAAm. **(E)** Particle size distribution of Prussian blue nanoparticles. **(F)** Zeta potential of PB shows positive charge.

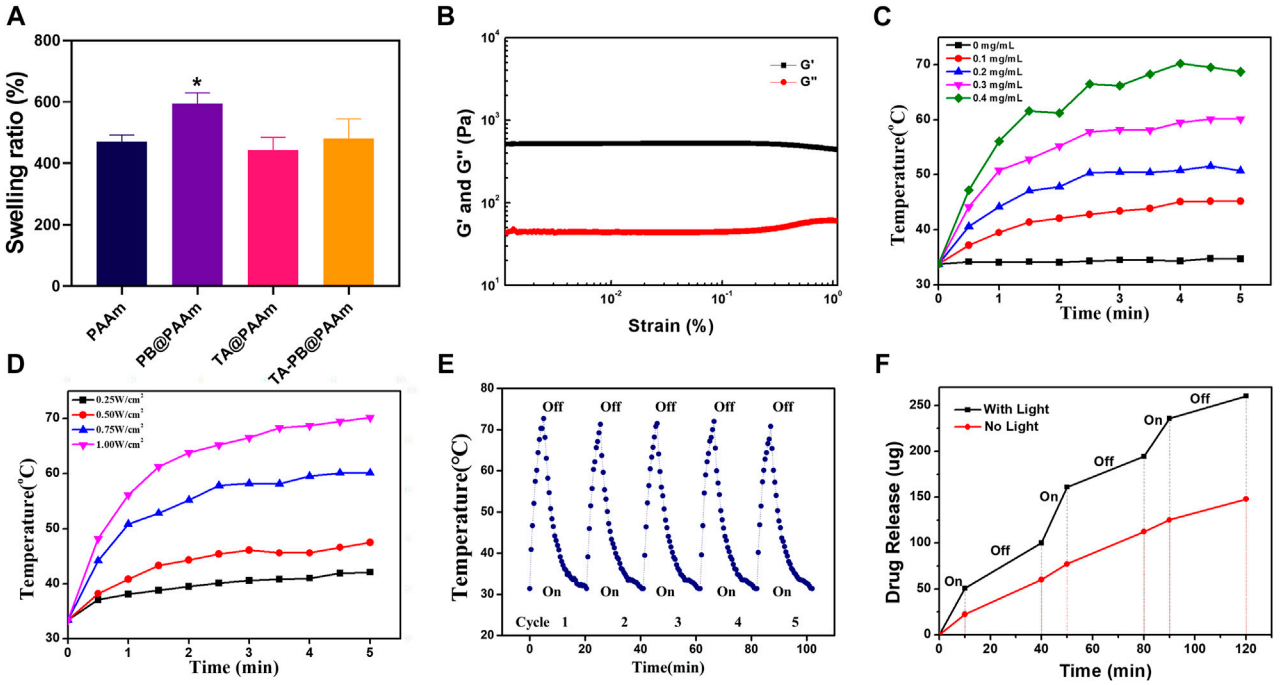

FIGURE 3 | Physical and chemical characterization of TA-PB@PAAm composite hydrogels. **(A)** Swelling rate for different contents of composite photothermal hydrogels. **(B)** The preservation modulus G′ is always higher than the loss modulus G″, which proves that the material has good crosslinking performance. **(C)** Photothermal effect curve for different PB concentrations. **(D)** Photothermal effect curve under different illumination intensities. **(E)** Curve of temperature changes after cyclic illumination of the hydrogels. **(F)** Drug release curve under alternating light.

solution, and TA-PB@PAAm hydrogel precursor solution were detected by particle size analyzer. The average particle size of PB was 205.6 nm and PDI was 0.156 (**Figure 2E**). Zeta potential results showed that the surface of PB was positively charged, TA was negatively charged, and finally the hydrogel was negatively charged (**Figure 2F**). The FTIR results are as follows. In the sample TA, the vibration peaks observed at 3402, 1716, and 1614cm^{-1} were respectively determined by the hydroxyl group, C=O in the carboxyl group and C-C in the benzene ring skeleton showed the presence of tannic acid. In sample PB, the vibration peaks caused by the metal -C≡N- metal at 2083 cm^{-1} and 594 cm^{-1} were observed, indicating the existence of PB. For the sample PAAm hydrogel, vibration peaks were not observed at 1,430 cm^{-1} and at 1,630 cm^{-1}, indicating that the stretching vibration of the C=C bond after acrylamide cross-linking polymerization disappeared. At 2,980 cm^{-1} and 1,450 cm^{-1}, the characteristic vibration peak was the C-H vibration peak which was in the -CH2- group. It was found that 1756 cm^{-1} represented the amide bond, 1,189 cm^{-1} represented the C-N bond, and 1,083 cm^{-1} represented the C-O-C bond. These characteristic vibration peaks indicated the formation of polyacrylamide. In addition to the characteristic vibration peak of PAAm, it could be observed that the vibration peak of the amide bond moved to 1,658 cm^{-1}, and the vibration peak of C-O-C moved to 1,116 cm^{-1}, which could be caused by the coordination effect between metal ions in Prussian blue and C-O functional groups in PAAm structure. For the TA-PB@PAAm sample, the characteristic vibration peak belonging to the benzene ring could be observed near 1,614 cm^{-1}, which proved that TA structure also existed in the PB@PAAm structure (**Supplementary Figure S1**). The XRD results are as follows: For sample PB, only a wide diffraction peak was observed at 19.6°, proving that the Prussian blue structure synthesized was amorphous. For sample TA, only a wide diffraction peak was observed at 25.2°, proving that the TA was an amorphous structure (**Supplementary Figure S2**).

All the above results indicated that PB and PAAm were crosslinked and successfully loaded. We then loaded the hydrogels with different concentrations of TA by the immersion method and calculated the drug loading rates, which were 0.25,0.5, and 2.5%. With the increase of TA concentration, the drug loading rate of polyacrylamide also increases, so it has excellent drug loading capacity. Therefore, 5 mg/mL TA concentration was selected as the later application concentration according to the results. We calculated the swelling rate of PAAm, PB@PAAm, TA@PAAm, and TA-PB@PAAm, and they are 470.8 ± 17.5%, 594.1 ± 28.6%, 442.6 ± 33.8%, and 480.3 ± 52.4%, respectively. The composite photothermal hydrogel could absorb about 4–5 times its own mass of water, so it had a good water absorption capacity (**Figure 3A**). This excellent swelling ability can effectively absorb the exudated and exfoliated necrotic tissue cells from the wound during the treatment process, so it has the function of autolytic debridement.

The rheology was used to test the viscoelastic properties of the composite photothermal hydrogel. Storage modulus G′ of the

hydrogel was always higher than loss modulus G″ by 500% strain, and G′ and G″ relatively represented pronounced plateau, indicating that the hydrogel could maintain a solid form and have a certain elasticity. This feature may be more suitable as a skin dressing (Van Den Bulcke et al., 2000) (**Figure 3B**).

Photothermal Properties of Composite Photothermal Hydrogel

Different concentrations of PB loaded on hydrogels have different photothermal effects (**Figure 3C**). Among them, 0.4 mg/mL PB hydrogel had the strongest photothermal effect and could reach 68.7°C within 5 min. With the decrease of PB content, the photothermal effect of the hydrogel gradually weakened, and the maximum temperature of 0.1mg/mL PB was 45.2°C. Different illumination intensities of NIR-808 laser had different photothermal effects (**Figure 3D**). The PB hydrogel with 1W/cm2 had the strongest photothermal effect and could increase to 70.2°C within 5 min. With the decrease of illumination intensity, the photothermal effect of hydrogel gradually weakened, and the maximum temperature was less than 47.5°C under the illumination intensity of 0.5W/cm2. It has been reported that when the ambient temperature of cells exceeds 50°C, cell necrosis will occur. When the ambient temperature of cells is below 50°C and above 40°C, apoptosis occurs, but it can be repaired by human heat shock proteins (Yang et al., 2017). Therefore, we chose the parameters of PB concentration of 0.1mg/ml and illumination intensity of 0.5W/cm^2 as the final photothermal conditions.

In order to test the reusability of the composite photothermal hydrogel, repeat irradiation was given. The temperature of the hydrogel reached its peak within 5 min. After the irradiation of NIR-808 was turned off, the temperature of the hydrogel dropped to the initial temperature within 15 min. With the increase of the number of cycles, the peak temperature and cycle time of hydrogel remain stable. It showed that the hydrogels had a good photothermal effect to ensure recycling and reuse (**Figure 3E**).

In Vitro NIR Light-Triggered Drug Release

In order to calculate the release amount of tannic acid, we tested the absorbance value of tannic acid in the ultraviolet absorption spectrum, which showed the maximum absorption peak at 275 nm (**Supplementary Figure S3**). With the increase of the concentration of tannic acid, the absorbance value also increased. In order to prove that the drug would be released by setting the photothermal switch in a NIR-triggered "off-on way", we measured the release profile of tannic acid by ultraviolet spectrum (**Figure 3F**). The TA-PB@PAAm hydrogel without NIR light had the ability of drug release in PBS solution, and the drug release amount slowly increased with a total release amount of 147.9 μg in 120 min. When the TA-PB@PAAm hydrogel was illuminated by NIR light, the drug release was significantly increased, and the total release reached 260.3 μg in 120 min. After the light was turned off, the drug release rate was the same as that without NIR light. The rate of drug release in the hydrogel changed as the light was switched on and off multiple times. It showed that the synergistic photothermal effect could promote the release of drugs in the hydrogel. NIR light acted as a switch in drug release, which might better promote the efficacy of hydrogel in the treatment of infection, and intelligently regulated the release rate of the drug, which was 1.76 times higher than that of the non-light group.

Cell Compatibility of NIH-3T3 With Composite Photothermal Hydrogel

Firstly, we measured the 50% lethality of tannic acid and Prussian blue to cells **(Supplementary Figure S4)**. The 50% lethal dose of tannic acid in NIH-3T3 cells was 200 μg/ml and the 50% lethal dose of PB was 100 μg/ml. After that, we evaluated the cell compatibility in different hydrogels at different time points (1, 3, 5 days) by CCK-8 assay **(Figures 4A–D)**. With the increase of culture time, cells in each group showed a steady growth trend. On day one, the absorbance of the control group was higher than that of the other three experiment groups (PB@PAAm, TA@PAAm, and TA-PB@PAAm) both in the non-light and light conditions (non-light: 0.230, 0.206, 0.212, 0.190; light: 0.258, 0.194, 0.242, 0.173). On day three, the CCK8 levels of PB@PAAm, TA@PAAm and TA-PB@PAAm both in the non-light and light conditions were significantly higher than those of the blank control group (non-light: 0.350, 0.696, 0.438, 0.531; light: 0.380, 0.522, 0.439, 0.517). On day five, the CCK8 of PB@PAAm, TA@PAAm, and TA-PB@PAAm both in the non-light and light conditions were significantly higher than that of the blank control group, but the increasing rate was lower than that of the third day (non-light: 0.397, 0.654, 0.466, 0.542; light: 0.414, 0.538, 0.464, 0.536). These results indicate that our composite photothermal hydrogel has good cytocompatibility and can support cell adhesion and growth after implantation. The result may be a slow release of the drug due to the encapsulation of the hydrogel, thus reducing the damage to the cells.

In Vitro Bactericidal Test of Composite Photothermal Hydrogel

We co-cultured *S. aureus* and *E. coli* with different kinds of hydrogels then inoculated the diluent solutions on the surface of the TSA plate for counting and evaluated the bactericidal effect of hydrogels. The survival rate of *S. aureus* was as follows (**Figure 5A, D**), NL control, L control, NL PB@PAAm, L PB@PAAm, N TA@PAAm, L TA@PAAm, NL TA-PB@PAAm, and L TA-PB@PAAm was 100, 98.5, 95.7, 44.2, 24.9, 17.9, 19.2, and 0.3%, respectively. Compared with the control group, the bacterial colony number of *S. aureus* inoculated on the surface of NL PB@PAAm was not significantly different, while the bacterial colony number of *S. aureus* inoculated on the surface of L PB@PAAm was significantly decreased. In addition, N TA@PAAm, TA@PAAm, and NL TA-PB@PAAm showed good bactericidal ability. It is worth noting that L TA-PB@PAAm hydrogel had a significant bactericidal effect, and the bacterial survival rate was only 0.3%. Prussian blue has a wide range of

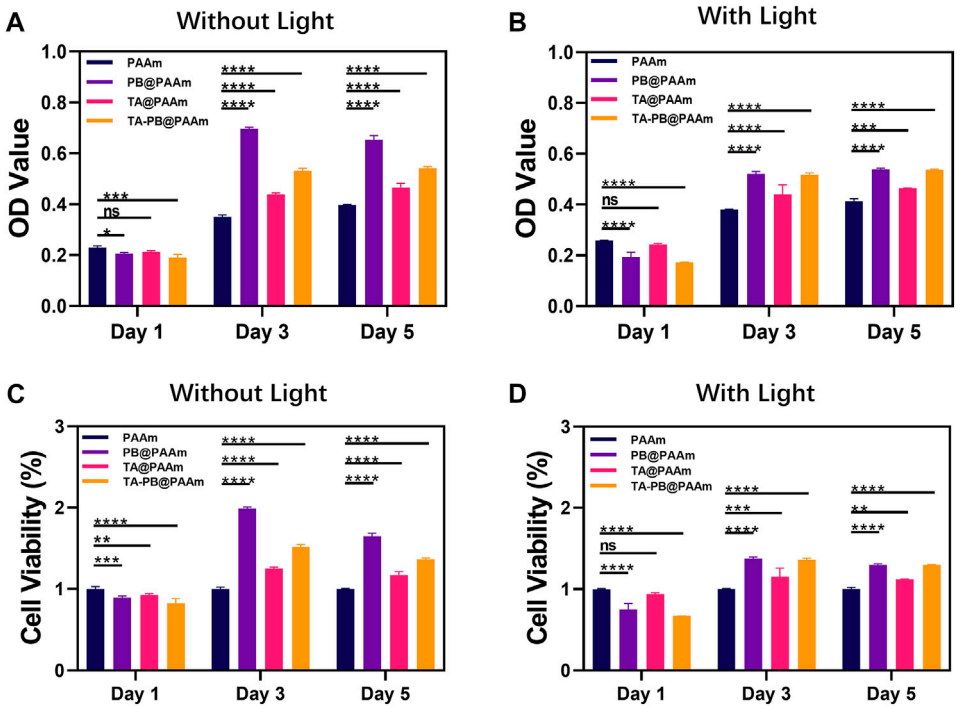

FIGURE 4 | CCK-8 results of NIH-3T3 cells co-cultured with composite photothermal hydrogels at different time points. **(A–B)** Absorbance in PAAm, PB@PAAm, TA@PAAm, TA-PB@PAAm with or without light. **(C–D)** Survival rate in PAAm, PB@PAAm, TA@PAAm, TA-PB@PAAm with or without light. Data are mean ± SD (n = 3, $^{*}p < 0.05$, $^{**}p < 0.01$, $^{***}p < 0.001$, $^{****}p < 0.0001$, ns = no statistical difference).

functions, including antibacterial, antioxidant, enzyme-mimetic, and detoxifying properties. Among them, because of its good biocompatibility, biological stability, and excellent photothermal effect, it has been widely studied by scholars (Busquets and Estelrich, 2020). Tannic acid is a kind of natural polyphenol, which has antibacterial and antioxidant ability25. This antioxidant molecule can trap large amounts of free radicals and thus play a key role in wound healing. Because it is non-toxic and non-carcinogenic, it is used by many scholars to study wound repair. On the one hand, in this experiment, in addition to using heat to directly kill bacteria, we can also use near-infrared radiation to trigger the release of local high concentrations of tannic acid from the hydrogel, so as to synergistically enhance the antibacterial activity. Tannic acid, on the other hand, is a polyphenolic substance that is effective against bacteria while reducing antibiotic overuse resulting in irreversible resistance. Here we speculate that the main reason why the photothermal effect can effectively kill bacteria is that it inhibitions the enzyme activity of bacteria, because the optimal activity temperature of enzymes in bacteria is between 30°C and 40°C, however, the enzyme activity is strongly inhibited at a higher temperature12.

Meanwhile, the survival rate of *E. coli* was as follows (**Figures 5A,E**), NL control, L control, NL PB@PAAm, L PB@PAAm, NL TA@PAAm, L TA@PAAm, NL TA-PB@PAAm, and L TA-PB@PAAm was 100, 95.6, 96.2, 41.9, 99.4, 93.7, 94.8, and 42.8%, respectively. We found that compared with the control group, there was no difference in the number of bacterial colonies when *E. coli* was inoculated on the surface of L Control, NL PB@PAAm, N TA@PAAm, L TA@PAAm, or NL TA-PB@PAAm. When inoculated on the surface of L PB@PAAm and L TA-PB@PAAm, the number of bacterial colonies decreased significantly, which was about 40% of the control group. It has been reported in the literature that tannic acid is not effective in killing *E. coli*25, which may be related to its extensive drug resistance. Fortunately, the main bacteria involved in skin infections is *S. aureus*, and the photothermal effect can achieve a certain antibacterial function, to fill this defect.

The killing effect of photothermal hydrogel composites on *S. aureus* and *E. coli* was characterized by SEM (**Figure 5B**). It was observed that with the addition of TA or photothermal effects, the membranes of *S. aureus* and *E. coli* were shrunk. In the bacteria with both TA and Prussian blue photohydrothermal action, obvious destruction of the membrane was observed. The significant efficacy of our photothermal hydrogel composites was illustrated.

We further tested the sustained antibacterial of *S. aureus* and *E. coli* with composite photothermal hydrogels by the bacterial inhibition ring test for 48 h (**Figures 5C,F**, **Supplementary Figure S5**). In NL control and L PB@PAAm groups, the diameter of the inhibition ring was 0 cm. The diameters of the inhibition rings of NL TA@PAAm, L TA@PAAm, NL TA, NL TA-PB@PAAm, and L TA-PB@PAAm were 1.13, 1.27, 1.37, 1.63, and 1.77 cm, respectively. Compared with the control group, the results of NL TA@PAAm, L TA@PAAm, NL TA, NL TA-PB@PAAm, and L TA-PB@PAAm were statistically different. Interestingly, the thermal effect could not be effectively

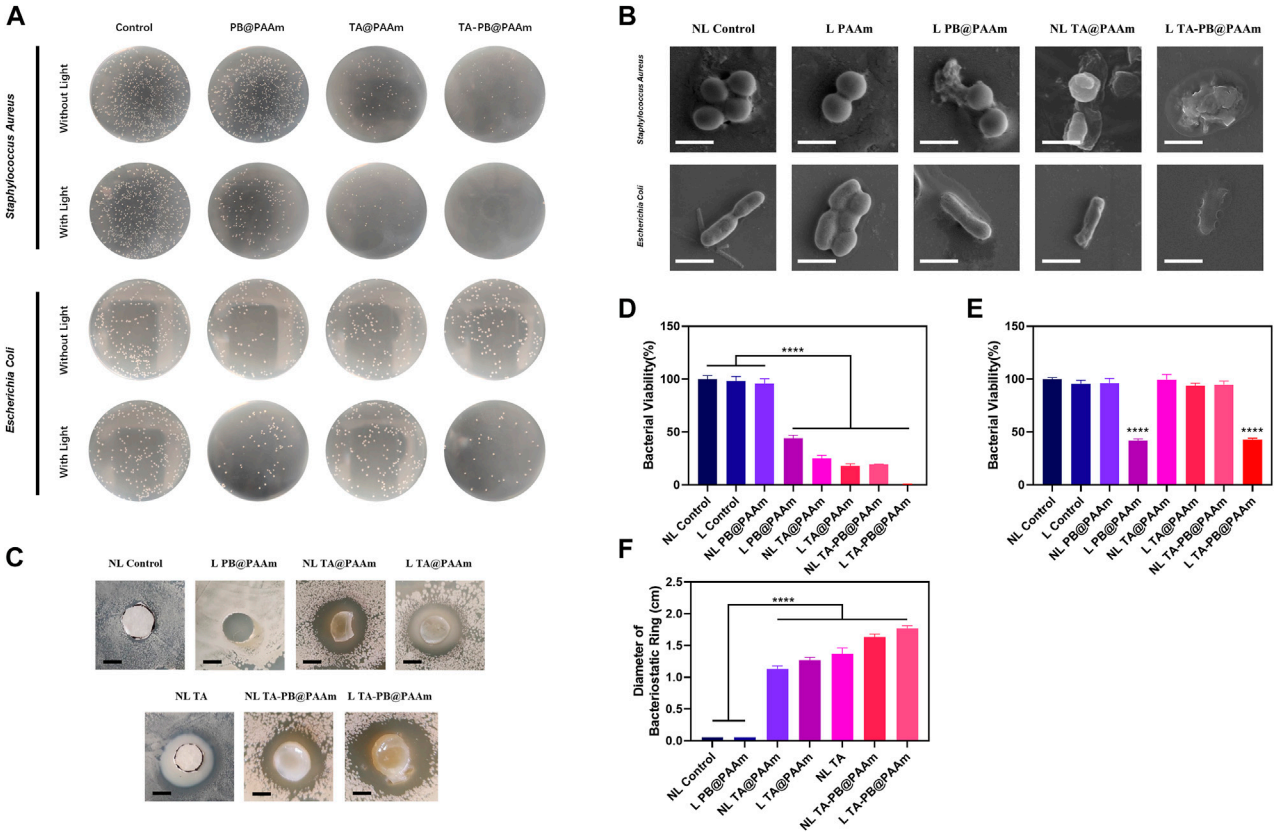

FIGURE 5 | *In-vitro* bactericidal test of composite photothermal hydrogel. **(A)** Bacteriostatic experiment of different hydrogels on *Staphylococcus aureus* and *Escherichia coli*. **(B)** The SEM result of the bacterial morphology through the treatment of different hydrogels on *S. aureus* and *E. coli*. Scale bar = 1 μm. **(C)** Bacterial inhibition ring test results of different materials. Scale bar = 5 mm. **(D)** Quantitative results of the survival rate of *S. aureus*. **(E)** Quantitative results of survival rate of *E. coli*. **(F)** Quantitative results of the diameters of bacterial inhibition ring tests. Data are mean ± SD (n = 3, ****$p < 0.0001$).

performed in the L PB@PAAm group perhaps due to the low water content in the plate. Since we can see that the surface of the hydrogel and the areas where it touched are free of bacteria, therefore, we can speculate that the photothermal effect of Prussian blue also has a certain bactericidal function in environments of a certain humidity. In summary, the above results indicated that illumination promoted the release of drugs, played a synergistic antibacterial effect and had the ability to produce a sustained release.

In Vivo Biological Assessment

Wound Healing Evaluation

The skin defects in all groups gradually healed (**Figure 6A**). From day 2 to day 4 after surgery, signs of skin infection were observed in the NL control, L control, NL PAAm, L PAAm, and NL PB@PAAm groups, while no signs of skin infection were observed in the other groups. By day 7, signs of infection were reduced in the NL Control, L Control, NL PAAm, L PAAm, and NL PB@PAAm groups. On day 14, infection in each group was significantly controlled, and skin healing in L PB@PAAm, NL TA@PAAm, L TA@PAAm, NL TA-PB@PAAm, and L TA-PB@PAAm was significantly higher than that in the other groups. Particularly, the skin healing in L TA-PB@PAAm was the best. The wound healing rate on day 14 was calculated (**Figure 6B**). NL control, L control, NL PAAm, L PAAm, NL PB@PAAm, L PB@PAAm, NL TA@PAAm, L TA@PAAm, NL TA-PB@PAAm, and L TA-PB@PAAm decreased to 26.5, 26.7, 26.7, 28.4, 22.2, 13.7, 11.7, 12.1, 9.8, and 1.5%, respectively.

In vivo Bacterial Plate Counting Test

We counted the bacteria numbers in the skin defect wound of rats 24 h after surgery, and the survival rate of *S. aureus* was as follows (**Figures 6C,D**). The survival rate in NL control, L control, NL PAAm, L PAAm, NL PB@PAAm, L PB@ PAAm, NL TA@ PAAm, L TA@ PAAm, NL TA-PB@ PAAm, and L TA-PB@ PAAm was 100, 92.4, 95.6, 98.0, 98.3, 20.6, 19.9, 26.7, 13.5, and 0.3%, respectively. The results were consistent with those of skin healing.

Histological Staining Evaluation

Histological analyses were also performed to evaluate the antimicrobial and tissue-repair properties of different composite photothermal hydrogels. In order to evaluate the

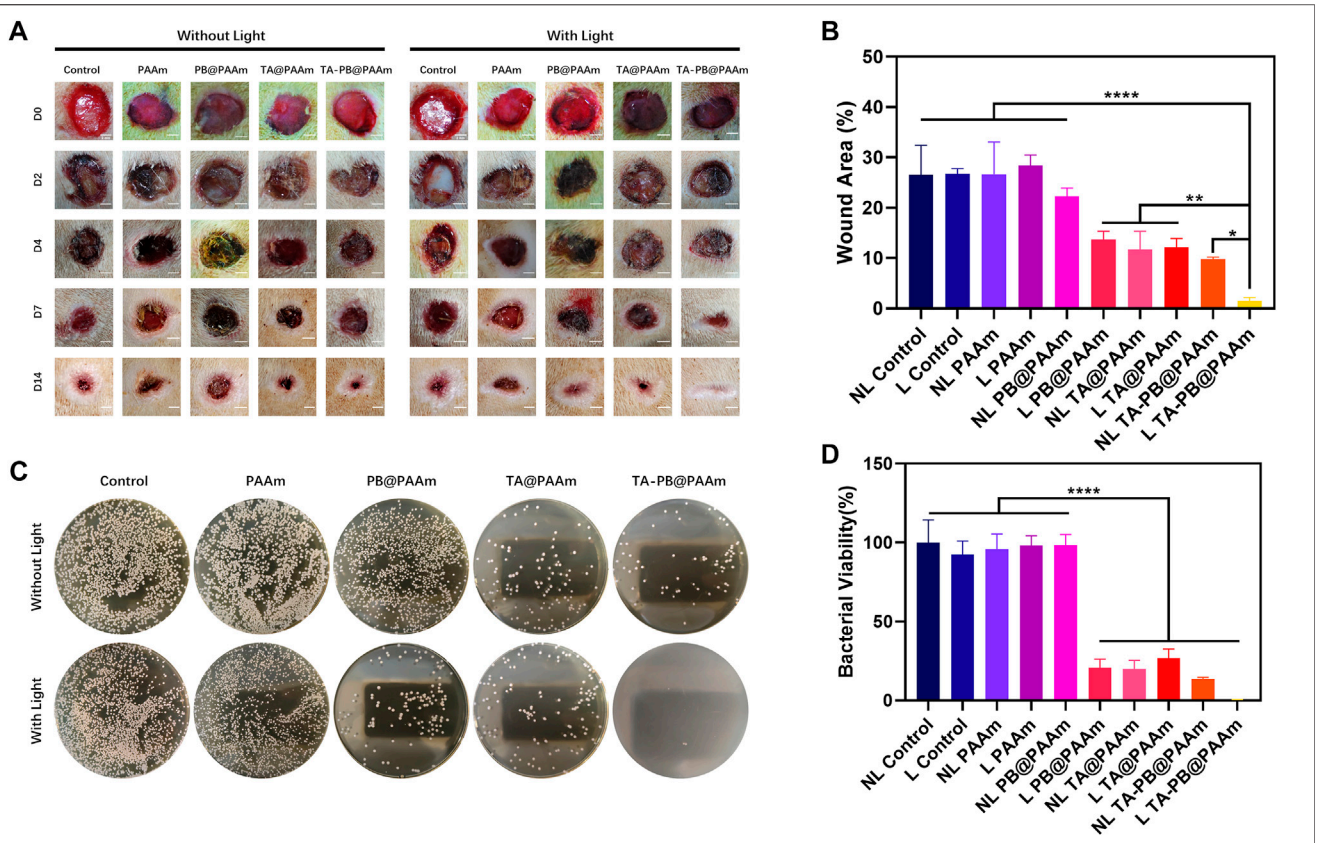

FIGURE 6 | Wound healing in SD rats. **(A)** Results of skin repair of infectious skin defect in animal model. Scale bar = 2 mm. **(B)** Quantitative results of the areas of wound healing. **(C)** *In-vivo* bacteriostatic experiments using different hydrogels on *Staphylococcus aureus*. **(D)** Quantitative results of the areas with a survival rate of *Staphylococcus aureus*. Data are mean ± SD (n = 3, $^{*}p < 0.05$,$^{**}p < 0.01$, $^{****}p < 0.0001$).

antibacterial properties of different composite photothermal hydrogels, we used Giemsa staining to observe the number of bacteria (**Figures 7A,B**). We could see at day 2, a large number of bacteria appeared in the skin tissue of NL control, L control, NL PAAm, L PAAm, NL PB@ PAAm group, while L PB@ PAAm, NL TA@ PAAm, L TA@ PAAm, NL TA-PB@ PAAm, and L TA-PB@ PAAm group had relatively few bacteria in the skin tissue, and the bacteria content of the L TA-PB@PAM group was significantly lower than that of the other groups. We carried out quantitative counting of bacteria by Giemsa staining in different groups. The bacterial counting in NL control, L control, NL PAAm, L PAAm, NL PB@PAAm, L PB@PAAm, NL TA@PAAm, L TA@PAAm, NL TA-PB@PAAm, and L TA-PB@PAAm was 408.0 ± 54.6, 399.7 ± 17.2, 391.7 ± 9.0, 360.3 ± 80.1, 336.3 ± 8.6, 197.3 ± 9.0, 196.0 ± 16.5, 199.7 ± 17.1, 160.0 ± 14.9, and 10.0 ± 2.6, respectively.

In order to evaluate the tissue repair function of different composite photothermal hydrogels, we used H and E staining to observe the number of inflammatory cells and skin repair conditions (**Figures 7C,D**). On 14 days after surgery, in the NL Control, L Control, NL PAAm, L PAAm, and NL PB@ PAAm groups, there was still necrotic tissue and a large number of neutrophils in the skin tissue, and poor tissue repair was also observed. However, the neutrophils in the L PB@PAAm, NL TA@PAAm, L TA@PAAm, NL TA-PB@ PAAm, and L TA-PB@PAAm groups were relatively less, while vessels and hair follicles were observed. Compared with the other groups, the bacterial content of neutrophils in the L TA-PB@PAM group was significantly reduced, and the skin tissue was repaired well, and a large number of hair follicles and vessels were found. We carried out quantitative counting of bacteria by H and E staining in different groups. The number of inflammatory cells in NL control, L control, NL PAAm, L PAAm, NL PB@ PAAm, L PB@ PAAm, NL TA@ PAAm, L TA@ PAAm, NL TA-PB@ PAAm, and L TA-PB@ PAAm was 766.0 ± 124.4, 786.7 ± 180.0, 781.3 ± 102.1, 654.7 ± 70.5, 709.3 ± 82.6, 418.7 ± 90.3, 328.7 ± 39.1, 304.3 ± 93.8, 264.7 ± 137.7, and 15.7 ± 2.5, respectively.

We also used Masson's trichrome staining to observe the type I collagen and skin repair conditions (**Figures 7E,F**). Fourteen days after surgery, in the NL Control, L Control, NL PAAm, L PAAm, and NL PB@PAAm group, there were still muscle fibers and a large number of red blood cells in the skin tissue, and poor tissue repair was also observed. However, the type I collagen in the L PB@PAAm, NL TA@ PAAm, L TA@PAAm, NL TA-PB@PAAm, and L TA-PB@PAAm groups were relatively higher. Compared with the other groups, the type I collagen in the L TA-PB@PAM group was significantly highest, and the skin tissue was repaired well. We carried out quantitative

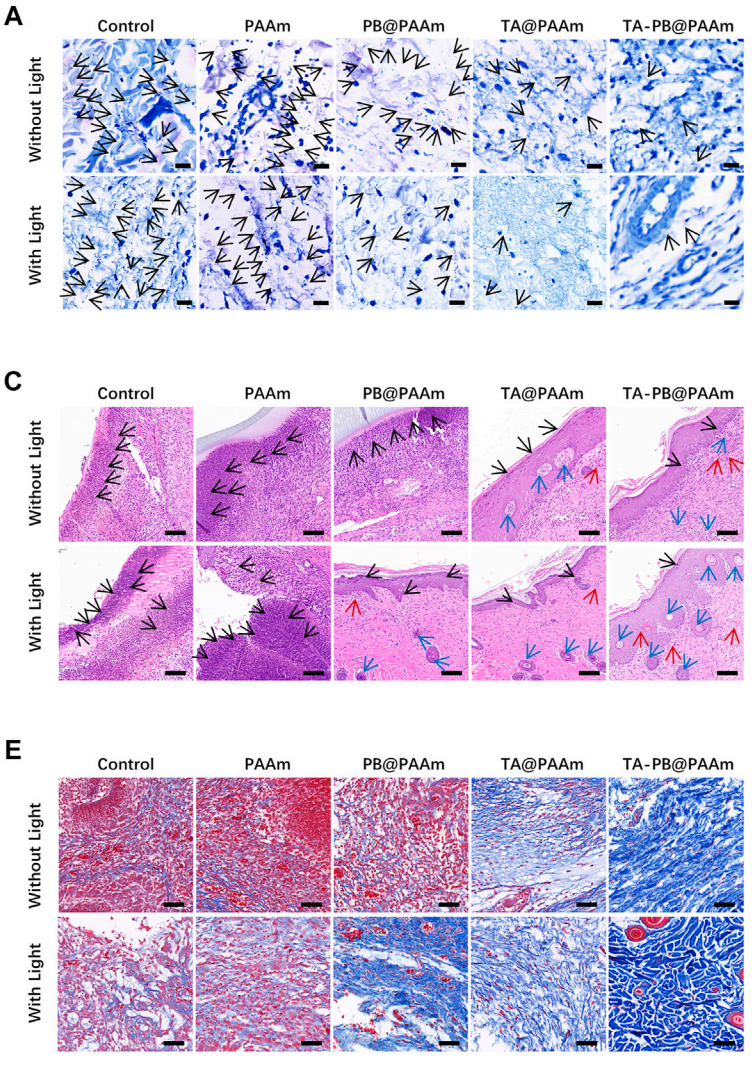

FIGURE 7 | Histological staining evaluation. **(A)** Giemsa staining of infective skin defects shows the smallest number of bacteria for the L TA-PB@PAAm group. Black arrow represents bacteria. Scale bar = 20 μm. **(B)** Quantitative results of bacterial viability in Giemsa staining. **(C)** H and E staining showed skin repair results, neutrophils are fewer in the L PB@PAAm, N TA@PAAm, L TA@PAAm, NL TA-PB@PAAm, L TA-PB@PAAm groups. Black arrows represent inflammatory cells, red arrows represent newly formed vessels, and blue arrows represent newly formed hair follicles. Scale bar = 100 μm. **(D)** Quantitative results of inflammatory cells in H and E staining. **(E)** Masson's trichrome staining shows the content of collagen are higher in the N TA@PAAm, L TA@PAAm, NL TA-PB@PAAm, L TA-PB@PAAm groups. **(F)** Quantitative results of collagen content in Masson's trichrome staining. Data are mean ± SD (n = 3, $^{*}p < 0.05$, $^{**}p < 0.01$, $^{****}p < 0.0001$). Scale bar = 100 μm.

counting of type I collagen in different groups. The content of type I collagen in NL control, L control, NL PAAm, L PAAm, NL PB@PAAm, L PB@ PAAm, NL TA@ PAAm, L TA@ PAAm, NL TA-PB@ PAAm, and L TA-PB@ PAAm was 13.4, 13.7, 13.8, 14.5, 12.7, 20.6, 21.8, 23.1, 28.9, and 51.6%, respectively.

The main reasons for this result are as follows: 1) Photothermal effect synergistic antibacterial can effectively kill bacteria and reduce tissue necrosis and cell destruction caused by toxins produced by bacteria, such as α-toxin produced by *S. aureus*, which is a kind of membrane penetrating toxin and can cause cell death. 2) Bacterial toxins can weaken the proliferation and differentiation of fibroblasts and reduce the ability of skin repair, while the antibacterial effect of composite photothermal hydrogels can indirectly enhance the repair ability of fibroblasts. 3) TA and PB have anti-inflammatory and anti-oxidant effects, and the good cellular compatibility of the composite photothermal hydrogel provides a stable environment for the growth of fibroblasts and further promotes tissue healing. 4) Thermal-disrupting interface induced mitigation (TRIM) provided by hydrogel can reduce the thermal effect and effectively protect normal tissues, so that the photothermal temperature reaches below 50°C and cells can be effectively protected from high-temperature damage. Therefore, combined with the above advantages, L TA-PB@PAAm hydrogel can better resist bacterial and repair tissue.

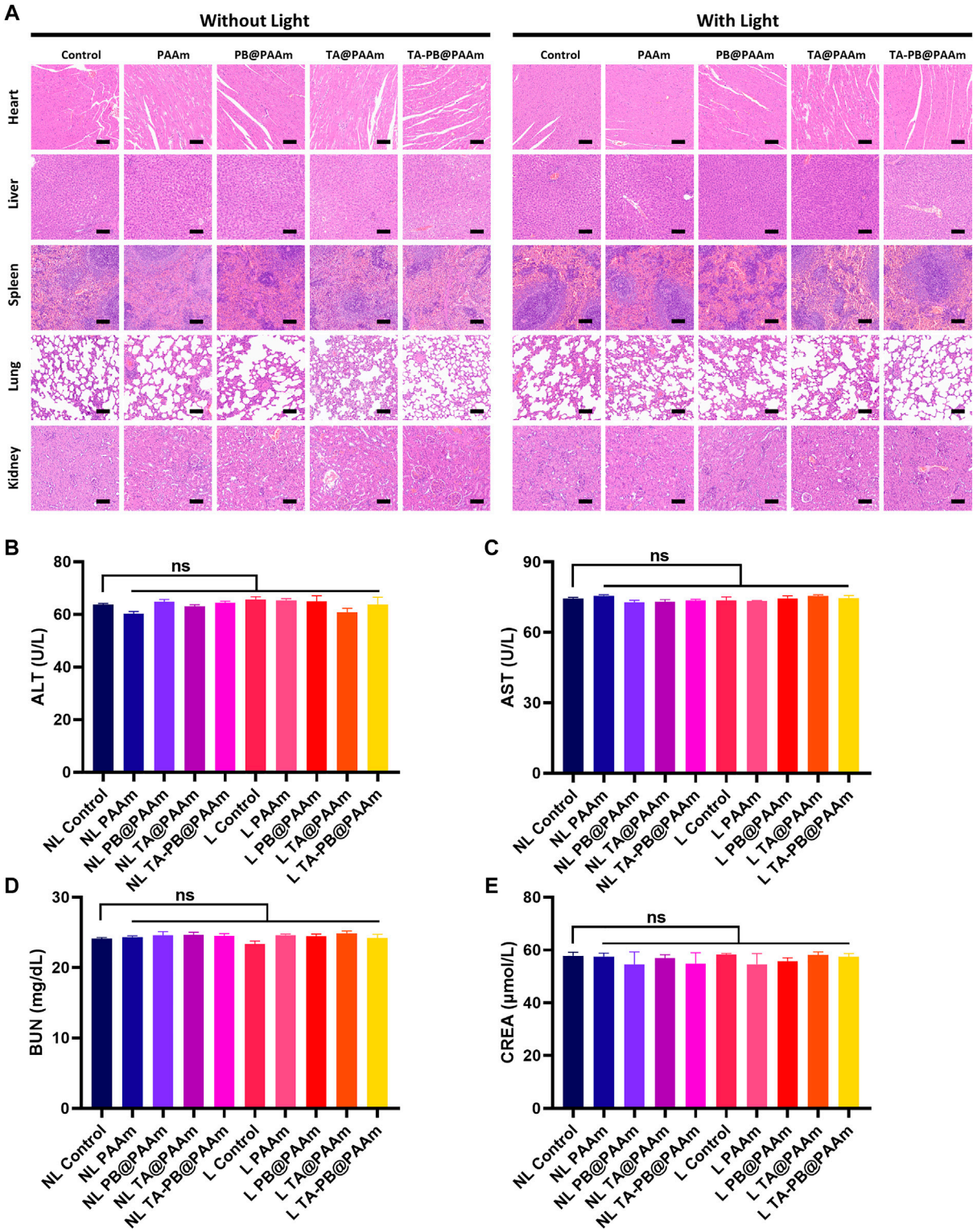

FIGURE 8 | a H and E staining of heart, liver, spleen, lung and kidney. Scale bar = 100 μm. b Results of ALT. c Results of AST. d Results of BUN. e Results of CREA. Data are mean ± SD (n = 3, ns = no statistical difference).

Histocompatibility Evaluation

H and E staining was performed on the sections of vital organs to further evaluate the biocompatibility of different samples (**Figure 8A**). Compared with the control group, there were no obvious organ damages or inflammatory lesions in the heart, liver, spleen, lung, and kidney of the composite photothermal hydrogel group. In addition, the results of liver and renal function were tested. ALT, AST, BUN, and CREA had no significant difference among different photothermal hydrogels (**Figures 8B–E**). These results showed that the composite photothermal hydrogels had good histocompatibility.

CONCLUSIONS

In conclusion, we fabricated a novel composite photothermal hydrogel with a simple synthetic method, triggering drug release rate, thermal-disrupting interface induced mitigation alleviating heat damage, transparent morphology observing wound healing, mechanical stability, strong adhesion, high swelling rate absorbing exudate, good biocompatibility, synergistic antibacterial ability, and excellent promotion of skin repair ability. As a new type of composite biomaterial, it has a strong guiding significance for the treatment of infectious skin defects in clinical use.

EXPERIMENTAL SECTION

Materials

Acrylamide, ferric chloride, potassium ferricyanide, citric acid, tannic acid, ammonium persulfate (APS), and 4-sulfanylbutanimidamide (MBA) were purchased from Sinopharm Chemical Reagent Co., Ltd. Solvents and buffer solutions were purchased from Servicebio (China). Lysogeny broth agar plates (LB), Fetal bovine serum, D-MEM medium were purchased from Thermo Fisher Scientific (China). Penicillin–streptomycin solution (PS) was purchased from HyClone (China). CCK-8 kits were purchased from Yeasen Biotech Co., Ltd. (China). NIH-3T3 cells (CL-0171) were purchased from Procell Life Science and Technology Co., Ltd. *S. aureus* and *E. coli* were purchased from China Center of Industrial Culture Collection (CICC, Beijing, China). All agents were used as received and used without further purification.

Synthesis of Materials

Fabrication of PBNPs

The synthesis of Prussian blue nanoparticles is based on previously reported methods (Maaoui et al., 2016). The brief description is as follows. Added 0.5 mmol (12.5% W/V %) citric acid to 20 ml ferric chloride solution containing 0.02 mmol (0.16% W/V %) and stirred it evenly at 60 °C to prepare 1 mM ferric chloride solution A. Then, 0.5 mmol (12.5% W/V %) citric acid was added to 20 ml of 0.02 mmol (0.33% W/V %) potassium ferricyanide solution to prepare 1 mM solution B. Dropped solution B dropwise into solution A (80–100 drops per minute) at 60 °C and stirred evenly. Finally, Prussian blue nanoparticles with a concentration of 0.5 mM were prepared after a 12 h reaction. The obtained product was purified with a dialysis membrane (MW: 1.4×10^3 Da) for 48 h to remove the excess reactants.

Fabrication of PAAm and PB@PAAm

The preparation method of polyacrylamide hydrogels is based on previous reports (Ning et al., 2014). The brief description is as follows: 1.42 g (0.02 mol) of acrylamide (142% W/V%), 4-sulfanylbutanimidamide (MBA) 3 mg (0.3% W/V%), then added 10 ml DI water to mix AAm and MBA solution, or added the appropriate amount of PB and stirred equally. Next step, added ammonium persulfate (APS) 4.7 mg (0.47% W/V %) to the above solution and stirred evenly. Polyacrylamide hydrogel or polyacrylamide hydrogel containing PB (abbreviated as PAAm and PB@PAAm) was prepared by placing the above solution in a 45°C water bath for 3 h. The obtained product was purified with a dialysis membrane for 48 h to remove the excess reactants.

Fabrication of TA@PAAm and TA-PB@PAAm by Immersion Method

Tannic acid is loaded by immersion method as previously reported (Zheng et al., 2018). The detailed steps are as follows: Tannic acid powder of different qualities was weighed and prepared into TA solutions of different concentrations (0.5, 1, 5 mg/ml). The prepared PAAm and PB@PAAm were immersed in the solution overnight, and the prepared hydrogel was centrifuged to remove the unattached TA. The obtained hydrogel was then washed three times with DI water. Finally, TA@PAAm and TA-PB@PAAm were prepared for further characterization.

Physical Characterization of Composite Photothermal Hydrogel

Observed the morphological appearance of TA-PB@PAAm. TA-PB@PAAm hydrogel was first frozen using liquid nitrogen, and then freeze-dried. After that, a scanning electron microscope (SEM, Quanta-200, United States) was used to observe the structure and surface morphology of TA-PB@PAAm and PB nanoparticles at the microscopic level. At the same time, FTIR and XRD were used to characterize the success of the material preparation.

The characteristic ultraviolet wavelength (UV) absorption at 700 nm of PB was used to quantify the content of PB and UV absorption at 270 nm of TA was used to quantify the content of TA in PB@PAAm and TA-PB@PAAm, which was measured by a spectrophotometer (UV- 2,450, Shimadzu, Japan). Measured the weight of drugs loaded on PAAm hydrogel (Wd), and the weight of PAAm hydrogel (Wg). The drugs loading ratio was calculated according to the following **Eq. 1** (Vieira et al., 2019):

$$\text{Drugs loading ratio}\,(\%) = \text{Wd}/(\text{Wd} + \text{Wg}) \times 100\% \quad (1)$$

Besides, Zeta potentials of PB, TA, TA + PB, andPAAm hydrogel precursor solution and TA-PB@PAAm hydrogel precursor solution were measured with a zeta-sizer instrument (Nano ZS, Malvern Instruments, United Kingdom).

The swelling ratio was calculated by following the conventional gravimetric method. Hydrogels were lyophilized and the dry weight of the hydrogels was recorded (Wi). Hydrogels were immersed in PBS (pH 7.4, 37°C) and measured the rehydrated weight (Wr) after specific time points. The swelling ratio was determined by the **Eq. 2** (Kumar et al., 2017).

$$\text{Swelling ratio}\,(\%) = (Wr - Wi)/Wi \times 100\% \quad (2)$$

The viscoelastic properties of TA-PB@PAAm were characterized by dynamic shear rotation measurement on Anton Paar MCR302 rheometer. Under the constant strain mode, the mechanical spectrum was recorded in the frequency range of 0.01–1 rad/s (Hz).

Photothermal Property

PB@PAAm or TA-PB@PAAm hydrogels (0.5 g) were formed in a 2 ml Eppendorf tube and then irradiated under fiber-coupled continuous semiconductor diode laser (808 nm, Beijing Viasho Technology Co., Ltd. China) with different PB concentrations (0, 0.1, 0.2, 0.3, 0.4 mg/ml) or a laser density of 0.25, 0.5, 0.75, 1.0W/cm^2 for 5 min. Then the temperature was recorded using an infrared thermal camera (Flir C2, United States) and data were recorded every 30 s.

In vitro NIR Light-Triggered Drug Release

Release of TA from TA-PB@PAAm hydrogels (2.5% drug loading) was determined in DI water. 4ml of DI water was placed in a 5 ml Eppendorf tube containing 1 g of TA-PB@PAAm hydrogels. TA-PB@PAAm hydrogels were irradiated using a fiber-coupled continuous semiconductor diode laser (808 nm, Beijing Viasho Technology Co., Ltd. China) with a power of 0.5W/cm^2 for 10 min, then followed by an interval of 30 min and the procedure was repeated three times. Before switching treatment conditions, 1 ml solution was taken and 1 ml PBS was added to keep the total amount of solution at 4 ml. Finally, a spectrophotometer (UV-2450, Shimadzu, Japan) was used to analyze the above solution to determine the release amount of TA. In comparison, the hydrogel without NIR light irradiation was set as a control.

Cell Compatibility of NIH-3T3 With TA-PB@PAAm

To culture NIH-3T3 cells, we used Complete Dulbecco's modified Eagle's medium, which contained 10% fetal bovine serum and 2% penicillin and streptomycin. Then put NIH-3T3 cells in an incubator at 37°C under 5% CO2.

For the CCK-8 test, the composite photothermal hydrogel was co-cultured with cells using a 48-well plate. NIH-3T3 cells with the number of 2*104 were inoculated into the blank well as the control group. The experimental group was inoculated on the top of PAAm, PB@PAAm, and TA-PB@PAAm, respectively. Another four groups of cells incubated on different kinds of hydrogel were treated with 808 nm NIR light. The medium should be changed every 24 h after washing 3 times with PBS. At the time point at 1, 3, and 5 days, CCK-8 medium and D-MEM medium were diluted at a ratio of 1:10 and incubated in each well for 2 h. Then, 100 μl of supernatant was taken and transferred to a 96-well plate. A microplate reader (Infinite M200Pro, Tecan, Switzerland) was used to detect the absorbance value at 450 nm wavelength (Xu et al., 2015). The cell metabolic rate was calculated according to the OD value. The experiment was repeated three times for each group of three samples.

In Vitro Bactericidal Test of Composite Photothermal Hydrogel

Gram-positive bacteria *S. aureus* and Gram-negative bacteria *E. coli* were cultured separately in an incubator at 37°C with fresh lysogeny broth (LB) medium (Thermo Fisher Scientific, China), which contained 5 mg/ml yeast extract, 10 mg/ml tryptone, and 10 mg/ml NaCl.

Selected overnight cultured *S. aureus* were diluted 10 times in LB medium and were diluted to 1 × 108 CFU/ml after 2 h of culture. Then take 2 ml of *S. aureus* suspension into a 2.5 ml Eppendorf tube containing 1 ml of TA-PB@PAAm hydrogel. After being irradiated with 808 nm (0.5W/cm2) near-infrared laser for 10 min, 100 μl diluted bacterial suspension (1:105 dilution) was taken and coated onto a TSA plate. After incubation for 24 h, the number of culture colonies was counted. Seven other groups (NL control, L control, NL PB@PAAm, L PB@PAAm, NL TA@PAAm, L TA@PAAm, and NL TA-PB@PAAm) were set to compare the antibacterial effect (NL for without NIR light, L for with NIR light). Three parallel samples were set in each group. The antibacterial activity of PB@PAAm hydrogels toward *E. coli in vitro* was tested in a similar way.

In order to observe the killing effect of photothermal hydrogel composites on *S. aureus* and *E. coli*, scanning electronic microscopic (SEM) characterization was carried out. The grouping is (NL Control, L PAAm, L PB@PAAm, NL TA@PAAm, and L TA-PB@PAAm).

In order to study the continuous antibacterial ability of the material, the antibacterial activity of PB@PAAm hydrogels toward *S. aureus* and *E. Coli* was tested by the bacterial inhibition ring test. Specifically, 100 μl of *S. aureus* suspension with the concentration of 1*106 CFU/ml was plated onto the TSA plate. Then the L TA-PB@PAAm was transferred to the *S. aureus*-coated TSA plate, irradiated with 808 nm (0.5W/cm^2) near-infrared laser for 10 min. Six other groups (NL control, L PB@PAAm, NL TA, NL TA@PAAm, L TA@PAAm, and NL TA-PB@PAAm) were set to compare the antibacterial activity. NL control group used sterile filter paper. NL TA group used sterile filter paper soaked in TA solution and dried. They were placed on the surface of the plate. NL TA@PAAm, NL TA-PB@PAAm were put on the surface of the plate. The above materials were not given light treatment. L PB@PAAm and L TA@PAAm were given light for 10 min. Three parallel samples were set in each group. After incubation at 37°C for 48 h, the diameters of the inhibition area were determined and the antibacterial activities were compared. The procedures are the same for the bacterial inhibition ring test of *E. coli*.

In Vivo Biological Assessment

Infective Skin Defect Model in SD Rats

Forty 8-week-old male SD rats, weighing 250–300 g, were provided by the Department of Animal Science and Ethics Committee, Xiangya Hospital, Central South University. The treatment of animals in the experiment conforms to the requirements of animal ethics according to the guidelines, principles, and procedures for the care and use of laboratory animals. To establish the *S. aureus*-infected skin defect model in rat, 100 μl (1 × 108 CFU/ml) of *S. aureus* in PBS was injected subcutaneously into the back of the rats. After infection for 2 days, the rats were randomly divided into 10 groups (n = 4).

The manufacturing method of the skin defects is reported in the literature1. The detailed method was that after 12 h of fasting, the rats were anesthetized with 2% pentobarbital sodium and skinned. Full-thickness skin defects were applied with an 8 mm diameter circular tissue extractor and then treated in different groups (NL control, L control, NL PAAm, L PAAm, NL PB@PAAm, L PB@ PAAm, NL TA@ PAAm, L TA@ PAAm, NL TA-PB@ PAAm, and L TA-PB@ PAAm), respectively. Vital signs of the rats were determined after operation.

in vivo Bacterial Plate Counting Test

After feeding for 24 h, the treated rats were photographed and killed, and the infected tissues were collected and homogenized with a homogenizer (500 μl normal saline). The homogenized supernatant was diluted at different multiples (10, 100, 1,000, 10,000) and inoculated on the TSA plat. After overnight incubation, colonies were counted to evaluate the *in vivo* antimicrobial activity.

Wound Healing and Histological Staining Evaluation

After feeding for 24 h, a group of rats was sacrificed by overinjection of pentobarbital sodium. Skin tissues were taken and soaked in 10% formalin solution for 24 h, and then embedded in paraffin for sectioning. The tissue sections were stained with Giemsa and captured using the Optical Microscope (Leica DMIL LED, Germany). After 14 days of feeding, all rats were sacrificed by overinjection of pentobarbital sodium. The skin defect was photographed, and defect area was calculated and the repair ability of the skin defect was evaluated. Then, skin tissues were taken and immersed in 10% formalin solution for 24 h, and then embedded in paraffin wax for sectioning. Hematoxylin and eosin (H and E) staining and Masson staining were performed and then the images captured.

Histocompatibility Evaluation

The tissues of the heart, liver, spleen, lung, and kidney were obtained and prepared into paraffin sections and performed with H and E staining. In addition, the liver and renal functions of rats in different groups were also evaluated, including ALT, AST, BUN, and CREA.

Statistical Analysis

Data analysis was performed using the GraphPad Instat 3.0 program (GraphPad Software, La Jolla, CA). The results were expressed as mean ± standard deviation. Student's t-test was used to analyze the comparison between two groups. A one-way ANOVA test was used to analyze the comparison between three or more groups. The q test (Student–Newman–Keuls method) was used for multiple comparisons between the groups when $p < 0.05$ was detected in the one-way ANOVA test. Among all results, $p < 0.05$ was statistically significant.

ASSOCIATED CONTENT

Supporting Information

FTIR characterization of different components (**Supplementary Figure S1**); XRD characterization of different components (**Supplementary Figure S2**); the standard curve of tannic acid in different concentrations, absorbance profiles of tannic acid in different concentrations (**Supplementary Figure S3**); absorbance values of NIH-3T3 cells after intervention with different concentrations of tannic acid or Prussian blue (**Supplementary Figure S4**); bacterial inhibition ring test of *E. coli* (**Supplementary Figure S5**).

DATA AVAILABILITY STATEMENT

The raw data supporting the conclusions of this article will be made available by the authors, without undue reservation.

ETHICS STATEMENT

The animal study was reviewed and approved by the Department of Animal Science and Ethics Committee, Xiangya Hospital, Central South University.

AUTHOR CONTRIBUTIONS

All authors listed have made a substantial, direct, and intellectual contribution to the work and approved it for publication.

FUNDING

This study was supported by the Natural Science Foundation of Hunan Province, China (Grant Nos. 2018JJ3844 and 2019JJ40499), the Scientific Research Project of Health and Family Planning Commission of Hunan Province, China (Grant No. B2019188), the Science and Technology Innovation Leading Project for High-tech Industry of Hunan Province (Grant No. 2020SK 2008), the Major science and technology projects of Changsha City (Grant No. kh2003016), the Young Science Foundation of Xiangya Hospital Central South University (Grant No. 2017Q07), the Postdoctoral Research Program of Xiangya Hospital Central South University (Grant No. 223551). National key research and development project (2016YFC1100605 and 2018YFB1105504), Natural Science Foundation of China (Grant Nos. 82002277 and 81672656). Clinical research fund of National Clinical Research Center for Geriatric Disorders (Xiangya Hospital, Grant No. 2020LNJJ15).

ACKNOWLEDGMENTS

Thanks to Juan Li for her support and guidance of experimental technology. Thank Yingjiao Wu, Xilong Li, Yandi Liu, Hongyang Wang, and Yijun Hao for their help and support in the synthetic experiment. Thank Yu Zhang for his help in cell and animal experiments.

SUPPLEMENTARY MATERIAL

The Supplementary Material for this article can be found online at: https://www.frontiersin.org/articles/10.3389/fbioe.2021.796602/full#supplementary-material

REFERENCES

Borzenkov, M., D'Alfonso, L., Polissi, A., Sperandeo, P., Collini, M., Dacarro, G., et al. (2019). Novel Photo-Thermally Active Polyvinyl Alcohol-Prussian Blue Nanoparticles Hydrogel Films Capable of Eradicating Bacteria and Mitigating Biofilms. *Nanotechnology* 30 (29), 295702. doi:10.1088/1361-6528/ab15f9

Busquets, M. A., and Estelrich, J. (2020). Prussian Blue Nanoparticles: Synthesis, Surface Modification, and Biomedical Applications. *Drug Discov. Today* 25, 1431–1443. doi:10.1016/j.drudis.2020.05.014

Cai, S., Qian, J., Yang, S., Kuang, L., and Hua, D. (2019). Acetylcysteine-decorated Prussian Blue Nanoparticles for strong Photothermal Sterilization and Focal Infection Treatment. *Colloids Surf. B: Biointerfaces* 181, 31–38. doi:10.1016/j.colsurfb.2019.05.007

Cao, C., Ge, W., Yin, J., Yang, D., Wang, W., Song, X., et al. (2020). Mesoporous Silica Supported Silver-Bismuth Nanoparticles as Photothermal Agents for Skin Infection Synergistic Antibacterial Therapy. *Small* 16 (24), e2000436. doi:10.1002/smll.202000436

Chen, T., Chen, Y., Rehman, H. U., Chen, Z., Yang, Z., Wang, M., et al. (2018). Ultratough, Self-Healing, and Tissue-Adhesive Hydrogel for Wound Dressing. *ACS Appl. Mater. Inter.* 10 (39), 33523–33531. doi:10.1021/acsami.8b10064

Dai, X., Zhao, Y., Yu, Y., Chen, X., Wei, X., Zhang, X., et al. (2017). Single Continuous Near-Infrared Laser-Triggered Photodynamic and Photothermal Ablation of Antibiotic-Resistant Bacteria Using Effective Targeted Copper Sulfide Nanoclusters. *ACS Appl. Mater. Inter.* 9 (36), 30470–30479. doi:10.1021/acsami.7b09638

Fang, J., Li, P., Lu, X., Fang, L., Lü, X., and Ren, F. (2019). A strong, Tough, and Osteoconductive Hydroxyapatite Mineralized Polyacrylamide/dextran Hydrogel for Bone Tissue Regeneration. *Acta Biomater.* 88, 503–513. doi:10.1016/j.actbio.2019.02.019

Gan, D., Han, L., Wang, M., Xing, W., Xu, T., Zhang, H., et al. (2018). Conductive and Tough Hydrogels Based on Biopolymer Molecular Templates for Controlling *In Situ* Formation of Polypyrrole Nanorods. *ACS Appl. Mater. Inter.* 10 (42), 36218–36228. doi:10.1021/acsami.8b10280

Han, D., Li, Y., Liu, X., Li, B., Han, Y., Zheng, Y., et al. (2020). Rapid Bacteria Trapping and Killing of Metal-Organic Frameworks Strengthened Photo-Responsive Hydrogel for Rapid Tissue Repair of Bacterial Infected Wounds. *Chem. Eng. J.* 396, 1. doi:10.1016/j.cej.2020.125194

Hao, S., Shao, C., Meng, L., Cui, C., Xu, F., and Yang, J. (2020). Tannic Acid-Silver Dual Catalysis Induced Rapid Polymerization of Conductive Hydrogel Sensors with Excellent Stretchability, Self-Adhesion, and Strain-Sensitivity Properties. *ACS Appl. Mater. Inter.* 12 (50), 56509–56521. doi:10.1021/acsami.0c18250

Hu, B., Berkey, C., Feliciano, T., Chen, X., Li, Z., Chen, C., et al. (2020). Thermal-disrupting Interface Mitigates Intercellular Cohesion Loss for Accurate Topical Antibacterial Therapy. *Adv. Mater.* 32 (12), e1907030. doi:10.1002/adma.201907030

Jiang, T., He, J., Sun, L., Wang, Y., Li, Z., Wang, Q., et al. (2018). Highly Efficient Photothermal Sterilization of Water Mediated by Prussian Blue Nanocages. *Environ. Sci. Nano* 5 (5), 1161–1168. doi:10.1039/c7en01245d

Kumar, M., Nandi, S. K., Kaplan, D. L., and Mandal, B. B. (2017). Localized Immunomodulatory Silk Macrocapsules for Islet-like Spheroid Formation and Sustained Insulin Production. *ACS Biomater. Sci. Eng.* 3 (10), 2443–2456. doi:10.1021/acsbiomaterials.7b00218

Li, J., Liu, X., Tan, L., Cui, Z., Yang, X., Liang, Y., et al. (2019). Zinc-doped Prussian Blue Enhances Photothermal Clearance of *Staphylococcus aureus* and Promotes Tissue Repair in Infected Wounds. *Nat. Commun.* 10 (1), 4490. doi:10.1038/s41467-019-12429-6

Li, M., Liu, X., Tan, L., Cui, Z., Yang, X., Li, Z., et al. (2018). Noninvasive Rapid Bacteria-Killing and Acceleration of Wound Healing through Photothermal/photodynamic/copper Ion Synergistic Action of a Hybrid Hydrogel. *Biomater. Sci.* 6 (8), 2110–2121. doi:10.1039/c8bm00499d

Liu, L., Ge, C., Zhang, Y., Ma, W., Su, X., Chen, L., et al. (2020). Tannic Acid-Modified Silver Nanoparticles for Enhancing Anti-biofilm Activities and Modulating Biofilm Formation. *Biomater. Sci.* 8 (17), 4852–4860. doi:10.1039/d0bm00648c

Luo, Y., Li, J., Liu, X., Tan, L., Cui, Z., Feng, X., et al. (2019). Dual Metal-Organic Framework Heterointerface. *ACS Cent. Sci.* 5 (9), 1591–1601. doi:10.1021/acscentsci.9b00639

Maaoui, H., Jijie, R., Pan, G.-H., Drider, D., Caly, D., Bouckaert, J., et al. (2016). A 980 Nm Driven Photothermal Ablation of Virulent and Antibiotic Resistant Gram-Positive and Gram-Negative Bacteria Strains Using Prussian Blue Nanoparticles. *J. Colloid Interf. Sci.* 480, 63–68. doi:10.1016/j.jcis.2016.07.002

Mao, C., Xiang, Y., Liu, X., Cui, Z., Yang, X., Li, Z., et al. (2018). Repeatable Photodynamic Therapy with Triggered Signaling Pathways of Fibroblast Cell Proliferation and Differentiation to Promote Bacteria-Accompanied Wound Healing. *ACS Nano* 12 (2), 1747–1759. doi:10.1021/acsnano.7b08500

Mukherjee, S., Kotcherlakota, R., Haque, S., Das, S., Nuthi, S., Bhattacharya, D., et al. (2020). Silver Prussian Blue Analogue Nanoparticles: Rationally Designed Advanced Nanomedicine for Multifunctional Biomedical Applications. *ACS Biomater. Sci. Eng.* 6 (1), 690–704. doi:10.1021/acsbiomaterials.9b01693

Ngo-Duc, T. T., Alibay, Z., Plank, J. M., Cheeney, J. E., and Haberer, E. D. (2020). Gold-Decorated M13 I-Forms and S-Forms for Targeted Photothermal Lysis of Bacteria. *ACS Appl. Mater. Inter.* 12 (1), 126–134. doi:10.1021/acsami.9b15682

Ninan, N., Forget, A., Shastri, V. P., Voelcker, N. H., and Blencowe, A. (2016). Antibacterial and Anti-inflammatory pH-Responsive Tannic Acid-Carboxylated Agarose Composite Hydrogels for Wound Healing. *ACS Appl. Mater. Inter.* 8 (42), 28511–28521. doi:10.1021/acsami.6b10491

Ning, C., Logsetty, S., Ghughare, S., and Liu, S. (2014). Effect of Hydrogel Grafting, Water and Surfactant Wetting on the Adherence of PET Wound Dressings. *Burns* 40 (6), 1164–1171. doi:10.1016/j.burns.2013.12.024

Sahiner, N., Sagbas, S., Sahiner, M., Silan, C., Aktas, N., and Turk, M. (2016). Biocompatible and Biodegradable poly(Tannic Acid) Hydrogel with Antimicrobial and Antioxidant Properties. *Int. J. Biol. Macromolecules* 82, 150–159. doi:10.1016/j.ijbiomac.2015.10.057

Sharma, S., Chakraborty, N., Jha, D., Gautam, H. K., and Roy, I. (2020). Robust Dual Modality Antibacterial Action Using Silver-Prussian Blue Nanoscale Coordination Polymer. *Mater. Sci. Eng. C* 113, 110982. doi:10.1016/j.msec.2020.110982

Van Den Bulcke, A. I., Bogdanov, B., De Rooze, N., Schacht, E. H., Cornelissen, M., and Berghmans, H. (2000). Structural and Rheological Properties of Methacrylamide Modified Gelatin Hydrogels. *Biomacromolecules* 1 (1), 31–38. doi:10.1021/bm990017d

Vieira, S., da Silva Morais, A., Garet, E., Silva-Correia, J., Reis, R. L., González-Fernández, Á., et al. (2019). Self-mineralizing Ca-Enriched Methacrylated Gellan Gum Beads for Bone Tissue Engineering. *Acta Biomater.* 93, 74–85. doi:10.1016/j.actbio.2019.01.053

Wang, Z., Yu, B., Alamri, H., Yarabarla, S., Kim, M.-H., and Huang, S. D. (2018). KCa(H2O)2[FeIII(CN)6]·H2O Nanoparticles as an Antimicrobial Agent againstStaphylococcus Aureus. *Angew. Chem. Int. Ed.* 57 (8), 2214–2218. doi:10.1002/anie.201713177

Xu, M., McCanna, D. J., and Sivak, J. G. (2015). Use of the Viability Reagent PrestoBlue in Comparison with alamarBlue and MTT to Assess the Viability of Human Corneal Epithelial Cells. *J. Pharmacol. Toxicol. Methods* 71, 1–7. doi:10.1016/j.vascn.2014.11.003

Xue, H., Hu, L., Xiong, Y., Zhu, X., Wei, C., Cao, F., et al. (2019). Quaternized Chitosan-Matrigel-Polyacrylamide Hydrogels as Wound Dressing for Wound Repair and Regeneration. *Carbohydr. Polym.* 226, 115302. doi:10.1016/j.carbpol.2019.115302

Yan, H., Ni, H., Jia, J., Shan, C., Zhang, T., Gong, Y., et al. (2019). Smart All-In-One Thermometer-Heater Nanoprobe Based on Postsynthetical Functionalization of a Eu(III)-Metal-Organic Framework. *Anal. Chem.* 91 (8), 5225–5234. doi:10.1021/acs.analchem.8b05960

Yang, Y., Zhu, W., Dong, Z., Chao, Y., Xu, L., Chen, M., et al. (2017). 1D Coordination Polymer Nanofibers for Low-Temperature Photothermal Therapy. *Adv. Mater.* 29 (40), 1. doi:10.1002/adma.201703588

Yu, P., Han, Y., Han, D., Liu, X., Liang, Y., Li, Z., et al. (2020). *In-situ* Sulfuration of Cu-Based Metal-Organic Framework for Rapid Near-Infrared Light Sterilization. *J. Hazard. Mater.* 390, 122126. doi:10.1016/j.jhazmat.2020.122126

Zhang, Y., Fu, H., Liu, D.-E., An, J., and Gao, H. (2019). Construction of Biocompatible Bovine Serum Albumin Nanoparticles Composed of Nano Graphene Oxide and AIEgen for Dual-Mode Phototherapy Bacteriostatic and Bacterial Tracking. *J. Nanobiotechnol* 17 (1), 104. doi:10.1186/s12951-019-0523-x

Zheng, Y., Liang, Y., Zhang, D., Sun, X., Liang, L., Li, J., et al. (2018). Gelatin-Based Hydrogels Blended with Gellan as an Injectable Wound Dressing. *ACS Omega* 3 (5), 4766–4775. doi:10.1021/acsomega.8b00308

Zhou, D., Gao, Y., A, S., Xu, Q., Meng, Z., Greiser, U., et al. (2016). Anticancer Drug Disulfiram for *In Situ* RAFT Polymerization: Controlled Polymerization, Multifacet Self-Assembly, and Efficient Drug Delivery. *ACS Macro Lett.* 5 (11), 1266–1272. doi:10.1021/acsmacrolett.6b00777

Conflict of Interest: The authors declare that the research was conducted in the absence of any commercial or financial relationships that could be construed as a potential conflict of interest.

Publisher's Note: All claims expressed in this article are solely those of the authors and do not necessarily represent those of their affiliated organizations, or those of the publisher, the editors and the reviewers. Any product that may be evaluated in this article, or claim that may be made by its manufacturer, is not guaranteed or endorsed by the publisher.

frontiers in Materials

ORIGINAL RESEARCH
published: 25 February 2022
doi: 10.3389/fmats.2022.834950

A Worldwide Bibliometric and Visualized Analysis in Publications of Research About Hydrogel in Cartilage Repair

Jieyu Lai[1,2†], *Dengjie Yu*[1,3†], *Changkai Ni*[2], *Aohan Zhang*[2], *Wenfeng Xiao*[1,3*] and *Yusheng Li*[1,3*]

[1]Department of Orthopaedics, Xiangya Hospital, Central South University, Changsha, China, [2]Xiangya School of Medicine, Central South University, Changsha, China, [3]National Clinical Research Center for Geriatric Disorders, Xiangya Hospital, Central South University, Changsha, China

OPEN ACCESS

Edited by:
Mingqiang Li,
Sun Yat-sen University, China

Reviewed by:
Zhao Tingxiao,
Zhejiang Provincial People's Hospital, China
Bin Wang,
Second Hospital of Shanxi Medical University, China

***Correspondence:**
Yusheng Li
Liyusheng@csu.edu.cn
Wenfeng Xiao
Xiaowenfeng@csu.edu.cn

[†]These authors have contributed equally to this work

Specialty section:
This article was submitted to Biomaterials, a section of the journal Frontiers in Materials

Received: 14 December 2021
Accepted: 04 February 2022
Published: 25 February 2022

Citation:
Lai J, Yu D, Ni C, Zhang A, Xiao W and Li Y (2022) A Worldwide Bibliometric and Visualized Analysis in Publications of Research About Hydrogel in Cartilage Repair. Front. Mater. 9:834950. doi: 10.3389/fmats.2022.834950

Background: Cartilage defect is a common joint disease. Hydrogels are widely used in the area of cartilage tissue engineering because of their ability to repair the defect cartilage. This study aimed to analyze published research on hydrogels in cartilage repair by using both bibliometric and visualized analysis.

Methods: The related articles about hydrogel in cartilage repair was extracted from the Web of Science Core Collection database. SPSS was used for the data analysis. Bibliographic coupling analysis, co-citation analysis, co-authorship analysis and co-occurrence analysis were conducted using VOSviewer. Burst detection conducted with CiteSpace helped to indicate the change of keywords.

Results: A total of 1,245 articles related to hydrogels in cartilage repair from 1997 to 2020 were identified and analyzed. Publication numbers grew steadily and reached 187 papers in 2020. The United States contributed the most to the research with the highest number of times cited, average citations and H-index. Over the studied period, *Acta Biomaterialia* published the most articles about hydrogels in cartilage repair, numbering 77. Johns Hopkins University was the institution that had the highest average citations per item, and Sichuan University, Harvard University, and Kyoto University were tied for the first by the H-index. Ranking first in the world were the National Institutes of Health, specifically the National Institute of Arthritis Musculoskeletal Skin Diseases, the National Institute of Biomedical Imaging and Engineering and the National Institute of Dental Craniofacial Research, which jointly sponsored 383 articles.

Conclusions: We provided the research trend of hydrogel in cartilage repair information for global researchers to better understand the facts and future development of research on hydrogels in cartilage repair. The number of publications on hydrogels in cartilage repair will probably still increase in the coming years according to the current trend.

Keywords: hydrogel, cartilage repair, bibliometric analysis, visualized analysis, cartilage

INTRODUCTION

Osteoarthritis (OA) is the most common degenerative joint diseases. The cartilage defect is the original pathological change among the OA process, which is closely related to the cartilage degeneration as well as both the initiation and progression of osteoarthritis. Lymphocytes and macrophages in synovial tissue secrete inflammatory factors, which can gradually affect and damage cartilage (Goldring and Goldring, 2016; Maudens et al., 2018). Cartilage lacks blood supply and located in a low-density environment, so it is difficult for defected cartilage to regenerate quickly (Fan et al., 2022). In addition, once the cartilage impaired, mechanical pressure can cause a greater damage to the defected cartilage. What's more, defected cartilage fragments can be produced by the wear, which may induce inflammation. Damaged cartilage needs early repair to achieve efficient regeneration (Zhang et al., 2019). The high incidence of OA has caused a heavy burden for individuals, families and even society as a whole.

Currently, various of methods for cartilage repair have been developed. Among them, tissue engineering has attracted many attentions (Huang et al., 2018). Tissue engineering consists of seed cells, biological scaffolds and favorable growth factors. Hydrogels are cross-linked hydrophilic polymers with a 3D network and high water content, which is similar to the soft tissue structure in the human body (Wang et al., 2018). Therefore, it can be used to deliver seed cells, growth factors and nutrients. Seed cells can constantly proliferate and secrete the extracellular matrix, and growth factors can induce chondrocyte expression and chondroblast differentiation (Kudva et al., 2019), eventually forming tissues and achieving the purpose of repairing cartilage defects and reconstructing functions. In addition, the ideal biological scaffold should display biocompatibility and bioabsorption. With the rapid progression of bioengineering, a variety of improved hydrogels have shown excellent biocompatibility and bioabsorption for the application of biological scaffolds. In recent years, tissue engineering based on hydrogels has displayed great advantages. It can repair large tissue defects, avoid donor complications and it shows better cartilage repair effects (Kwon et al., 2019).

Bibliometric analysis is an important method to analyze related studies in various fields, and it has been increasingly used to assess research. More specifically, bibliometric analysis is excellent for the discovery of undiscovered public knowledge, and relational bibliometrics provide some of more thrilling modes of research (Zou et al., 2018; Iqbal et al., 2019). Bibliometric methods can be applied to examine many publications, and the research can be expanded from institutions to the world level. The main purpose of bibliometric analysis is to transform something intangible into a manageable entity (Wallin, 2005). The information extracted from the databases was analyzed *via* bibliometric methodology, which can provide researchers with vast quantities of intuitive information. With the help of bibliometric analysis, information about different authors, countries, journals and institutions can be compared, and the differences between them can be displayed as an intuitive graph. Moreover, the visualized analysis makes it easier to discover the relationships among authors, keywords, countries, institutions and journals. Because of these outstanding advantages, bibliometric analysis has been frequently applied in various fields, such as stem cells for osteoarthritis (Xing et al., 2018), spines (Jia et al., 2015) and neoplasms (Ugolini et al., 2007). However, the quantitative and qualitative characteristics of global research on hydrogels in cartilage repair have not been analyzed before. This study aims to evaluate the current trends and status of the publications.

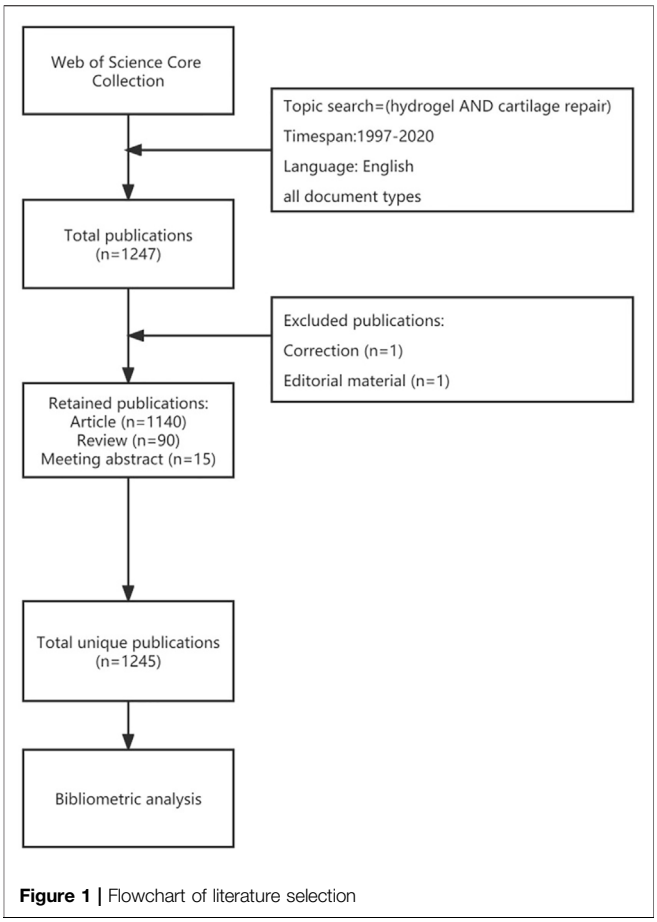

Figure 1 | Flowchart of literature selection

MATERIALS AND METHODS

Data Collection

Literature was extracted on 4 September 2021 from the Web of Science Core Collection. The search strategy are as follows: [TS = (hydrogel AND cartilage repair) AND PY = (1997-2020)] and English (Languages). A total of 1,247 publications from the Web of Science Core Collection were collected. We excluded invalid documents, including correction and editorial material. Articles, reviews, book chapters, proceedings papers and meeting abstracts were included (See **Figure 1**). Finally, a total of 1,245 publications were selected for our study. All data from the Web of Science Core Collection, which included titles, abstracts, author names, journals, publishers and countries, was saved as a TXT file.

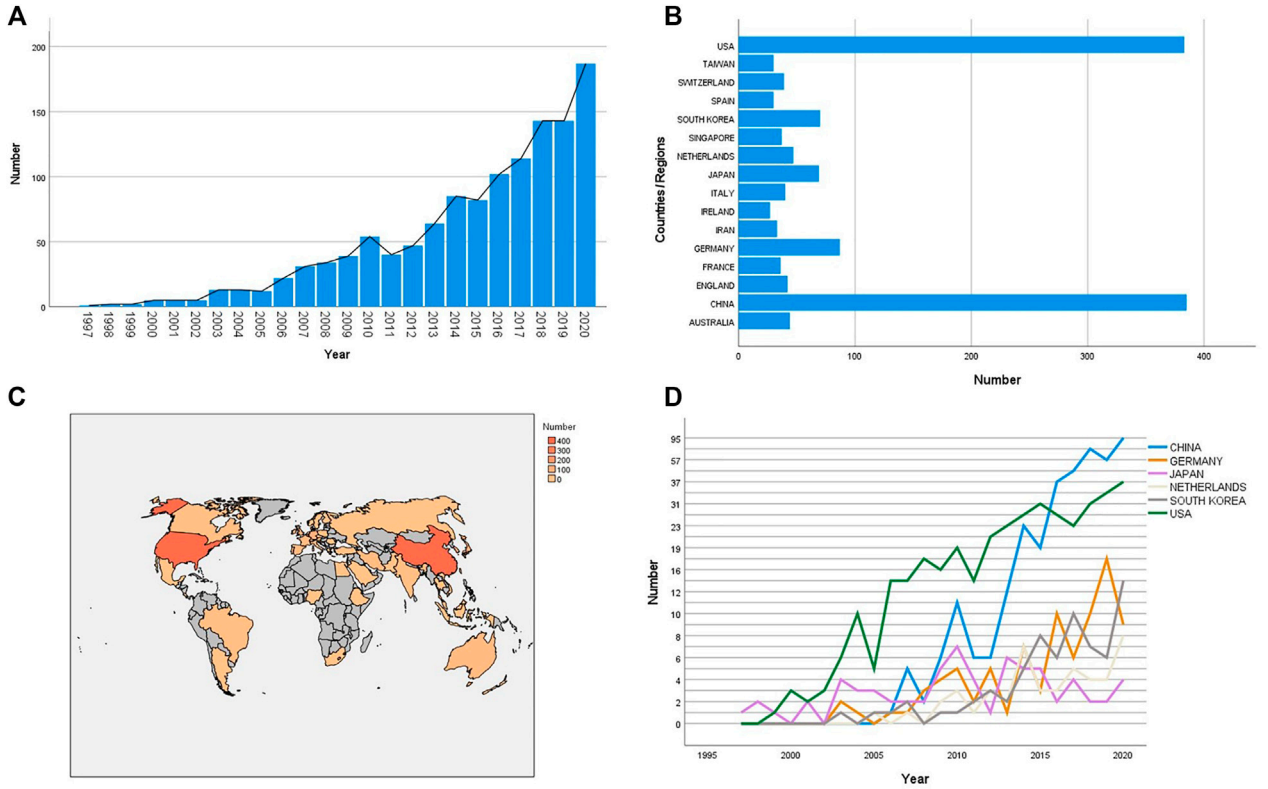

Figure 2 | Global trends and countries contributing to research of hydrogel in Cartilage repair **(A)** The Annual number of publications related to research of hydrogel in cartilage repair. **(B)** The sum of publications about research of hydrogel in cartilage repair from the top 16 countries. **(C)** The Worldwide heat map showing the contribution of different countries to research of hydrogel in cartilage repair.The area with the darker color contributes more to researches. **(D)** The Number of publications from top 6 countries over time.

Data Analysis

All data extracted from Web of Science Core Collection were converted into SPSS, VOSviewer, and CiteSpace to perform visual analysis. SPSS software (v.28.0, IBM) was used to analyze the data. The number of papers published globally and in different countries or regions every year, the heat map of studies worldwide and indicators of the quality of a country's papers, including total times of citation, average citation per item and H-index, were all protracted in graphs by SPSS. Meanwhile, by using VOSviewer (v.1.6.17.0), bibliographic coupling analysis, co-authorship analysis, co-citation analysis and co-occurrence analysis were finished, and visualized maps were produced. Burst detection performed by CiteSpace (5.8.2.0) also played an important role in the analysis of keywords. The trends in the number of publications from the top six countries over time were analyzed using linear regression, and statistical significance was considered when p values were less than 0.05.

RESULTS

Analysis of Global Publications

Changes in the number of publications can reflect the development of this field. The future trend of research can be shown directly by carrying out data analysis and drawing charts. There were a total of 1,245 articles derived from the WOS databases from 1997 to 2020. It is clear that the number of studied related to hydrogels in cartilage repair grew steadily over this period, and the literature published in the last five years (2016-2020) made up a large part in the sum of publications, accounting for 55.3% of the total publications (**Figure 2A**). **Figure 2B** showed different countries' contributions to worldwide research. China had the most contributions with 385 articles (30.9%), followed by the United States (383 articles, 30.8%), Germany (87 articles, 7.0%), South Korea (70 articles, 5.6%) and Japan (69 articles, 5.5%). Meanwhile, the top 16 countries jointly made great contributions to global research on hydrogels in cartilage repair. Shown in **Figure 2C**, the world heat map effectively showed the contributions of different countries. The areas covered by a darker color contribute more to worldwide research. Compared with countries in developing areas, countries in developed areas published more papers from 1997 to 2020. From **Figure 2D**, it is easy to see that the publications of each top country also increased annually: China ($R^2 = 0.695$, $p < 0.001$), the United States ($R^2 = 0.943$, $p < 0.001$), Germany ($R^2 = 0.663$, $p < 0.001$), South Korea ($R^2 = 0.695$, $p < 0.001$), Japan ($R^2 = 0.206$, $p < 0.05$) and Netherlands ($R^2 = 0.701$, $p < 0.001$).

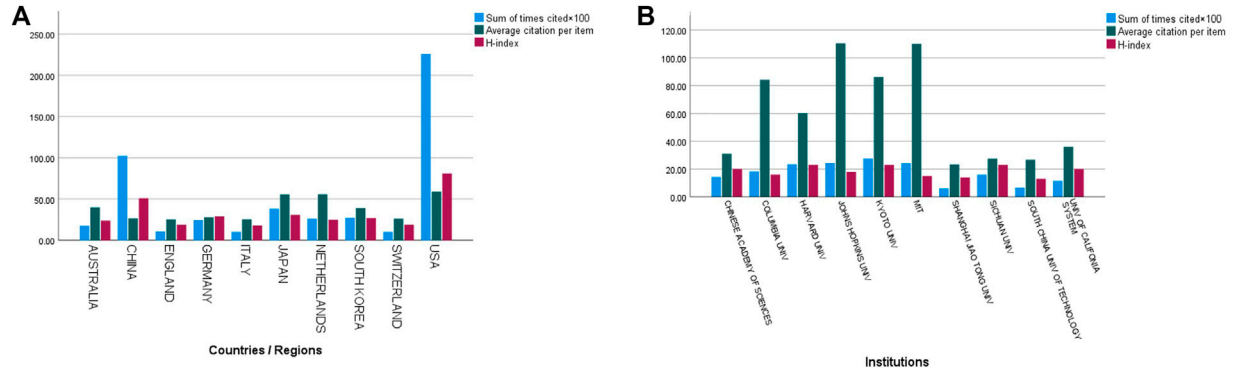

Figure 3 | Analysis of citation and H-index of different countries/regions and institutions.**(A)** Sum of times cited average citation per item and H-index of top 10 countries or regions.**(B)** Sum of times cited average citation per item and H-index of top 10 institutions MIT; Massachusetts Institute Of Technology.

Analysis of Citation and H-Index

Figure 3A shows the sum of times cited, average citation of each item and H-index of the top 10 countries/regions worldwide. Among them, with 22,589 citations, 58.98 average citations per item and an H-index of 81, the United States undoubtedly played a leading role in this field, ranking first in these three aspects. The total number of citations, average citations per item and H-index of the top 10 institutions are included in **Figure 3B**. Sichuan University, Harvard University, and Kyoto University were tied for the first in the world in regard to H-index (23). Johns Hopkins University had the highest average citations per item (110.45), and Kyoto University's total number of citations was the highest in the world (2,758). In addition, there were six other top institutions: Chinese Academy of Sciences (20 H-index), University of California system (20 H-index), Columbia University (16 H-index), Shanghai Jiao Tong University (14 H-index), University of Colorado system (14 H-index) and South China University of Technology (13 H-index).

Study Category and Article Type Analysis

Globally, studies about hydrogels in cartilage repair were categorized into 78 study types. As is shown in **Figure 4A**, materials science biomaterials with 525 articles (42.169%) were observed most frequently. followed by engineering biomedical with 481 articles (38.635%), cell tissue engineering with 178 articles (14.297%), cell biology with 159 articles (12.771%), polymer science with 134 articles (10.763%) and orthopedics with 128 articles (10.281%). Additionally, 1,114 articles (89.478%), 90 review articles (7.229%), 44 proceeding articles (3.534%), 24 book chapters (1.928%) and 15 meeting abstracts (1.205%) were published in this field (**Figure 4B**). The number of publications of articles and review articles from China are respectively 350 and 30, which both exceeded that of any other country.

Journals and Funding Agency Analysis

In total, 352 journals published papers related to hydrogels in cartilage repair. The top 10 journals that published the most papers are presented in **Figure 5A**. Among them, *Acta Biomaterialia* made the greatest contribution to global research related to hydrogels in cartilage repair, with 77 articles (6.2%), followed by *Biomaterials* (67, 5.4%), *Tissue Engineering Part A* (55, 4.4%), *Journal of Biomedical Materials Research Part A* (41, 3.3%) and *Materials Science Engineering C Materials for Biological Applications* (33, 2.7%).

As **Figure 5B** shows, the NIH United States, NIAMS, NIBIB and NIDCR jointly sponsored 383 articles (30.8%), making the greatest contribution to related research worldwide. NSFC was also an active contributor and ranked second worldwide by sponsoring 267 articles (21.4%).

Bibliographic Coupling Analysis

By analyzing the sum of the reference items used together, bibliographic coupling analysis can help to discover the relatedness of items. The resulting maps of primary authors, institutions and countries directly displayed the connection network among them in research on hydrogels in cartilage repair. As **Figure 6** shows, an author, institution or country is represented by a point, and the line between any two points symbolizes their collaborations. The thickness of the line is called the link strength, and the thicker the line is, the stronger the collaboration. The same applies to co-authorship analysis, co-citation analysis and co-occurrence analysis.

According to the total link strength (TLS), 114 authors are presented in **Figure 6A**. Moreover, in **Figure 6A**, the larger the dots are, the stronger the power of the author in global hydrogel cartilage repair research. Based on papers with a minimum number of documents of an author greater than 5, the top 5 authors were Zhang Xingdong (TLS = 14,341), Mauck Robert L (TLS = 9,734), Kitamura Nobuto (TLS = 9,709), Yasuda Kazunori (TLS = 9,709), Gong Jianping (TLS = 8,872) and Kurokawa Takayuki (TLS = 8,853). There were 123 institutions in **Figure 6B** based on the minimum number of documents of an institution of more than 5. The top 5 institutions with the most TLSs were listed: Chinese Academy Sciences (TLS = 22,786), Sichuan University (TLS = 22,167), Massachusetts Institute of Technology (TLS = 14,897), Utrecht University (TLS = 14,337) and Pennsylvania University. (TLS = 14,284). The top 5 countries

Figure 4 | Analysis of study category and article type related to research on hydrogels in cartilage repair. **(A)** Study categories of research on hydrogels in cartilage repair. **(B)** Article types of research on hydrogels in cartilage repair.

based on the minimum number of documents of a university greater than 5 included the United States (TLS = 141,965), China (TLS = 116,108), Germany (TLS = 38,981), Netherlands (TLS = 32,763) and South Korea (TLS = 32,271) (**Figure 6C**).

Co-authorship Analysis

By analyzing the sum of co-authored documents, co-authorship analysis can help to discover the relatedness of items. The resulting maps of primary authors, institutions and countries directly displayed the connection network among them in research on hydrogels in cartilage repair. Valuable information can guide researchers in finding authors to cooperate with, institutions to making the acquaintance of other institutions, and countries to developing cooperation at the world level. After analyzing the data in VOSviewer, there were 44 authors, 118 institutions and 28 countries in the resulting maps. Authors, institutions and countries were all based on the minimum number of documents of an author, an institution or a country of no less than 5. Zhang Xingdong had the most TLSs (94), followed by Fan Yujiang (TLS = 59), Kitamura Nobuto (TLS = 36), Yasuda Kazunori (TLS = 36) and Kurokawa Takayuki (TLS = 34) (**Figure 7A**). In terms of TLS, the top 5 institutions were Chinese Academy Science (TLS = 62), Harvard University (TLS = 35), Sichuan

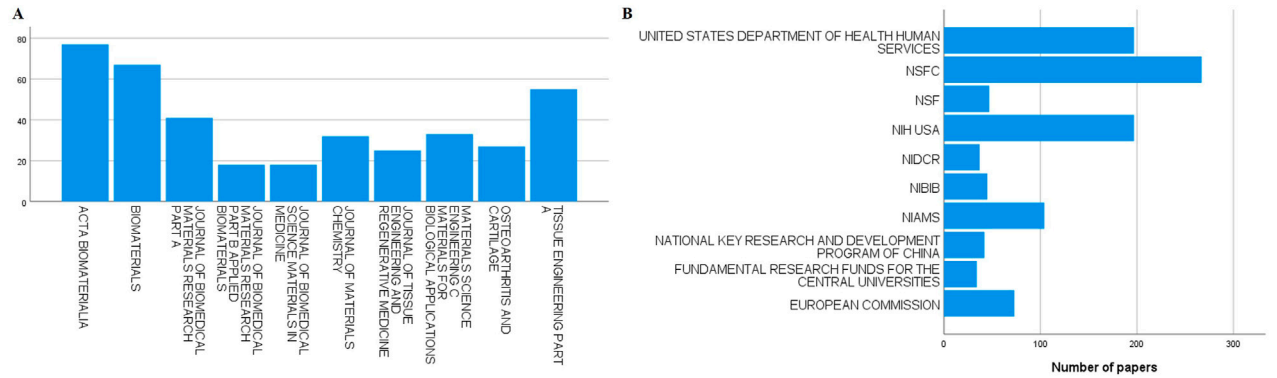

Figure 5 | Analysis of journals and fundings agency related to researches of hydrogel in cartilage repair. **(A)** The number of papers published by the top 10 journals. **(B)** Top 10 funding agency Contributing to the global research hydrogel in cartilage repair. NSFC, National Institute of Dental Carniofacial Research; NIBIB, National Institute of Biomedical Imaging Bioengineering; NIAMS, National Institute Of Arthritis Musculoskeletal Skin Diseases.

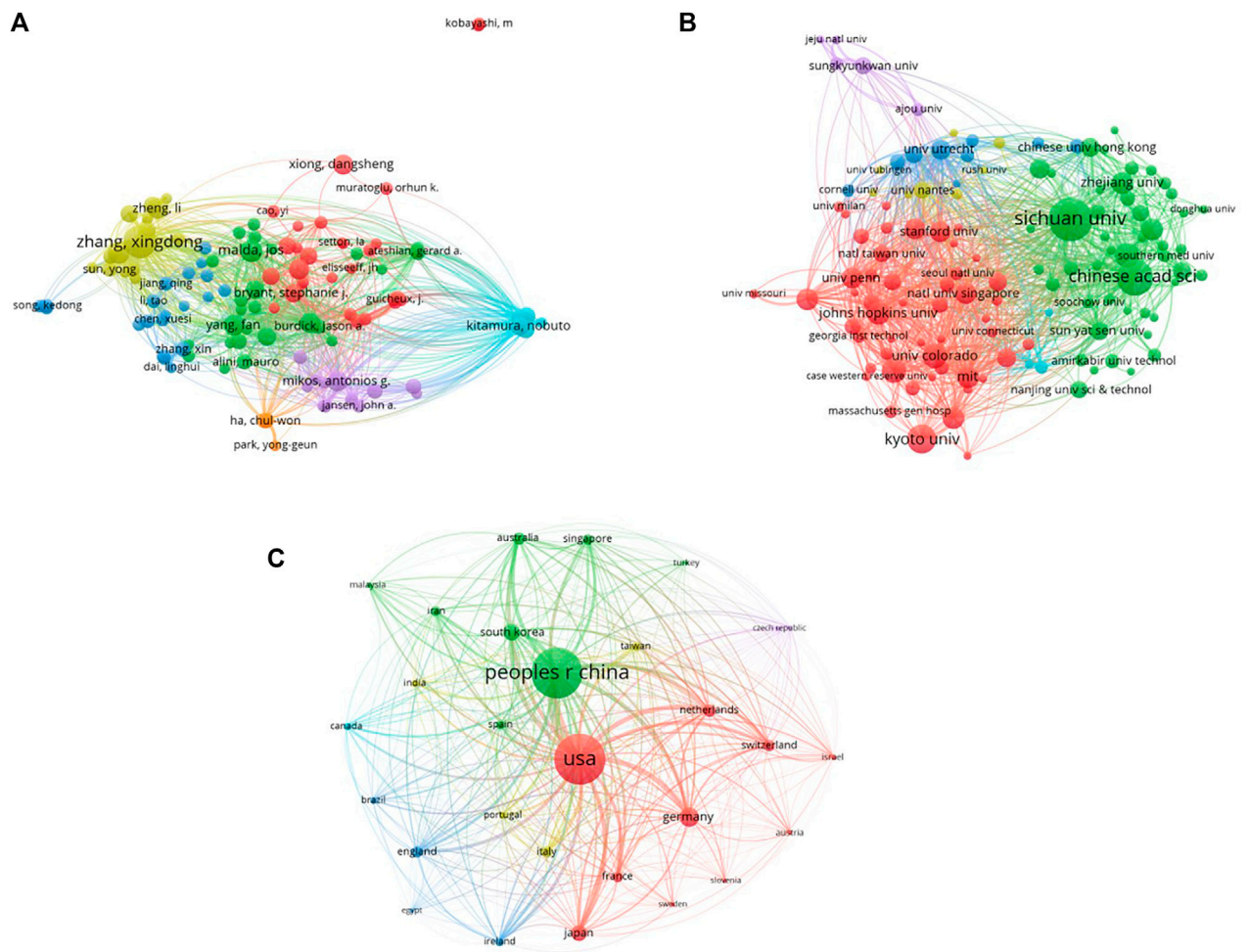

Figure 6 | Bibliographic coupling analysis of research on hydrogels in cartilage repair. **(A)** Map of 113 authors related to research on hydrogels in cartilage repair. **(B)** Map of 123 institutions related to research on hydrogels in cartilage repair. **(C)** Map of 29 countries related to research on hydrogels in cartilage repair. The thicker the connecting line the stronger the relationship between two dots.

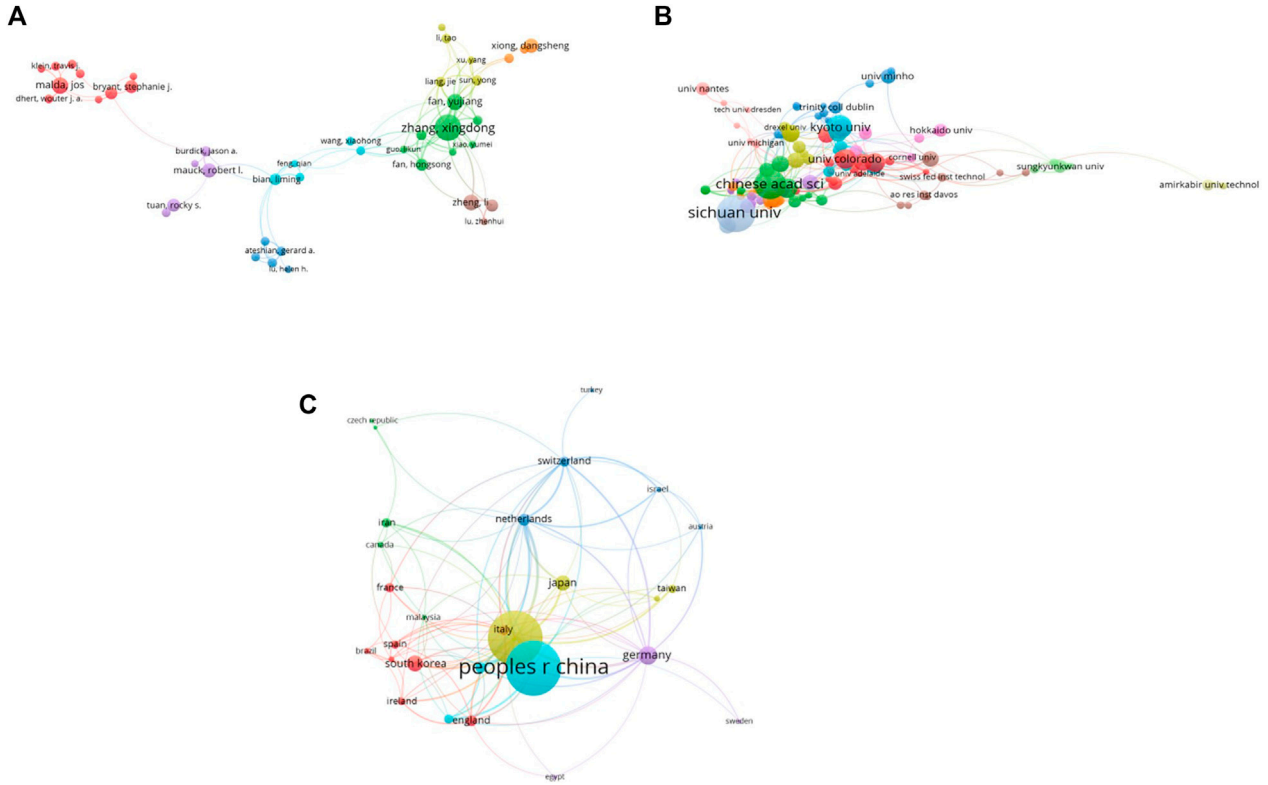

Figure 7 | Co-authorship analysis of researches about hydrogel in cartilage repair. **(A)** Map 44 authors related to researches about hydrogel in cartilage repair. **(B)** map of 118 institutions related to researches about hydrogel in cartilage repair. **(C)** Map of 28 countries related to researches about hydrogel in cartilage repair. The frequency is represented by the size of the dots and the cooperation between two authors/institutions/countries is represented by the line between two dots. The thicker the connecting line, the stronger the relationship between two dots.

University (TLS = 32), Chinese University Hong Kong (TLS = 31) and Utrecht University (TLS = 31) (**Figure 7B**). Similarly, the United States (TLS = 169), China (TLS = 108), Netherlands (TLS = 63), Germany (TLS = 59) and Australia (TLS = 47 times) were the top 5 countries with the most TLSs (**Figure 7C**).

Co-citation Analysis

By analyzing the number of times items are cited together, co-citation analysis can help to discover the relatedness of the items. Significant information can be rapidly and conveniently obtained from a very large number of cited papers. Moreover, the resulting maps will show the relevance of items intuitively. A total of 186 references were analyzed *via* VOSviewer with the minimum number of citations of a cited reference of no less than 20, and the top 5 were as follows (**Figure 8A**): *The New England Journal of Medicine*.1994 OCT; 331(14):889-905 (TLS = 897), *Osteoarthritis And Cartilage* (Brittberg et al., 1994). 2002 JUL; 10(7):564-572 (TLS = 823) *Science*. 1999 (Hunziker, 2002), APR; 284(5,411): 143-147 (TLS = 688), *Science*. 2012 NOV (Pittenger et al., 1999); 338(6,109):917-921 (TLS = 671) and *Biomaterials*. 2011 DEC (Huey et al., 2012); 32(34):8,771-8,782 (TLS = 612) (Kim et al., 2011). Based on papers with the minimum number of citations of a source, more than 30, 260 sources are shown in **Figure 8B**. *Biomaterials* (TLS = 368,025), *Acta Biomaterialia* (TLS = 130,985), *Osteoarthritis Cartilage* (TLS = 106,674), *Journal of Biomedical Materials Research Part A* (TLS = 94,737) and *Tissue Engineering Part A* (TLS = 93,501) were the top 5 journals with the largest TLS. Similarly, 214 authors with papers of the minimum number of citations of an author more than 30 were analyzed through the VOSviewer, and the top 5 authors with largest TLS were listed (See **Figure 8C**): Hunziker EB (TLS = 4,236), Bryant SJ (TLS = 3,945), Mauck RL (TLS = 3,545), Chung C (TLS = 3,448) and Park H (TLS = 3,227).

Co-occurrence Analysis

By analyzing the number of papers in which items occur together, co-occurrence analysis aims to discover the relatedness of items and to show the internal relationship of a certain scientific field. From the resulting maps of keywords, it is also easier to obtain advanced information in this field. Popular topics were demonstrated in keyword maps *via* co-occurrence analysis, which can help researchers follow up on the development of domain research. Keywords based on the minimum number of occurrences greater than 4 from 1988 to 2000 are included in **Figure 9A**. There were only 3 keywords: articular cartilage, tissue and hydrogel. **Figure 9B** shows 76 keywords with a minimum number of occurrences greater than 10 for 2010. Research on hydrogels in cartilage repair has expanded to the protein level and

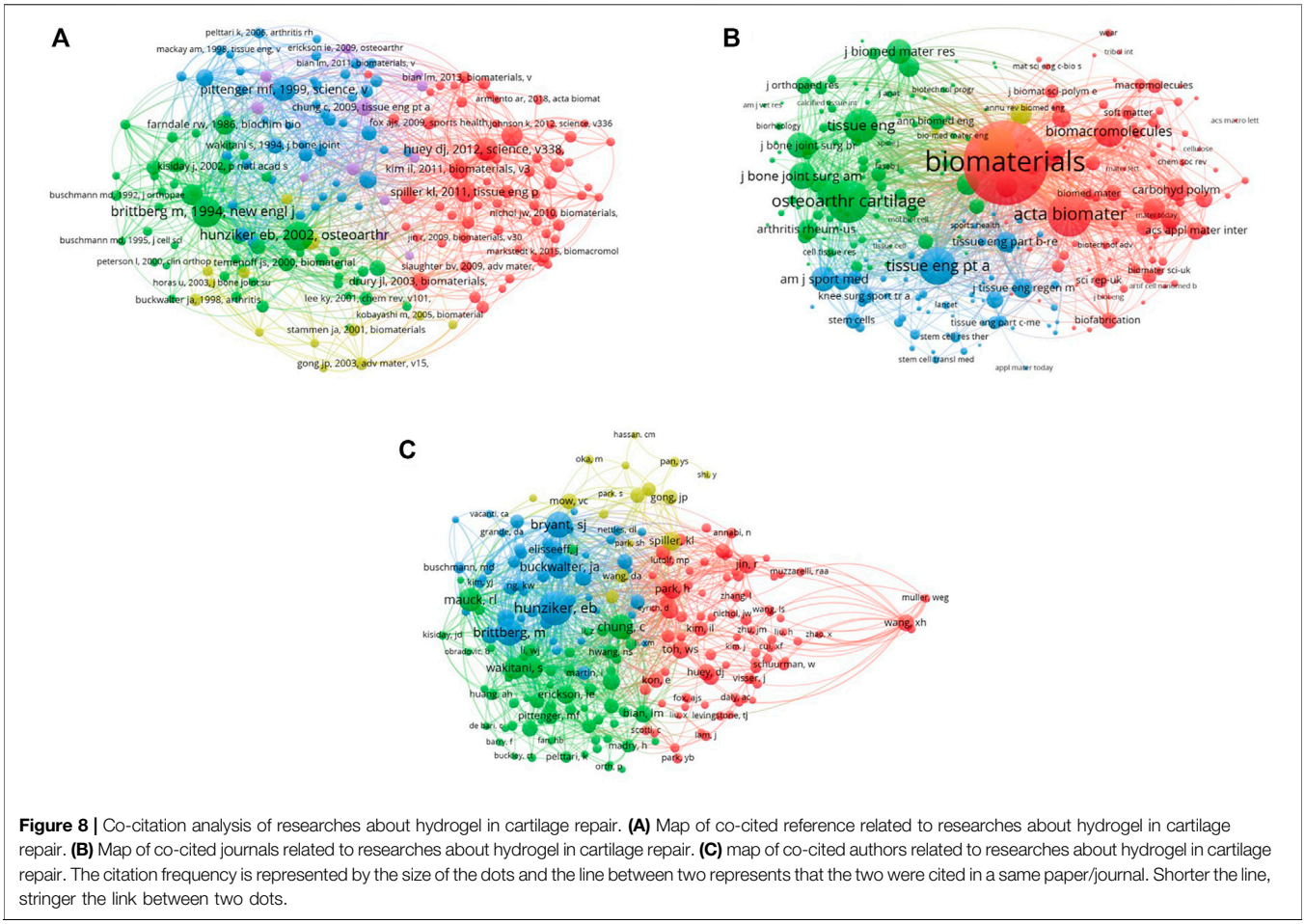

Figure 8 | Co-citation analysis of researches about hydrogel in cartilage repair. **(A)** Map of co-cited reference related to researches about hydrogel in cartilage repair. **(B)** Map of co-cited journals related to researches about hydrogel in cartilage repair. **(C)** map of co-cited authors related to researches about hydrogel in cartilage repair. The citation frequency is represented by the size of the dots and the line between two represents that the two were cited in a same paper/journal. Shorter the line, stringer the link between two dots.

added new topics, such as mesenchymal stem cells, growth factors, collagen type, viability, scaffolds and tissue engineering. Most studies have been carried out *in vitro* or *in vivo* in animals, and the mechanism of cartilage damage and repair has been recognized and gradually explained. Moreover, new materials have been applied to improve the composition of hydrogels (Miljkovic et al., 2009). For 2020, keywords with the minimum number of occurrences greater than 10 increased rapidly to 371 (**Figure 9C**). Some keywords that appeared before were also included, such as mesenchymal stem cells and articular cartilage. In addition, there were also some new keywords, such as engineering, bioprinting, polymers, osteochondral defect, implantation and transplantation. At this time, some studies were carried out *in vivo* in humans. In addition, new methods have been applied to treat cartilage damage, such as tissue engineering and 3D bioprinting (Duchi et al., 2020).

Figure 9D shows the burst detection of the top 10 keywords. From the burst time, implant was the earliest keyword to emerge (1998) in this field and lasted the longest (12 years), which indicates that implantation was likely the ideal therapy for cartilage damage in the early years. In addition, regeneration became a popular topic from 2017 to 2018, indicating that the direction of therapy changed from inserting new cells in patients from the outside to helping patients' cells regenerate.

DISCUSSION

Trends of Papers of Researches About Hydrogel in Cartilage Repair

By bibliometric analysis and visualized analysis, this study aimed to evaluate the trends and predict the development of research on hydrogels in cartilage repair. From 1997 to 2020, the sum of publications increased steadily, and it is easy to predict the growth of publications in coming years. Articular cartilage will be damaged to varying degrees in cases of acute trauma and chronic wear. With the aging and increasing obesity of the world population, there is a large increase in the demand for clinical treatment of osteoarthritis (Cross et al., 2014). Tissue engineering is a promising way to treat cartilage damage caused by osteoarthritis and hydrogels are considered as the ideal materials for tissue engineering, which can explain the growth of publications in the field of hydrogels in cartilage repair to some extent. Meanwhile, hydrogel has shown its promising prospect in acute cartilage defects. Jeong et al. demonstrated a injectable hyaluronate hydrogel, which successfully repaired *in situ* cartilage defect (Jeong et al., 2020). It

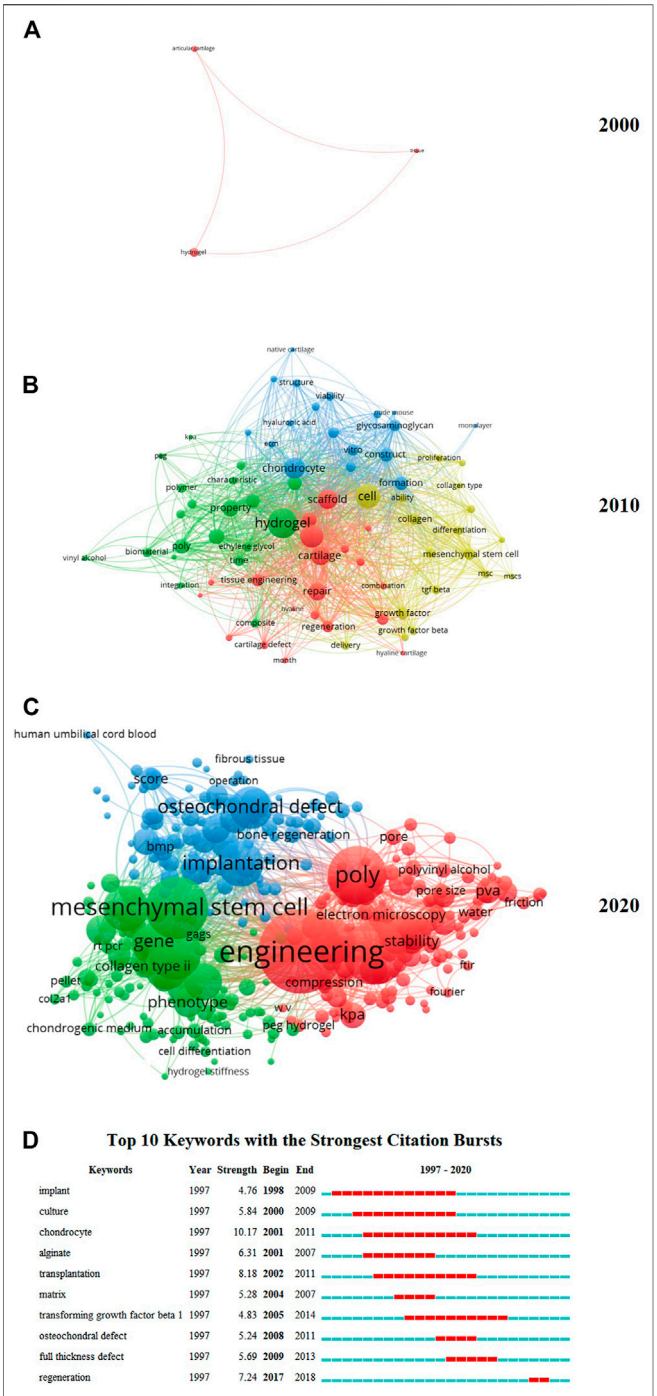

Figure 9 | Co-occurrence analysis of researches about hydrogel in cartilage repair. **(A)** Map of keywords of researches about hydrogel in cartilage repair from 1988 to 2000. **(B)** map of researches about hydrogel in cartilage repair from 1988 to 2010. **(C)** map of keywords is represented by a dot and the size of the dot represents the number of publications in this dot. The line between two dotsa shows the collaboration and co-occurrence. The Larger the number of publications for which two dots are both found, the stronger the relationship between the dots. **(D)** Burst detections of top 10 keywords with the strongest citation bursts.

showed the potential in treating early cartilage defect caused by athletic injury and preventing occurrence and development of osteoarthritis in the future. There were 27 countries or regions that had published papers related to hydrogels in cartilage repair. The top six countries or regions, which published the most documents, all made great progress in the number of publications in recent years. Popular topics and promising research orientations were also shown in our study. Compared with traditional drug therapy, tissue engineering is a better choice for clinical treatment and hydrogels are considered as suitable scaffolds for the transplantation of mesenchymal stem cells (He et al., 2017). Treated by tissue engineering, the patients who have cartilage damage will have less complications and better cartilage repair effects. Researchers can study in a more specific field and further study can be carried out for promising and significant applications.

Current Situation and Quality of Global Publications

China made the greatest contribution to the global publications according to the graph of contributions of countries/regions. For journals, *Acta Biomaterialia* published the most papers. In terms of funding agencies, NIH United States, NIAMS, NIBIB and NIDCR jointly ranked first in the world by sponsoring a great number of publications. The sum of citation times, average citation per item and H-index were the criteria for judging the quantity and quality of the papers of a country, a region and an institution. With the highest number of citations, average citations per item and H-index, the United States can be considered the leading country for and best contributor to global research associated with hydrogels in cartilage repair. The average citations per item and H-index are both recommended criteria for judging the quality of papers published by a country, a region or an institution, and they can represent the academic impact of a country, a region or an institution. The average citations per item are in accord with the H-index because the United States ranked first in both aspects. In terms of institutions, some universities in the United States also made great contributions. For instance, Johns Hopkins University had the highest average citation per item, and its H-index ranked 6th in all institutions worldwide. Meanwhile, with the largest H-index, Harvard University took a lead globally. Also, Sichuan University and Kyoto University, also had the largest H-index and contributed greatly to this field.

Bibliographic coupling means two publications cite the same third publications in their references. In this study, through bibliographic coupling analysis, the internal relationship of a great number of authors, institutions and countries was demonstrated and illustrated. The authors shown in **Figure 6A** probably contributed most to the research on hydrogels in cartilage repair. Their latest publications and research should receive more attention, and they are likely to have significantly advanced discoveries in this field. In **Figure 6B**, the top 2 institutions with the most TLSs were from China and are Sichuan University and Chinese Academy Sciences respectively. This proved that China played an important role in this field by creating excellent institutions at the world level. As **Figure 6C** showed, the United States is the country that contributed most to global research. In addition, China also made great contributions to research, which echoed the bibliographic coupling analysis results

of institutions. Co-authoring can help researchers innovate and obtain new information. By co-authorship analysis, the collaboration among different authors, institutions and countries was assessed and demonstrated. Authors, institutions and countries with higher TLSs were more willing to cooperate with others, which provided directions for research to find partners. Therefore, Zhang Xingdong, Chinese Academy Sciences and the United States may be ideal choices for researchers to collaborate with. Through counting times that papers were cited together, co-citation analysis can also evaluate the influence of studies. In **Figure 8A**, a variety of frequently cited references were included. Biomaterials was the journal with the largest frequency of citations, and Hunziker EB, Bryant SJ and Mauck RL had great achievements in this domain.

Researches Concentrated on Hydrogel in Cartilage Repair

Keywords from titles and abstracts of all extracted publications were analyzed by co-occurrence analysis. Keywords for 2000, 2010 and 2020 were shown in **Figure 9**. The yearly sum of the keywords increased from 4 in 2000 to 371 in 2020, which indicates that the content of this field was enriched. Moreover, popular topics were also represented in the resulting maps. Tissue engineering, polymers, collagen and human mesenchymal stem cells were all hotspots in this research field. Articular cartilage was an important keyword from 2000 to 2020, which indicated that studies of hydrogels in cartilage repair were related to osteoarthritis. Plolymers, such as polyethylene glycol (PEG) hydrogels, are a new type of chemical hydrogels, which characterize in its 3D network and are similar with soft tissue structure in human body. Mesenchymal stem cells, as the ideal seed cells for tissue engineering, have many advantages. Compared with chondrocytes, it is easy to obtain mesenchymal stem cells and mesenchymal stem cells have the ability to differentiate into other cell types (Ferrand et al., 2011), which can explain the popularity of mesenchymal stem cells in researches of hydrogels in cartilage repair. Most studies were original articles and many of them concentrated on the materials science biomaterials and engineering biomedical fields. The studies were mainly carried out *in vitro* or *in vivo* in animals while *in vivo* studies in humans were gradually carried out.

Advantages and Limitations

Publications of research on hydrogels in cartilage repair were all extracted from the Web of Science Core Collection. In addition, the current situation and quality of studies were analyzed *via* bibliometric analysis and visualized analysis so that the study is relatively comprehensive and objective. Nevertheless, there were still some limitations in this study. Publications published in 2021 were not included in this study, and non-English papers were also excluded. Thus, further study should introduce newly published papers and non-English papers.

CONCLUSION

This study presented the current global situation and trends in research on hydrogels in cartilage repair. The United States was the best contributor to research and took a lead in worldwide research over the examined period. *Acta Biomaterialia* had the most publications related to hydrogels in cartilage repair. What is most remarkable is that there is likely to be an increasing number of publications in the future. Tissue engineering and mesenchymal stem cells are popular topics in this field. Because of the promising biocompatibility and bioabsorption of hydrogels, tissue engineering based on hydrogels shows unique advantages, including better cartilage repair and the decrease of donor complications. Mesenchymal stem cell, as the ideal seed cell in tissue engineering because of its great potential for differentiation, is also a hot spot. Therefore, an increasing number of researchers will pay attention to these fields, which may lead to great achievements in the coming years. With the development of medical technology, the experiments of hydrogels in cartilage repair have been carried out *in vivo*. In addition, tissue engineering has already been used to treat cartilage repair in clinic.

DATA AVAILABILITY STATEMENT

The original contributions presented in the study are included in the article/supplementary material, further inquiries can be directed to the corresponding authors.

AUTHOR CONTRIBUTIONS

This article was written by JL and DY. Data was collected and analyzed by CN and AZ. WX and YL designed and revised this study. All authors consent to the final vision of the manuscript and are willing to take responsibility for the content of all works provided.

FUNDING

This work was supported by National Natural Science Foundation of China (No. 81874030, 82072506), National Key R&D Program of China (2019YFA0111900), National Clinical Research Center for Geriatric Disorders (Xiangya Hospital,Grant No. 2021KFJJ02), National Clinical Research Center for Orthopedics, Sports Medicine and Rehabilitation (2021-NCRC-CXJJ-PY-40), Science and Technology Innovation Program of Hunan Province (No. 2021RC3025), Provincial Natural Science Foundation of Hunan (No. 2020JJ3060), Provincial Clinical Medical Technology Innovation Project of Hunan (No. 2020SK53709), the Administration of Traditional Chinese Medicine of Hunan Province (No. 2021075), Innovation-Driven Project of Central South university (No. 2020CX045), Wu Jieping Medical Foundation (320.6750.2020-03-14), CMA Young and Middle-aged Doctors Outstanding Development Program – Osteoporosis Specialized Scientific Research Fund Project (G-X-2019-1107-12) and the Independent Exploration and Innovation Project for Postgraduate Students of Central South University (No. 2021XQLH041).

REFERENCES

Brittberg, M., Lindahl, A., Nilsson, A., Ohlsson, C., Isaksson, O., and Peterson, L. (1994). Treatment of Deep Cartilage Defects in the Knee with Autologous Chondrocyte Transplantation. *N. Engl. J. Med.* 331, 889–895. doi:10.1056/nejm199410063311401

Cross, M., Smith, E., Hoy, D., Nolte, S., Ackerman, I., Fransen, M., et al. (2014). The Global burden of Hip and Knee Osteoarthritis: Estimates from the Global burden of Disease 2010 Study. *Ann. Rheum. Dis.* 73, 1323–1330. doi:10.1136/annrheumdis-2013-204763

Duchi, S., Onofrillo, C., O'Connell, C., Wallace, G. G., Choong, P., and Di Bella, C. (2020). "Bioprinting Stem Cells in Hydrogel for *In Situ* Surgical Application: A Case for Articular Cartilage, *Methods Mol. Biol.*, 2140, 145–157. doi:10.1007/978-1-0716-0520-2_9

Fan, X., Wu, X., Trevisan Franca De Lima, L., Stehbens, S., Punyadeera, C., Webb, R., et al. (2022). The Deterioration of Calcified Cartilage Integrity Reflects the Severity of Osteoarthritis-A Structural, Molecular, and Biochemical Analysis. *Faseb J.* 36. doi:10.1096/fj.202101449r

Ferrand, J., Noël, D., Lehours, P., Prochazkova-Carlotti, M., Chambonnier, L., Ménard, A., et al. (2011). Human Bone Marrow-Derived Stem Cells Acquire Epithelial Characteristics through Fusion with Gastrointestinal Epithelial Cells. *PLoS One* 6, e19569e19569. doi:10.1371/journal.pone.0019569

Goldring, S. R., and Goldring, M. B. (2016). Changes in the Osteochondral Unit during Osteoarthritis: Structure, Function and Cartilage-Bone Crosstalk. *Nat. Rev. Rheumatol.* 12, 632–644. doi:10.1038/nrrheum.2016.148

He, Z., Wang, B., Hu, C., and Zhao, J. (2017). An Overview of Hydrogel-Based Intra-articular Drug Delivery for the Treatment of Osteoarthritis. *Colloids Surf. B: Biointerfaces* 154, 33–39. doi:10.1016/j.colsurfb.2017.03.003

Huang, K., Li, Q., Li, Y., Yao, Z., Luo, D., Rao, P., et al. (2018). Cartilage Tissue Regeneration: The Roles of Cells, Stimulating Factors and Scaffolds. *Cscr* 13, 547–567. doi:10.2174/1574888x12666170608080722

Huey, D. J., Hu, J. C., and Athanasiou, K. A. (2012). Unlike Bone, Cartilage Regeneration Remains Elusive. *Science* 338, 917–921. doi:10.1126/science.1222454

Hunziker, E. B. (2002). Articular Cartilage Repair: Basic Science and Clinical Progress. A Review of the Current Status and Prospects. *Osteoarthritis and Cartilage* 10, 432–463. doi:10.1053/joca.2002.0801

Iqbal, U., Rehan, A., Akmal, M., Jamali, M., Iqbal, A., Khan, B. A., et al. (2019). Top 100 Most Influential Articles in the Field of Myeloid Neoplasms: A Bibliometric Study. *Acta Haematol.* 141, 68–78. doi:10.1159/000493251

Jeong, S. H., Kim, M., Kim, T. Y., Kim, H., Ju, J. H., and Hahn, S. K. (2020). Supramolecular Injectable Hyaluronate Hydrogels for Cartilage Tissue Regeneration. *ACS Appl. Bio Mater.* 3, 5040–5047. doi:10.1021/acsabm.0c00537

Jia, Z. W., Wu, Y. H., Li, H., Li, H. F., Zhao, X. Y., Tang, Y., et al. (2015). Growing Trend of China's Contribution to the Field of Spine: a 10-year Survey of the Literature. *Eur. Spine J.* 24, 1806–1812. doi:10.1007/s00586-015-4030-y

Kim, I. L., Mauck, R. L., and Burdick, J. A. (2011). Hydrogel Design for Cartilage Tissue Engineering: a Case Study with Hyaluronic Acid. *Biomaterials* 32, 8771–8782. doi:10.1016/j.biomaterials.2011.08.073

Kudva, A. K., Dikina, A. D., Luyten, F. P., Alsberg, E., and Patterson, J. (2019). Gelatin Microspheres Releasing Transforming Growth Factor Drive *In Vitro* Chondrogenesis of Human Periosteum Derived Cells in Micromass Culture. *Acta Biomater.* 90, 287–299. doi:10.1016/j.actbio.2019.03.039

Kwon, H., Brown, W. E., Lee, C. A., Wang, D., Paschos, N., Hu, J. C., et al. (2019). Surgical and Tissue Engineering Strategies for Articular Cartilage and Meniscus Repair. *Nat. Rev. Rheumatol.* 15, 550–570. doi:10.1038/s41584-019-0255-1

Maudens, P., Jordan, O., and Allémann, E. (2018). Recent Advances in Intra-articular Drug Delivery Systems for Osteoarthritis Therapy. *Drug Discov. Today* 23, 1761–1775. doi:10.1016/j.drudis.2018.05.023

Miljkovic, N. D., Lin, Y.-C., Cherubino, M., Minteer, D., and Marra, K. G. (2009). A Novel Injectable Hydrogel in Combination with a Surgical Sealant in a Rat Knee Osteochondral Defect Model. *Knee Surg. Sports Traumatol. Arthrosc.* 17, 1326–1331. doi:10.1007/s00167-009-0881-2

Pittenger, M. F., Mackay, A. M., Beck, S. C., Jaiswal, R. K., Douglas, R., Mosca, J. D., et al. (1999). Multilineage Potential of Adult Human Mesenchymal Stem Cells. *Science* 284, 143–147. doi:10.1126/science.284.5411.143

Ugolini, D., Puntoni, R., Perera, F. P., Schulte, P. A., and Bonassi, S. (2007). A Bibliometric Analysis of Scientific Production in Cancer Molecular Epidemiology. *Carcinogenesis* 28, 1774–1779. doi:10.1093/carcin/bgm129

Wallin, J. A. (2005). Bibliometric Methods: Pitfalls and Possibilities. *Basic Clin. Pharmacol. Toxicol.* 97, 261–275. doi:10.1111/j.1742-7843.2005.pto_139.x

Wang, L., Huang, J., Huang, C., Li, Q., Liu, L., Luo, S., et al. (2018). Adult Stem Cells and Hydrogels for Cartilage Regeneration. *Cscr* 13, 533–546. doi:10.2174/1574888x12666170511142917

Xing, D., Zhao, Y., Dong, S., and Lin, J. (2018). Global Research Trends in Stem Cells for Osteoarthritis: a Bibliometric and Visualized Study. *Int. J. Rheum. Dis.* 21, 1372–1384. doi:10.1111/1756-185x.13327

Zhang, Y., Liu, S., Guo, W., Hao, C., Wang, M., Li, X., et al. (2019). Coculture of hWJMSCs and pACs in Oriented Scaffold Enhances Hyaline Cartilage Regeneration *In Vitro*. *Stem Cell Int.* 2019, 5130152. doi:10.1155/2019/5130152

Zou, X., Yue, W. L., and Vu, H. L. (2018). Visualization and Analysis of Mapping Knowledge Domain of Road Safety Studies. *Accid. Anal. Prev.* 118, 131–145. doi:10.1016/j.aap.2018.06.010

Conflict of Interest: The authors declare that the research was conducted in the absence of any commercial or financial relationships that could be construed as a potential conflict of interest.

frontiers | Frontiers in Bioengineering and Biotechnology

REVIEW
published: 27 April 2022
doi: 10.3389/fbioe.2022.863969

Implantable Biomaterials for Peripheral Nerve Regeneration–Technology Trends and Translational Tribulations

Angela Sanchez Rezza[1†], *Yalcin Kulahci*[2], *Vijay S. Gorantla*[2], *Fatih Zor*[2*] and *Norman M. Drzeniek*[1,3,4*†]

[1]Charité— Universitätsmedizin Berlin, Corporate Member of Freie Universität Berlin and Humboldt–Universität zu Berlin, Institute of Medical Immunology, Berlin, Germany, [2]Wake Forest School of Medicine, Department of Surgery, Wake Forest Institute for Regenerative Medicine, Winston-Salem, NC, United States, [3]Berlin Institute of Health at Charité—Universitätsmedizin Berlin, BIH Center for Regenerative Therapies (BCRT), Berlin, Germany, [4]Charité — Universitätsmedizin Berlin, corporate member of Freie Universität Berlin and Humboldt- Universität zu Berlin, Berlin-Brandenburg School for Regenerative Therapies (BSRT), Berlin, Germany

OPEN ACCESS

Edited by:
Yusheng Li,
Central South University, China

Reviewed by:
Justus P. Beier,
University Hospital RWTH Aachen, Germany
Wen Shi,
University of Nebraska Medical Center, United States

***Correspondence:**
Fatih Zor
fzor@wakehealth.edu
Norman M. Drzeniek
norman.drzeniek@charite.de

†ORCID:
Angela Sanchez Rezza
orcid.org/0000-0001-6420-9100
Norman M. Drzeniek
orcid.org/0000-0001-6562-2351

Specialty section:
This article was submitted to Biomaterials, a section of the journal Frontiers in Bioengineering and Biotechnology

Received: 27 January 2022
Accepted: 05 April 2022
Published: 27 April 2022

Citation:
Sanchez Rezza A, Kulahci Y, Gorantla VS, Zor F and Drzeniek NM (2022) Implantable Biomaterials for Peripheral Nerve Regeneration–Technology Trends and Translational Tribulations. Front. Bioeng. Biotechnol. 10:863969. doi: 10.3389/fbioe.2022.863969

The use of autografted nerve in surgical repair of peripheral nerve injuries (PNI) is severely limited due to donor site morbidity and restricted tissue availability. As an alternative, synthetic nerve guidance channels (NGCs) are available on the market for surgical nerve repair, but they fail to promote nerve regeneration across larger critical gap nerve injuries. Therefore, such injuries remain unaddressed, result in poor healing outcomes and are a limiting factor in limb reconstruction and transplantation. On the other hand, a myriad of advanced biomaterial strategies to address critical nerve injuries are proposed in preclinical literature but only few of those have found their way into clinical practice. The design of synthetic nerve grafts should follow rational criteria and make use of a combination of bioinstructive cues to actively promote nerve regeneration. To identify the most promising NGC designs for translation into applicable products, thorough mode of action studies, standardized readouts and validation in large animals are needed. We identify design criteria for NGC fabrication according to the current state of research, give a broad overview of bioactive and functionalized biomaterials and highlight emerging composite implant strategies using therapeutic cells, soluble factors, structural features and intrinsically conductive substrates. Finally, we discuss translational progress in bioartificial conduits for nerve repair from the surgeon's perspective and give an outlook toward future challenges in the field.

Keywords: biomaterial, peripheral nerve regeneration, nerve guidance conduit, biofabrication, bioactive material, material structure, growth factors, peripheral nerve injuries (PNI)

1 INTRODUCTION

Peripheral nerve injury (PNI) occurs predominantly in the upper limb, including digital nerves and nerves of the brachial plexus and its terminal branches and results in pain, loss of motor functions and sensation of the limb, significantly impacting the patient's quality of life (Ciaramitaro et al., 2010). PNI occurs most often due to trauma, but also as a consequence of metabolic diseases such as diabetes (Sahin et al., 2012), nerve compression such as carpal tunnel syndrome or even vessel thrombosis. In most cases other tissues are affected by the injury as well, but even if an amputated limb can be replanted micro-surgically, the functional outcome of the limb is often limited by the degree of nerve injury and its capacity to regenerate.

PNI regeneration is often categorized by the Sunderland classification, where grade I is defined as a defect of the myelin layer without any damage to the axons and grade II describes injury to the axons without disruption of supporting connective tissue sheaths such as the epi-, peri-, and endoneurium. Grades III-V describe additional injury to the endoneurium, perineurium, or complete transection of the nerve and are associated with significantly worse healing outcomes (Sunderland, 1951). This observation highlights the outcome-determining role that the (micro-) anatomical guiding sheaths play in nerve regeneration and reconstruction.

Axonal injury triggers a series of events especially at the distal nerve segment called Wallerian degeneration, which is driven by Schwann cells. Activated Schwann cells increase their mitotic rate with upregulation of several genes to orchestrate the degeneration and repair process. Following migration of macrophages, Schwann cells and macrophages work together to clear all myelin lipid and other axonal debris and prepare the nerve for regeneration (Burnett and Zager, 2004).

Proliferating and migrating Schwann cell later develop glial bands of Büngner which encase basal lamina. These bands provide neurotrophic and structural support and guide the regrowing axon back to innervate its former target (Stoll and Müller, 1999; Burnett and Zager, 2004; Namgung, 2014). Although the regeneration process of the nerve seems to be a standard sequence of events, there are many variations in the detail, especially in the regeneration of sensory and motor nerves. There are intrinsic (the embryonic origin) and extrinsic (environmental) differences between these two fiber types causing different regenerative capacities. Although activation of class II and III b-tubulin genes and downregulation of neurofilament genes NF-L, NF-M, and NF-H are common in both type of fibers, their cytokine milieu is different: IL6, IL1b and TNFa and LIF are more prominent in sensory fiber regeneration while NGF-R, trkB, BDNF and NT-4 are more prominent in motor fiber regeneration (Stoll and Müller, 1999). To differenciate in detail between motor and sensory nerve regeneration is beyond the aim of this article, but because most nerves are a combination of these two fibers, a strategy which enables regeneration of both fiber types is needed.

Indeed, although peripheral nerves possess the theoretical ability to regenerate at a rate of about 1 mm/day, successful regrowth is dependent on surgical reconstruction of these anatomical guiding sheaths (Seddon et al., 1943). However, unless neurorrhaphy is performed within a day after injury, the stumps of a transected nerve recoil and a gap is formed, making tension-free coaptation impossible. A graft is then needed to bridge the anatomical gap (Sahin et al., 2014).

A "critical nerve gap" is defined as a nerve gap over which no recovery will occur without nerve grafting or bridging. It is generally accepted that all vertebrate species posess the same velocity of nerve regeneration. However, intrinsic differences of each species result in different nerve gap size being considered critical. In rats, the critical nerve gap is considered ~1.5 cm, in rabbits ~3 cm, and in pigs and humans ~4 cm (Kaplan et al., 2015).

While in terms of healing outcome the autograft approach is still the gold standard to bridge a critical gap defect, it creates another nerve defect at the donor site and in most cases consists of a small-diameter cutaneous nerve unsuitable to repair large-diameter nerves. Therefore, there is a need for bioartificial, off-the-shelf nerve guidance conduits (NGCs) that promote nerve regeneration. In this review we provide an overview of classic and emerging conduit design strategies, highlight how principles derived from the regenerative medicine field are being used to augment bioactivity of the implants and discuss their potential value for clinical practice.

1.1 Bioartificial Nerve Grafts Available on the Market

Years of preclinical research in nerve regeneration have resulted in only few products on the market. Perhaps the most popular and widely accepted one is the decellularized allograft from deceased human donors, known as Avance (AxoGen, Alachua, FL). Although the use of AxoGen eliminates donor site morbidity, it has the limitation of usage of biological material that can be characterized only to a certain extent (Rbia et al., 2019). Another product developed by Integra Life Sciences (Plainsboro, NJ) and composed of semi-permeable Type I collagen is marketed under name Neuragen. A practical limitation of tubular collagen products is their tendency to collapse and kink and their potential for scarring (Kornfeld et al., 2021a).

Currently, more biocompatible synthetic polymer product made from polyglycolic acid (PGA) or poly-lactidecaprolactone (PLCL) are gaining popularity in nerve gap repair. Neurotube is produced from woven polyglycolic acid (PGA); by Synovis Micro Companies Alliance (Birmingham, AL) while Neurolac is a PLCL conduit (Hussain et al., 2020). The newest FDA approved product is Nerbridge, which is composed of polyglycolic acid and collagen derived from porcine skin. This product is composed of resorbable and semipermeable tubular membrane matrix filled with porous collagen and provides a non-constricting encasement for injured peripheral nerves (Matsui et al., 2016). Despite many advantages of synthetic materials, their biologcial performance cannot reach allogenic nerve grafts. Therefore, they have only limited application for repair of short gaps (Kaplan et al., 2015).

2 TRANSLATIONAL DESIGN CRITERIA FOR NERVE GUIDANCE CHANNELS

With experience gained from over three decades of translation-oriented development and *in vivo* evaluation of NGCs, several general requirements and desirable properties have been identified (**Figure 1**).

- Sufficient availability: The limited availability of natural grafts, such as autografts, allografts or xenografts is a major incentive to develop bioartificial NGCs.
- Size/diameter: In contrast to naturally harvested grafts, bioartificial implants can be tailored to match a specific defect or the diameter of the nerve to be reconstructed.
- Mechanical strength: The tensile strength of a peripheral nerve lies in the megapascal (MPa) range (Borschel et al.,

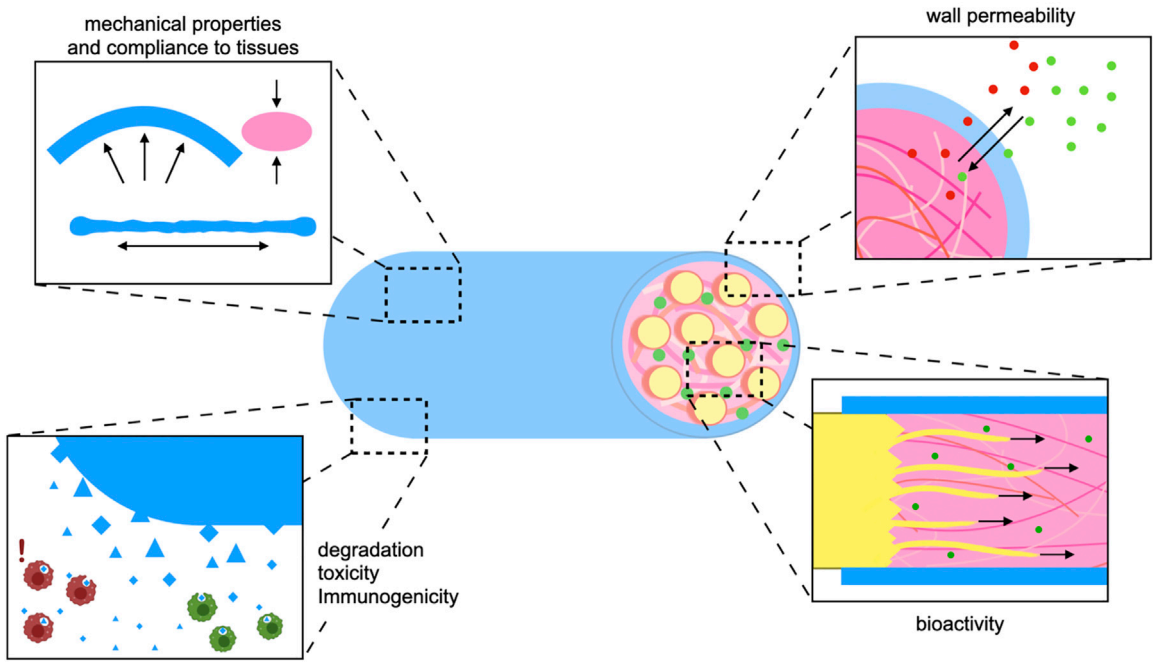

FIGURE 1 | Design criteria for nerve guidance implants: For the development of effective synthetic nerve grafts biomaterial and biofabrication strategies should be applied in the service of established design criteria. The implant needs to comply with living tissue but possess enough strength and stability to withstand forces resulting from joint and muscle movement (top right). In order to avoid a surgical removal, the implant should degrade biologically and its degradation products must not harm the regenerating nerve nor other surrounding tissues (bottom right). The conduit wall should be permeable enough to allow for entry of nutrients and efflux of metabolic waste. At the same time the conduit wall creates a compartment that retains biochemical cues and soluble growth factors at the site of regeneration (top left). In order to bridge larger nerve gap injuries the implant should actively promote axon growth in a setting where regeneration would be otherwise ineffective or take too long. This can be achieved both by intrinsic properties of bioactive polymers, as well as their functionalization through biochemical or physical cues (bottom left).

2003). Ideally, the conduit should match the mechanical properties of the native nerve (**Figure 1**). The NGC wall should be strong enough to allow for suturing and to prevent collapsing, but too much rigidity can cause trauma to surrounding tissues during movement of joints and muscles. For example, empty vein grafts may kink and collapse across larger defects (Tang et al., 1995).

- Biodegradability: If the implanted material is not degradable it needs to be removed surgically in time before it starts to compress the newly sprouted axon bundles. Silicone tubes are an early historic example of non-degradable synthetic conduits. Since then, biodegradable polymers have been investigated for PNI repair (Weber et al., 2000). Because depending on defect size healing might take more or less time, the degradation rate, which is depends on the polymer used and on the micromilieu at the implantation site, should also be considered, as discussed by Barrows (1986). So far there is no consensus on the ideal degradation time of an NGC *in vivo*.
- Toxicity/immunogenicity: When implanting degradable biomaterials *in vivo*, no matter if natural or synthetic, low toxicity of degradation products should be a top priority (**Figure 1**). Additionally, the immune response to the graft might cause excessive inflammation which hampers successful healing in different tissues (Reinke et al., 2013; Benga et al., 2017).
- Wall permeability: The conduit wall should let nutrients in and waste metabolites out (**Figure 1**). However, a certain degree of compartmentalization is necessary to prevent scar tissue and inflammatory cells from entering the lumen (Zor et al., 2014).
- Bioactivity: Bioactive substances can actively support neuron survival and axon attachment, reduce scarring or inflammation, and promote axon sprouting or vascularization (Benga et al., 2017; Yapici et al., 2017). As critical-size defects still pose an unsolved problem, current NGC design should aim at incorporating biochemical, mechanical, and structural bio-instructive cues into the implant without sacrificing any of the criteria listed above (**Figure 1**).

3 SUBSTRATE CHOICE

3.1 Synthetic Biodegradable Polymers

To date aliphatic polyester NGCs are the only fully synthetic NGCs with FDA approval.

In contrast to naturally harvested materials such as the autograft or NGCs fabricated from naturally occurring proteins, their chemically defined synthesis, well understood *in vivo* performance and superior control over material properties allow for mass production and commercialization, providing a

potential alternative in surgical management of PNI. While the exact degradation time depends on polymer formulation, implant size and location and its surface exposure to water, polyglycolic acid (PGA), polylactic acid (PLA), polycaprolactone (PCL) and copolymers such as polylactide-co-glycolide (PLGA) or polylactide-co-caprolactone (PLCL) are all hydrolytically degraded within weeks to months and absorbed in a controlled process that is accompanied by only a moderate inflammatory reaction (Pavan et al., 1979; Barrows, 1986; Ginde and Gupta, 1987).

Because the presence of methyl groups results in stronger hydrophobicity, hydrolytic degradation of PLA takes longer than for PGA. Depending on the expected regeneration rate this can be an advantage as rapid degradation could lead to premature NGC breakdown and loss of mechanical strength (Ginde and Gupta, 1987; Matsumine et al., 2014). On the other hand, continuous degradation is needed to gradually relieve pressure on regenerated axons. A potential solution to this dilemma, the copolymer PLGA has been found to degrade faster than PGA or PLA but retained strength longer (Craig et al., 1975). The degradation and mechanical strength of PLGA can be further adjusted by changing the PLA/PGA ratio (Makadia and Siegel, 2011).

Biodegradable polyesters were promising early candidates for NGC design because in contrast to a silicon tube they eliminated the need for surgical removal. Weber et al. (2000) found that a PGA-based NGC commercialized as NeurotubeTM led to better functional recovery than autograft after digital nerve injury which is among the most common types of PNI (Ciaramitaro et al., 2010). Key principles of structural design are found in this early product: the corrugated wall prevents collapsing of the tube *in vivo*, while porosity allows for an oxygen-rich environment (Dellon and Mackinnon, 1988; Weber et al., 2000; Rosson et al., 2009).

Despite early commercialization and some positive results in the repair of short nerve gaps, the aliphatic polyesters did not lead to a breakthrough in the field of surgical nerve repair due to their lack of bioactive cues that could support nerve growth across larger gaps. Bioactive proteins such as growth factors or adhesion ligands are difficult to incorporate as the high process temperatures of the polymers lead to protein degradation (Benga et al., 2017). In the following sections we will discuss strategies that aim at combining advantages of synthetic polymers and bioactive materials.

3.2 Bioactive Natural Polymers

The success of the autograft is likely attributable to the presence of Schwann cells and growth factors as well as attachment sites and guiding sheaths for the sprouting axon. These properties are most easily recapitulated using naturally occurring biopolymers like polysaccharides (HA, chitosan) or proteins (collagen, gelatin, silk). Some of these natural polymers like collagen and laminin are physiologically present within the nerve and are natural candidates for re-engineering the damaged microanatomy (Wallquist et al., 2002). Other naturally occurring polymers such as silk, gelatin or chitosan can interact with human tissue and provide bioactive cues for healing although they are not physiologically present within the human body.

Because natural polymers need to be harvested form animal sources, their purity and their physicochemical and immunological properties are more difficult to control, making translation potentially challenging. An alternative to harvested materials are recombinant sources, which offer potentially well-defined biopolymers with minimized impurity, but are significantly more costly and require advanced production methods. For example, production of recombinant collagen from bacterial, yeast or mammalian cells allows to recreate a variety of its native structures or even introduce new derivatives. Despite these advancements and great demand for collagen in both the biomedical and the food industry, both industries still rely on animal-derived sources, because there is no consensus on the preferred structure or production method and production of recombinant protein remains more expensive than the well-established harvesting from animal herds, as discussed in detail by Fertala (2020) and colleagues.

3.2.1 Decellularized Extracellular Matrix Allograft

As an alternative to the autograft, allografts from cadaveric donors could avoid donor site morbidity but would be rejected by the host immune system due to human leukocyte antigen (HLA) mismatch. To avoid graft rejection, the tissue needs to be decellularized, removing the HLA epitopes presented on the cell surface but processed nerve allografts maintain the extracellular matrix and its structure, which is advantageous as discussed in **Section 4.3** (Whitlock et al., 2009). Cell removal can be achieved by chemical processing with a detergent or physical methods such as irradiation, lyophilization or thermal treatment. Moore and colleagues showed that the processing method has an influence on graft performance, with chemical decellularization leading to better graft function than physical processing (Moore et al., 2011).

Decellularized allograft resulted in regeneration superior to bioartificial collagen-based conduits, but still inferior to autograft in rat models (Whitlock et al., 2009; Giusti et al., 2012). More recently however, a direct comparison in digital nerve repair in human patients with a commercially available collagen NGC (NeuraGen by Integra) versus an allograft (Avance by AxoGen) showed similar results for both products (Rbia et al., 2019). However, both products failed to achieve an outcome that was evaluated as excellent in most patients. This and further limitations related to availability and storage of allografts as well as the high cost, create a strong incentive to engineer synthetic NGCs that can be mass produced and are available off the shelf at different sizes, sufficient quantity and accessible cost.

3.2.2 Collagen and Gelatin

The most abundant extracellular matrix (ECM) protein Collagen type I is widely implemented as a biomaterial for tissue repair. Collagen consists of a triple helix of three polypeptide chains. Fibrils are formed by cross-links between telopeptides that contribute to the relatively high moduli of telo-collagen, as discussed in depth elsewhere (Gelse et al., 2003).

Collagen provides attachment sites for neurons, that have been shown to contribute to neurite outgrowth (Ivins et al., 2000). Additionally, collagen can act as a scaffold for growth factors and cytokines and thus play an important role in mimicking a biologically relevant healing environment.

A collagen nerve guidance conduit was developed for the regeneration of a 4 mm nerve gap and demonstrated comparable nerve growth to the autograft method in rats and monkeys (Archibald et al., 1991). This product was FDA-approved and commercialized under the name NeuraGen and allowed for regeneration of nerve gaps of 6–18 mm in human patients (Lohmeyer et al., 2007).

As gelatin is denatured collagen that lacks the triple helix structure, it seems that it could be used for NGC construction as well. However, its weak mechanical properties and its tendency to move quickly away from the implant site make additional modification and cross-linking necessary to increase mechanical stability of the NGC (Ko et al., 2017). A clear advantage of both collagen and gelatin is their biodegradability by enzymes present in the healing milieu (van Amerongen et al., 2006; Kuwahara et al., 2011).

3.2.3 Laminin

Laminin, a glycoprotein of the basal lamina secreted by Schwann cells, has been described as a particularly favorable substrate for adhesion, migration, and regeneration of axons (Mammadov et al., 2016). Laminin is naturally present within the lesioned nerve and exerts its function through interaction with integrin receptors that are upregulated on the neuron cell membrane upon PNI such as integrins α6β1 and α7β1 (Wallquist et al., 2004; Gardiner et al., 2005). The 18 laminin isoforms have varying affinities for different integrins, which have been reviewed in detail elsewhere (Nieuwenhuis et al., 2018). Rather than as a base material, laminin is used in the tissue engineering field to functionalize other synthetic or natural polymer networks (Barros et al., 2019; Drzeniek et al., 2021). Drzeniek et al. (2021) have demonstrated covalent linking of laminin into a methacrylated collagen hydrogel, which improved the material's bioactive properties. Chang et al. (2020) have recently used laminin to functionalize a synthetic PCL NGC, demonstrating its use as a pro-regenerative additive in PNI.

3.2.4 Hyaluronic Acid

HA is a highly hydrophilic glycosaminoglycan of the ECM, that contributes to the cushioning function of cartilage due to its high-water content. Already applied clinically in several indications reviewed by Abatangelo et al. (2020) HA is suitable for implantation, injection and tissue engineering purposes due to its viscoelastic properties, biocompatibility, biodegradability and bioactivity. In the field of peripheral nerve regeneration, hyaluronic acid was used as a conduit filler to facilitate axon migration and myelination in the regeneration of a 10 mm rat sciatic nerve gap (Wang et al., 1998). HA can also be implemented to overcome extraneural scarring, as it has been shown to reduce adhesion of the nerve to the neural bed (Ikeda et al., 2003; Zor et al., 2014).

3.2.5 Chitosan

Chitosan is a linear polysaccharide derived from chitin, the major component of the exoskeleton of crustaceans and insects, through chemical or enzymatic processes. Its reactive groups make chitosan accessible to a myriad of chemical modifications and biofabrication techniques, resulting in fibers, beads, films, gels, scaffolds or nanoparticles (reviewed by El Knidri et al. (El Knidri et al., 2018)). Additionally, chitosan possesses an antimicrobial activity probably due to its positive charge and interactions with the negatively charged cell membrane and thus could be a useful component of implantable biomedical devices (D'Almeida et al., 2017). In peripheral nerve regeneration the positive charge of chitosan interacts with the negatively charged axons and significantly improved functional outcome in human patients in a randomized controlled trial of primary surgical nerve repair (Neubrech et al., 2018). In preclinical models chitosan has also been shown to improve regeneration of critical sized nerve injuries (30 mm dog sciatic nerve) and to reduce neuroma formation and fibrosis (Wang et al., 2005; Marcol et al., 2011). Limiting to the use of chitosan are its weak mechanical properties and the low mechanical strength of chitosan is even reduced in physiological environments (Madihally and Matthew, 1999; El Knidri et al., 2018). This challenge can be overcome by additional chemical modification, cross-linking or hybrid use of chitosan with other materials. Thus, most recent NGC designs implement combinations of chitosan and collagen or gelatin (Singh et al., 2019; Itai et al., 2020).

3.2.6 Silk

Silk is a protein fiber produced by insects, among others silkworms, spiders and bees, to construct webs and cocoons. Its major component is silk fibroin, a semicrystalline protein, which has been studied for peripheral nerve applications mostly in the form of a silk fibroin protein solution from the silkworm *Bombyx mori* or the spider *Nephila clavipes* (Radtke et al., 2011; Radtke, 2016). Silk has been FDA-approved for decades and is used as a surgical suture material. In contrast to the other natural biomaterials mentioned above, silk convinces due to its extremely high tensile strength paired with natural proteolytic degradability (Wongpinyochit et al., 2018). Importantly, silk is biocompatible with nerve and has been shown to support attachment and survival of neurons and Schwann cells not only *in vitro* (Yang et al., 2007) but also in a large animal model (Radtke et al., 2011).

The protein structure of silk can be modified through genetic engineering and its many functional groups offer a myriad of opportunities for functionalization with additional bioactive domains or growth factors (Kong et al., 2020). In a recent study, a silk fibroin-HA-composite matrix was proposed and implanted subcutaneously into immunocompetent mice to assess immunogenicity. The addition of silk fibroin to HA resulted in a faster regrowth of blood vessels and synthesis of new ECM compared to HA alone, without triggering any excessive inflammation. This demonstrates that silk could be used in multimodal NGC designs to improve the bioactivity and mechanical strength of other materials (Gisbert Roca et al., 2020). The modifiable properties of silk can be implemented

for functionalization with neurotrophic factors. A controlled-release-NGC implant successfully restored motor function and reduced distal muscle atrophy in a 10 mm rat sciatic nerve gap study, as the controlled release of GDNF from the proximal conduit led to retrograde neuroprotection not noticed in the plain silk conduit group (Carvalho et al., 2021).

Beyond preclinical rodent models, Kornfeld et al. (2021b) have recently demonstrated that spider silk nerve implants can support axonal regeneration in a 6 cm nerve defect in adult sheep with comparable efficacy to autologous nerve grafts. This result represents one of the most translationally mature implementations of a biomaterial graft in a large nerve gap and paves the way for translation of silk-based conduits into clinical practice.

3.3 Conductive Materials

As an electrified tissue, the peripheral nerve offers the opportunity to be stimulated through electrical cues, in addition to classical soluble or material-mediated bioinstructive cues used in other areas of tissue engineering and regenerative medicine. Conceptually, this can involve the use of intrinsically conductive organic polymers as a substrate for electric communication between cells or the inclusion of soft neural interfaces and electrode arrays with read or write functionalities (Kim et al., 2015; Chen et al., 2019; Paggi et al., 2021). In addition to implantable biomaterial strategies, electrical stimulation of the healing nerve is a clinically validated procedure which could be applied in synergy with an NGC strategy and has been reviewed elsewhere (Gordon, 2016).

3.3.1 Intrinsically Conductive Polymers

Organic polymers such as polyaniline, PEDOT and polypyrrole owe their electrical properties to their conjugated bonds as discussed by Le and colleagues (Le et al., 2017). When included in an NGC without an external electricity source, these materials do not actively actuate the healing nerve, instead they can respond to and conduct electrical activity of interfacing neurons. Recently, Vijayavenkataraman et al. (2019)a have demonstrated that neural crest stem cells on conductive a polypyrrole-PCL substrate differentiated into peripheral neurons without any external electrical stimulation. The advantage of these organic polymers is their biocompatibility, the disadvantage being their lack of biodegradability and biochemical motifs that can be recognized by cells. To overcome the latter issue, Khor and colleagues attempted almost three decades ago to impregnate entire animal tissues with polypyrrole, but found that the coated tissues did not conduct electricity, likely due to the discontinuity of the polypyrrole in the surface layer of the tissue (Khor et al., 1995). To integrate the conductive polymers homogenously into a biologically relevant ECM, more recent studies blend them with collagen or other biopolymers prior to gelation (Vijayavenkataraman et al., 2019b; Zarei et al., 2021). With increasing proportions of the conductive polymer, conductivity improves, while biological properties are reduced. To add biological cues without disrupting conductivity, conductive polymers can also be functionalized with cell-adhesive peptides such as the laminin-derived YIGSR motif (Green et al., 2009). Alternatively, biodegradability can be introduced, by co-polymerizing the conductive polymer with a biodegradable polymer, instead of blending (Durgam et al., 2010; Vijayavenkataraman et al., 2019b). Recently conductive polymers have been gaining attention in the nerve regeneration community and the implementation of different combinations of conductive materials in NGCs has been shown to enhance axonal growth *in vivo* (Sun et al., 2019). Furthermore, Zhao and colleagues have shown that not only neurons, but also Schwann cells (SCs) respond to the electrical stimulation (Zhao et al., 2020).

3.3.2 Neural Interfaces

Peripheral nerve interfaces' primary function is to interrogate or actuate the peripheral nervous system with electrode arrays for applications such as neuropathic pain management, nerve recording for limb prosthetics or replacement of peripheral nerve function for bladder control, as reviewed by Paggi and colleagues (Paggi et al., 2021). However, depending on their design and geometry, the interfaces may be used in synergy with a regenerative implant to actively stimulate regenerating axons or monitor healing success both as a research question and as a medical theranostic device. Such strategies involve either a sieve electrode which allows for the passage of growing axons (Lago et al., 2005; MacEwan et al., 2016) or a multichannel electrode conduit (Musick et al., 2015). Although implantable nerve interfaces often face similar problems as NGCs, including mechanical compatibility, biocompatibility and immunogenicity, the material choice for neural interfaces is not typically motivated by questions of bioactivity. Instead, a metal electrode such as gold or platinum is supported by a bioinert substrate such as silicone or polyimide (MacEwan et al., 2016; Paggi et al., 2021). Approaches that combine a neural interface with neuroregenerative functionality would have to draw from both research fields, pairing a spatiotemporally precise interface with a bioactive and biodegradable polymer.

4 BIOLOGICAL FUNCTIONALIZATION BEYOND THE HOLLOW TUBE

A possible middle ground between the translatability of synthetic polymers and the biological advantages of natural polymers is the controlled bio-functionalization of well defined NGCs. When a PNI occurs, neurotrophins, chemoattractants and pro-angiogenic factors are naturally secreted in increased amounts, each targeting different mechanistic aspects of nerve regeneration. Thus, studies on advanced NGCs often aim to combine the desirable physicochemical properties of a polymer with defined bioactive agents such as soluble growth factors or cells. Additionally, recent studies demonstrate the use of structural features and electrically conductive materials to promote and guide nerve regeneration.

4.1 Functionalization With Soluble Factors

Soluble factors that affect nerve regeneration have been reviewed in detail elsewhere (Benga et al., 2017). Here we give an overview

of functional classes of relevant factors and how they are implemented in an NGC approach.

4.1.1 Neurotrophins

As the name suggests, neurotrophins such as NGF, BDNF or NT-3, exert primarily trophic effects on neurons, although some axon guiding effects have also been discussed (Guthrie, 2007; Lykissas et al., 2007).

The most studied member of the neurotrophin family, Nerve Growth Factor (NGF), acts mostly on sensory and sympathetic neurons by promoting neurite sprouting and elongation. Xia and Lv, (2018) loaded an electrospun nanofibrous scaffold with VEGF and NGF, allowing NGF to be released continuously for more than a month. The NGF condition induced stronger proliferation of neural crest stem cells *in vitro* and better functional recovery after sciatic nerve gap injury *in vivo*. NGF was also tested as an axon guidance molecule, showing a chemoattractant function on growth cones *in vitro* (Dontchev and Letourneau, 2002). However, this effect could not be reliably confirmed in a milieu required for ganglionic cell growth, resulting in no directionality and disorganized growth (Fornaro et al., 2020). Brain Derived Neurotrophic Factor (BDNF) is known for its involvement in hippocampal neurogenesis and its protective role in neuronal survival after a PNI, as higher expression of BDNF in Schwann cells and dorsal root ganglia (DRG) were detected after PNI (Kobayashi et al., 2008). Lopes et al. (2017) used tetanus toxin-conjugated nerve targeting nanoparticles to overexpress BDNF DNA in a nerve crush injury model. Their approach led not only to a significantly higher count of myelinated axons but also protected the denervated muscle. This shows that neurotrophins can be valuable therapeutic targets for PNI both on a protein and a gene therapy level.

Neurotrophin-3 (NT-3) can enhance Schwann cell migration and ensure their survival. Donsante et al. (2020) showed that a continuous release of NT-3 from collagen-based electrospun fibers over a 2 week-period led to increased axon counts in the distal nerve. In a co-culture of DRG-derived neurons and then in dorsal root ganglia (DRG) explants NT-3 ensured ordinate and oriented axonal elongation (Fornaro et al., 2020). These recent studies indicate NT-3 as a potential axon guiding component for next generation anisotropic NGCs, although further studies are needed to confirm its axon guiding function *in vivo* and determine the optimal time and mode of delivery.

Glial cell line-Derived Neurotrophic Factor (GDNF), a neurotrophic factor produced by Schwann cells (SCs) has been shown to promote the survival of sensory neurons and axon outgrowth from DRG explants *in vitro* (Leclere et al., 1997) but when released at high concentrations from an NGC it impeded nerve regeneration *in vivo* (Kong et al., 2021). Kong and colleagues discuss this unexpected observation in the context of the "candy store effect," a term used to describe the entrapment of growing axons in a microenvironment oversaturated with growth factor (Eggers et al., 2013; Kong et al., 2021). It has been suggested that to harness the pro-regenerative function of GDNF a concentration gradient or continuous delivery at low levels via gene therapy is needed (Shi et al., 2010; Eggers et al., 2013).

This last example reminds us, that observations from *in vitro* studies on neurons or explanted dorsal root ganglions (DRG) treated with recombinant growth factors cannot always be directly translated into conclusions about the factor's beneficial role in a therapeutic application. The optimal dose, timing, release kinetic and localization may be entirely different for each therapeutic protein and the current challenge lies in understanding and modulating the application-specific pharmacokinetics and pharmacodynamics. While there is a strong consensus on the pro-regenerative potential of soluble factors such as neurotrophic growth factors or the matrix remodeling enzyme chondroitinase in PNI, these potent factors are not a one one-size-fits-all solution and their biological function is dependent on the timing, microanatomical localization and often gradient.

4.1.2 Chemoattractant Gradients

An anisotropic aspect could be added to NGC implants by exposing growth cones to chemical gradients of chemoattractants that determine growth directionality rather than growth rate only. Netrin-1 (Ntn1) and its receptor "Deleted in colorectal carcinoma" have been shown to attract the tip of a sprouting axon *in vitro* and promote peripheral nerve regeneration, as well as Schwann cell proliferation and migration (Lv et al., 2015; Wang et al., 2019). Other classes of molecules, such as slits act as axon repellent cues, preventing disorganized growth (Long et al., 2004). Lykissas et al. (2007) discussed that while axon attracting effects have also been reported as an additional function for some members of the neurotrophin family, other classes of soluble molecules that predominantly guide axon growth cones constitute a novel and largely unexplored opportunity in the NGC field. Ntn1 was first used for NGC design in a recent study by Huang and colleagues. A graphene mesh-supported double-network hydrogel scaffold was engineered in which Ntn1 promoted Schwann cell migration successfully and guided their alignment, outperforming even the autologous graft (Huang et al., 2021). Thus, chemoattractant agents should be investigated in further studies, as many *in vitro* findings on axon guidance are yet to be validated in an *in vivo* PNI model.

4.1.3 Adjuvant Soluble Factors

Because every growing tissue is dependent on nutrient supply, sufficient vascularization has an important supportive role in the process of nerve regeneration. As Yapici et al. (2017) have shown, vascularized conduits significantly outperformed non-vascularized conduits in a sciatic nerve gap model. Therefore, Vascular Endothelial Growth Factor (VEGF) was used in combination with mesenchymal stem cells (MSCs) to functionalize autogenous vein grafts. The VEGF group resulted in a higher degree of regeneration of a 10 mm nerve gap, compared to MCSs alone (Eren et al., 2016). Beside its pro-angiogenic activity, VEGF can stimulate axonal outgrowth and promote Schwann cell proliferation and migration, suggesting an entire palette of additional mechanisms through which VEGF could enhance nerve regeneration (Sondell et al., 1999; Muratori et al., 2018).

If the PNI is older and repair occurs with a significant delay, a glial scar consisting of chondroitin sulfate proteoglycans (CSPG) and glycosaminoglycans can interfere with axon regeneration even after successful readaptation of transected nerve ends. Chondroitinase ABC, an enzyme derived from the bacterium Proteus vulgaris, catalyzes the degradation of the polysaccharides. Enzymatic removal of the CSPG scar by chondroitinase treatment is an established strategy in the field of spinal cord repair, but also in PNI (Kostereva et al., 2016; Donsante et al., 2020). Chondroitinase may be an especially valuable factor in a setting of delayed repair because its mode of action could complement the pro-regenerative or trophic approaches discussed above. A recent study has identified an additional mechanism through which the enzyme can disinhibit a BDNF receptor, leading to increased neuroplasticity (Lesnikova et al., 2021).

4.2 Functionalization With Transplanted Cells

Aside from the sprouting axons of the injured nerve, different cell types play a role in PNI and can support regeneration. In the NGC approach, the goal is not to grow new neurons in the nerve gap, but instead to regenerate the neurites of lower motor neurons and sensory DRG neurons, the cell bodies of which are located proximal to the injury. Transplanted cells can provide a supportive structure for axons, secrete cytokines, or be engineered to produce and release specific paracrine factors. The challenge for most cell types lies in securing a reliable cell source that ensures controllable product quality, minimal batch to batch differences and off-the-shelf availability. The therapeutic cells' functionality depends strongly on their microenvironment and can be harnessed by considering cell-material interactions in the NGC design strategy (Keshavarz et al., 2020; Panzer et al., 2020; Drzeniek et al., 2021).

4.2.1 Schwann Cells

SCs are the principal glial cells of the peripheral nervous system (PNS) and ensure the formation of myelin sheaths around the axons and the accelerated conduction of nerve impulses as reviewed elsewhere (Berrocal et al., 2013; Fallon and Tadi, 2021). A recent study shows that SCs exist in functionally diverse differentiation states, as they can dedifferentiate into a precursor-like, proliferating state, which can downregulate myelin genes and remove pre-existing myelin debris that would inhibit axonal regrowth (Arthur-Farraj et al., 2012; Stratton et al., 2018). Beside their ability to myelinate regenerated axons, SCs enhance axonal sprouting and form bands of Büngner, important guiding structures for the growing axon. To mimic the bands, SCs could be compressed into bundles and surrounded by a hydrogel microcolumn. Such tissue engineered Büngner bands accelerated axonal growth *in vitro* up to 8 fold and resulted in significantly longer neurite length than an NGC with unaligned SCs (Panzer et al., 2020). An early study of SCs for PNI treatment reported that *in vitro* cultured SCs would align along the axis of the NGC in structures reminiscent of Büngner's bands. The same study also found that only syngeneic SCs promoted the growth of myelinated axons, while heterologous SCs induced a host immune response that impaired regeneration (Guénard et al., 1992). The importance of autologous SC sources poses a considerable challenge in terms of NGC availability, standardized product quality control and mass fabrication.

4.2.2 Induced Pluripotent Stem Cells

iPSCs are a personalized self-renewing source of stem cells which enables autologous treatment. iPSCs can be reprogrammed from patient-derived somatic cells and then differentiated into a broad spectrum of cell types, enabling researchers to generate large quantities of cells that are difficult to harvest, such as SCs (Takahashi et al., 2007). On the downside, iPSCs' pluripotent state has demonstrated the risk of teratoma formation if some undifferentiated iPSCs remain in the transplanted iPSC-derived cell population. Different strategies, including cell sorting or the introduction of suicide genes into iPSCs prior to differentiation are being investigated to provide the safety, necessary for human application of iPSC-derived cells (Bedel et al., 2017). For preclinical evaluation in PNI, iPSCs were differentiated into neural crest stem cells (NCSCs) or SCs without teratoma formation. Huang et al. (2017) used these two cell types to create a tissue-engineered NGC that successfully regenerated a 10 mm gap in a rat model. NCSCs, showed stronger paracrine signaling than the further differentiated SCs, pointing out the importance of selecting the iPSC differentiation state.

Because generating patient-derived iPSCs and differentiating them into a desired cell type takes time, their usefulness for PNI management is limited. Strategies for off-the-shelf clinical use and for complete depletion of undifferentiated iPSCs needs to be developed to fully unleash their potential.

4.2.3 Mesenchymal Stromal/Stem Cells

MSCs are adult multipotent stromal cells isolated from bone marrow, adipose or perinatal tissues. MSCs have attracted attention due to their well-documented clinical safety, rich pro-regenerative secretome, and immunomodulatory properties (Drzeniek et al., 2021). Additionally they can differentiate into SC-like cells when exposed to a combination of soluble factors and produce even more growth factors in this pre-differentiated state (Drzeniek et al., 2021; Liu et al., 2022). Despite many functional similarity and a similar mode of action, MSCs derived from different sources differ in characteristics such as expansion speed and hemocompatibility, as reviewed by Moll and colleagues (Moll et al., 2019).

Intravenously infused MSCs can migrate to the site of injury (Marconi et al., 2012; Matthes et al., 2013), but are often transplanted into the vicinity of the lesioned nerve during the reconstructive surgery, resulting in a more concentrated effect and reduced local fibrosis (Wang et al., 2015; Cooney et al., 2016). MSCs are a natural source of pro-angiogenic and

regenerative growth factors and act as a "living drug factory" for the healing nerve (Drzeniek et al., 2021). Their paracrine effects result in a better electrophysiological and functional outcome and micromorphological intactness of the healed nerve (Marconi et al., 2012; Matthes et al., 2013; Cooney et al., 2016; Bucan et al., 2019). Because the local microenvironment can affect MSC survival and function *in vivo*, protective carrier materials can shield MSCs from the harsh microenvironment, hold them in place and stimulate them to augment their growth factor secretion (Mao et al., 2017; Drzeniek et al., 2021). In recent years, it has been proposed to transplant MSC-derived vesicles, exosomes, instead of the entire living cell. These exosomes have also been shown to promote peripheral nerve regeneration, similarly to the parent cell (Bucan et al., 2019). Another recent study shows that exosomes from MSC-derived SC-like cells play a supporting role by protecting endogenous SCs from oxidative stress and promoting angiogenesis (Liu et al., 2022).

4.3 Functionalization Through Structural Material Design and Multimodal Strategies

Neurites can recognize surface geometry and their growth pattern follows local topography such as groves *in vitro* (Miller et al., 2001a). In order to recapitulate the microanatomical guiding sheaths, the intactness of which is outcome-determining according to the Sunderland classification, biomimetic NGC designs experiment with different anisotropic microstructures and micropatterns to provide more precise physical guidance at the cellular level *in vivo*. The field of architectured materials and NGCs is currently growing fast thanks to the rapid progress in spatiotemporally precise biofabrication methods, such as 3D bioprinting [reviewed by Dixon (Dixon et al., 2018)]. Many NGC designs discussed in this section combine several of the synthetic or natural polymers mentioned above and experiment with additional biological cues to achieve results comparable to the autograft.

4.3.1 Bulk Filler Hydrogel

An easy way to functionalize the NGC lumen is with bulk hydrogel, which can provide a cell friendly environment, allows for easy incorporation of biochemical cues and soluble factors, but does not provide any topographical cues for directional determination and may even reduce the permissiveness of the NGC lumen for growing axons (Yoo et al., 2020; Drzeniek et al., 2021). Therefore, the opinion on bulk fillers is controversial and evidence which favors spatial patterning of hydrogels is growing (Yoo et al., 2020).

4.3.2 Grooved Surfaces

The use of molded grooves on the inner NGC wall has been proposed with the rationale that grooves could not only provide anisotropic physical guidance to sprouting axons but also increase the surface area for cell attachment, cell-material interactions and potentially for controlled release of incorporated growth factors. In practice however, patterning 10 μm grooves on the inner NGC wall did not yield a relevant effect compared to an unpatterned chitosan NGC and failed to outperform the autograft control (Li et al., 2018). Similarly, in an older study a micropatterned inner lumen designed to regenerate a 10 mm rat sciatic nerve gap could only impact functional outcome when implemented in synergy with pre-seeded SCs (Rutkowski et al., 2004).

As an alternative to molded groves, longitudinally oriented collagen strips were 3D-printed on a porous PLCL membrane. It could be shown that the 3D-printed collagen lines led to a better axonal regeneration and remyelination than bulk collagen hydrogel filling, indicating that spatially controlled patterning of substrates that promote cell attachment can be a promising strategy that combines structural and substrate-mediated cues (Yoo et al., 2020). Similarly, in a very recent study a grooved PLCL conduit in combination with a patterned gradient of a laminin-derived peptide showed synergistic effects on aligned migration of SCs *in vitro* and significantly accelerated nerve recovery *in vivo* (Zhang et al., 2021).

It seems that the benefit of grooves manifests in combination with other factors such as biochemical cues or cells, or maybe acts on axons indirectly by influencing SC biology. Early *in vitro* studies had found that groove width versus depth differently influence the alignment of SCs versus neurites (Miller et al., 2001a; Miller et al., 2001b). *In vivo* studies often lack such comparisons and possibly successful use of grooves in NGC design would require more attention to detail and systematic optimization *in vivo*.

4.3.3 Intraluminal Microchannels

Microchannels mimic the nerve fascicular (perineural) anatomy and prevent axon dispersion and can be introduced into the scaffold either by precise 3D bioprinting or through more conventional fabrication such as directional freeze drying or molding (**Figure 2**) (Hu et al., 2009; Wray et al., 2012; Zhang et al., 2022). Chang et al. (2017) used an NGC with micromolded intraluminal channels that resulted in increased axon diameter and myelin layer thickness compared to a control NGC without internal channels. While additional aligned nanofibers within the microchannels contributed only slightly to regeneration, adding an additional neurotrophic factor gradient, yielded an effect comparable to autograft. Similarly, the combination of a multichannel design with controlled release of 4-aminopyridine, a potassium channel blocker thought to improve nerve conduction in neurological disorders such as multiple sclerosis, was comparable to autograft in a 15 mm sciatic nerve gap rat model (Manoukian et al., 2021). Here the multichannels were fabricated by unidirectional freeze drying. For a simple yet clever spiral-shaped design, a grooved surface was rolled to fabricate multichannels which were combined with aligned nanofibers, but the structural cues alone failed to compete with the autograft control (Shah et al., 2019). The disadvantage of the aforementioned fabrication techniques is that the material architecture needs to be fabricated before therapeutic cells can be added to the conduit. In contrast to

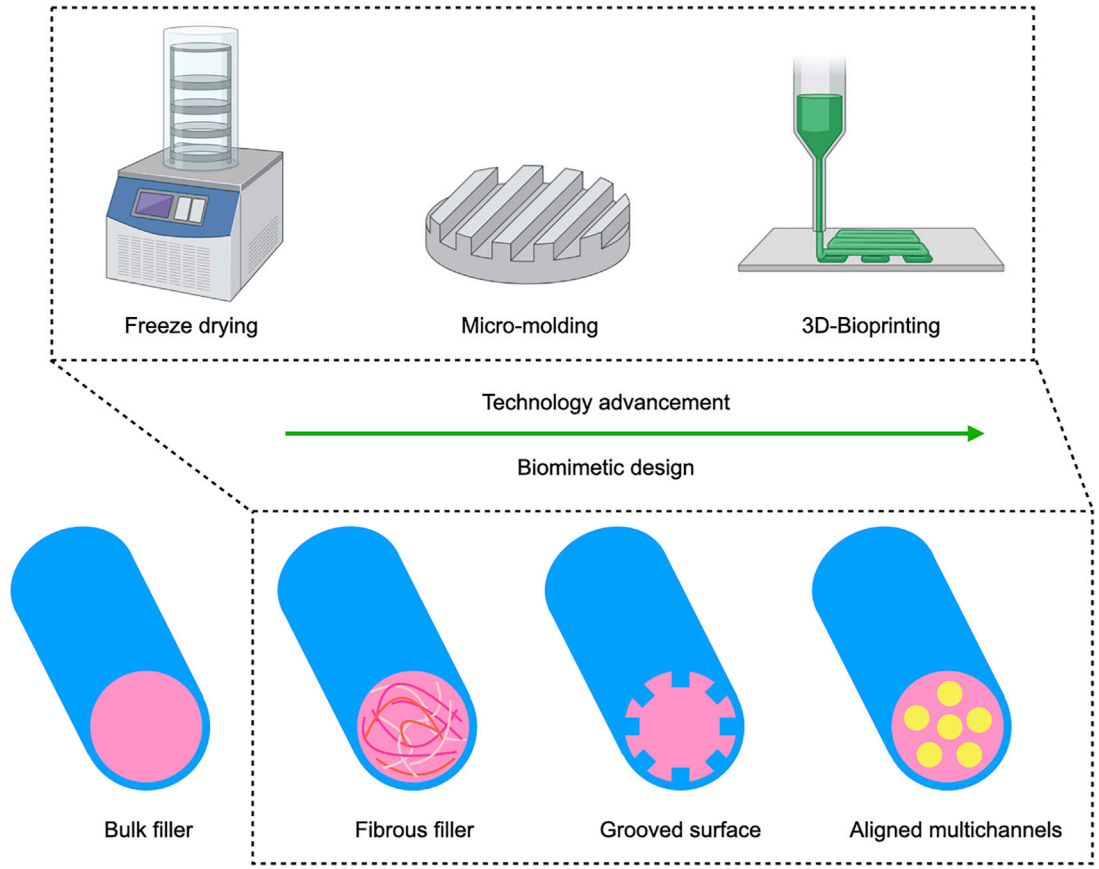

FIGURE 2 | Advancement of structural cues for biomimetic NGC design: With the advancement of biofabrication techniques, structural cues for axon guidance are gaining relevance as an additional bioinstructive modality besides substrate mediated and soluble cues. The design of NGCs has evolved from very early nerve repair with hollow tubes to added anisotropic bulk gel or fibrous fillers. From the early 2000s on, research on longitudinally oriented fibers and grooves intensified and most recent studies increasingly investigate biomimetic multichannel conduits. 3D bioprinting allows to freely pattern multiple materials with or without cells and growth factors, thereby opening up new possibilities for multimodal implant fabrication.

freeze drying, 3D bioprinting allows to integrate cells directly into the biomaterial. Recently, Zhang and colleagues used bioprinting to fabricate an advanced NGC (Zhang et al., 2022). SCs were incorporated into a methacrylated gelatin bioink and printed directly into the multi-channeled conduit.

These studies show that different fabrication techniques can be used to achieve an internal microchannel structure that mimics the natural anatomy of guiding sheaths. Emerging study design combining different modalities of bioactive cues stress the importance of synergistic biological and structural cues for NGC constructs that could promote nerve regeneration across larger gaps.

5 CHALLENGES FOR TRANSLATING NEW NGC DESIGNS BEYOND PRECLINICAL STUDIES

Engineering a clinically usable alternative to the autograft for repair of large peripheral nerve gap injuries still poses an unsolved challenge. The first FDA-approved artificial NGCs were implants fabricated from biodegradable synthetic polymers that could bridge a short defect but failed at promoting axon regrowth across larger gaps. In an effort to increase the conduits' bioactivity, the design of synthetic NGCs has progressed over the past decades from hollow tubes to the implementation of bioactive substrates and intraluminal structures for refined topographical guidance. In 2014, the FDA approved the first NGC with a porous lumen filler (NeuraGen® 3D Nerve Guide Matrix), which is composed of a bioactive collagen-glycosaminoglycan blend and has substantially improved the conduit's performance (Lee et al., 2012). Since then, preclinical studies have advanced to multimodal strategies that explore synergistic effects of substrate-, structure-, and soluble factor-mediated cues (**Figure 3A**). While some of these more intricate synthetic grafts have reached functional outcomes that are comparable to autografting in preclinical models, none have been approved for clinical use so far. As the conduits tested preclinically are becoming more complex and bioactive,

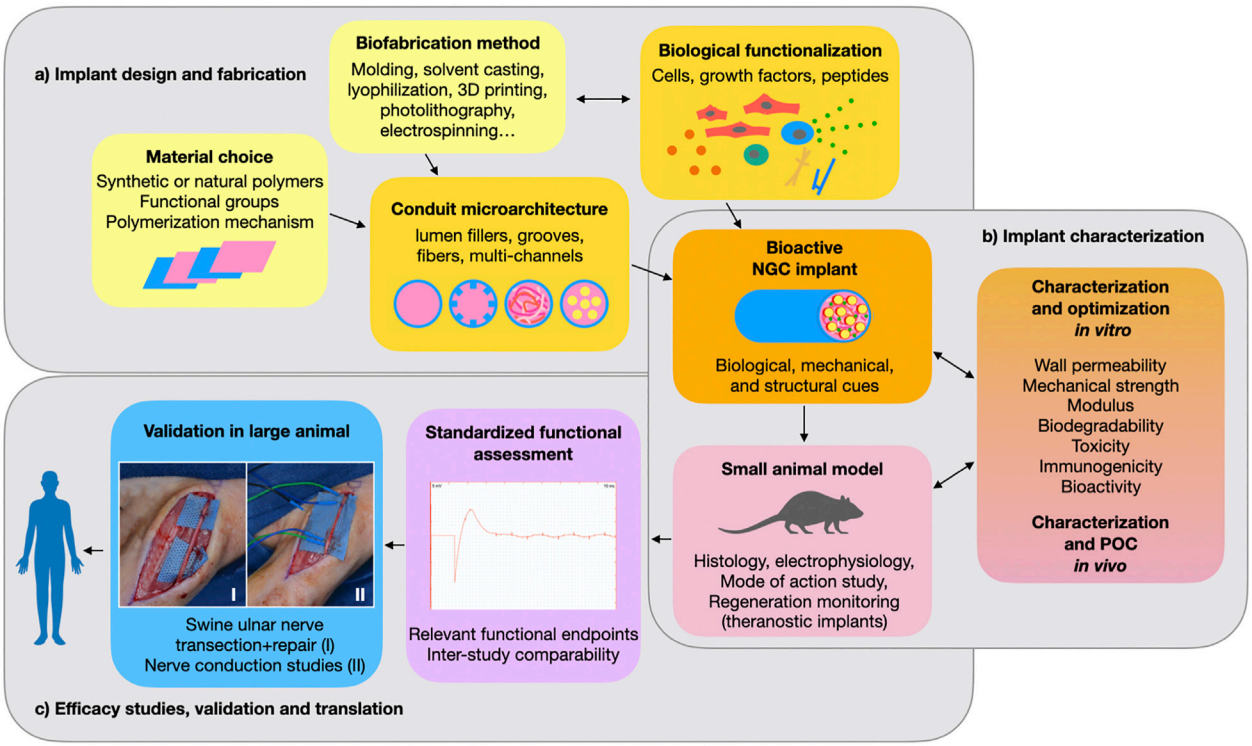

FIGURE 3 | Preclinical development of a nerve conduit: **(A)** The choice of a suitable polymer and fabrication method determine the implant's structural features and allow for biological functionalization with cells, proteins or peptides. **(B)** The resulting nerve guidance conduit (NGC) promotes nerve regeneration through a combination of biological, mechanical and structural cues. Several parameters are critical for safe and effective performance. These need to be thoroughly characterized both *in vitro* and *in vivo*. Most commonly, a rodent model is used for initial *in vivo* proof of concept (POC) and evaluation of safety and efficacy. **(C)** In order to identify the most promising implant designs and progress toward clinical application, performance of NGCs should be compared using standardized relevant endpoints and validated in large animal studies. Photographs I and II belong to the Gorantla lab.

their clinical acceptance declines compared to that of simpler and well understood hollow tube grafts. This could be in part because the more active components an implant has, the more challenging it becomes to translate it into a safe, well characterized, and reliable medical device.

A major translational challenge lies in choosing the correct preclinical *in vivo* model for translation to human application. Most preclinical studies show efficacy of their NGC in a rat sciatic nerve gap injury, usually of 10 mm gap size (**Table 1**). (Kaplan et al., 2015) showed that nearly 90% of the peripheral nerve gap repair studies are being conducted in rats and rabbits (78% rats and 12% rabbits). For translation, these studies have major limitations due to a species-specific neurobiological regenerative profile. Small animal studies have little relevance for translation without supporting large animal studies. Thus, more large animal studies are needed to identify truly promising conduits among the countless designs found in literature (**Figure 3C**).

Additionally, while many studies show efficacy of their design and use meaningful internal controls, they are hardly comparable with other studies in the field as there is little consensus on which readouts, time points and effect sizes are considered most relevant for clinical translation. The evaluation timepoint following nerve repair is crucial for thoroughly understanding the effect of the experimental technique on nerve regeneration. Brenner et al. (2008) demonstrated that while the nerve regenerative effect of tacrolimus is significant at 40 days, it is undetectable at 70 days. Similar results are found in a metanalysis by DeLeonibus et al., 2021.

As discussed in the "structural design" section of this review, synergistic biological effects of multimodal NGC functionalization are still poorly understood and would require extensive comparisons and scrutinous experimental design to optimize each component (**Figures 3A,B**). Furthermore, the already vast choice of individual bioactive factors such as cells and growth factors (cf. "biological functionalization" section) makes it difficult to choose the optimal combination. Therefore, rather than further expanding the choice of bioactive polymers, soluble factors, transplantable cells and structural designs, an important challenge for the NGC field lies in better understanding how different modes of action of each component can be synergized into combination therapies (**Figure 3B**). This can only be achieved in a collective effort, by improving and standardizing study design and readouts towards better inter-study comparability. Fortunately, recent studies in the field have recognized this issue and are combining more

TABLE 1 | Chronological overview of NGC design and animal studies.

Year	Authors	NGC design	*In vivo* Model
1988	Dellon AL. et al. (Dellon and Mackinnon, 1988)	PGA	Monkey
1991	Archibald SJ. et al. (Archibald et al., 1991)	Collagen	Rat and monkey
1992	Guénard V. et al. (Guénard et al., 1992)	Semipermeable PAN/PVC conduit loaded with Schwann cells	Rat
1995	Tang JB. et al. (Tang et al., 1995)	Vein graft	Human
2000	Weber RA. et al. (Weber et al., 2000)	PGA	Human
2001	Miller C. et al. (Miller et al., 2001a)	Laminin-coated PDLA seeded with Schwann cells	Rat
2004	Rutkowski GE. et al. (Rutkowski et al., 2004)	PDLLA conduit seeded with Schwann cells	Rat
2005	Wang X. et al. (Wang et al., 2005)	Chitosan/PGA	Dog
2009	Hu X. et al. (Hu et al., 2009)	Collagen/Chitosan conduit with microchannels	Rat
2009	Rosson GD. et al. (Rosson et al., 2009)	PGA conduit	Human
2009	Whitlock EL. et al. (Whitlock et al., 2009)	Commercially available collagen versus allograft	Rat
2010	Durgam H. et al.	NGCs coated with PPy-PCL and PPy-PECA co-polymers	Rat
2011	Marcol W. et al. (Marcol et al., 2011)	Chitosan gel covered proximal nerve end	Rat
2011	Radtke C. et al. (Radtke et al., 2011)	Decellularized vein grafts filled with spider silk fibers	Sheep
2012	Lee JY. et al. (Lee et al., 2012)	Collagen conduit filled with collagen-glycosaminoglycan	Rat
2012	Wray LF. et al. (Wray et al., 2012)	Silk-based scaffold with hollow channels	—
2012	Giusti, G. et al. (Giusti et al., 2012)	Collagen versus allograft	Rat
2013	Berrocal YA. et al. (Berrocal et al., 2013)	Collagen conduits seeded with Schwann cells	Rat
2014	Matsumine H. et al. (Matsumine et al., 2014)	PLA-conduit and silicon conduit filled with Collagen	Rat
2014	Sahin C. et al. (Sahin et al., 2014)	Vein filled with minced nerve	Rat
2015	Kim B. et al.	PDMS (polydimethylsiloxane) microchannel scaffold with microwires (used as recording electrodes) embedded within the microchannels	Rat
2015	Musick KM. et al.	Microchannel electrode implants with silicone rubber and elastic thin-film metallization	Rat
2016	Eren F. et al. (Eren et al., 2016)	Vein graft with VEGF and stem cells	Rat
2016	MacEwan MR. et al.	GDNF loaded nerve guidance silicone-conduits with chronically implanted macro-sieve electrode	Rat
2017	Chang YC. et al. (Chang et al., 2017)	Multi-channeled scaffolds with electrospun nanofibers and NGF and BDNF	Rabbit
2017	Ko CH. et al. (Ko et al., 2017)	Bisvinyl sulfonemethyl (BVSM)-crosslinked gelatin conduit	Rat
2017	Yapici AK. et al. (Yapici et al., 2017)	Vascularized neurotube	Rat
2018	Li G. et al. (Li et al., 2018)	Chitosan conduit with micropatterned inner wall	Rat
2018	Neubrech F. et al. (Neubrech et al., 2018)	Chitosan wrap	Human
2018	Xia B. et al. (Xia and Lv, 2018)	PLLA-electrospun nanofibrous conduit loaded with VEGF and NGF	Rat
2019	Sun B. et al. (Sun et al., 2019)	Ppy-coated nerve guidance conduit	Rat
2019	Chen X. et al. (Chen et al., 2019)	Carboxylic graphene oxide-composited polypyrrole conduits loaded with mouse fibroblast cells and rat pheochromocytoma cells	Rat
2019	Shah MB. et al. (Shah et al., 2019)	Multichannel PCL spiral with aligned collagen nanofibers	Rat
2019	Singh A. et al. (Singh et al., 2019)	Polyurethane conduit filled with aligned chitosan-gelatin cryogel filler	—
2019	Vijayavenkataraman S. et al. (Vijayavenkataraman et al., 2019a)	PPy-b-PCL based conductive scaffolds seeded with peripheral neuronal cells	—
2019	Rbia N. et al. (Rbia et al., 2019)	Commercially available collagen versus allograft	Human
2020	Chang W. et al. (Chang et al., 2020)	Laminin cross-linked PCL/PEG spiral conduit with outer nanofibrous tube	Rat
2020	Donsante A. et al. (Donsante et al., 2020)	PCL conduit integrated with phase-change material loaded with NT-3 and ChABC	Rat
2020	Gisbert Roca F. et al. (Gisbert Roca et al., 2020)	Hyaluronic acid and silk fibroin conduits	Rat
2020	Itai S. et al. (Itai et al., 2020)	Chitosan-collagen hydrogel conduit loaded with Schwann cells	—
2020	Keshavarz M. et al. (Keshavarz et al., 2020)	Polycarbonate conduit with poly-L-ornithine and double-walled carbon nanotubes	—
2020	Panzer KV. et al. (Panzer et al., 2020)	Tissue engineered bands of Büngner	—
2020	Yoo J. et al. (Yoo et al., 2020)	PLCL conduit with 3D printed collagen hydrogel	Rat
2020	Zhao Y. et al. (Zhao et al., 2020)	Polypyrrole/silk fibroin (PPy/SF) conductive composite scaffold seeded with Schwann Cells	Rat
2021	Carvalho CR. et al. (Carvalho et al., 2021)	Silk fibroin loaded with NGF and GDNF	Rat
2021	Huang Q. et al. (Huang et al., 2021)	Alginate-gelatin hydrogel with graphene mesh, loaded with netrin-1	Rat
2021	Kong Y. et al. (Kong et al., 2021)	HA-phenylboronic acid-poly (vinyl alcohol) -heparin hydrogel loaded with GDNF	Mouse
2021	Kornfeld T. et al. (Kornfeld et al., 2021b)	Spider silk-based artificial nerve graft	Sheep
2021	Manoukian OS. et al. (Manoukian et al., 2021)	Chitosan-halloysite nanotubes conduit loaded with 4-aminopyridin	Rat
2021	Zhang D. et al. (Zhang et al., 2021)	Grooved PLCL with laminin peptide gradient	Rat
2022	Zhang L. et al. (Zhang et al., 2022)	Schwann Cells 3D printed in gelatin-based microchannel conduit	—

extensive *in vitro* comparisons and mode-of-action studies with a functional *in vivo* investigation.

Finally, in order to identify both biological mechanisms as well as translationally relevant readout, some attention should be brought to *in vivo* live monitoring of peripheral nerve regeneration. This could be achieved through theranostic implants that track the regenerative process *in vivo* (**Figure 3**). For example, some nerve interface studies use

bioelectronics to track axon growth and electrophysiological performance (cf. **Section 3.3.2**), but other monitoring approaches are also conceivable and remain largely unexplored in the nerve regeneration field to date (Kim et al., 2015; Musick et al., 2015; Paggi et al., 2021).

AUTHOR CONTRIBUTIONS

All authors contributed to conception of the article. AR and ND wrote the manuscript. ND designed the storyline. All authors contributed to manuscript revision and approved the submitted version.

ACKNOWLEDGMENTS

The authors gratefully acknowledge the German Research Foundation (DFG) for funding ND (SFB 1444). ND would like to thank Drs. Hans-Dieter Volk (Charité Universitätsmedizin Berlin, Institute of Medical Immunology, Berlin, Germany) and Manfred Gossen (Helmholtz-Zentrum Hereon, Institute of Active Polymers, Teltow, Germany) for their continuous support and valuable advice. ND would like to thank the Berlin-Brandenburg School for Regenerative Therapies GSC 203 for its support. **Figures 1** and **2** were created in part using BioRender.com.

REFERENCES

Abatangelo, G., Vindigni, V., Avruscio, G., Pandis, L., and Brun, P. (2020). Hyaluronic Acid: Redefining its Role. *Cells* 9 (7), 1743. doi:10.3390/cells9071743

Archibald, S. J., Krarup, C., Shefner, J., Li, S.-T., and Madison, R. D. (1991). A Collagen-Based Nerve Guide Conduit for Peripheral Nerve Repair: an Electrophysiological Study of Nerve Regeneration in Rodents and Nonhuman Primates. *J. Comp. Neurol.* 306 (4), 685–696. doi:10.1002/cne.903060410

Arthur-Farraj, P. J., Latouche, M., Wilton, D. K., Quintes, S., Chabrol, E., Banerjee, A., et al. (2012). c-Jun Reprograms Schwann Cells of Injured Nerves to Generate a Repair Cell Essential for Regeneration. *Neuron* 75 (4), 633–647. doi:10.1016/j.neuron.2012.06.021

Barros, D., Conde-Sousa, E., Gonçalves, A. M., Han, W. M., García, A. J., Amaral, I. F., et al. (2019). Engineering Hydrogels with Affinity-Bound Laminin as 3D Neural Stem Cell Culture Systems. *Biomater. Sci.* 7 (12), 5338–5349. doi:10.1039/c9bm00348g

Barrows, T. (1986). Degradable Implant Materials: a Review of Synthetic Absorbable Polymers and Their Applications. *Clin. Mater.* 1 (4), 233–257. doi:10.1016/s0267-6605(86)80015-4

Bedel, A., Beliveau, F., Lamrissi-Garcia, I., Rousseau, B., Moranvillier, I., Rucheton, B., et al. (2017). Preventing Pluripotent Cell Teratoma in Regenerative Medicine Applied to Hematology Disorders. *Stem Cell Transl Med* 6 (2), 382–393. doi:10.5966/sctm.2016-0201

Benga, A., Zor, F., Korkmaz, A., Marinescu, B., and Gorantla, V. (2017). The Neurochemistry of Peripheral Nerve Regeneration. *Indian J. Plast. Surg.* 50 (1), 5–15. doi:10.4103/ijps.IJPS_14_17

Berrocal, Y. A., Almeida, V. W., Gupta, R., and Levi, A. D. (2013). Transplantation of Schwann Cells in a Collagen Tube for the Repair of Large, Segmental Peripheral Nerve Defects in Rats. *Jns* 119 (3), 720–732. doi:10.3171/2013.4.jns121189

Borschel, G. H., Kia, K. F., Kuzon, W. M., Jr., and Dennis, R. G. (2003). Mechanical Properties of Acellular Peripheral Nerve. *J. Surg. Res.* 114 (2), 133–139. doi:10.1016/s0022-4804(03)00255-5

Brenner, M. J., Moradzadeh, A., Myckatyn, T. M., Tung, T. H. H., Mendez, A. B., Hunter, D. A., et al. (2008). Role of Timing in Assessment of Nerve Regeneration. *Microsurgery* 28 (4), 265–272. doi:10.1002/micr.20483

Bucan, V., Vaslaitis, D., Peck, C.-T., Strauß, S., Vogt, P. M., and Radtke, C. (2019). Effect of Exosomes from Rat Adipose-Derived Mesenchymal Stem Cells on Neurite Outgrowth and Sciatic Nerve Regeneration after Crush Injury. *Mol. Neurobiol.* 56 (3), 1812–1824. doi:10.1007/s12035-018-1172-z

Burnett, M. G., and Zager, E. L. (2004). Pathophysiology of Peripheral Nerve Injury: a Brief Review. *Neurosurg. Focus* 16 (5), E1. doi:10.3171/foc.2004.16.5.2

Carvalho, C. R., Chang, W., Silva-Correia, J., Reis, R. L., Oliveira, J. M., and Kohn, J. (2021). Engineering Silk Fibroin-Based Nerve Conduit with Neurotrophic Factors for Proximal Protection after Peripheral Nerve Injury. *Adv. Healthc. Mater.* 10 (2), e2000753. doi:10.1002/adhm.202000753

Chang, W., Shah, M. B., Zhou, G., Walsh, K., Rudraiah, S., Kumbar, S. G., et al. (2020). Polymeric Nanofibrous Nerve Conduits Coupled with Laminin for Peripheral Nerve Regeneration. *Biomed. Mater.* 15 (3), 035003. doi:10.1088/1748-605x/ab6994

Chang, Y.-C., Chen, M.-H., Liao, S.-Y., Wu, H.-C., Kuan, C.-H., Sun, J.-S., et al. (2017). Multichanneled Nerve Guidance Conduit with Spatial Gradients of Neurotrophic Factors and Oriented Nanotopography for Repairing the Peripheral Nervous System. *ACS Appl. Mater. Inter.* 9 (43), 37623–37636. doi:10.1021/acsami.7b12567

Chen, X., Liu, C., Huang, Z., Pu, X., Shang, L., Yin, G., et al. (2019). Preparation of Carboxylic Graphene Oxide-composited Polypyrrole Conduits and Their Effect on Sciatic Nerve Repair under Electrical Stimulation. *J. Biomed. Mater. Res.* 107 (12), 2784–2795. doi:10.1002/jbm.a.36781

Ciaramitaro, P., Mondelli, M., Logullo, F., Grimaldi, S., Battiston, B., Sard, A., et al. (2010). Traumatic Peripheral Nerve Injuries: Epidemiological Findings, Neuropathic Pain and Quality of Life in 158 Patients. *J. Peripher. Nerv Syst.* 15 (2), 120–127. doi:10.1111/j.1529-8027.2010.00260.x

Cooney, D. S., Wimmers, E. G., Ibrahim, Z., Grahammer, J., Christensen, J. M., Brat, G. A., et al. (2016). Mesenchymal Stem Cells Enhance Nerve Regeneration in a Rat Sciatic Nerve Repair and Hindlimb Transplant Model. *Sci. Rep.* 6 (1), 31306. doi:10.1038/srep31306

Craig, P. H., Williams, J. A., Davis, K. W., Magoun, A. D., Levy, A. J., Bogdansky, S., et al. (1975). A Biologic Comparison of Polyglactin 910 and Polyglycolic Acid Synthetic Absorbable Sutures. *Surg. Gynecol. Obstet.* 141 (1), 1–10.

D'Almeida, M., Attik, N., Amalric, J., Brunon, C., Renaud, F., Abouelleil, H., et al. (2017). Chitosan Coating as an Antibacterial Surface for Biomedical Applications. *PLoS One* 12 (12), e0189537. doi:10.1371/journal.pone.0189537

DeLeonibus, A., Rezaei, M., Fahradyan, V., Silver, J., Rampazzo, A., and Bassiri Gharb, B. (2021). A Meta-analysis of Functional Outcomes in Rat Sciatic Nerve Injury Models. *Microsurgery* 41 (3), 286–295. doi:10.1002/micr.30713

Dellon, A. L., and Mackinnon, S. E. (1988). An Alternative to the Classical Nerve Graft for the Management of the Short Nerve gap. *Plast. Reconstr. Surg.* 82 (5), 849–856. doi:10.1097/00006534-198811000-00020

Dixon, A. R., Jariwala, S. H., Bilis, Z., Loverde, J. R., Pasquina, P. F., and Alvarez, L. M. (2018). Bridging the gap in Peripheral Nerve Repair with 3D Printed and Bioprinted Conduits. *Biomaterials* 186, 44–63. doi:10.1016/j.biomaterials.2018.09.010

Donsante, A., Xue, J., Poth, K. M., Hardcastle, N. S., Diniz, B., O'Connor, D. M., et al. (2020). Controlling the Release of Neurotrophin-3 and Chondroitinase ABC Enhances the Efficacy of Nerve Guidance Conduits. *Adv. Healthc. Mater.* 9 (14), e2000200. doi:10.1002/adhm.202000200

Dontchev, V. D., and Letourneau, P. C. (2002). Nerve Growth Factor and Semaphorin 3A Signaling Pathways Interact in Regulating Sensory Neuronal Growth Cone Motility. *J. Neurosci.* 22 (15), 6659–6669. doi:10.1523/jneurosci.22-15-06659.2002

Drzeniek, N. M., Mazzocchi, A., Schlickeiser, S., Forsythe, S. D., Moll, G., Geißler, S., et al. (2021). Bio-instructive Hydrogel Expands the Paracrine Potency of Mesenchymal Stem Cells. *Biofabrication* 13, 1. doi:10.1088/1758-5090/ac0a32

Durgam, H., Sapp, S., Deister, C., Khaing, Z., Chang, E., Luebben, S., et al. (2010). Novel Degradable Co-polymers of Polypyrrole Support Cell Proliferation and Enhance Neurite Out-Growth with Electrical Stimulation. *J. Biomater. Sci. Polym. Edition* 21 (10), 1265–1282. doi:10.1163/092050609x12481751806330

Eggers, R., de Winter, F., Hoyng, S. A., Roet, K. C. D., Ehlert, E. M., Malessy, M. J. A., et al. (2013). Lentiviral Vector-Mediated Gradients of GDNF in the Injured Peripheral Nerve: Effects on Nerve Coil Formation, Schwann Cell

Maturation and Myelination. *PLoS One* 8 (8), e71076. doi:10.1371/journal.pone.0071076

El Knidri, H., Belaabed, R., Addaou, A., Laajeb, A., and Lahsini, A. (2018). Extraction, Chemical Modification and Characterization of Chitin and Chitosan. *Int. J. Biol. Macromolecules* 120 (Pt A), 1181–1189. doi:10.1016/j.ijbiomac.2018.08.139

Eren, F., Öksüz, S., Küçükodaci, Z., Kendırlı, M. T., Cesur, C., Alarçın, E., et al. (2016). Targeted Mesenchymal Stem Cell and Vascular Endothelial Growth Factor Strategies for Repair of Nerve Defects with Nerve Tissue Implanted Autogenous Vein Graft Conduits. *Microsurgery* 36 (7), 578–585. doi:10.1002/micr.22401

Fallon, M., and Tadi, P. (2021). "Histology, Schwann Cells," in *StatPearls* (Treasure Island (FL): StatPearls Publishing LLC.) 1.

Fertala, A. (2020). Three Decades of Research on Recombinant Collagens: Reinventing the Wheel or Developing New Biomedical Products? *Bioengineering (Basel)* 7 (4), 155. doi:10.3390/bioengineering7040155

Fornaro, M., Giovannelli, A., Foggetti, A., Muratori, L., Geuna, S., Novajra, G., et al. (2020). Role of Neurotrophic Factors in Enhancing Linear Axonal Growth of Ganglionic Sensory Neurons *In Vitro*. *Neural Regen. Res.* 15 (9), 1732–1739. doi:10.4103/1673-5374.276338

Gardiner, N. J., Fernyhough, P., Tomlinson, D. R., Mayer, U., von der Mark, H., and Streuli, C. H. (2005). α7 Integrin Mediates Neurite Outgrowth of Distinct Populations of Adult Sensory Neurons. *Mol. Cell Neurosci.* 28 (2), 229–240. doi:10.1016/j.mcn.2004.08.017

Gelse, K., Poschl, E., and Aigner, T. (2003). Collagens-structure, Function, and Biosynthesis. *Adv. Drug Deliv. Rev.* 55 (12), 1531–1546. doi:10.1016/j.addr.2003.08.002

Ginde, R. M., and Gupta, R. K. (1987). *In Vitro* chemical Degradation of Poly(glycolic Acid) Pellets and Fibers. *J. Appl. Polym. Sci.* 33 (7), 2411–2429. doi:10.1002/app.1987.070330712

Gisbert Roca, F., Lozano Picazo, P., Pérez-Rigueiro, J., Guinea Tortuero, G. V., Monleón Pradas, M., and Martínez-Ramos, C. (2020). Conduits Based on the Combination of Hyaluronic Acid and Silk Fibroin: Characterization, *In Vitro* Studies and *In Vivo* Biocompatibility. *Int. J. Biol. Macromolecules* 148, 378–390. doi:10.1016/j.ijbiomac.2020.01.149

Giusti, G., Willems, W. F., Kremer, T., Friedrich, P. F., Bishop, A. T., and Shin, A. Y. (2012). Return of Motor Function after Segmental Nerve Loss in a Rat Model: Comparison of Autogenous Nerve Graft, Collagen Conduit, and Processed Allograft (AxoGen). *J. Bone Jt. Surg Am* 94 (5), 410–417. doi:10.2106/jbjs.k.00253

Gordon, T. (2016). Electrical Stimulation to Enhance Axon Regeneration after Peripheral Nerve Injuries in Animal Models and Humans. *Neurotherapeutics* 13 (2), 295–310. doi:10.1007/s13311-015-0415-1

Green, R. A., Lovell, N. H., and Poole-Warren, L. A. (2009). Cell Attachment Functionality of Bioactive Conducting Polymers for Neural Interfaces. *Biomaterials* 30 (22), 3637–3644. doi:10.1016/j.biomaterials.2009.03.043

Guénard, V., Kleitman, N., Morrissey, T. K., Bunge, R. P., and Aebischer, P. (1992). Syngeneic Schwann Cells Derived from Adult Nerves Seeded in Semipermeable Guidance Channels Enhance Peripheral Nerve Regeneration. *J. Neurosci.* 12 (9), 3310–3320.

Guthrie, S. (2007). Neurotrophic Factors: Are They Axon Guidance Molecules? *Adv. Exp. Med. Biol.* 621, 81–94. doi:10.1007/978-0-387-76715-4_6

Hu, X., Huang, J., Ye, Z., Xia, L., Li, M., Lv, B., et al. (2009). A Novel Scaffold with Longitudinally Oriented Microchannels Promotes Peripheral Nerve Regeneration. *Tissue Eng. A* 15 (11), 3297–3308. doi:10.1089/ten.tea.2009.0017

Huang, C.-W., Huang, W.-C., Qiu, X., Fernandes Ferreira da Silva, F., Wang, A., Patel, S., et al. (2017). The Differentiation Stage of Transplanted Stem Cells Modulates Nerve Regeneration. *Sci. Rep.* 7 (1), 17401. doi:10.1038/s41598-017-17043-4

Huang, Q., Cai, Y., Zhang, X., Liu, J., Liu, Z., Li, B., et al. (2021). Aligned Graphene Mesh-Supported Double Network Natural Hydrogel Conduit Loaded with Netrin-1 for Peripheral Nerve Regeneration. *ACS Appl. Mater. Inter.* 13 (1), 112–122. doi:10.1021/acsami.0c16391

Hussain, G., Wang, J., Rasul, A., Anwar, H., Qasim, M., Zafar, S., et al. (2020). Current Status of Therapeutic Approaches against Peripheral Nerve Injuries: A Detailed Story from Injury to Recovery. *Int. J. Biol. Sci.* 16 (1), 116–134. doi:10.7150/ijbs.35653

Ikeda, K., Yamauchi, D., Osamura, N., Hagiwara, N., and Tomita, K. (2003). Hyaluronic Acid Prevents Peripheral Nerve Adhesion. *Br. J. Plast. Surg.* 56 (4), 342–347. doi:10.1016/s0007-1226(03)00197-8

Itai, S., Suzuki, K., Kurashina, Y., Kimura, H., Amemiya, T., Sato, K., et al. (2020). Cell-encapsulated Chitosan-Collagen Hydrogel Hybrid Nerve Guidance Conduit for Peripheral Nerve Regeneration. *Biomed. Microdevices* 22 (4), 81. doi:10.1007/s10544-020-00536-x

Ivins, J. K., Yurchenco, P. D., and Lander, A. D. (2000). Regulation of Neurite Outgrowth by Integrin Activation. *J. Neurosci.* 20 (17), 6551–6560. doi:10.1523/jneurosci.20-17-06551.2000

Kaplan, H. M., Mishra, P., and Kohn, J. (2015). The Overwhelming Use of Rat Models in Nerve Regeneration Research May Compromise Designs of Nerve Guidance Conduits for Humans. *J. Mater. Sci. Mater. Med.* 26 (8), 226. doi:10.1007/s10856-015-5558-4

Keshavarz, M., Wales, D. J., Seichepine, F., Abdelaziz, M. E. M. K., Kassanos, P., Li, Q., et al. (2020). Induced Neural Stem Cell Differentiation on a Drawn Fiber Scaffold-Toward Peripheral Nerve Regeneration. *Biomed. Mater.* 15 (5), 055011. doi:10.1088/1748-605x/ab8d12

Khor, E., Li, H. C., and Wee, A. (1995). *In Situ* polymerization of Pyrrole in Animal Tissue in the Formation of Hybrid Biomaterials. *Biomaterials* 16 (8), 657–661. doi:10.1016/0142-9612(95)93864-a

Kim, B., Reyes, A., Garza, B., and Choi, Y. (2015). A Microchannel Neural Interface with Embedded Microwires Targeting the Peripheral Nervous System. *Microsyst Technol.* 21 (7), 1551–1557. doi:10.1007/s00542-014-2340-3

Ko, C.-H., Shie, M.-Y., Lin, J.-H., Chen, Y.-W., Yao, C.-H., and Chen, Y.-S. (2017). Biodegradable Bisvinyl Sulfonemethyl-Crosslinked Gelatin Conduit Promotes Regeneration after Peripheral Nerve Injury in Adult Rats. *Sci. Rep.* 7 (1), 17489. doi:10.1038/s41598-017-17792-2

Kobayashi, H., Yokoyama, M., Matsuoka, Y., Omori, M., Itano, Y., Kaku, R., et al. (2008). Expression Changes of Multiple Brain-Derived Neurotrophic Factor Transcripts in Selective Spinal Nerve Ligation Model and Complete Freund's Adjuvant Model. *Brain Res.* 1206, 13–19. doi:10.1016/j.brainres.2007.12.004

Kong, N., Wan, F., Dai, W., Wu, P., Su, C., Peng, C., et al. (2020). A Cuboid Spider Silk: Structure-Function Relationship and Polypeptide Signature. *Macromol Rapid Commun.* 41 (6), e1900583. doi:10.1002/marc.201900583

Kong, Y., Shi, W., Zhang, D., Jiang, X., Kuss, M., Liu, B., et al. (2021). Injectable, Antioxidative, and Neurotrophic Factor-Deliverable Hydrogel for Peripheral Nerve Regeneration and Neuropathic Pain Relief. *Appl. Mater. Today* 24, 101090. doi:10.1016/j.apmt.2021.101090

Kornfeld, T., Borger, A., and Radtke, C. (2021). Reconstruction of Critical Nerve Defects Using Allogenic Nerve Tissue: A Review of Current Approaches. *Int. J. Mol. Sci.* 22 (7), 3515. doi:10.3390/ijms22073515

Kornfeld, T., Nessler, J., Helmer, C., Hannemann, R., Waldmann, K. H., Peck, C. T., et al. (2021). Spider Silk Nerve Graft Promotes Axonal Regeneration on Long Distance Nerve Defect in a Sheep Model. *Biomaterials* 271, 120692. doi:10.1016/j.biomaterials.2021.120692

Kostereva, N. V., Wang, Y., Fletcher, D. R., Unadkat, J. V., Schnider, J. T., Komatsu, C., et al. (2016). IGF-1 and Chondroitinase ABC Augment Nerve Regeneration after Vascularized Composite Limb Allotransplantation. *PLoS One* 11 (6), e0156149. doi:10.1371/journal.pone.0156149

Kuwahara, K., Fang, J. Y., Yang, Z., and Han, B. (2011). Enzymatic Crosslinking and Degradation of Gelatin as a Switch for Bone Morphogenetic Protein-2 Activity. *Tissue Eng. Part. A.* 17 (23-24), 2955–2964. doi:10.1089/ten.tea.2011.0290

Lago, N., Ceballos, D., J Rodrı´guez, F., Stieglitz, T., and Navarro, X. (2005). Long Term Assessment of Axonal Regeneration through Polyimide Regenerative Electrodes to Interface the Peripheral Nerve. *Biomaterials* 26 (14), 2021–2031. doi:10.1016/j.biomaterials.2004.06.025

Le, T. H., Kim, Y., and Yoon, H. (2017). Electrical and Electrochemical Properties of Conducting Polymers. *Polymers (Basel)* 9 (4), 150. doi:10.3390/polym9040150

Leclere, P., Ekström, P., Edström, A., Priestley, J., Averill, S., and Tonge, D. A. (1997). Effects of Glial Cell Line-Derived Neurotrophic Factor on Axonal Growth and Apoptosis in Adult Mammalian Sensory Neurons *In Vitro*. *Neuroscience* 82 (2), 545–558. doi:10.1016/s0306-4522(97)00307-2

Lee, J.-Y., Giusti, G., Friedrich, P. F., Archibald, S. J., Kemnitzer, J. E., Patel, J., et al. (2012). The Effect of Collagen Nerve Conduits Filled with Collagen-Glycosaminoglycan Matrix on Peripheral Motor Nerve Regeneration in a Rat Model. *The J. Bone Jt. Surgery-American Volume* 94 (22), 2084–2091. doi:10.2106/jbjs.k.00658

Lesnikova, A., Casarotto, P. C., Fred, S. M., Voipio, M., Winkel, F., Steinzeig, A., et al. (2021). Chondroitinase and Antidepressants Promote Plasticity by

Releasing TRKB from Dephosphorylating Control of PTPσ in Parvalbumin Neurons. *J. Neurosci.* 41 (5), 972–980. doi:10.1523/jneurosci.2228-20.2020

Li, G., Xue, C., Wang, H., Yang, X., Zhao, Y., Zhang, L., et al. (2018). Spatially Featured Porous Chitosan Conduits with Micropatterned Inner wall and Seamless Sidewall for Bridging Peripheral Nerve Regeneration. *Carbohydr. Polym.* 194, 225–235. doi:10.1016/j.carbpol.2018.04.049

Liu, B., Kong, Y., Shi, W., Kuss, M., Liao, K., Hu, G., et al. (2022). Exosomes Derived from Differentiated Human ADMSC with the Schwann Cell Phenotype Modulate Peripheral Nerve-Related Cellular Functions. *Bioactive Mater.* 14, 61–75. doi:10.1016/j.bioactmat.2021.11.022

Lohmeyer, J., Zimmermann, S., Sommer, B., Machens, H.-G., Lange, T., and Mailänder, P. (2007). Überbrückung peripherer Nervendefekte durch den Einsatz von Nervenröhrchen. *Chirurg* 78 (2), 142–147. doi:10.1007/s00104-006-1269-1

Long, H., Sabatier, C., Le Ma, L., Plump, A., Yuan, W., Ornitz, D. M., et al. (2004). Conserved Roles for Slit and Robo Proteins in Midline Commissural Axon Guidance. *Neuron* 42 (2), 213–223. doi:10.1016/s0896-6273(04)00179-5

Lopes, C. D. F., Gonçalves, N. P., Gomes, C. P., Saraiva, M. J., and Pêgo, A. P. (2017). BDNF Gene Delivery Mediated by Neuron-Targeted Nanoparticles Is Neuroprotective in Peripheral Nerve Injury. *Biomaterials* 121, 83–96. doi:10.1016/j.biomaterials.2016.12.025

Lv, J., Sun, X., Ma, J., Ma, X., Zhang, Y., Li, F., et al. (2015). Netrin-1 Induces the Migration of Schwann Cells via P38 MAPK and PI3K-Akt Signaling Pathway Mediated by the UNC5B Receptor. *Biochem. Biophysical Res. Commun.* 464 (1), 263–268. doi:10.1016/j.bbrc.2015.06.140

Lykissas, M., Batistatou, A., Charalabopoulos, K., and Beris, A. (2007). The Role of Neurotrophins in Axonal Growth, Guidance, and Regeneration. *Cnr* 4 (2), 143–151. doi:10.2174/156720207780637216

MacEwan, M. R., Zellmer, E. R., Wheeler, J. J., Burton, H., and Moran, D. W. (2016). Regenerated Sciatic Nerve Axons Stimulated through a Chronically Implanted Macro-Sieve Electrode. *Front. Neurosci.* 10, 557. doi:10.3389/fnins.2016.00557

Madihally, S. V., and Matthew, H. W. T. (1999). Porous Chitosan Scaffolds for Tissue Engineering. *Biomaterials* 20 (12), 1133–1142. doi:10.1016/s0142-9612(99)00011-3

Makadia, H. K., and Siegel, S. J. (2011). Poly Lactic-Co-Glycolic Acid (PLGA) as Biodegradable Controlled Drug Delivery Carrier. *Polymers* 3 (3), 1377–1397. doi:10.3390/polym3031377

Mammadov, B., Sever, M., Gecer, M., Zor, F., Ozturk, S., Akgun, H., et al. (2016). Sciatic Nerve Regeneration Induced by Glycosaminoglycan and Laminin Mimetic Peptide Nanofiber Gels. *RSC Adv.* 6 (112), 110535–110547. doi:10.1039/c6ra24450e

Manoukian, O. S., Rudraiah, S., Arul, M. R., Bartley, J. M., Baker, J. T., Yu, X., et al. (2021). Biopolymer-nanotube Nerve Guidance Conduit Drug Delivery for Peripheral Nerve Regeneration: *In Vivo* Structural and Functional Assessment. *Bioactive Mater.* 6 (9), 2881–2893. doi:10.1016/j.bioactmat.2021.02.016

Mao, A. S., Shin, J.-W., Utech, S., Wang, H., Uzun, O., Li, W., et al. (2017). Deterministic Encapsulation of Single Cells in Thin Tunable Microgels for Niche Modelling and Therapeutic Delivery. *Nat. Mater* 16 (2), 236–243. doi:10.1038/nmat4781

Marcol, W., Larysz-Brysz, M., Kucharska, M., Niekraszewicz, A., Slusarczyk, W., Kotulska, K., et al. (2011). Reduction of post-traumatic Neuroma and Epineural Scar Formation in Rat Sciatic Nerve by Application of Microcrystallic Chitosan. *Microsurgery* 31 (8), 642–649. doi:10.1002/micr.20945

Marconi, S., Castiglione, G., Turano, E., Bissolotti, G., Angiari, S., Farinazzo, A., et al. (2012). Human Adipose-Derived Mesenchymal Stem Cells Systemically Injected Promote Peripheral Nerve Regeneration in the Mouse Model of Sciatic Crush. *Tissue Eng. Part. A.* 18 (11-12), 1264–1272. doi:10.1089/ten.TEA.2011.0491

Matsui, H., Tsui, H., and Saka, M. (2016). Clinical Study of Sensory Recovery of Artificial Nerve Grafts (Nerbridge). *Hand (New York, N,Y.)* 11 (1_Suppl. l), 88S. doi:10.1177/1558944716660555fl

Matsumine, H., Sasaki, R., Yamato, M., Okano, T., and Sakurai, H. (2014). A Polylactic Acid Non-woven Nerve Conduit for Facial Nerve Regeneration in Rats. *J. Tissue Eng. Regen. Med.* 8 (6), 454–462. doi:10.1002/term.1540

Matthes, S. M., Reimers, K., Janssen, I., Liebsch, C., Kocsis, J. D., Vogt, P. M., et al. (2013). Intravenous Transplantation of Mesenchymal Stromal Cells to Enhance Peripheral Nerve Regeneration. *Biomed. Res. Int.* 2013, 573169. doi:10.1155/2013/573169

Miller, C., Jeftinija, S., and Mallapragada, S. (2001). Micropatterned Schwann Cell-Seeded Biodegradable Polymer Substrates Significantly Enhance Neurite Alignment and Outgrowth. *Tissue Eng.* 7 (6), 705–715. doi:10.1089/107632701753337663

Miller, C., Shanks, H., Witt, A., Rutkowski, G., and Mallapragada, S. (2001). Oriented Schwann Cell Growth on Micropatterned Biodegradable Polymer Substrates. *Biomaterials* 22 (11), 1263–1269. doi:10.1016/s0142-9612(00)00278-7

Moll, G., Ankrum, J. A., Kamhieh-Milz, J., Bieback, K., Ringdén, O., Volk, H.-D., et al. (2019). Intravascular Mesenchymal Stromal/Stem Cell Therapy Product Diversification: Time for New Clinical Guidelines. *Trends Mol. Med.* 25 (2), 149–163. doi:10.1016/j.molmed.2018.12.006

Moore, A. M., MacEwan, M., Santosa, K. B., Chenard, K. E., Ray, W. Z., Hunter, D. A., et al. (2011). Acellular Nerve Allografts in Peripheral Nerve Regeneration: a Comparative Study. *Muscle Nerve* 44 (2), 221–234. doi:10.1002/mus.22033

Muratori, L., Gnavi, S., Fregnan, F., Mancardi, A., Raimondo, S., Perroteau, I., et al. (2018). Evaluation of Vascular Endothelial Growth Factor (VEGF) and its Family Member Expression after Peripheral Nerve Regeneration and Denervation. *Anat. Rec.* 301 (10), 1646–1656. doi:10.1002/ar.23842

Musick, K. M., Rigosa, J., Narasimhan, S., Wurth, S., Capogrosso, M., Chew, D. J., et al. (2015). Chronic Multichannel Neural Recordings from Soft Regenerative Microchannel Electrodes during Gait. *Sci. Rep.* 5, 14363. doi:10.1038/srep14363

Namgung, U. (2014). The Role of Schwann Cell-Axon Interaction in Peripheral Nerve Regeneration. *Cells Tissues Organs* 200 (1), 6–12. doi:10.1159/000370324

Neubrech, F., Sauerbier, M., Moll, W., Seegmüller, J., Heider, S., Harhaus, L., et al. (2018). Enhancing the Outcome of Traumatic Sensory Nerve Lesions of the Hand by Additional Use of a Chitosan Nerve Tube in Primary Nerve Repair. *Plast. Reconstr. Surg.* 142 (2), 415–424. doi:10.1097/prs.0000000000004574

Nieuwenhuis, B., Haenzi, B., Andrews, M. R., Verhaagen, J., and Fawcett, J. W. (2018). Integrins Promote Axonal Regeneration after Injury of the Nervous System. *Biol. Rev.* 93 (3), 1339–1362. doi:10.1111/brv.12398

Paggi, V., Akouissi, O., Micera, S., and Lacour, S. P. (2021). Compliant Peripheral Nerve Interfaces. *J. Neural Eng.* 18 (3), 031001. doi:10.1088/1741-2552/abcdbe

Panzer, K. V., Burrell, J. C., Helm, K. V. T., Purvis, E. M., Zhang, Q., Le, A. D., et al. (2020). Tissue Engineered Bands of Büngner for Accelerated Motor and Sensory Axonal Outgrowth. *Front. Bioeng. Biotechnol.* 8, 580654. doi:10.3389/fbioe.2020.580654

Pavan, A., Bosio, M., and Longo, T. (1979). A Comparative Study of Poly(glycolic Acid) and Catgut as Suture Materials. Histomorphology and Mechanical Properties. *J. Biomed. Mater. Res.* 13 (3), 477–496. doi:10.1002/jbm.820130312

Radtke, C. (2016). Natural Occurring Silks and Their Analogues as Materials for Nerve Conduits. *Int. J. Mol. Sci.* 17 (10), 1754. doi:10.3390/ijms17101754

Radtke, C., Allmeling, C., Waldmann, K.-H., Reimers, K., Thies, K., Schenk, H. C., et al. (2011). Spider Silk Constructs Enhance Axonal Regeneration and Remyelination in Long Nerve Defects in Sheep. *PLoS One* 6 (2), e16990. doi:10.1371/journal.pone.0016990

Rbia, N., Bulstra, L. F., Saffari, T. M., Hovius, S. E. R., and Shin, A. Y. (2019). Collagen Nerve Conduits and Processed Nerve Allografts for the Reconstruction of Digital Nerve Gaps: A Single-Institution Case Series and Review of the Literature. *World Neurosurg.* 127, e1176–e1184. doi:10.1016/j.wneu.2019.04.087

Reinke, S., Geissler, S., Taylor, W. R., Schmidt-Bleek, K., Juelke, K., Schwachmeyer, V., et al. (2013). Terminally Differentiated $CD8^+$ T Cells Negatively Affect Bone Regeneration in Humans. *Sci. Transl Med.* 5 (177), 177ra36. doi:10.1126/scitranslmed.3004754

Rosson, G. D., Williams, E. H., and Dellon, A. L. (2009). Motor Nerve Regeneration across a Conduit. *Microsurgery* 29 (2), 107–114. doi:10.1002/micr.20580

Rutkowski, G. E., Miller, C. A., Jeftinija, S., and Mallapragada, S. K. (2004). Synergistic Effects of Micropatterned Biodegradable Conduits and Schwann Cells on Sciatic Nerve Regeneration. *J. Neural Eng.* 1 (3), 151–157. doi:10.1088/1741-2560/1/3/004

Sahin, C., Karagoz, H., Kulahci, Y., Sever, C., Akakin, D., Kolbasi, B., et al. (2014). Minced Nerve Tissue in Vein Grafts Used as Conduits in Rat Tibial Nerves. *Ann. Plast. Surg.* 73 (5), 540–546. doi:10.1097/sap.0000000000000060

Sahin, C., Karagoz, H., Yuksel, F., Kulahci, Y., Akakin, D., Dagbasi, N., et al. (2012). The Effect of Perineurotomy on Nerve Regeneration in Diabetic Rats. *Plast. Reconstr. Surg.* 130 (5), 651e–661e. doi:10.1097/prs.0b013e318267d3bd

Seddon, H. J., Medawar, P. B., and Smith, H. (1943). Rate of Regeneration of Peripheral Nerves in Man. *J. Physiol.* 102 (2), 191–215. doi:10.1113/jphysiol.1943.sp004027

Shah, M. B., Chang, W., Zhou, G., Glavy, J. S., Cattabiani, T. M., and Yu, X. (2019). Novel Spiral Structured Nerve Guidance Conduits with Multichannels and Inner Longitudinally Aligned Nanofibers for Peripheral Nerve Regeneration. *J. Biomed. Mater. Res.* 107 (5), 1410–1419. doi:10.1002/jbm.b.34233

Shi, J. Y., Liu, G. S., Liu, L. F., Kuo, S. M., Ton, C. H., Wen, Z. H., et al. (2011). Glial Cell Line–Derived Neurotrophic Factor Gene Transfer Exerts Protective Effect on Axons in Sciatic Nerve Following Constriction-Induced Peripheral Nerve Injury. *Hum. Gene Ther.* 22 (6), 721–731.

Singh, A., Shiekh, P. A., Das, M., Seppälä, J., and Kumar, A. (2019). Aligned Chitosan-Gelatin Cryogel-Filled Polyurethane Nerve Guidance Channel for Neural Tissue Engineering: Fabrication, Characterization, and *In Vitro* Evaluation. *Biomacromolecules* 20 (2), 662–673. doi:10.1021/acs.biomac.8b01308

Sondell, M., Lundborg, G., and Kanje, M. (1999). Vascular Endothelial Growth Factor Has Neurotrophic Activity and Stimulates Axonal Outgrowth, Enhancing Cell Survival and Schwann Cell Proliferation in the Peripheral Nervous System. *J. Neurosci.* 19 (14), 5731–5740. doi:10.1523/jneurosci.19-14-05731.1999

Stoll, G., and Müller, H. W. (1999). Nerve Injury, Axonal Degeneration and Neural Regeneration: Basic Insights. *Brain Pathol.* 9 (2), 313–325. doi:10.1111/j.1750-3639.1999.tb00229.x

Stratton, J. A., Holmes, A., Rosin, N. L., Sinha, S., Vohra, M., Burma, N. E., et al. (2018). Macrophages Regulate Schwann Cell Maturation after Nerve Injury. *Cel Rep.* 24 (10), 2561–2572. e2566. doi:10.1016/j.celrep.2018.08.004

Sun, B., Zhou, Z., Li, D., Wu, T., Zheng, H., Liu, J., et al. (2019). Polypyrrole-coated Poly(l-Lactic Acid-Co-ε-Caprolactone)/silk Fibroin Nanofibrous Nerve Guidance Conduit Induced Nerve Regeneration in Rat. *Mater. Sci. Eng. C* 94, 190–199. doi:10.1016/j.msec.2018.09.021

Sunderland, S. (1951). A Classification of Peripheral Nerve Injuries Producing Loss of Function. *Brain* 74 (4), 491–516. doi:10.1093/brain/74.4.491

Takahashi, K., Tanabe, K., Ohnuki, M., Narita, M., Ichisaka, T., Tomoda, K., et al. (2007). Induction of Pluripotent Stem Cells from Adult Human Fibroblasts by Defined Factors. *Cell* 131 (5), 861–872. doi:10.1016/j.cell.2007.11.019

Tang, J.-B., Shi, D., and Zhou, H. (1995). Vein Conduits for Repair of Nerves with a Prolonged gap or in Unfavorable Conditions: An Analysis of Three Failed Cases. *Microsurgery* 16 (3), 133–137. doi:10.1002/micr.1920160303

van Amerongen, M. J., Harmsen, M. C., Petersen, A. H., Kors, G., and van Luyn, M. J. A. (2006). The Enzymatic Degradation of Scaffolds and Their Replacement by Vascularized Extracellular Matrix in the Murine Myocardium. *Biomaterials* 27 (10), 2247–2257. doi:10.1016/j.biomaterials.2005.11.002

Vijayavenkataraman, S., Vialli, N., Fuh, J. Y. H., and Lu, W. F. (2019). Conductive Collagen/polypyrrole-B-Polycaprolactone Hydrogel for Bioprinting of Neural Tissue Constructs. *Int. J. Bioprint* 5, 229. doi:10.18063/ijb.v5i2.1.229

Vijayavenkataraman, S., Kannan, S., Cao, T., Fuh, J. Y. H., Sriram, G., and Lu, W. F. (2019). 3D-Printed PCL/PPy Conductive Scaffolds as Three-Dimensional Porous Nerve Guide Conduits (NGCs) for Peripheral Nerve Injury Repair. *Front. Bioeng. Biotechnol.* 7, 266. doi:10.3389/fbioe.2019.00266

Wallquist, W., Patarroyo, M., Thams, S., Carlstedt, T., Stark, B., Cullheim, S., et al. (2002). Laminin Chains in Rat and Human Peripheral Nerve: Distribution and Regulation during Development and after Axonal Injury. *J. Comp. Neurol.* 454 (3), 284–293. doi:10.1002/cne.10434

Wallquist, W., Zelano, J., Plantman, S., Kaufman, S. J., Cullheim, S., and Hammarberg, H. (2004). Dorsal Root Ganglion Neurons Up-Regulate the Expression of Laminin-Associated Integrins after Peripheral but Not central Axotomy. *J. Comp. Neurol.* 480 (2), 162–169. doi:10.1002/cne.20345

Wang, K.-K., Nemeth, I. R., Seckel, B. R., Chakalis-Haley, D. P., Swann, D. A., Kuo, J.-W., et al. (1998). Hyaluronic Acid Enhances Peripheral Nerve Regeneration *In Vivo*. *Microsurgery* 18 (4), 270–275. doi:10.1002/(sici)1098-2752(1998)18:4<270::aid-micr11>3.0.co;2-v

Wang, P., Zhang, Y., Zhao, J., and Jiang, B. (2015). Intramuscular Injection of Bone Marrow Mesenchymal Stem Cells with Small gap Neurorrhaphy for Peripheral Nerve Repair. *Neurosci. Lett.* 585, 119–125. doi:10.1016/j.neulet.2014.11.039

Wang, X., Hu, W., Cao, Y., Yao, J., Wu, J., and Gu, X. (2005). Dog Sciatic Nerve Regeneration across a 30-mm Defect Bridged by a Chitosan/PGA Artificial Nerve Graft. *Brain* 128 (Pt 8), 1897–1910. doi:10.1093/brain/awh517

Wang, X., Chen, Q., Yi, S., Liu, Q., Zhang, R., Wang, P., et al. (2019). The microRNAs Let-7 and miR-9 Down-Regulate the Axon-Guidance Genes Ntn1 and Dcc during Peripheral Nerve Regeneration. *J. Biol. Chem.* 294 (10), 3489–3500. doi:10.1074/jbc.ra119.007389

Weber, R. A., Breidenbach, W. C., Brown, R. E., Jabaley, M. E., and Mass, D. P. (2000). A Randomized Prospective Study of Polyglycolic Acid Conduits for Digital Nerve Reconstruction in Humans. *Plast. Reconstr. Surg.* 106 (5), 1036–1045. discussion 1046-1038. doi:10.1097/00006534-200010000-00013

Whitlock, E. L., Tuffaha, S. H., Luciano, J. P., Yan, Y., Hunter, D. A., Magill, C. K., et al. (2009). Processed Allografts and Type I Collagen Conduits for Repair of Peripheral Nerve Gaps. *Muscle Nerve* 39 (6), 787–799. doi:10.1002/mus.21220

Wongpinyochit, T., Johnston, B. F., and Seib, F. P. (2018). Degradation Behavior of Silk Nanoparticles-Enzyme Responsiveness. *ACS Biomater. Sci. Eng.* 4 (3), 942–951. doi:10.1021/acsbiomaterials.7b01021

Wray, L. S., Rnjak-Kovacina, J., Mandal, B. B., Schmidt, D. F., Gil, E. S., and Kaplan, D. L. (2012). A Silk-Based Scaffold Platform with Tunable Architecture for Engineering Critically-Sized Tissue Constructs. *Biomaterials* 33 (36), 9214–9224. doi:10.1016/j.biomaterials.2012.09.017

Xia, B., and Lv, Y. (2018). Dual-delivery of VEGF and NGF by Emulsion Electrospun Nanofibrous Scaffold for Peripheral Nerve Regeneration. *Mater. Sci. Eng. C* 82, 253–264. doi:10.1016/j.msec.2017.08.030

Yang, Y., Chen, X., Ding, F., Zhang, P., Liu, J., and Gu, X. (2007). Biocompatibility Evaluation of Silk Fibroin with Peripheral Nerve Tissues and Cells *In Vitro*. *Biomaterials* 28 (9), 1643–1652. doi:10.1016/j.biomaterials.2006.12.004

Yapici, A. K., Bayram, Y., Akgun, H., Gumus, R., and Zor, F. (2017). The Effect of *In Vivo* Created Vascularized Neurotube on Peripheric Nerve Regeneration. *Injury* 48 (7), 1486–1491. doi:10.1016/j.injury.2017.05.014

Yoo, J., Park, J. H., Kwon, Y. W., Chung, J. J., Choi, I. C., Nam, J. J., et al. (2020). Augmented Peripheral Nerve Regeneration through Elastic Nerve Guidance Conduits Prepared Using a Porous PLCL Membrane with a 3D Printed Collagen Hydrogel. *Biomater. Sci.* 8 (22), 6261–6271. doi:10.1039/d0bm00847h

Zarei, M., Samimi, A., Khorram, M., Abdi, M. M., and Golestaneh, S. I. (2021). Fabrication and Characterization of Conductive Polypyrrole/chitosan/collagen Electrospun Nanofiber Scaffold for Tissue Engineering Application. *Int. J. Biol. Macromolecules* 168, 175–186. doi:10.1016/j.ijbiomac.2020.12.031

Zhang, D., Li, Z., Shi, H., Yao, Y., Du, W., Lu, P., et al. (2021). Micropatterns and Peptide Gradient on the Inner Surface of a Guidance Conduit Synergistically Promotes Nerve Regeneration *In Vivo*. *Bioactive Mater.* 9, 134–146. doi:10.1016/j.bioactmat.2021.07.010

Zhang, L., Zhang, H., Wang, H., Guo, K., Zhu, H., Li, S., et al. (2022). Fabrication of Multi-Channel Nerve Guidance Conduits Containing Schwann Cells Based on Multi-Material 3D Bioprinting. *3D Printing and Additive Manufacturing* 1, 1. doi:10.1089/3dp.2021.0203

Zhao, Y., Liang, Y., Ding, S., Zhang, K., Mao, H.-q., and Yang, Y. (2020). Application of Conductive PPy/SF Composite Scaffold and Electrical Stimulation for Neural Tissue Engineering. *Biomaterials* 255, 120164. doi:10.1016/j.biomaterials.2020.120164

Zor, F., Deveci, M., Kilic, A., Ozdag, M. F., Kurt, B., Sengezer, M., et al. (2014). Effect of VEGF Gene Therapy and Hyaluronic Acid Film Sheath on Peripheral Nerve Regeneration. *Microsurgery* 34 (3), 209–216. doi:10.1002/micr.22196

Conflict of Interest: The authors declare that the research was conducted in the absence of any commercial or financial relationships that could be construed as a potential conflict of interest.

Publisher's Note: All claims expressed in this article are solely those of the authors and do not necessarily represent those of their affiliated organizations, or those of the publisher, the editors and the reviewers. Any product that may be evaluated in this article, or claim that may be made by its manufacturer, is not guaranteed or endorsed by the publisher.

frontiers | Frontiers in Bioengineering and Biotechnology

ORIGINAL RESEARCH
published: 28 June 2022
doi: 10.3389/fbioe.2022.876157

The Thermosensitive Injectable Celecoxib-Loaded Chitosan Hydrogel for Repairing Postoperative Intervertebral Disc Defect

Yukun Du[1†], Jianyi Li[1†], Xiaojie Tang[2], Yingying Liu[3], Guoshuai Bian[3], Jianzhuang Shi[3], Yixin Zhang[1,4], Baomeng Zhao[5], Hongri Zhao[2], Kunyan Sui[3] and Yongming Xi[1]**

[1]Department of Spinal Surgery, The Affiliated Hospital of Qingdao University, Qingdao, China, [2]Department of Spinal Surgery, Yantai Affiliated Hospital of Binzhou Medical University, Yantai, China, [3]State Key Laboratory of Bio-Fibers and Eco-Textiles, College of Materials Science and Engineering, Shandong Collaborative Innovation Center of Marine Biobased Fibers and Ecological Textiles, Qingdao University, Qingdao, China, [4]Health Care Ward III, The Affiliated Hospital of Qingdao University, Qingdao, China, [5]Department of Surgery teaching and research, Binzhou Medical University, Yantai, China

OPEN ACCESS

Edited by:
Jun Lin,
First Affiliated Hospital of Soochow University, China

Reviewed by:
Joana C. Antunes,
University of Minho, Portugal
Björn Rath,
Klinikum Wels-Grieskirchen, Austria

***Correspondence:**
Kunyan Sui
sky@qdu.edu.cn
Yongming Xi
xym700118@163.com

[†]These authors have contributed equally to this work and share first authorship

Specialty section:
This article was submitted to Biomaterials, a section of the journal Frontiers in Bioengineering and Biotechnology

Received: 15 February 2022
Accepted: 18 May 2022
Published: 28 June 2022

Citation:
Du Y, Li J, Tang X, Liu Y, Bian G, Shi J, Zhang Y, Zhao B, Zhao H, Sui K and Xi Y (2022) The Thermosensitive Injectable Celecoxib-Loaded Chitosan Hydrogel for Repairing Postoperative Intervertebral Disc Defect. Front. Bioeng. Biotechnol. 10:876157. doi: 10.3389/fbioe.2022.876157

Percutaneous endoscopic lumbar discectomy has been widely used in clinical practice for lumbar spine diseases. But the postoperative disc re-herniation and inflammation are the main reason for pain recurrence after surgery. The postoperative local defect of the intervertebral disc will lead to the instability of the spine, further aggravating the process of intervertebral disc degeneration. In this work, we successfully synthesized the thermosensitive injectable celecoxib-loaded chitosan hydrogel and investigated its material properties, repair effect, biocompatibility, and histocompatibility in *in vitro* and in vivo study. *In vitro* and in vivo, the hydrogel has low toxicity, biodegradability, and good biocompatibility. In an animal experiment, this composite hydrogel can effectively fill local tissue defects to maintain the stability of the spine and delay the process of intervertebral disc degeneration after surgery. These results indicated that this composite hydrogel will be a promising way to treat postoperative intervertebral disc disease in future clinical applications.

Keywords: intervertebral disc degeneration, celecoxib, lumbar disc herniation, chitosan hydrogel, percutaneous endoscopic lumbar discectomy

INTRODUCTION

Low back pain (LBP) is one of the common conditions which everyone experiences in their lifetime (Yang;Zhang;Ma and Ding, 2020; Van Zundert and Cohen, 2021). LBP has been regarded as a significant global public health problem, which was given more attention with the development of society (Tendulkar;Chen;Ehnert;Kaps and Nüssler, 2019). Studies indicated that intervertebral disc degeneration (IDD) is the most common reason for LBP (Kos;Gradisnik and Velnar, 2019).

The intervertebral disc (IVD) is the complex tissue including the jelly-like elastic nucleus pulposus, which is surrounded by layers of collagen fibers, the annulus fibrosus (AF), together with cartilaginous and bony end-plates (Liyew, 2020; Urban and Fairbank, 2020). The NP, one of the most critical components of the IVD, provides an avascular hypoxic microenvironment to support chondrocyte-like cells in a proteoglycan and type II collagen-rich ECM, regulating disc functions and deformation (Cannata et al., 2020). The AF is the circumferential ring that withstands the tension created during IVD deformation, which is enabling the uniform distribution and transfer of

compressive loads between the vertebral bodies. The cartilaginous and bony end-plates are the thin layers of hyaline cartilage placed between the IVD and the adjacent vertebral bodies, which is the main approach for nutrient supply to all IVD cells through diffusion, as well as removal of waste products. With the development of IDD, the annulus fibrosus will be broken, with the consequence of the protrusion of the nucleus pulposus (NP), which is called lumbar disc herniation (LDH) (Chen;Tseng;Sun; Chang and Chen, 2021; Deng et al., 2021). Patients with LDH usually present with symptoms such as pain, numbness, and weakness, which have a significant negative influence on their social functions. Percutaneous endoscopic lumbar discectomy (PELD) was first introduced in 1992 and has been widely used in clinical practice for lumbar spine diseases due to less invasiveness and faster recovery than traditional surgery (Aprile;Amato and de Oliveira, 2020; Hu;Zheng;Chen and Chen, 2020; Tacconi;Baldo; Merci and Serra, 2020).

The PELD can significantly release nerve compression and attenuate pain caused by the protrusion of the nucleus pulposus. But the trauma of tissue caused by the operation will induce inflammation in local tissue. Also, the defect of AF is that it can no longer keep the NP residue in place, leading to pain recurrence due to NP re-herniation. The control of postoperative pain depends on oral drugs, such as celecoxib. However, oral medication alone cannot provide effective concentrations locally, and for some patients, such as those with gastric ulcers, hypertension, and cardiovascular accident, there are unavoidable additional side effects (Kocak et al., 2019; Patel et al., 2019; Schectman, 2020). Controllable release of celecoxib could decrease potential side effects and allow less administration. Other methods, such as physical therapy strengthening and muscle training, are also considered to improve clinical symptoms after surgery, but there is no effective research and clinical effect statistics supporting this. Therefore, injecting anti-inflammatory functional materials into the defect tissue after discectomy is a feasible strategy to control the inflammation microenvironment locally (Wang et al., 2019; Borrelli and Buckley, 2020).

The chitosan hydrogel is a novel choice as a carrier for controllable release of anti-inflammatory drugs due to its similarity to the natural extracellular matrix and excellent biocompatibility (Alinejad et al., 2019; Zhang et al., 2021). In addition, the thermosensitive injectable chitosan-based hydrogel can be used for local treatment and is beneficial for the repair of tissue defects. Celecoxib is a new generation of non-steroidal anti-inflammatory and analgesic drugs, which is one of the commonly used anti-inflammatory and pain-relieving drugs in the orthopedic clinic. It can inhibit the production of prostaglandins by selectively inhibiting cyclooxygenase-2 (COX-2) to achieve anti-inflammatory and analgesic effects. The hydrogel delivery system could increase the release of celecoxib and further improve bioavailability, avoid burst drug release, and reduce toxicity and side effects. In this study, we designed a thermosensitive injectable chitosan hydrogel-based celecoxib (TICHC) delivery system with injectability and fixation properties to prevent NP re-protrusion and degeneration after discectomy. After injection, the thermosensitive composite chitosan-based hydrogel could repair the defect and provide the necessary mechanical support after being crosslinked, alleviating the degeneration process aggravated by mechanical changes. The locally released celecoxib could inhibit the postoperative inflammatory response of residual tissue and effectively delay the development of degeneration (**Figure 1**). Finally, the thermosensitive injectable chitosan-based hydrogel has been widely applied and intensively studied, and its safety and reliability have been widely verified, thus supporting its clinical application in the future.

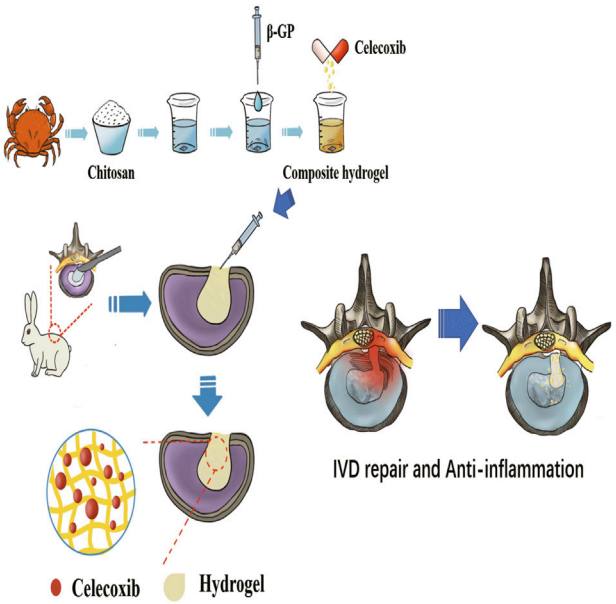

FIGURE 1 | The schematic diagram of the preparation process of thermosensitive injectable celecoxib-loaded chitosan hydrogel and its effect on preventing the recurrence of lumbar disc herniation and pain after partial discectomy.

METHODS AND MATERIALS

Materials

Celebrex (CAS: 169590-42-5), chitosan (degree of deacetylation: 95%; molecular weight: 20 w; CAS: 9012-76-4), and β-glycerophosphate (β-GP) (CAS: 154804-51-0) were all purchased from Sigma-Aldrich (St. Louis, United States).

Synthesis of TICHC

The 2, 3, and 5 g chitosan powder were, respectively, weighed and dissolved with 0.1 mol dilute hydrochloric acid. A total of 5.6 g of β-glycerophosphate sodium (β-GP) powder was weighed and dissolved in 10 ml ultrapure water with the assistance of magnetic stirring. A 56% β-GP solution was obtained and sterilized by using a filter membrane (22 μm) and stored in the refrigerator at 4°C for further experiment. A total of 1 g of Celecoxib powder was weighed and dissolved in 50 ml ultrapure water with the assistance of magnetic stirring. 1 ml of 56% β-GP solution was,

respectively, added to 9 ml of 2%, 3%, and 5% chitosan solutions with slow stirring. According to the previous relevant literature, a total of 1–1.5 ml of 2% celecoxib solution was added to 9 ml of 2% chitosan solution with constant stirring (Choi et al., 2020).

Characterization of TICHC

After freeze-drying, the chitosan hydrogel samples with different concentrations were fixed on the specimen platform. The samples were covered with gold produced by the sputter coater, and its morphology was observed by using a scanning electron microscope (SEM). Different parts of the hydrogels were randomly selected for further analyses of celecoxib and the hydrogel. Therefore, the hydrogels were analyzed by using an energy dispersive spectrometer (EDS) to observe the distribution of celecoxib in chitosan hydrogels. After coating gold on the surface of the sample, samples were placed into the sample chamber of the scanning electron microscope, and its morphology was observed with 15 kV accelerating voltage. The qualitative and semi-quantitative analyses of samples were conducted by using an X-ray energy spectrum analyzer.

The Temperature Sensitivity Study of TICHC

According to the former study, a total of 3 ml TICHC was placed into sample tubes. Then, the tubes were placed in 37°C incubators to analyze temperature-sensitive characteristics of the hydrogel using the tube inversion method.

The Injectability Study of TICHC

Samples of 5 ml liquid 2% TICHC were, respectively, extracted by using a 10-ml syringe. The 10-ml syringe was used to inject hydrogel with the appropriate force to simulate the injection process *in vivo*.

Cell Viability

In order to evaluate the cytocompatibility of TICHC samples, the cytotoxicity was analyzed by using the cell counting kit (CCK; Sigma-Aldrich Co., Ltd., United States) and the Hoechst staining experiment (Sigma-Aldrich Co., Ltd., United States), respectively. The different extraction concentrations of hydrogel samples were divided into three groups including the control group, 50% extraction group, and 25% extraction group. The cultured L929 cells were dissociated to obtain a single cell after adding trypsin. After 1, 3, and 5 days of culture, the fresh medium and CCK reagent were added and incubated for 30 min at 37°C after the removal of the old medium. Then, the measurement of absorbance was conducted at 450 nm. After adding the hydrogel solution for 5 days, 10 ug/ml Hoechst 33342 staining solution was added to the plate at 37°C for 15 min. The cell cultured glass was fixed with 4% paraformaldehyde for 15 min and then washed with PBS solution three times to be observed under a fluorescence microscope (Leica DMI4000B, Germany).

The Biocompatibility and Degradability Analysis

Eighteen female New Zealand rabbits (6 months old, approximately 2.0–2.5 kg) were provided from the animal center of Binzhou Medical University (Yantai, China) and were used to analyze the biocompatibility and degradability of hydrogel *in vivo*. Eighteen rabbits were divided into 3 groups, 6 in each group. They were the control group, the hydrogel group, and the drug-loaded hydrogel group, respectively. About 3 ml of normal saline, chitosan hydrogel, or drug-loaded hydrogel was injected subcutaneously in the front of the thigh of each New Zealand white rabbit, depending on its group. After injection, 2 rabbits in each group were selected and the skin of the right thigh was cut at 2 weeks, 1 month, and 2 months after injection. The histocompatibility and degradation of the hydrogel samples *in vivo* were observed.

Animal Surgery

This study was approved by the Affiliated Hospital of Qingdao University Ethics Committee. The animal experiment and feed were in accordance with the guidelines of the animal center of the Binzhou Medical University, Yantai, Shandong. The fifteen New Zealand rabbits (5–6 months, 2.0–2.5 kg) in the in vivo study were obtained from the animal center of Binzhou Medical University. They were divided into three groups based on the different times including 2 weeks, 1 month, and 2 months. Five rabbits were selected to conduct the X-ray and MRI at different times. All rabbits were housed in single cages under controlled conditions (17–23°C, and 30–70% air humidity with appreciative air circulations) and provided with adequate feed and water. All rabbits fasted for 12 h and were forbidden water for 6 h before anesthesia. Each rabbit was fixed into the anesthesia box to be anesthetized by urethane through the marginal ear vein and the penicillin was injected before the operation. The rabbit was placed on the small operation table in the left lateral position. After the removal of the fur from the dorsal surface, the anterolateral intervertebral disc 2–6 were, respectively, exposed through an anterolateral approach by blunt dissection of muscles. The IDD model of rabbits was obtained by using a 20G needle puncture at L3/4, L4/5, and L5/6, respectively. Each disc was punctured five times by using a needle and continuously aspirated with a 10-ml syringe for 30 s. The annulus fibrosus was punctured to establish the local defect, and the nucleus pulposus was partially sucked by the needle. In order to avoid individual differences, the different lumbar segment of the rabbit was conducted with different interventions on the same rabbit. A total of four groups were established including a control group (L2/3), a degeneration group (L3/4), a chitosan hydrogel treatment group (L4/5), and a chitosan hydrogel–loaded with celecoxib treatment group (L5/6). The 1-ml injection with an 18G needle was used to inject the hydrogel into different intervertebral discs. After the injection of hydrogel, the incision was sutured and the rabbits were placed on the operation table at a constant temperature to wait for recovery. The rabbits were injected with penicillin for 3 consecutive days after surgery.

The X-Ray and MRI Evaluation

The X-ray can show the height changes of each segment to indirectly prove the instability. After 2 weeks, 1 month, and

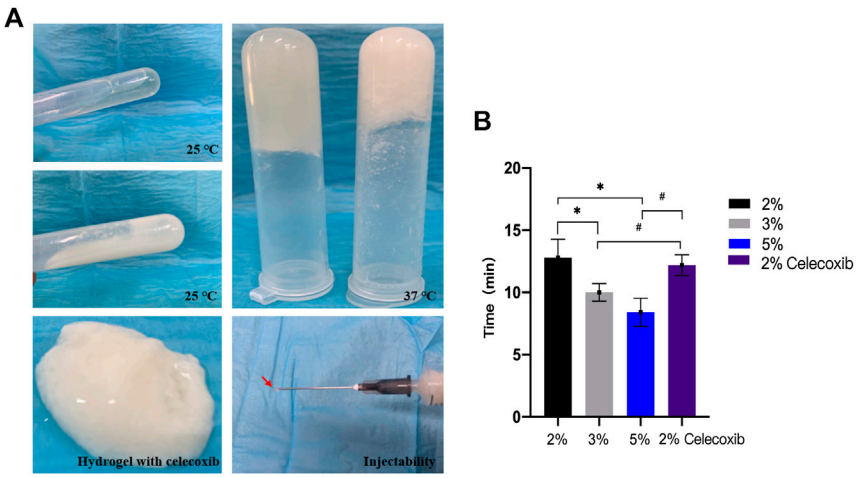

FIGURE 2 | (A) Photographs of *in situ* gel formation of 2 wt% hydrogels (upper left) and hydrogel with celecoxib (middle left) solution with temperature increased from 25°C to 37°C (upper right), gel stability (below left), and injectability (below right). **(B)** The thermosensitive sol-gel conversion time of hydrogel solutions with different concentrations. (*,# = $p < 0.05$).

2 months following the establishment of the IDD model, five rabbits were randomly selected for X-ray and magnetic resonance imaging (MRI) assessments at each time point. The X-ray imaging was performed by an X-ray system (Siemens, German), and the MRI tests were conducted using a 3.0-T MRI system (Siemens, German).

The X-ray and MRI image analysis and measurements were analyzed by two independent radiologists. The Bradner disc index (BDI) was used to evaluate the intervertebral height changes. The modified Thompson classification was used to evaluate the disc degeneration changes by using the T2-weighted MRI images with grades I to IV.

Histological Analysis

The air embolism after anesthesia was used to euthanize the rabbits after 2 months. The spine samples were fixed by using formalin (10%) for 1–3 days, and the different intervertebral discs were, respectively, cut off from the spine. We used EDTA (10%) to decalcify the surrounding bone of intervertebral discs for 1–2 months. We selected the coronal median section of the intervertebral disc for the histological examination. After obtaining the wax-embedded intervertebral disc samples, we, respectively, stained the samples with H&E. The histological classification was conducted based on the observation by using light microscopy.

Statistical Analysis

The data are shown as the mean ± standard deviation (SD). All the experiments were conducted at least three times independently. The data of results were analyzed by SPSS 23.0 statistical software. The statistical significance of the differences between the groups was calculated by using the one-way ANOVA and Tukey's post-hoc test or nonparametric test. $p < 0.05$ is considered to be statistically significant.

RESULTS

Preparation and Characterization of TICHC

The different concentrations of chitosan hydrogel in this study were the liquid state with different viscosity at room temperature. The appearance of chitosan hydrogel loaded with celecoxib was a milk-white liquid at room temperature. For this reason, it can be injected by using a different-sized injector. As shown in **Figures 2A,B**, the thermosensitive chitosan liquid hydrogels with/without celecoxib were able to turn solid at 37°C in 8–15 min. Hence, it was suitable for the repair of intervertebral disc defects through injection in a narrow surgical space. The thermosensitive chitosan liquid hydrogel was able to convert to a solid state at a local defect under the normal body temperature in a short time. As shown in **Figure 3**, the different concentrations of hydrogel showed the porous structure with different densities (higher the concentration, higher the density) by scanning electron microscopy. After comparing the different concentrations of chitosan hydrogel, the 2% hydrogel was more suitable for injection and better porous density. As shown in **Figure 4**, the F (red) and S (green) elements were uniformly distributed within the chitosan hydrogel by EDS, and it was indirect proof that the celecoxib was successfully loaded in the chitosan hydrogel.

In order to evaluate its liquid–solid transformation ability, we used the tube inversion method and different time measurement methods to analyze the liquid–solid conversion time of different hydrogels. As shown in **Figure 2B**, the results showed that the liquid–solid conversion time of 2% chitosan hydrogel with/without celecoxib was, respectively, 12.20 ± 0.84 min and 12.80 ± 1.48 min. So, the celecoxib was not able to significantly affect the liquid–solid conversion time of hydrogel. The shortest liquid–solid conversion time was 8.40 ± 1.14 min (5% chitosan hydrogel). The results indicated that the higher concentration chitosan hydrogel had a shorter liquid–solid conversion time. ($p < 0.05$).

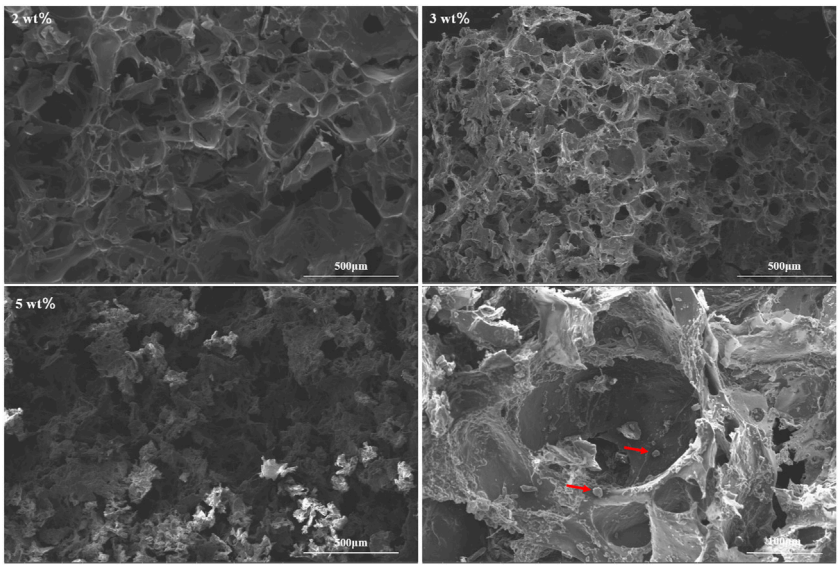

FIGURE 3 | Morphologies of hydrogels with different concentrations of 2, 3, and 5 wt% and celecoxib are observed in the porous hydrogel structure (red arrow).

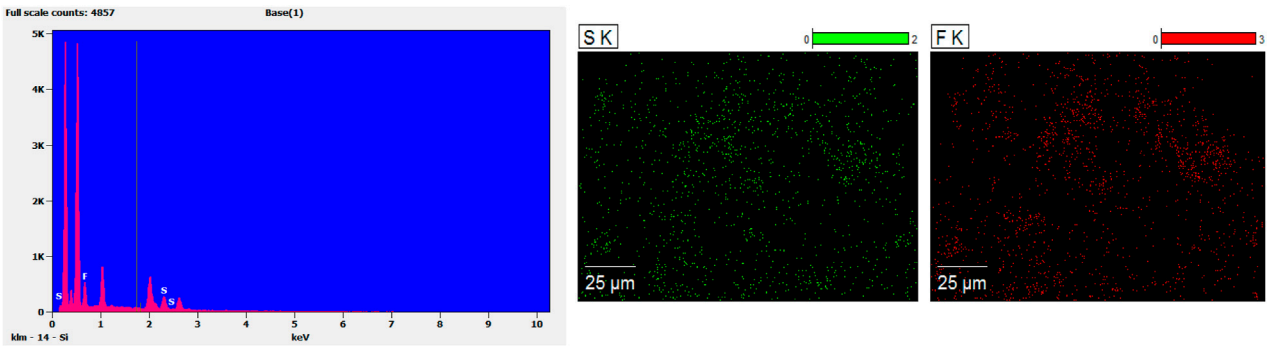

FIGURE 4 | The EDS results showed the F (red) and S (green) were evenly distributed in the hydrogel, and indirectly indicated that the hydrogel had successfully encapsulated celecoxib.

In vitro Toxicity Evaluation

The cytotoxicity of hydrogel was analyzed by using L929 cells. As shown in **Figures 5A,B**, the chitosan hydrogel with/without celecoxib had no significant effect on the proliferation of L929 cells than the control group at 1, 3, and 5 days of incubation. Moreover, the high concentration extracts of chitosan hydrogel loaded with celecoxib slightly inhibited the proliferation of L929 cells, displaying 79.56 ± 3.55%, 71.35 ± 1.39%, and 70.56 ± 6.10% cell viability for the hydrogel solution with the prolongation of culture time. Overall, the hydrogel with/without celecoxib solutions showed low cellular toxicity.

A live/dead staining assay of L929 cells was conducted using Hoechst 33342 to further confirm the cellular toxicity of hydrogels. Hoechst 33342 is a blue fluorescent dye with low toxicity, which is able to penetrate the cell membrane of the cell. The fluorescence microscopy was used to observe the proliferation of L929 cells after dyeing. As shown in **Figure 5C**, the results showed that the cell numbers of the three samples had no significant difference. Compared with the control group, there was no significant reduction of cell numbers in the hydrogel with/without celecoxib simples. The results indicated that the hydrogel loaded with celecoxib has satisfying biocompatibility and is a suitable injectable biomaterial for biomedical fields.

In vivo Toxicity Evaluation

There was no significant infection in 18 rabbits after local hydrogel injection. In 2 weeks, there was no normal saline residue under the skin of the rabbits in the control group. No significant infection was found in the subcutaneous fascia and surrounding muscles. So, it was not necessary for further observation of the rest rabbits in the control group. As shown in **Figure 6**, there was obvious hydrogel residue under the skin of the rabbits of the other two groups for 2 weeks.

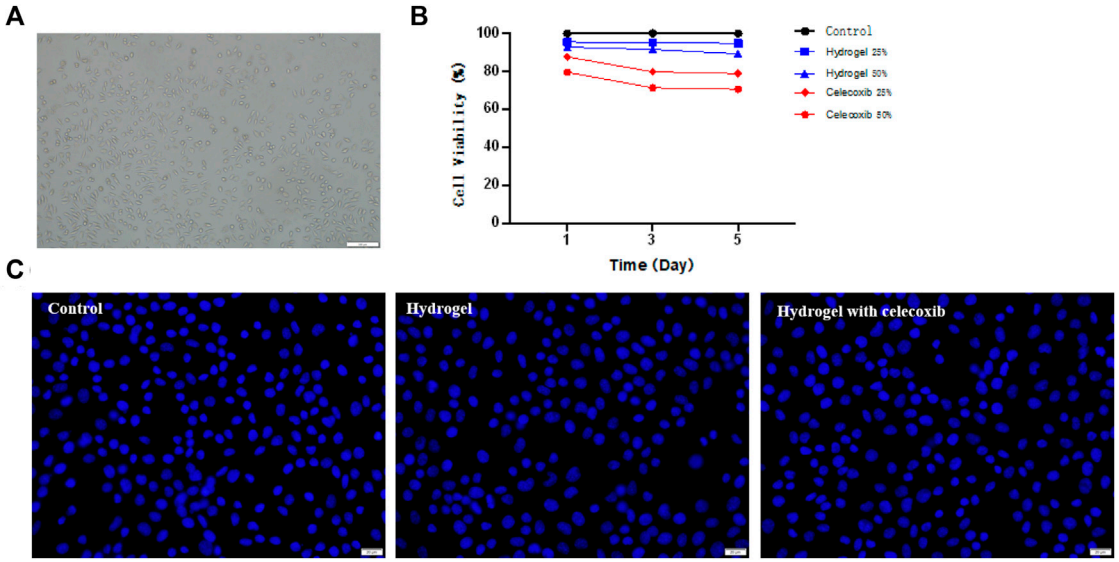

FIGURE 5 | (A) The culture and proliferation of L929 cells. **(B)** The CCK-8 test of hydrogels. **(C)** The Hoechst staining experiment of cells cultured on the different groups.

FIGURE 6 | The degradation and histocompatibility analysis of hydrogel implanted subcutaneously at time of 2 weeks, 1 month, and 2 months after injection.

Moreover, there was no sign of infection with the obvious distinction between hydrogel residue and surrounding tissue. With the extension of observation time, the hydrogel residues were gradually degraded under the skin, and there was no obvious hydrogel residue under the skin in 2 months. The results indicated that the injectable thermosensitive celecoxib-loaded chitosan hydrogel was able to be used as non-toxic material with good biocompatibility and histocompatibility for biomedical application.

In vivo Study by X-Ray and MRI

In a total of two New Zealand white rabbits, death occurred in the process of anesthesia and post-operation. There was no obvious sign of infection, and all rabbits were in good condition after surgery. The postoperative X-ray and MRI showed the success of the establishment of the intervertebral disc degeneration model by needle puncture. Therefore, the composite hydrogel showed good sealing properties of the AF defect by injecting the exogenous hydrogel.

Postoperative X-rays can visually display the intervertebral disc height. The postoperative intervertebral disc height changes were judged using the Bradner disc index (BDI). In addition, the intervertebral disc degeneration can be evaluated by the observation of sagittal MRI T2-weighted image. At 2 weeks, 1 month, and 2 months after the initial surgery, the X-ray imaging showed that a relatively normal BDI was maintained in the hydrogel treatment groups than in the degeneration group (**Figures 7A,B**) ($p < 0.05$). Moreover, the degeneration group had a weaker MRI signal than the hydrogel

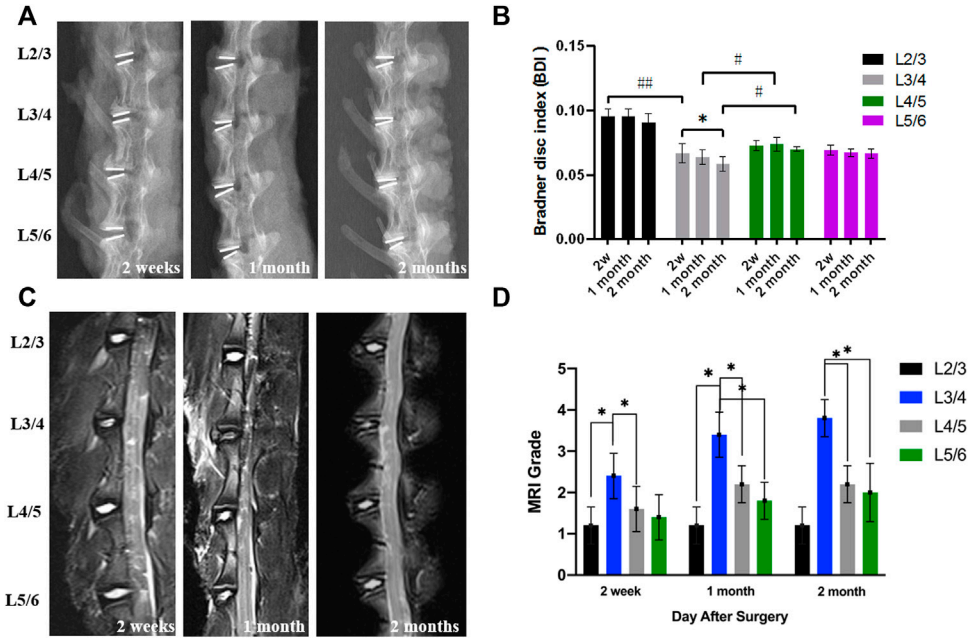

FIGURE 7 | (A) The representative X-ray images. **(B)** The BDI changes in different groups after surgery. **(C)** The representative MRI shows the intervertebral disc signal intensity of different groups. **(D)** The MRI grade changes of different groups after the operation (*,# = $p < 0.05$).

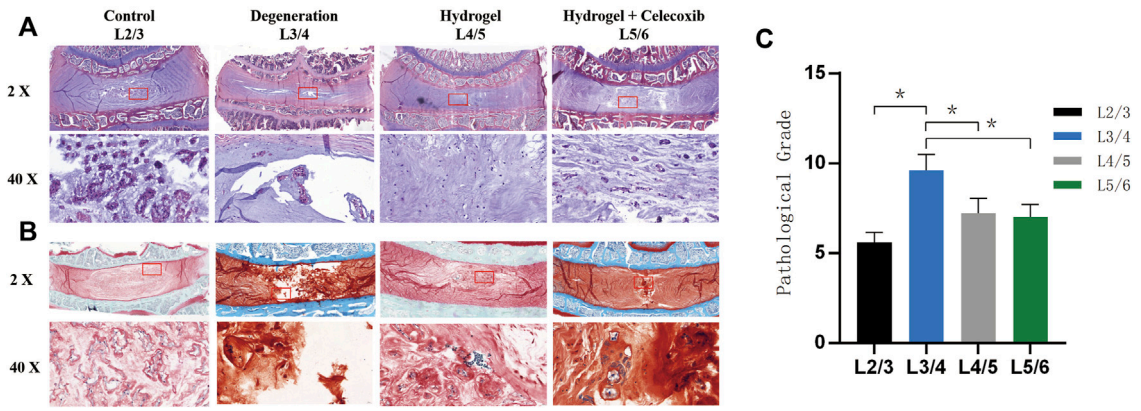

FIGURE 8 | Morphological staining *in vivo*. **(A)** The representative paraffin sections with H&E. **(B)** The representative paraffin sections with H&E. **(C)** The histological grades of different groups after the operation (*,# = $p < 0.05$).

treatment groups after the operation (**Figures 7C,D**). With the extension of time, the difference became more obvious. However, the intervertebral height and the degeneration grade of IVD still gradually decreased in hydrogel groups than in the degeneration group.

The Histological Analysis of Intervertebral Discs

The H&E staining (**Figure 8A**) and safranin O-fast green staining (**Figure 8B**) were able to show the chromatin in the cell nucleus, cytoplasmic ribosome, cytoplasm, and the extracellular matrix. Normal nucleus pulposus tissue after staining can clearly show the NP cells and onion-shaped AF. As shown in **Figure 8**, the staining showed an obvious decrease in NP cells and height of IVD with a local defect in the degeneration group. However, there still was NP cell residue in the center of IVD without an obvious local defect in the hydrogel loaded with the celecoxib group. The histological grade was 9.6 ± 0.9 in the degeneration group and 7.0 ± 1.0 in the hydrogel loaded with the celecoxib group (**Figure 8C**). In the hydrogel loaded with the celecoxib group, there was no significant difference in histological grade compared with the hydrogel group, but it was worse than that in the control

group. In addition, the number of NP cells can be observed by staining. Compared with the degeneration group, there were more NP cells residual in hydrogel groups which is beneficial for delaying the progress of IVD.

DISCUSSION

According to some studies, the recurrence of lumbar disc herniation is one of the main reasons for postoperative leg pain after lumbar discectomy (Hao et al., 2020; Paulsen;Rasmussen;Carreon and Andersen, 2020). At present, most scholars think the local defect of the annulus fibrosus is one of the pathogeny element of the recurrent lumbar disc herniation and reoperation. Because of the postoperative annulus fibrosus defect, the residual nucleus pulposus has a high risk of disc prolapse after surgery, especially for young patients with strong activities. Some studies showed that the incidence of recurrent lumbar disc herniation could reach nearly 62% after surgery (Huang;Han;Liu;Yu and Yu, 2016; Yaman;Kazancı;Yaman; Baş and Ayberk, 2017; Shin;Cho;Kim and Park, 2019). In addition, the intervertebral disc degeneration will be accelerated due to the damage caused by PELD, leading to the local spinal instability. Thus, the effective measures to prevent the re-protrusion of the intervertebral disc are the key issues for surgeons after PELD.

In addition, inflammation is also an important aspect that cannot be neglected in postoperative leg pain. Studies showed that the inflammatory response will be formed by the accumulation of neutrophils and lymphocytes (Djuric et al., 2019; Peng et al., 2019). The molecular mediators of inflammation, such as IL-1β, IL-6, and TNF-α, will be released to cause the inflammation (Huang et al., 2018;Ford;Kaddour;Gonzales;Page and Hahne, 2020). In fact, studies also showed that the degeneration grade of IVD was aggravated by the accumulation of inflammatory cytokines. TNF-α and IL-1β are the important inflammatory factors for intervertebral disc degeneration, which can induce intervertebral disc degeneration by reducing the anabolism of extracellular matrix proteins (Chen; Hodges;James and Diwan, 2021; Kim;Hong;Lee;Jeon and Ha, 2021). TNF-α is able to inhibit the production of extracellular matrix and increase the expression of MMP-3, MMP-9, and MMP-13. The extracellular matrix synthesis could decrease because of affected mitochondrial function and protein synthesis caused by inflammatory mediators (Lambrechts et al., 2021). Moreover, the expression of MMPs and ADAMTSs could also be affected by inflammatory mediators, leading to the degradation of collagen-2 and aggrecan. Spinal instability can be caused by the decreased extracellular matrix and reduced moisture content. Due to the important pathological role of inflammation after discectomy, it is very important to control postoperative inflammation.

Celecoxib is a selective COX-2 inhibitor, with the effect of anti-inflammatory and analgesic (Choi et al., 2020). Due to the characteristics of its chemical structure, it can be combined with COX-2 to inhibit COX-2 in the conversion of arachidonic acid to prostaglandins. It has a good anti-inflammatory analgesic with the protection of gastric mucosa. However, studies showed that systemic medication can increase the risk of serious cardiovascular thrombotic events including myocardial infarction and stroke for patients with pre-existing cardiovascular disease (Zhou et al., 2020). Some studies have already shown that the local management using celecoxib not only had an anti-inflammatory effect but also avoided the systemic adverse effects (Salgado;Guénée;Černý;Allémann and Jordan, 2020).

Considering the narrow operation space, we designed and developed the injectable thermosensitive composite chitosan-based hydrogel as the drug delivery system to attenuate local inflammation and improve degeneration in order to meet the clinical requirement. The composite hydrogel also can sustain mechanical stability by repairing the local defect after surgery. Unlike other light-sensitive materials, our thermosensitive chitosan-based hydrogel can crosslink at body temperature in a short time. We can also use electrocoagulation to reduce the crosslink time in operation.

Chitosan is widely used in biomedicine and preparation because of its biodegradability, low toxicity, and good biocompatibility (Gullbrand et al., 2017; Li et al., 2018). The degradation products of chitosan can be absorbed without accumulation or immunogenicity in the body (George;Tandon and Kandasubramanian, 2020; Qu and Luo, 2020). In recent years, studies on the role of chitosan in cartilage repair are also gradually being carried out (Rusu et al., 2019; George;Tandon and Kandasubramanian, 2020). NP cells are the main components of NP, belonging to the chondroid cells, which can secrete aggrecan and type-II collagen to synthesize extracellular matrix and then maintain the stability of NP (Liu et al., 2020). Theoretically, the gel made of chitosan is also suitable for the nucleus pulposus scaffold of the IVD nucleus pulposus cells. Roughley et al. inoculated and cultured NP cells on the prepared chitosan hydrogel (Roughley et al., 2006). They found that chitosan hydrogel has no obvious inhibitory effect on the proliferation of nucleus pulposus cells, maintaining its phenotype and promoting the growth of the extracellular matrix. In this study, these advantages of chitosan allowed NP cells to normally proliferate and had no obvious adverse effects on cells. The in vivo experiment results also indicated that the chitosan-based hydrogel had effects on the delay of degeneration of IVD to some extent. In addition, the crosslinked chitosan hydrogel is able to maintain a specific local concentration of celecoxib. The porous structure of chitosan hydrogel can provide space to contain and protect celecoxib to improve its bioavailability. In addition, the slowed degradation of the hydrogel further prolonged the drug release time.

All in all, postoperative leg pain can be caused by numerous reasons. Because of the complex structure and function of the intervertebral disc, the in vitro and animal experiments hardly simulate the actual situation encountered in clinical practice. Indeed, biomechanical tests can well explain the problem of preventing re-herniation, and biomechanical tests will continue to be added in the future. We will try large mammal animal models (such as monkeys and sheep) to better evaluate the application potential of more bioremediation materials. In the future, it is also necessary to explore the research of biological materials to repair intervertebral discs at the genetic level.

CONCLUSION

In this experiment, we successfully synthesized a chitosan-based hydrogel loaded with celecoxib with thermo-

sensitivity, injectability, and anti-inflammatory characteristics. The composite chitosan-based hydrogel, with the characteristics of biodegradability, low toxicity, and good biocompatibility, is able to repair the defect of IVD to prevent postoperative recurrence of disc herniation, to further maintain the stability of the spine, and to delay the IDD to some extent.

DATA AVAILABILITY STATEMENT

The raw data supporting the conclusion of this article will be made available by the authors, without undue reservation.

ETHICS STATEMENT

The animal study was reviewed and approved by the ethics committee of the affiliated hospital of Qingdao University. Written informed consent was obtained from the owners for the participation of their animals in this study.

AUTHOR CONTRIBUTIONS

YD: Methodology, investigation, and writing—original draft. JL: Experiment and writing—review and editing. XT: Experiment, review, and editing. YZ: Review and image editing. YL: Experiment, review, and editing. GB: Experiment. JS: Experiment. BZ: Animal experiment. HZ: Animal experiment. KS: Supervision and writing—review and editing. YX: Supervision and writing—review and editing.

FUNDING

This study was support by Taishan Scholar Project ofShandong Province, China (No. ts20190985).

REFERENCES

Alinejad, Y., Adoungotchodo, A., Grant, M. P., Epure, L. M., Antoniou, J., Mwale, F., et al. (2019). Injectable Chitosan Hydrogels with Enhanced Mechanical Properties for Nucleus Pulposus Regeneration. *Tissue Eng. Part A* 25 (5-6), 303–313. doi:10.1089/ten.TEA.2018.0170

Aprile, B. C., Amato, M. C. M., and De Oliveira, C. A. (2020). Evolução funcional após discectomia endoscópica lombar, uma avaliação mais precoce de 32 casos. *Rev. Bras. Ortop. (Sao Paulo)* 55 (4), 415–418. doi:10.1055/s-0039-3402473

Borrelli, C., and Buckley, C. T. (2020). Injectable Disc-Derived ECM Hydrogel Functionalised with Chondroitin Sulfate for Intervertebral Disc Regeneration. *Acta Biomater.* 117, 142–155. doi:10.1016/j.actbio.2020.10.002

Cannata, F., Vadalà, G., Ambrosio, L., Fallucca, S., Napoli, N., Papalia, R., et al. (2020). Intervertebral Disc Degeneration: A Focus on Obesity and Type 2 Diabetes. *Diabetes Metab. Res. Rev.* 36 (1), e3224. doi:10.1002/dmrr.3224

Chen, K.-T., Tseng, C., Sun, L.-W., Chang, K.-S., and Chen, C.-M. (2021). Technical Considerations of Interlaminar Approach for Lumbar Disc Herniation. *World Neurosurg.* 145, 612–620. doi:10.1016/j.wneu.2020.06.211

Chen, X., Hodges, P. W., James, G., and Diwan, A. D. (2021). Do Markers of Inflammation And/or Muscle Regeneration in Lumbar Multifidus Muscle and Fat Differ between Individuals with Good or Poor Outcome Following Microdiscectomy for Lumbar Disc Herniation? *Spine (Phila Pa 1976)* 46 (10), 678–686. doi:10.1097/brs.0000000000003863

Choi, J.-S., Lee, D.-H., Ahn, J. B., Sim, S., Heo, K.-S., Myung, C.-S., et al. (2020). Therapeutic Effects of Celecoxib Polymeric Systems in Rat Models of Inflammation and Adjuvant-Induced Rheumatoid Arthritis. *Mater. Sci. Eng. C* 114, 111042. doi:10.1016/j.msec.2020.111042

Deng, L., Yang, H., Liu, M., Liang, T., Wang, F., Ning, X., et al. (2021). The Role of Positive Nerve Root Sedimentation Sign in the Treatment of Patients Undergoing Lumbar Disc Herniation. *Br. J. Neurosurg.* 35. 1–6. doi:10.1080/02688697.2021.1923652

Djuric, N., Yang, X., Ostelo, R. W. J. G., van Duinen, S. G., Lycklama à Nijeholt, G. J., van der Kallen, B. F. W., et al. (2019). Disc Inflammation and Modic Changes Show an Interaction Effect on Recovery after Surgery for Lumbar Disc Herniation. *Eur. Spine J.* 28 (11), 2579–2587. doi:10.1007/s00586-019-06108-9

Ford, J. J., Kaddour, O., Gonzales, M., Page, P., and Hahne, A. J. (2020). Clinical Features as Predictors of Histologically Confirmed Inflammation in Patients with Lumbar Disc Herniation with Associated Radiculopathy. *BMC Musculoskelet. Disord.* 21 (1), 567. doi:10.1186/s12891-020-03590-x

George, S. M., Tandon, S., and Kandasubramanian, B. (2020). Advancements in Hydrogel-Functionalized Immunosensing Platforms. *ACS Omega* 5 (5), 2060–2068. doi:10.1021/acsomega.9b03816

Gullbrand, S. E., Schaer, T. P., Agarwal, P., Bendigo, J. R., Dodge, G. R., Chen, W., et al. (2017). Translation of an Injectable Triple-Interpenetrating-Network Hydrogel for Intervertebral Disc Regeneration in a Goat Model. *Acta Biomater.* 60, 201–209. doi:10.1016/j.actbio.2017.07.025

Hao, L., Li, S., Liu, J., Shan, Z., Fan, S., and Zhao, F. (2020). Recurrent Disc Herniation Following Percutaneous Endoscopic Lumbar Discectomy Preferentially Occurs when Modic Changes Are Present. *J. Orthop. Surg. Res.* 15 (1), 176. doi:10.1186/s13018-020-01695-6

Hu, Y., Zheng, Y., Chen, G., and Chen, W. (2020). Comparison of Percutaneous Endoscopic Discectomy and Microendoscopic Discectomy in Treatment of Symptomatic Lumbar Disc Herniation. *Med. Baltim.* 99 (42), e22709. doi:10.1097/md.0000000000022709

Huang, W., Han, Z., Liu, J., Yu, L., and Yu, X. (2016). Risk Factors for Recurrent Lumbar Disc Herniation. *Med. Baltim.* 95 (2), e2378. doi:10.1097/md.0000000000002378

Huang, K.-Y., Hsu, Y.-H., Chen, W.-Y., Tsai, H.-L., Yan, J.-J., Wang, J.-D., et al. (2018). The Roles of IL-19 and IL-20 in the Inflammation of Degenerative Lumbar Spondylolisthesis. *J. Inflamm.* 15, 19. doi:10.1186/s12950-018-0195-6

Kim, H., Hong, J. Y., Lee, J., Jeon, W.-J., and Ha, I.-H. (2021). IL-1β Promotes Disc Degeneration and Inflammation through Direct Injection of Intervertebral Disc in a Rat Lumbar Disc Herniation Model. *Spine J.* 21 (6), 1031–1041. doi:10.1016/j.spinee.2021.01.014

Knezevic, N. N., Candido, K. D., Vlaeyen, J. W. S., Van Zundert, J., and Cohen, S. P. (2021). Low Back Pain. *Lancet* 398 (10294), 78–92. doi:10.1016/s0140-6736(21)00733-9

Kocak, A. O., Ahiskalioglu, A., Sengun, E., Gur, S. T. A., and Akbas, I. (2019). Comparison of Intravenous NSAIDs and Trigger Point Injection for Low Back Pain in ED: A Prospective Randomized Study. *Am. J. Emerg. Med.* 37 (10), 1927–1931. doi:10.1016/j.ajem.2019.01.015

Kos, N., Gradisnik, L., and Velnar, T. (2019). A Brief Review of the Degenerative Intervertebral Disc Disease. *Med. Arch.* 73 (6), 421–424. doi:10.5455/medarh.2019.73.421-424

Lambrechts, M. J., Pitchford, C., Hogan, D., Li, J., Fogarty, C., Rawat, S., et al. (2021). Lumbar Spine Intervertebral Disc Desiccation Is Associated with Medical Comorbidities Linked to Systemic Inflammation. *Arch. Orthop. Trauma Surg.* 141. 1. doi:10.1007/s00402-021-04194-3

Li, Z., Shim, H., Cho, M. O., Cho, I. S., Lee, J. H., Kang, S.-W., et al. (2018). Thermo-sensitive Injectable Glycol Chitosan-Based Hydrogel for Treatment of Degenerative Disc Disease. *Carbohydr. Polym.* 184, 342–353. doi:10.1016/j.carbpol.2018.01.006

Liu, Y., Li, Y., Nan, L.-P., Wang, F., Zhou, S.-F., Feng, X.-M., et al. (2020). Insights of Stem Cell-Based Endogenous Repair of Intervertebral Disc Degeneration. *Wjsc* 12 (4), 266–276. doi:10.4252/wjsc.v12.i4.266

Liyew, W. A. (2020). Clinical Presentations of Lumbar Disc Degeneration and Lumbosacral Nerve Lesions. *Int. J. Rheumatology* 2020, 1–13. doi:10.1155/2020/2919625

Patel, H. D., Uppin, R. B., Naidu, A. R., Rao, Y. R., Khandarkar, S., and Garg, A. (2019). Efficacy and Safety of Combination of NSAIDs and Muscle Relaxants in the Management of Acute Low Back Pain. *Pain Ther.* 8 (1), 121–132. doi:10.1007/s40122-019-0112-6

Paulsen, R. T., Rasmussen, J., Carreon, L. Y., and Andersen, M. Ø. (2020). Return to Work after Surgery for Lumbar Disc Herniation, Secondary Analyses from a Randomized Controlled Trial Comparing Supervised Rehabilitation versus Home Exercises. *Spine J.* 20 (1), 41–47. doi:10.1016/j.spinee.2019.09.019

Peng, H., Tang, G., Zhuang, X., Lu, S., Bai, Y., and Xu, L. (2019). Minimally Invasive Spine Surgery Decreases Postoperative Pain and Inflammation for Patients with Lumbar Spinal Stenosis. *Exp. Ther. Med.* 18 (4), 3032–3036. doi:10.3892/etm.2019.7917

Qu, B., and Luo, Y. (2020). Chitosan-based Hydrogel Beads: Preparations, Modifications and Applications in Food and Agriculture Sectors - A Review. *Int. J. Biol. Macromol.* 152, 437–448. doi:10.1016/j.ijbiomac.2020.02.240

Roughley, P., Hoemann, C., DesRosiers, E., Mwale, F., Antoniou, J., and Alini, M. (2006). The Potential of Chitosan-Based Gels Containing Intervertebral Disc Cells for Nucleus Pulposus Supplementation. *Biomaterials* 27 (3), 388–396. doi:10.1016/j.biomaterials.2005.06.037

Rusu, A. G., Chiriac, A. P., Nita, L. E., Bercea, M., Tudorachi, N., Ghilan, A., et al. (2019). Interpenetrated Polymer Network with Modified Chitosan in Composition and Self-Healing Properties. *Int. J. Biol. Macromol.* 132, 374–384. doi:10.1016/j.ijbiomac.2019.03.136

Salgado, C., Guénée, L., Černý, R., Allémann, E., and Jordan, O. (2020). Nano Wet Milled Celecoxib Extended Release Microparticles for Local Management of Chronic Inflammation. *Int. J. Pharm.* 589, 119783. doi:10.1016/j.ijpharm.2020.119783

Schectman, J. M. (2020). In Non-low Back Musculoskeletal Injuries, NSAIDs and Acetaminophen Reduce Acute Pain. *Ann. Intern Med.* 173 (12), Jc65. doi:10.7326/acpj202012150-065

Shin, E.-H., Cho, K.-J., Kim, Y.-T., and Park, M.-H. (2019). Risk Factors for Recurrent Lumbar Disc Herniation after Discectomy. *Int. Orthop. (SICOT)* 43 (4), 963–967. doi:10.1007/s00264-018-4201-7

Tacconi, L., Baldo, S., Merci, G., and Serra, G. (2021). Transforaminal Percutaneous Endoscopic Lumbar Discectomy: Outcome and Complications in 270 Cases. *J. Neurosurg. Sci.* 64 (6), 531–536. doi:10.23736/s0390-5616.18.04395-3

Tendulkar, G., Chen, T., Ehnert, S., Kaps, H.-P., and Nüssler, A. K. (2019). Intervertebral Disc Nucleus Repair: Hype or Hope? *Ijms* 20 (15), 3622. doi:10.3390/ijms20153622

Urban, J. P. G., and Fairbank, J. C. T. (2020). Current Perspectives on the Role of Biomechanical Loading and Genetics in Development of Disc Degeneration and Low Back Pain; a Narrative Review. *J. Biomechanics* 102, 109573. doi:10.1016/j.jbiomech.2019.109573

Wang, F., Nan, L.-p., Zhou, S.-f., Liu, Y., Wang, Z.-y., Wang, J.-c., et al. (20192019). Injectable Hydrogel Combined with Nucleus Pulposus-Derived Mesenchymal Stem Cells for the Treatment of Degenerative Intervertebral Disc in Rats. *Stem Cells Int.* 2019, 1–17. doi:10.1155/2019/8496025

Yaman, M. E., Kazancı, A., Kazancı, A., Yaman, N. D., Baş, F., and Ayberk, G. (2017). Factors that Influence Recurrent Lumbar Disc Herniation. *Hong Kong Med. J.* 23 (3), 258–263. doi:10.12809/hkmj164852

Yang, S., Zhang, F., Ma, J., and Ding, W. (2020). Intervertebral Disc Ageing and Degeneration: The Antiapoptotic Effect of Oestrogen. *Ageing Res. Rev.* 57, 100978. doi:10.1016/j.arr.2019.100978

Zhang, C., Gullbrand, S. E., Schaer, T. P., Boorman, S., Elliott, D. M., Chen, W., et al. (2021). Combined Hydrogel and Mesenchymal Stem Cell Therapy for Moderate-Severity Disc Degeneration in Goats. *Tissue Eng. Part A* 27 (1-2), 117–128. doi:10.1089/ten.TEA.2020.0103

Zhou, J., Xiong, W., Gou, P., Chen, Z., Guo, X., Huo, X., et al. (2020). Clinical Effect of Intramuscular Calcitonin Compared with Oral Celecoxib in the Treatment of Knee Bone Marrow Lesions: a Retrospective Study. *J. Orthop. Surg. Res.* 15 (1), 230. doi:10.1186/s13018-020-01746-y

Conflict of Interest: The authors declare that the research was conducted in the absence of any commercial or financial relationships that could be construed as a potential conflict of interest.

Publisher's Note: All claims expressed in this article are solely those of the authors and do not necessarily represent those of their affiliated organizations, or those of the publisher, the editors, and the reviewers. Any product that may be evaluated in this article, or claim that may be made by its manufacturer, is not guaranteed or endorsed by the publisher.

frontiers | Frontiers in Bioengineering and Biotechnology

ORIGINAL RESEARCH
published: 12 July 2022
doi: 10.3389/fbioe.2022.929699

Early Pixel Value Ratios to Assess Bone Healing During Distraction Osteogenesis

Qi Liu[1,2†], Haibo Mei[3†], Guanghui Zhu[3], Ze Liu[1,2], Hongbin Guo[1,2], Min Wang[4], Jieyu Liang[1,2] and Yi Zhang[1,2*]*

[1]Department of Orthopaedics, Xiangya Hospital, Central South University, Changsha, China, [2]National Clinical Research Center for Geriatric Disorders, Xiangya Hospital, Central South University, Changsha, China, [3]Department of Pediatric Orthopedics, Hunan Children's Hospital, Pediatric Academy of University of South China, Changsha, China, [4]Department of Endocrinology, Xiangya Hospital, Central South University, Changsha, China

OPEN ACCESS

Edited by:
Jun Lin,
First Affiliated Hospital of Soochow University, China

Reviewed by:
Sien Lin,
The Chinese University of Hong Kong, China
Weimin Shen,
Children's Hospital of Nanjing Medical University, China

***Correspondence:**
Yi Zhang
zhangyi0205@csu.edu.cn
Jieyu Liang
jamesliang8@aliyun.com

[†]These authors have contributed equally to this work and share the first authorship

Specialty section:
This article was submitted to Biomaterials, a section of the journal Frontiers in Bioengineering and Biotechnology

Received: 27 April 2022
Accepted: 13 June 2022
Published: 12 July 2022

Citation:
Liu Q, Mei H, Zhu G, Liu Z, Guo H, Wang M, Liang J and Zhang Y (2022) Early Pixel Value Ratios to Assess Bone Healing During Distraction Osteogenesis. Front. Bioeng. Biotechnol. 10:929699. doi: 10.3389/fbioe.2022.929699

Background: Distraction osteogenesis (DO) is an approach for bone lengthening and reconstruction. The pixel value ratio (PVR), an indicator calculated from X-ray images, is reported to assess the final timing for the external fixator removal. However, the early PVR and its potential influencing factors and the relationship between the early PVR and clinical outcomes are rarely discussed. Therefore, this study was employed to address these issues.

Methods: A total of 125 patients with bone lengthening were investigated retrospectively. The early PVR of regenerated bone was monitored in the first 3 months after osteotomy. The potential effect of sex, chronological age, BMI, lengthening site, and involvement of internal fixation during the consolidation period was analyzed. Moreover, the associations of the healing index (HI) and lengthening index (LI) with early PVR were also investigated.

Results: The early PVRs were 0.78 ± 0.10, 0.87 ± 0.06, and 0.93 ± 0.06 in the first 3 months after osteotomy, respectively. Moreover, the PVR in juvenile was significantly higher than that in adults in the first 3 months after osteotomy (0.80 ± 0.09 vs. 0.74 ± 0.10; $p = 0.008$), (0.89 ± 0.06 vs. 0.83 ± 0.06; $p = 0.018$), and (0.94 ± 0.05 vs. 0.87 ± 0.05; $p = 0.003$). In addition, the PVR in males was significantly higher than that in females in the first month after osteotomy (0.80 ± 0.09 vs. 0.76 ± 0.10; $p = 0.015$), and the PVR in femur site was significantly higher than that in the tibia site in the second and third months after osteotomy (0.88 ± 0.07 vs. 0.87 ± 0.06; $p = 0.015$) and (0.93 ± 0.06 vs. 0.92 ± 0.06, $p = 0.037$). However, the BMI and involvement of the internal fixator during the consolidation period seem to not influence the early PVR of regenerated callus during DO. Interestingly, the early PVR seems to be moderately inversely associated with HI (mean = 44.98 ± 49.44, r = -0.211, and $p = 0.029$) and LI (mean = 0.78 ± 0.77, r = -0.210, and $p = 0.029$), respectively.

Conclusion: The early PVR is gradually increasing in the first 3 months after osteotomy, which may be significantly influenced by chronological age, sex, and the lengthening site. Moreover, the early PVR of callus may reflect the potential clinical outcome for DO. Our results may be beneficial to the clinical management of the subjects with bone lengthening.

Keywords: distraction osteogenesis, bone lengthening, pixel value ratio, X-ray, external fixator

1 INTRODUCTION

Distraction osteogenesis (DO) is an approach for bone lengthening and reconstruction. Generally speaking, the regeneration system in living tissue is activated under a physiological continuous, stable, and slow distraction force: the bone and its attached muscles, fascia, blood vessels, and nerve tissue grow synchronously. This technique is utilized to treat severely damaged limb tissues and complicated orthopedic disorders (Malkova and Borzunov, 2021). Basically, DO is an effective treatment for significant bone defects, limb shortening, bone non-union, limb deformities, and neurovascular skin injuries (Shchudlo et al., 2017).

Currently, a variety of evaluation methods have been employed to monitor bone lengthening during DO, including standard radiography (X-ray), dual-energy X-ray absorptiometry (DXA), quantitative computed tomography (QCT), ultrasound, biomechanical evaluation, and biochemical markers (Tesiorowski et al., 2005; Babatunde et al., 2010). In general, the cost and radiation of QCT and DXA are high, and the scope of their application is also limited (Babatunde et al., 2010; Engelke et al., 2013; Anna et al., 2021). Moreover, ultrasound cannot penetrate the cortex of mature bone, and the limb line of force is not intuitive enough to be presented either (Eyres et al., 1993). Biomechanical testing is usually considered for laboratory fundamental research (Floerkemeier et al., 2005; Ishimoto et al., 2011). Nevertheless, X-ray is the most common choice for being inexpensive and convenient. However, this evaluation is relatively subjective (relied on the experience of clinicians) (Starr et al., 2004; Anand et al., 2006). Therefore, an objective quantitative assessment based on X-ray is quite needed.

The pixel value (PV) is an assessment of the bone mineral density in pixels. On this basis, the pixel value ratio (PVR) is calculated by comparing the PV of regenerated bone with that of the adjacent bone (Bafor et al., 2020). Hazra et al. (2008) found that there was a good correlation between the BMD (bone mineral density) ratio and PVR, which suggested decent reliability of the PVR. The density of the regenerated bone increases with healing and leads to a higher PVR (approach to 1). Furthermore, the PVR can be calculated in the clinical setting without any additional expense or radiation for the patient, which makes it a potentially attractive method to objectively measure the status of regenerated bone healing. Therefore, PVR is a quantifiable, convenient and reliable evaluative indicator to monitor the formation of newborn callus.

To the best of our knowledge, PVR is mainly utilized to assess the maturity of the late callus and to confirm the timing to remove the external fixator (Hazra et al., 2008; Zhao et al., 2009; Song et al., 2012; Vulcano et al., 2018; Bafor et al., 2020). However, the early PVR of the callus during DO is rarely discussed. Importantly, the early PVR can assess the progress of callus maturation, which may be important for deciding the lengthening speed during the early DO stage (slow down or speed up the lengthening). Moreover, it has been reported that age, sex, BMI, lengthening site, and the involvement of internal fixation during the consolidation period may significantly affect osteogenesis (Mehta et al., 2011; Sun et al., 2011; Ko et al., 2019; Zak et al., 2021), which may further exert impact on PVR as a consequence. On the other hand, the lengthening index (LI) is the number of months required to achieve 1 cm lengthening, whereas the healing index (HI) is calculated as the duration of complete consolidation in days divided by the length gained in centimeters. Both LI and HI are reliable indicators of the bone healing potential (Koczewski and Shadi, 2013; Wright et al., 2020). However, the associations of LI and HI with early PVR have never been explored yet. Therefore, this study was employed to investigate: 1) the early PVR of the callus in bone lengthening; 2) the potential influencing factors for the early PVR; and 3) the associations of LI and HI with the early PVR of the callus.

2 MATERIALS AND METHODS

2.1 Study Design and Patients

This study was approved by the ethics committee of the Xiangya Hospital of Central South University. We retrospectively reviewed the clinical and imaging data of patients who completed bone lengthening in the Xiangya Hospital of Central South University and Hunan Children's Hospital from January 2010 to December 2021. The inclusion criteria were as follows: 1) lower limb lengthening by using the Ilizarov technique; 2) primary surgery; and 3) patients with successful bone lengthening. The exclusion criteria were as follows: 1) patients with the bone non-union or delayed union; 2) patients with a skeletal disorder affecting the healing index, for example, congenital pseudarthrosis of the tibia; and 3) patients with missing follow-up data. Finally, a total of 125 subjects were recruited for our study. A chart for the study design has been shown in **Figure 1**.

2.2 Surgical Method

All patients were operated on by experienced surgeons, and the Ilizarov technique was used for bone lengthening in the femur and tibia. The patients were subjected with or without the involvement of an internal fixator during the consolidation period (after reaching the final length) randomly. As a consequence, 72 patients were kept with an external fixator until the callus was completely healed, whereas 53 patients were replaced with an internal fixator during the consolidation period. The distraction was initiated 1 week after the osteotomy (at the speed of 0.75–1 mm per day). Then, the patients were examined by X-ray monthly. The conditions to end the bone lengthening and remove the external fixator are listed as follows (patients kept with external fixator): 1) bridging callus is shown on three of the four cortices based on the anteroposterior and lateral X-ray photos of the extension segment; 2) the fixation time is generally in line with the average extension index (the total fixation time of the external fixator is the average time of soft callus consolidation calculated from the date of lengthening. Each 1 cm is fixed for 1 month, called the average extension index); and 3) no

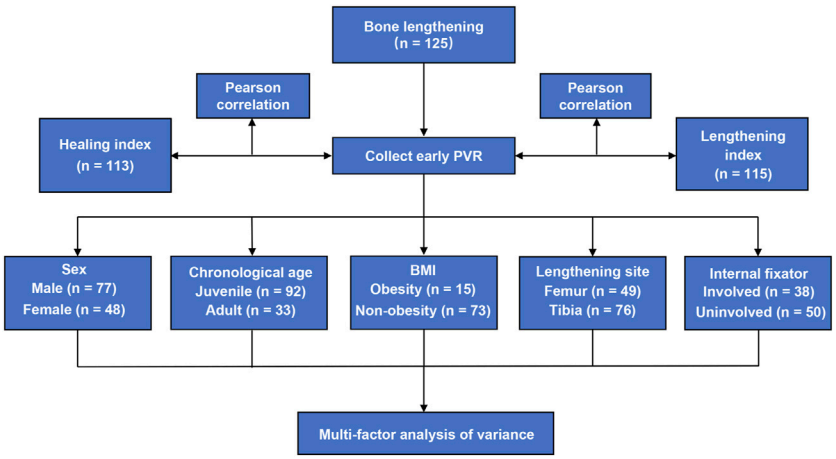

FIGURE 1 | Flowchart for the study design of this study.

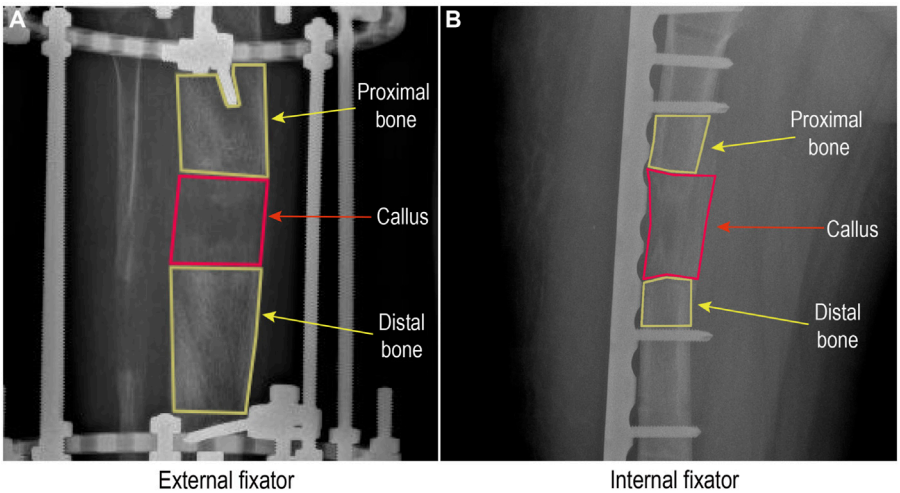

FIGURE 2 | Pixel value assessment from a radiograph in a picture archiving and communication system.

abnormal feeling of weight-bearing after loosening the nut (Iobst et al., 2017).

2.3 Pixel Value Ratio Measurement Based on X-Ray

The X-ray image measurement tool of the picture archiving and communication system (PACS) was employed to depict the regenerated bone area and its distal and proximal normal bone areas (**Figure 2**). In order to improve the accuracy of the PVR, the part of the metal bar was rigorously avoided in the targeted area. Then, the ratio of the regenerated bone PV to the average value of the distal and proximal normal bone PV was calculated. The higher PVR (approach to 1) indicates that the regenerated callus is closer to the adjacent normal bone, whereas the lower PVR reflects a lower immaturity (Zhao et al., 2009). The formula for calculating PVR is as follows:

$$\mathrm{PVR} = \frac{\text{Regenerated bone pixel value}}{(\text{Distal normal bone pixel value} + \text{Proximal normal bone pixel value}) \div 2}.$$

2.4 Potential Influencing Factors for the Early Pixel Value Ratio of the Callus During Distraction Osteogenesis

The overall PVR is analyzed first. Then, the subjects were divided into several subgroups according to sex, chronological age, BMI, lengthening site, and the involvement of the internal fixator during the consolidation period, respectively.

TABLE 1 | Early PVR value of the regenerated callus during distraction osteogenesis.

	First month (n = 118)	Second month (n = 107)	Third month (n = 102)	p-value
PVR value (mean ± SD)	0.78 ± 0.10	0.87 ± 0.06	0.93 ± 0.06	<0.001

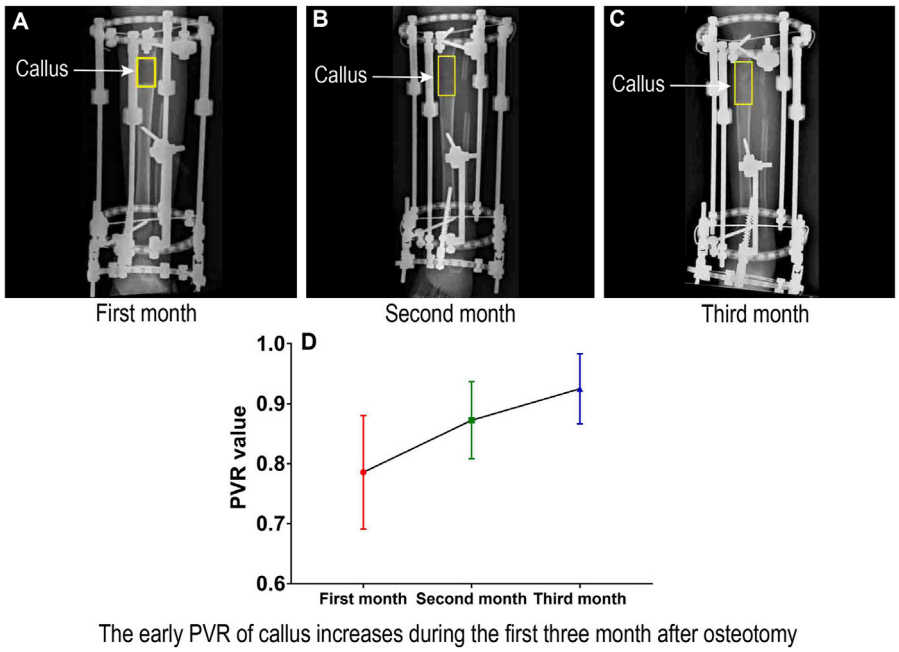

FIGURE 3 | Early PVR of the regenerated callus during distraction osteogenesis.

2.5 Associations of the Healing Index and Lengthening Index With the Early Pixel Value Ratio of the Callus

The LI is the number of months required to achieve 1 cm lengthening, whereas the HI is calculated as the duration of complete consolidation (three cortices in the distraction callus) in days divided by the length gained in centimeters (Koczewski and Shadi, 2013; Wright et al., 2020). The mean of the HI and LI in these patients and the associations of HI and LI with the early PVR of the callus have been analyzed.

2.6 Statistical Analysis

All the analyses were performed by using the SPSS 26.0 version. The mean value and standard deviation (SD) of the PVR for the first 3 months were calculated. The PVR differences according to sex (male vs. female), chronological age (juvenile: under 18 years old vs. adult: 18 years or older), BMI (non-obesity vs. obesity), lengthening site (femur vs. tibia), and involvement of the internal fixator were assessed by a multi-factor analysis of variance. The associations of the HI and LI with the early PVR of callus were assessed by Pearson's correlation coefficient. $p < 0.05$ was regarded as statistically significant.

3 RESULTS

3.1 Pixel Value Ratio in Subjects With Bone Lengthening Is Gradually Increasing During the First Three Months After Osteotomy

A total of 125 patients were recruited for this analysis. The PVRs in subjects with bone lengthening were 0.78 ± 0.10, 0.87 ± 0.06, and 0.93 ± 0.06 in the first 3 months, respectively (**Table 1**). Obviously, the PVR increased gradually during the first 3 months after osteotomy (**Figure 3**).

3.2 Subgroup Analysis for the Pixel Value Ratio

3.2.1 Subgroup Analysis for the Pixel Value Ratio Based on Sex

A total of 77 male and 48 female subjects were recruited for this analysis. The PVR in males with bone lengthening was significantly higher than that in females in the first month after osteotomy (0.80 ± 0.09 vs. 0.76 ± 0.10; $p = 0.015$). However, there was no significant difference in the second and

TABLE 2 | Subgroup analysis for the early PVR based on sex.

PVR value (mean ± SD)	Sex		*p*-value
	Male (*n* = 77)	Female (*n* = 48)	
First month	0.80 ± 0.09	0.76 ± 0.10	0.015
Second month	0.87 ± 0.07	0.87 ± 0.06	0.690
Third month	0.93 ± 0.06	0.92 ± 0.06	0.504

TABLE 3 | Subgroup analysis for the early PVR based on chronological age.

PVR value (mean ± SD)	Chronological age		*p*-value
	Juvenile (*n* = 92)	Adult (*n* = 33)	
First month	0.80 ± 0.09	0.74 ± 0.10	0.008
Second month	0.89 ± 0.06	0.83 ± 0.06	0.018
Third month	0.94 ± 0.05	0.87 ± 0.05	0.003

TABLE 4 | Subgroup analysis for the early PVR based on BMI.

PVR value (mean ± SD)	BMI		*p*-value
	Obesity (*n* = 15)	Non-obesity (*n* = 73)	
First month	0.76 ± 0.11	0.79 ± 0.10	0.854
Second month	0.87 ± 0.07	0.88 ± 0.06	0.116
Third month	0.90 ± 0.06	0.94 ± 0.05	0.154

TABLE 5 | Subgroup analysis for the early PVR based on the lengthening site.

PVR value (Mean ± SD)	Lengthening site		*p* value
	Femur (*n* = 49)	Tibia (*n* = 76)	
First month	0.80 ± 0.10	0.76 ± 0.09	0.349
Second month	0.88 ± 0.07	0.87 ± 0.06	0.015
Third month	0.93 ± 0.06	0.92 ± 0.06	0.037

third month (0.87 ± 0.07 vs. 0.87 ± 0.06; p = 0.690), (0.93 ± 0.06 vs. 0.92 ± 0.06; p = 0.504) (**Table 2**).

3.2.2 Subgroup Analysis for the Pixel Value Ratio Based on Chronological Age

A total of 92 juvenile and 33 adult subjects were recruited in this analysis. The PVR in juveniles with bone lengthening was significantly higher than that in adults in the first 3 months after osteotomy (0.80 ± 0.09 vs. 0.74 ± 0.10; p = 0.008), (0.89 ± 0.06 vs. 0.83 ± 0.06; p = 0.018), and (0.94 ± 0.05 vs. 0.87 ± 0.05; p = 0.003) (**Table 3**).

3.2.3 Subgroup Analysis for the Pixel Value Ratio Based on BMI

A total of 15 obese and 73 non-obese subjects were recruited for this analysis. There was no significant difference in the PVR between the obese and non-obese subjects with bone lengthening in the first 3 months after osteotomy (0.76 ± 0.11 vs. 0.79 ± 0.10; p = 0.854), (0.87 ± 0.07 vs. 0.88 ± 0.06; p = 0.116), and (0.90 ± 0.06 vs. 0.94 ± 0.05; p = 0.154) (**Table 4**).

3.2.4 Subgroup Analysis for the Pixel Value Ratio Based on the Lengthening Site

A total of 49 femoral and 76 tibial site subjects were recruited for this analysis. The PVR in the femur site was significantly higher than that in the tibia site in the second and third months after osteotomy (0.88 ± 0.07 vs. 0.87 ± 0.06; p = 0.015) and (0.93 ± 0.06 vs. 0.92 ± 0.06; p = 0.037). However, there was no difference in the first month (0.80 ± 0.10 vs. 0.76 ± 0.09; p = 0.349) (**Table 5**).

3.2.5 Subgroup Analysis for the Pixel Value Ratio Growth Value Based on the Involvement of the Internal Fixator During the Consolidation Period

A total of 38 and 50 subjects with or without the involvement of an internal fixator during the consolidation period were recruited for this analysis. There was no significant difference in the PVR growth value between the subjects with and without the involvement of the internal fixator (0.04 ± 0.04 vs. 0.04 ± 0.04; p = 0.422) (**Table 6**).

3.3 Associations of the Healing Index and Lengthening Index With the Early Pixel Value Ratio of the Callus

A total of 113 patients were recruited for HI analysis, whereas 115 patients were employed for LI analysis. The average HI was 44.98 ± 49.44 days per centimeter, and the LI was 0.78 ± 0.77 months per centimeter, respectively. The results showed that the early PVR of the regenerated callus in the first month after osteotomy was moderately inversely associated with the HI (r = −0.211; p = 0.029) and LI (r = −0.210; p = 0.029) (**Table 7**).

4 DISCUSSION

Our results showed that the early PVR is gradually increasing in the first 3 months after osteotomy, and the early PVRs in juvenile, male, and femur sites are significantly higher than those in adult, female, and tibial site subjects. Moreover, the early PVR is moderately inversely associated with the HI and LI, respectively (**Figure 4**).

Generally speaking, the PVR is mainly utilized to assess the maturity of the late bone callus in order to identify the time to remove the external fixator. Zhao et al. (2009) demonstrated that the PVR could be served as an objective parameter for callus measurement, which provided guidance for the timing of external fixator removal. Bafor et al. found that there were no adverse effects when subjects commenced full weight-bearing when three out of the four cortices of the anteroposterior and lateral radiographs had a PVR of 0.93. Moreover, both Song et al. (2012) and Vulcano et al. (2018) indicated that the PVR could be utilized as a criterion for callus maturation and full weight-bearing. On this basis, our study further analyzed the early PVR of the callus during DO and its potential influencing factors and association with HI and LI.

Interestingly, Koczewski and Shadi (2013) found that the LI was increased with aging, and the LI for the femur was significantly lower than that for the tibia. Indeed, the bone metabolism system with an equilibrium of bone resorption and formation changes with aging

TABLE 6 | Subgroup analysis for the PVR growth based on the involvement of the internal fixator during the consolidation period.

	Internal fixator		*p*-value
	Involved (*n* = 38)	Uninvolved (*n* = 50)	
PVR growth value (mean ± SD)	0.04 ± 0.04	0.04 ± 0.04	0.422

TABLE 7 | Associations of the healing index and lengthening index with the early PVR value.

PVR value	Index	
	Healing index (*n* = 113)	Lengthening index (*n* = 115)
First month	r = −0.211; *p* = 0.029	r = −0.210; *p* = 0.029
Second month	r = −0.125; *p* = 0.210	r = −0.191; *p* = 0.053
Third month	r = 0.026; *p* = 0.801	r = −0.017; *p* = 0.867

(Kloss and Gassner, 2006), and the arterial blood supply of the femur is also richer than that of the tibia (Kizilkanat et al., 2007) (the nutrient artery is the main blood supply to the long bone). Moreover, Mehta et al. (2011) found that being female was an independent risk factor for bone healing *in vivo*, which may be attributed to a reduction in the mesenchymal stem cell quantity in the bone marrow (Strube et al., 2009). Consistently, we did find that the early PVRs in male, juvenile, and femur sites were significantly higher than those in female, adult, and tibial site subjects, respectively. On the other hand, obesity may induce ectopic adipocyte accumulation in bone marrow cavities, which is considered to impair osteogenic regeneration (Ambrosi et al., 2017). Furthermore, Sun et al. (2011) found more favorable progress in callus regeneration during bone lengthening with the involvement of an internal fixator. Nevertheless, no significant difference in the PVR with regard to BMI and the involvement of the internal fixator was identified in our study. It was speculated that the PVR might not be sensitive enough to reflect the issues. More importantly, the number of obese subjects is rather small, which may inevitably influence our results. Basically, a series of clinical issues caused by an external fixator (for example, inconvenient activities, psychological impact, and uncomfortableness) (Castelein and Docquier, 2016; Nguyen Van and Le Van, 2021) may be avoided by the involvement of an internal fixator. However, our results showed that the early PVR value might not reflect the clinical benefit of an internal fixator (additional medical resources are also consumed). Therefore, the involvement of the internal fixator in bone lengthening still needs to be discussed further. In addition, it is well known that both the LI and HI indicate the bone healing potential (Koczewski and Shadi, 2013; Wright et al., 2020). Our study suggests that the early PVR is moderately inversely associated with LI and HI, which may partly reflect the potential clinical outcome of bone lengthening. However, our results are restricted to the nature of the retrospective design. Taken together, further large well-designed prospective studies are still needed.

The advantages of this study are as follows: first, this is the first study to assess the early PVR value and its potential influencing factors (sex, chronological age, and lengthening site) in bone lengthening. Second, the associations of the HI and LI with the early PVR were also discussed first. Third, this is the largest sample-sized study for PVR analysis until now (others only involved tens of subjects). Fourth, our results may provide the potential clinical value of the early PVR in subjects with bone lengthening. The limitations to the present study should also be acknowledged. First, several issues cannot be addressed due to the nature of the retrospective study design.

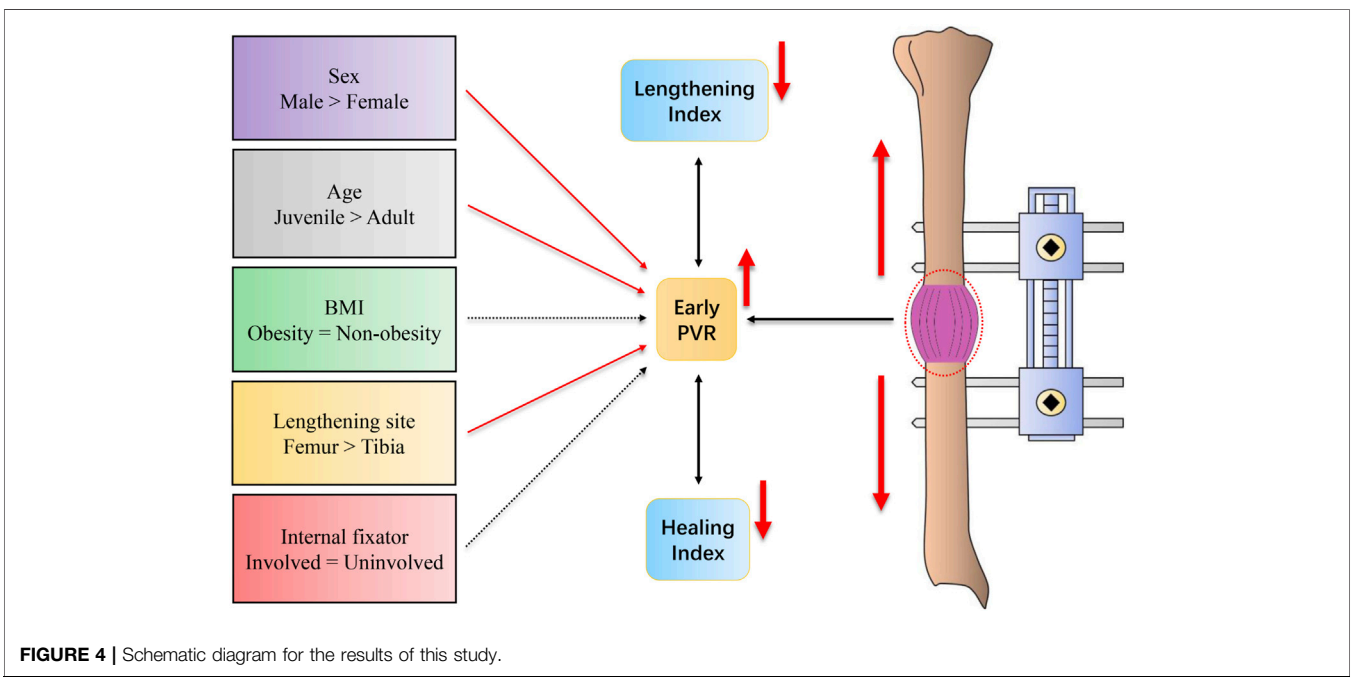

FIGURE 4 | Schematic diagram for the results of this study.

Second, due to the limited available evidence, bone nonunion cannot be considered in the present study. Third, the disturbance by metal fixtures during the PVR measurement may still slightly influence the PVR assessment. Fourth, some data for BMI and PVR growth were lost in our study, which leads to a different sample size between overall and subgroup analysis. Fifth, the disuse osteopenia of the adjacent bone caused by DO has been ignored in our study. Last but not the least, the number of obese subjects is relatively small in our study.

Our results showed that the early PVR is gradually increasing in the first 3 months after osteotomy, which may be significantly influenced by chronological age, sex, and lengthening site. Moreover, the early PVR of the callus may reflect the potential clinical outcome for DO. Our results may be beneficial to the clinical management of the subjects with bone lengthening.

DATA AVAILABILITY STATEMENT

The original contributions presented in the study are included in the article/supplementary material; further inquiries can be directed to the corresponding authors.

AUTHOR CONTRIBUTIONS

JL and YZ decided and conceptualized this manuscript and revised the draft. QL and HM wrote the manuscript. GZ and ZL collected and analyzed the data. HG and MW prepared the figures and tables. JL and YZ was the guarantor of the overall content. All authors approved the final version of the manuscript and agreed to be accountable for all specs of the work.

FUNDING

This study was supported by the National Natural Science Foundation of China (82102581), the National Postdoctoral Science Foundation of China (2021M693562), the Provincial Natural Science Foundation of Hunan (2019JJ40517), the Provincial Outstanding Postdoctoral Innovative Talents Program of Hunan (2021RC2020), the Young Investigator Grant of Xiangya Hospital, Central South University (2020Q14), the FuQing Postdoc Program of Xiangya Hospital, Central South University (176), and the Fund of Reform and Practice of Ideological and Political in Xiangya Hospital, Central South University (36, 40).

REFERENCES

Ambrosi, T. H., Scialdone, A., Graja, A., Gohlke, S., Jank, A.-M., Bocian, C., et al. (2017). Adipocyte Accumulation in the Bone Marrow during Obesity and Aging Impairs Stem Cell-Based Hematopoietic and Bone Regeneration. *Cell Stem Cell* 20, 771–784. doi:10.1016/j.stem.2017.02.009

Anand, A., Feldman, D. S., Patel, R. J., Lehman, W. B., van Bosse, H. J. P., Badra, M. I., et al. (2006). Interobserver and Intraobserver Reliability of Radiographic Evidence of Bone Healing at Osteotomy Sites. *J. Pediatr. Orthop. B* 15, 271–272. doi:10.1097/01202412-200607000-00007

Anna, U.-M., Maria, S., and Kerstin, B. (2021). Comparison of Quantitative Ultrasound of Calcaneus and Dual Energy X-Ray Absorptiometry in Measuring Bone Density and Predicting Fractures in Patients with Diabetic Polyneuropathy: A Prospective Cohort Study. *Diabetes Res. Clin. Pract.* 180, 109064. doi:10.1016/j.diabres.2021.109064

Babatunde, O. M., Fragomen, A. T., and Rozbruch, S. R. (2010). Noninvasive Quantitative Assessment of Bone Healing after Distraction Osteogenesis. *HSS Jrnl* 6, 71–78. doi:10.1007/s11420-009-9130-y

Bafor, A., Iobst, C., and Duncan, M. E. (2020). Evaluating the Utility of the Pixel Value Ratio in the Determination of Time to Full Weight-Bearing in Patients Undergoing Intramedullary Limb Lengthening. *Strateg. Trauma Limb Reconstr.* 15, 74–78. doi:10.5005/jp-journals-10080-1461

Castelein, S., and Docquier, P. L. (2016). Complications Associated with Bone Lengthening of the Lower Limb by Callotasis. *Acta Orthop. Belg* 82, 806–813.

Engelke, K., Libanati, C., Fuerst, T., Zysset, P., and Genant, H. K. (2013). Advanced CT Based *In Vivo* Methods for the Assessment of Bone Density, Structure, and Strength. *Curr. Osteoporos. Rep.* 11, 246–255. doi:10.1007/s11914-013-0147-2

Eyres, K., Bell, M., and Kanis, J. (1993). Methods of Assessing New Bone Formation during Limb Lengthening. Ultrasonography, Dual Energy X-Ray Absorptiometry and Radiography Compared. *J. Bone Jt. Surg. Br. volume* 75-B, 358–364. doi:10.1302/0301-620X.75B3.8496200

Floerkemeier, T., Hurschler, C., Witte, F., Wellmann, M., Thorey, F., Vogt, U., et al. (2005). Comparison of Various Types of Stiffness as Predictors of the Load-Bearing Capacity of Callus Tissue. *J. Bone Jt. Surg. Br. volume* 87-B, 1694–1699. doi:10.1302/0301-620X.87B12.16247

Hazra, S., Song, H.-R., Biswal, S., Lee, S.-H., Lee, S. H., Jang, K.-M., et al. (2008). Quantitative Assessment of Mineralization in Distraction Osteogenesis. *Skelet. Radiol.* 37, 843–847. doi:10.1007/s00256-008-0495-7

Iobst, C. A., Mohammed, W., and Colley, R. (2017). Determining when it Is Safe to Remove the External Fixator: Results from a Survey of the Limb Lengthening and Reconstruction Society. *Orthopedics* 40, e876–e879. doi:10.3928/01477447-20170810-06

Ishimoto, T., Nakano, T., Yamamoto, M., and Tabata, Y. (2011). Biomechanical Evaluation of Regenerating Long Bone by Nanoindentation. *J. Mater Sci. Mater Med.* 22, 969–976. doi:10.1007/s10856-011-4266-y

Kizilkanat, E., Boyan, N., Ozsahin, E. T., Soames, R., and Oguz, O. (2007). Location, Number and Clinical Significance of Nutrient Foramina in Human Long Bones. *Ann. Anat. - Anatomischer Anzeiger* 189, 87–95. doi:10.1016/j.aanat.2006.07.004

Kloss, F. R., and Gassner, R. (2006). Bone and Aging: Effects on the Maxillofacial Skeleton. *Exp. Gerontol.* 41, 123–129. doi:10.1016/j.exger.2005.11.005

Ko, K. R., Shim, J. S., Chung, C. H., and Kim, J. H. (2019). Surgical Results of Limb Lengthening at the Femur, Tibia, and Humerus in Patients with Achondroplasia. *Clin. Orthop. Surg.* 11, 226–232. doi:10.4055/cios.2019.11.2.226

Koczewski, P., and Shadi, M. (2013). Factors Influencing Bone Regenerate Healing in Distraction Osteogenesis. *Ortop. Traumatol. Rehabil.* 15, 591–599. doi:10.5604/15093492.1091515

Malkova, T. A., and Borzunov, D. Y. (2021). International Recognition of the Ilizarov Bone Reconstruction Techniques: Current Practice and Research (Dedicated to 100th Birthday of G. A. Ilizarov). *Wjo* 12, 515–533. doi:10.5312/wjo.v12.i8.515

Mehta, M., Duda, G. N., Perka, C., and Strube, P. (2011). Influence of Gender and Fixation Stability on Bone Defect Healing in Middle-Aged Rats: a Pilot Study. *Clin. Orthop. Relat. Res.* 469, 3102–3110. doi:10.1007/s11999-011-1914-y

Nguyen Van, L., and Le Van, D. (2021). Complications and Functional, Psychological Outcomes of Bilateral Tibial Lengthening over Intramedullary Nail: Evidence from Vietnam. *Int. Orthop. (SICOT)* 45, 2007–2015. doi:10.1007/s00264-021-05059-5

Shchudlo, N., Varsegova, T., Stupina, T., Shchudlo, M., Saifutdinov, M., and Yemanov, A. (2017). Benefits of Ilizarov Automated Bone Distraction for Nerves and Articular Cartilage in Experimental Leg Lengthening. *Wjo* 8, 688–696. doi:10.5312/wjo.v8.i9.688

Song, S.-H., Agashe, M., Kim, T.-Y., Sinha, S., Park, Y.-E., Kim, S.-J., et al. (2012). Serial Bone Mineral Density Ratio Measurement for Fixator Removal in Tibia

Distraction Osteogenesis and Need of a Supportive Method Using the Pixel Value Ratio. *J. Pediatr. Orthop. B* 21, 137–145. doi:10.1097/BPB.0b013e32834f04f3

Starr, K. A., Fillman, R., and Raney, E. M. (2004). Reliability of Radiographic Assessment of Distraction Osteogenesis Site. *J. Pediatr. Orthop.* 24, 26–29. doi:10.1097/00004694-200401000-0000610.1097/01241398-200401000-00006

Strube, P., Mehta, M., Baerenwaldt, A., Trippens, J., Wilson, C. J., Ode, A., et al. (2009). Sex-specific Compromised Bone Healing in Female Rats Might Be Associated with a Decrease in Mesenchymal Stem Cell Quantity. *Bone* 45, 1065–1072. doi:10.1016/j.bone.2009.08.005

Sun, X.-T., Easwar, T. R., Stephen, M., Song, S.-H., Kim, S.-J., and Song, H.-R. (2011). Comparative Study of Callus Progression in Limb Lengthening with or without Intramedullary Nail with Reference to the Pixel Value Ratio and the Ru Li's Classification. *Arch. Orthop. Trauma Surg.* 131, 1333–1340. doi:10.1007/s00402-011-1302-9

Tesiorowski, M., Kacki, W., Jasiewicz, B., Rymarczyk, A., and Sebastianowicz, P. (2005). Methods for the Evaluation of Bone Regeneration during Distraction Osteogenesis. *Chir. Narzadow Ruchu Ortop. Pol.* 70, 127–130.

Vulcano, E., Markowitz, J. S., Ali, S., Nguyen, J., Fragomen, A. T., and Rozbruch, S. R. (2018). Assessment of Bone Healing during Antegrade Intramedullary Rod Femur Lengthening Using Radiographic Pixel Density. *J. Am. Acad. Orthop. Surg.* 26, e388–e394. doi:10.5435/JAAOS-D-16-00949

Wright, S. E., Goodier, W. D., and Calder, P. (2020). Regenerate Deformity with the Precice Tibial Nail. *Strateg. Trauma Limb Reconstr.* 15, 98–105. doi:10.5005/jp-journals-10080-1457

Zak, L., Arnhold, R., Tiefenboeck, T. M., and Wozasek, G. E. (2021). The Influence of Advanced Age in Bone Healing after Intramedullary Limb Lengthening. *Orthop. Traumatology Surg. Res.* 107, 103055. doi:10.1016/j.otsr.2021.103055

Zhao, L., Fan, Q., Venkatesh, K. P., Park, M. S., and Song, H. R. (2009). Objective Guidelines for Removing an External Fixator after Tibial Lengthening Using Pixel Value Ratio: a Pilot Study. *Clin. Orthop. Relat. Res.* 467, 3321–3326. doi:10.1007/s11999-009-1011-7

Conflict of Interest: The authors declare that the research was conducted in the absence of any commercial or financial relationships that could be construed as a potential conflict of interest.

Publisher's Note: All claims expressed in this article are solely those of the authors and do not necessarily represent those of their affiliated organizations, or those of the publisher, the editors, and the reviewers. Any product that may be evaluated in this article, or claim that may be made by its manufacturer, is not guaranteed or endorsed by the publisher.

frontiers | Frontiers in Bioengineering and Biotechnology

SYSTEMATIC REVIEW
published: 22 July 2022
doi: 10.3389/fbioe.2022.956614

Peripheral Blood-Derived Stem Cells for the Treatment of Cartilage Injuries: A Systematic Review

*Yanlin Zhu and Weili Fu**

Department of Orthopedics, Orthopedic Research Institute, West China Hospital, Sichuan University, Chengdu, China

Background: The treatment of cartilage damage is a hot topic at present, and cell therapy is an emerging alternative therapy. Stem cells derived from peripheral blood have become the focus of current research due to the ease of obtaining materials and a wide range of sources.

Methods: We used a text search strategy using the ["mesenchymal stem cells" (MeSH term) OR "MSC" OR "BMMSC" OR "PBMSC" OR" PBMNC" OR "peripheral blood stem cells"] AND (cartilage injury [MeSH term] OR "cartilage" OR "chondral lesion"). After searching the literature, through the inclusion and exclusion criteria, the last included articles were systematically reviewed.

Result: We found that peripheral blood-derived stem cells have chondrogenic differentiation ability and can induce chondrogenic differentiation and repair *in vivo* and have statistical significance in clinical and imaging prognosis. It is an improvement of academic differences. Compared with the bone marrow, peripheral blood is easier to obtain, widely sourced, and simple to obtain. In the future, peripheral blood will be a more potential cell source for cell therapy in the treatment of cartilage damage.

Conclusion: Stem cells derived from peripheral blood can repair cartilage and are an important resource for the treatment of cartilage damage in the future. The specific mechanism and way of repairing cartilage need further study.

Keywords: peripheral blood-derived stem cells, cartilage injuries, PBMSC, BMSC, PBMNCs

OPEN ACCESS

Edited by:
Jun Lin,
First Affiliated Hospital of Soochow University, China

Reviewed by:
Hang Lin,
University of Pittsburgh, United States
Dong Jiang,
Peking University Third Hospital, China

****Correspondence:***
Weili Fu
foxwin2008@163.com

Specialty section:
This article was submitted to Biomaterials, a section of the journal Frontiers in Bioengineering and Biotechnology

Received: *30 May 2022*
Accepted: *22 June 2022*
Published: *22 July 2022*

Citation:
Zhu Y and Fu W (2022) Peripheral Blood-Derived Stem Cells for the Treatment of Cartilage Injuries: A Systematic Review. Front. Bioeng. Biotechnol. 10:956614. doi: 10.3389/fbioe.2022.956614

1 INTRODUCTION

Cartilage is a special, low-friction articular surface tissue that is essential for weight absorption and smooth gliding of the articulating surfaces in diarthrodial joints, whose primary function is to absorb, cushion, and protect the underlying bone from the forces that arise when the joint is being used. Chondral lesions can lead to direct contact with bone, ultimately leading to osteoarthritis (Rackwitz et al., 2014). Due to the lack of native blood vessels and lymphatic return, the spontaneous healing capacity of cartilage is low and is generally replaced by fibrocartilage (Frisch et al., 2017a). The newly generated fibrocartilage can withstand far less mechanical stress than the original cartilage tissue (Hunziker, 2002). Numerous studies have reported that the newly formed fibrocartilage tends to deteriorate over time (Orth et al., 2014). Therefore, the treatment of chondral lesions is currently an important research topic in traumatology.

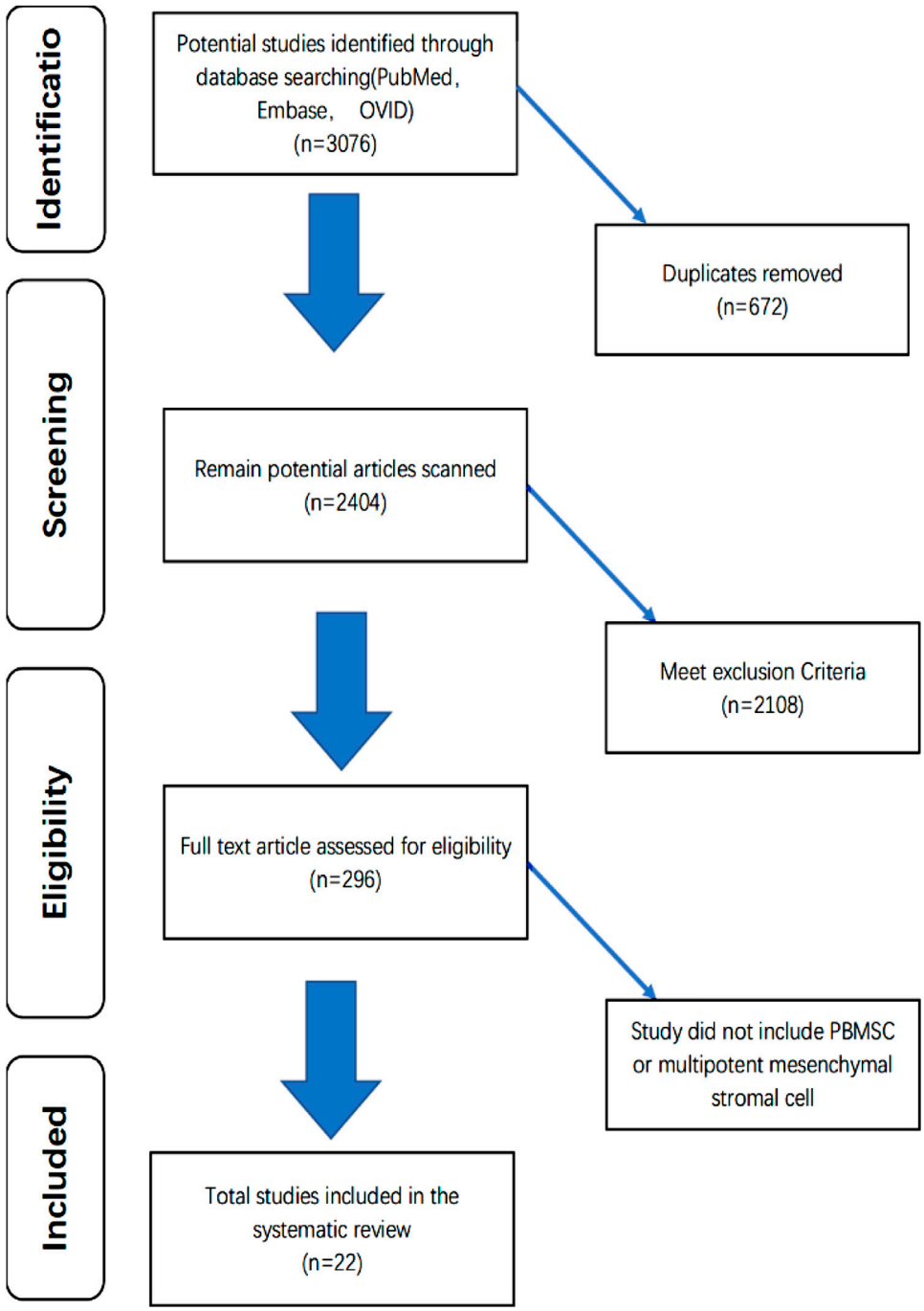

FIGURE 1 | Flow Chart.

Conservative treatment of cartilage damage usually includes corticosteroids, nonsteroidal anti-inflammatory drugs, hyaluronan, and polysulfated glycosaminoglycan (Ferris et al., 2011). However, the abovementioned drugs can only control the symptoms and cannot prevent the occurrence of osteoarthritis (Frisbie et al., 2009). Marrow stimulation techniques, including microfracture and microdrilling, have been widely reported as promoting chondral healing, with microfracture being the most commonly performed (Madry et al., 2011). It penetrates the underlying subchondral bone marrow through drilling, allowing bone marrow mesenchymal stem cells (MSC) and other progenitor cells to enter the cartilage defect for repair and present good clinical outcomes (Bieback et al., 2008). However, after bone marrow stimulation, the joint normally covered by hyaline cartilage is repaired by fibrocartilage, which is biochemically and mechanically inferior to hyaline cartilage

(Saris et al., 2009; Seol et al., 2012; Jiang and Tuan, 2015). Continued stress can lead to tissue degeneration and deteriorating results in the long term (Vinatier et al., 2009). Therefore, improving the quality of prosthetic tissue has become a new issue.

The application of autologous mesenchymal stem cells in the joint cavity shows the effect of enhancing cartilage repair in a lasting way (Saw et al., 2013; Skowroński and Rutka, 2013; Reissis et al., 2016). Thus, lately researchers have focused on cell therapy as a therapeutic alternative (Brittberg et al., 1994). There are many sources of mesenchymal stem cells, including bone marrow, adipose tissue, skin, or peripheral blood, or from an umbilical cord donor (Kassis et al., 2006; Larochelle et al., 2006; Huang et al., 2009). While bone marrow (BM) MSCs show a decline in the number and differentiation potential of MSCs with aging or transformation in long-term *in vitro* culture, the peripheral blood mononuclear cell fraction has been shown to enhance cartilage repair in an ovine osteochondral defect model (Emadedin et al., 2012; Hopper et al., 2015a). The use of peripheral blood may provide workable and less invasive translational procedures as this resource also contains MSC with the same potency for chondrogenic differentiation as that of bone marrow MSC (Zvaifler et al., 2000; Huang et al., 2009; Raghunath et al., 2010; Al Faqeh et al., 2012). The purpose of this systematic review is to evaluate the potential of peripheral blood-derived stem cells in the treatment of cartilage injury by collecting relevant literature on the treatment of cartilage injury with peripheral blood-derived stem cells in the past two decades, including *in vitro* and *in vivo* experimental articles.

2 MATERIALS AND METHODS

2.1 Data Sources and Search Strategy

We conducted a systematic review based on the PRISMA (Preferred Reporting Items for Systematic Review and Meta-Analysis) guidelines (Moher et al., 2009). We used a text search strategy using the ["mesenchymal stem cells" (MeSH term) OR "MSC" OR "BMMSC" OR "PBMSC" OR" PBMNC" OR "peripheral blood stem cells"] AND [cartilage injury (MeSH term) OR "cartilage" OR "chondral lesion"]. Specifically, we searched the PubMed, Embase, and OVID databases from inception to 20 April 2022. We also assessed the bibliographies of identified studies to seek additional articles. We did not add language restrictions.

Along with the database search, we examined the references of included studies and previously published systematic reviews to identify additional studies. We also checked the International Clinical Trials Registry Platform Search Portal and ClinicalTrials.gov (https://clinicaltrials.gov/) to identify the currently ongoing or recently completed trials.

2.2 Inclusion and Exclusion Criteria

2.2.1 Inclusion

1. Any basic English-language scientific studies of the PB-derived primitive cells that exhibited chondrogenic or multipotent mesenchymal differentiation abilities.
2. *in vivo* animals using PB as a source of chondrogenic progenitor cells for cartilage regeneration were also included.
3. Human studies using PB as a source of chondrogenic progenitor cells for cartilage regeneration were also included.
4. Any study that has at least one outcome that can be documented.

2.3 Exclusion

Any studies of primitive cells that were not chondrogenic or not derived from the PB and *in vivo* studies that only used non-PB sources were excluded.

2.4 Quality Assessment

The risk of bias graph in Review Manager 5.3 was used to evaluate the methodologic quality of included RCT studies in this systematic review. This seven-element checklist qualitatively assesses various aspects of trial quality (random sequence generation, allocation concealment, blinding of participant and personnel, blinding of outcome assessment, incomplete outcome data, selective reporting, and other bias) using an ordinal scoring system comprising high risk, low risk, or unclear risk response options for each statement in Review Manager 5.3. A higher score obtained with the Review Manager 5.3 is indicative of higher methodological study quality. We did not assess publication bias with a funnel chart because we had less than 10studies for each comparison in this review.

QUADAS (Quality Assessment of Diagnostic Accuracy Studies) was used to evaluate the methodologic quality of other studies. The detailed items of the scale are as follows:

1. Was a consecutive or random sample of patients enrolled? Yes/No/Unclear
2. Was a case-control design avoided? Yes/No/Unclear
3. Did the study avoid inappropriate exclusions? Yes/No/Unclear
4. Could the selection of patients have introduced bias? RISK: LOW/HIGH/UNCLEAR
5. Is there a concern that the included patients do not match the review question? CONCERN: LOW/HIGH/UNCLEAR
6. Were the index test results interpreted without the knowledge of the results of the reference standard? Yes/No/Unclear
7. If a threshold was used, was it prespecified? Yes/No/Unclear
8. Could the conduct or interpretation of the index test have introduced bias? RISK: LOW /HIGH/UNCLEAR
9. Is there a concern that the index test, its conduct, or interpretation differ from the review question? CONCERN: LOW /HIGH/UNCLEAR
10. Is the reference standard likely to correctly classify the target condition? Yes/No/Unclear
11. Were the reference standard results interpreted without the knowledge of the results of the index test? Yes/No/Unclear
12. Could the reference standard, its conduct, or its interpretation have introduced bias? RISK: LOW /HIGH/UNCLEAR
13. Is there a concern that the target condition, as defined by the reference standard, does match the review questions? CONCERN: LOW /HIGH/UNCLEAR

TABLE 1 | PBSCs in animals.

First author	Species	Number	Character	Type of study	Evaluation method	Injury site(number)	Degree of damage
Henson et al. (2021)	Welsh Mountain female sheep	40	3–4 year-old (adult) (mean age 3.2 years), 40–42 kg	Comparative study	MRI, Gross Morphology, Histology, and Immunohistochemistry	the medial femoral condyle	Full-thickness chondral defects of 8 mm diameter
Broeckx et al. (2019)	Horse	75	22 mares, 16 geldings and 37 stallions	RCTs	visual lameness assessment, flexion test	Fetlock joint	Early staged fetlock degenerative joint disease
Broeckx et al. (2019)	horse	12	3 geldings and 9 mares (median age 8.5 years)	RCTs	weekly joint assessment, AAEP score, an inertial sensor-based system, X-ray, Synovial fluid analysis, OARSI, and Immunohistochemistry	Metacarpophalangeal OA	surgically induced OA
Fu et al. (2014)	Rabbit	30	New Zealand White rabbits, aged about 4 months	Controlled laboratory study	histological scoring, histochemical staining, and immunohistochemistry	the trochlear groove of the distal femur	Full-thickness articular osteochondral defects (5 mm in diameter and 1–2 mm in depth)
Broeckx et al. (2014)	Horse	50	clinical lameness for at least 3 months	Preliminary study	Cytological Staining, Immunocytochemistry, Flow Cytometry, RT-PCR, and AAEP	fetlock	NA
Broeckx et al. (2014)	Horse	165	NA	Pilot study	Clinical lameness; locomotory disorder; and positive flexion test	Stifle joint (30), fetlock joint (58), coffin joint (43), pastern joint (34)	Degenerative joint disease

First author	Cell source	Cultivation and extraction methods	Cell character markers	number of cells	Cell implantation method	Surgical approach
Henson et al. (2021)	Autologous G-CSF activated PB	Apheresis	*CD34*, *CD45*, *CD73*, *CD90, and CD105*	NA	intra-articular injections	intra-articular injections
Broeckx et al. (2019)	Chondrogenic induced PBMSCs	DGC and PA	*CD45*, *MHC II*, *CD29*, *CD44, and CD90*	2×10^6 cells/ml	Articular injection	Articular injection
Broeckx et al. (2019)	Chondrogenic induced PBMSCs	DGC and PA	Aggrecan+, Col II+, COMP+, p63+ and GAG+; decrease in Ki67.	2×10^6 cells in/ml	Articular injection	Articular injection
Fu et al. (2014)	Autologous G-CSF activated PB	Erythrocyte Lysis and PA	*CD44*, *CD45*, and *MHC II*	4×10^6 cells/ scaffold	Surgical implantation	Establishment of animal model
Broeckx et al. (2014)	PB-MSCs (native or chondrogenic induction)	DGC and PA	Col II, Ki67 p63, vimentin, and MHCII aggrecan	NA	Single IA injection	PB-MSCs with or without PRP injection
Broeckx et al. (2014)	PB-MSCs (native or chondrogenic induced)	DGC and PA	Col II, Ki67 p63, vimentin, and MHCII aggrecan	NA	Single IA injection	PB-MSCs with PRP injections

First author	Time	Postoperative treatment	Clinical outcome	Imaging results	Experimental results	Adverse event
Henson et al. (2021)	8 weeks	NA	NA	SPION labeled cells could not be detected within the defect at any of the time points studied despite using MRI sequences	ICRS found No significant difference between treatment groups the repaired tissue was fibrocartilagenous in nature rather than hyaline cartilage	no adverse event
Broeckx et al. (2019)	1 year	Dexmedetomidine hydrochloride and Ketoprofen	Improved AAEP score*, Flexion score* and Pain score*	NA	NA	3 mild infections of the upper respiratory tract
Broeckx et al. (2019)	11 weeks	Dexmedetomidine hydrochloride	AAEP scores in week 7*	radiographic changes were not significantly different	higher viscosity score*, less wear lines were present in the intervention group*, higher COMP in the cartilage adjacent*	1 horse had an increase in local temperature 2 horses had a limited range of motion
Fu et al. (2014)	24 weeks	allowed to move freely and had free access to food pellets and water	NA	NA	PB MSCs had a greater chondrogenic ability than BM MSCs* The histological scores were significantly better in PB MSCs* defects were synthesized with abundant cartilage matrices with a regular arrangement in PB MSCs	NA

(Continued on following page)

TABLE 1 | (*Continued*) PBSCs in animals.

First author	Time	Postoperative treatment	Clinical outcome	Imaging results	Experimental results	Adverse event
Broeckx et al. (2014)	12 months	NA	Improved short- and long-term clinical evolution scores*; Relief from clinical lameness, flexion pain and joint effusion	NA	exhibiting increases in the levels of Col II, aggrecan and cartilage oligomeric matrix protein	NA
Broeckx et al. (2014)	18 weeks	NA	Improved short- and long-term clinical evolution scores*; Relief from clinical lameness and locomotor disorder	NA	NA	Moderate flare reaction (without long-term effects, 3 horses)

DGC, density gradient centrifugation; PA, plastic adherence; AAEP, American association of equine practitioners; OARSI, the Osteoarthritis research society international; OA, osteoarthritis; COMP, cartilage oligomeric matrix protein; NI, not involving; AAV, human adeno-associated virus; rAAV:recombinant AAV; AAPBSC, autologous activated peripheral blood stem cells; IA, intraarticular; rt-PCR, reverse transcriptase-polymerase chain reaction; HHS, the Harris Hip score. means statistically different.*

14. Was there an appropriate interval between index test(s) and reference standard? Yes/No/Unclear
15. Did all patients receive reference standard? Yes/No/Unclear
16. Did patients receive the same reference standard? Yes/No/Unclear
17. Were all patients included in the analysis? Yes/No/Unclear
18. Could the patient flow have introduced bias? RISK: LOW /HIGH/UNCLEAR

2.5 Data Extraction

A single reviewer screened all the citations and abstracts generated by the literature search and applied the selection criteria. Identified randomized trials were assessed for inclusion by two reviewers. Any disagreement between them on the eligibility of certain studies was resolved through discussion with a third reviewer. The titles of journals and names of authors were not masked during the study selection process.

Each investigator independently extracted the following data:

1. Study characteristics, including species, number, character of included species, type of study, evaluation method, injury site, and degree of damage.
2. Experimental details including cell source, cultivation and extraction methods, cell character markers, number of cells, cell implantation method, and surgical approach.
3. Experimental results and adverse events.

3 RESULT

3.1 Basic Characteristic

According to our retrieval strategy abovementioned, we retrieved a total of 3,076 articles. After a brief reading of the abstracts and titles, duplicate articles and irrelevant articles were excluded, and a total of 296 articles were reviewed in detail (**Figure 1**). After excluding articles that do not contain related stem cells, we ultimately included 24 articles between 2008 and 2022 for the systematic review (Jancewicz et al., 1995; Pufe et al., 2008; Saw et al., 2011; Casado et al., 2012; Chong et al., 2012; Kim et al., 2012; Skowroński et al., 2012; Saw et al., 2013; Skowroński and Rutka, 2013; Turajane et al., 2013; Broeckx et al., 2014a; Fu et al., 2014a; Broeckx et al., 2014b; Fu et al., 2014b; Turajane et al., 2014; Hopper et al., 2015b; Frisch et al., 2017b; Broeckx et al., 2019a; Broeckx et al., 2019b; Monckeberg et al., 2019; Ying et al., 2020; Henson et al., 2021). The data from 24 studies were analyzed, including seven fully *in vitro* studies and 17 *in vivo* studies (**Table 1**). The experimental subject includes humans, sheep, rabbits, and horses. A total of nine articles included *in vitro* experiments, all (100%) of which confirmed the tendency of peripheral blood-derived stem cells to differentiate into chondrocytes. In terms of cell sources, 10 articles used G-CSF-stimulated PBMSCs, four articles used chondro-induced PBMSCs, and eight articles directly used the peripheral blood stem cells after apheresis or gradient centrifugation. *In vivo* experiments include three comparative studies, one prospective study, three RCTs, five case reports, one preliminary study, and one pilot study. Cartilage defects in nine of the studies were graded with ICRS and were all greater than grade 3. All characteristics of the included literature are listed in **Tables 1**, **2**, **3**. **Figures 2**, **3** demonstrates the basic experimental procedure. **Table 1** and **Figure 4** show the methodological quality evaluation results. The detailed results of the quality evaluation are shown in **Figure 4** and **Table 4**.

3.2 PBMSC in Humans

We included nine studies with human subjects, including one prospective study, three comparative studies, 4 case reports, and one RCTs (Jancewicz et al., 1995; Saw et al., 2011; Skowroński et al., 2012; Saw et al., 2013; Skowroński and Rutka, 2013; Fu et al., 2014b; Turajane et al., 2014; Monckeberg et al., 2019; Ying et al., 2020). A total of 225 people were included. Most injuries are concentrated in the patella and femoral condyle, and a few in the hip joint. Cartilage damage in all patients included in the study was degenerative. Except for the study conducted by Ying et al.

TABLE 2 | PBSCs in human.

First author	Species	Number	Character	Type of Study	Evaluation method	Injury site(number)	Degree of damage
Ying et al. (2020)	Human	37(15 males)	age range 31–64 years	prospective study	HHS, μCT Scanning, Histochemistry, Immunohistochemistry (IHC), and Immunofluorescence analyses,	hip	microfracture and/or cystic degeneration existed between cartilage and subchondral bone
Monckeberg et al. (2019)	Human	20	7 women and 13 man with average age of 32.7	Comparative study	IKDC, VAS, MRI, and ICRS	1.Trochlea(9) 2.Femoral condyle(5) 3.Patella(6)	ICRS grade>3
Fu et al. (2014)	Human	1	19 years old	case report	X-rays, CT and MRI, Tegner, Lysholm, and IKDC 2000 scores.	Lateral femoral trochlea	Full-thickness cartilage defects(ICRS grade IV)
Turajane et al. (2013)	Human	5	52–59 years old	Case report	WOMAC and KOOS	Medial condyle (4) and patellofemoral (1)	Early-stage OA(ICRS grade III and IV)
Skowroński and Rutka. (2013)	Human	46	7–52 years old (average age: 26 years)	Comparative study	KOOS and Lysholm and VAS scales	Medial femoral condyle	Osteochondral lesions(ICRS grade IV)
Saw et al. (2013)	Human	50	22–50 years old	RCTs	IKDC, MRI scan, and ICRS	Knee	Chondral defects(ICRS grade III and IV)
Skowroński et al. (2012)	Human	52	16–55 years old	Case report	KOOS, Lysholm and VAS scales, and MRI	Patella (22), medial femoral condyle (38), and lateral femoral condyle (6)	Cartilage lesions (ICRS grade III and IV)
Saw et al. (2013)	Human	5	19–52 years old	case report	Second-Look Arthroscopy and Histology	Knee	Chondral defects (ICRS grade III and IV)
Jancewicz, P.(2004)	Human	9	NA	Case report	clinical examination, Magee score, and MRI	Talus	Osteochondral defects(ICRS IV)

First author	Cell source	Cultivation and extraction methods	Cell character markers	Number of cells	Cell implantation method	Surgical approach
Ying et al. (2020)	G-CSF activated PB	apheresis	NA	minimum concentration of $8 \times l0^6$/l	arterial injection	infused through the medial circumflex femoral artery.
Monckeberg et al. (2019)	PBSCs	autologous PB (Apheresis)	N/A	430,000 PBSC ± 270.000/ml	articular injection with PRP	knee arthroscopy
Fu et al. (2014)	Autologous G-CSF mobilized PB	Blood cell separation	NA	3.496×10^7 cells/ml	Surgical implantation	Debridement + PBSCs with autologous periosteum flap cover
Turajane et al. (2013)	Autologous G-CSF activated PB	Leukapheresis	*CD34*$^+$ *CD105*$^+$	$2.67–5.99 \times 10^3$ cells/ injection	Repeated IA injections	Debridement + BMS + repeated IA injections
Skowroński and Rutka. (2013)	Autologous G-CSF activated PB,	NA	NA	$1.25 \times 10^6–5.2 \times 10^6$ cells/ml	Surgical implantation	Debridement + modified sandwich technique
Saw et al. (2013)	Autologous G-CSF mobilized PB	Apheresis	NA	NA	IA injections	IA injections
Skowroński et al. (2012)	Autologous G-CSF mobilized PB	Apheresis	NA	2.0×10^7 cells/injection	Repeated IA injections	Debridement + BMS + HTO(1) + repeated IA injections
Saw et al. (2013)	Autologous G-CSF activated PB	Blood cell separation	*CD34*$^+$	NAC	Surgical implantation	Debridement + sandwich technique

First author	Time	Postoperative treatment	Clinical outcome	Imaging results	Experimental results	Adverse event
Ying et al. (2020)	36 months	NA	no significant difference in HHSs between the two groups at 36 months	no significant differences between the control group and the combination treatment group in μCT Scanning,	no significant difference in osteoclast number was found between the control group and the combination treatment group	
Monckeberg et al. (2019)	5 years	Nonsteroidal anti-inflammatory drugs and acetaminophen, rehabilitation protocol	Improved IKDC score* and lower VAS score*	improved	Improved ICRS score*	2: myalgia and fever
Fu et al. (2014)	7.5 years	Strict rehabilitation program	improved IKDC 2000 subjective score*, Lysholm score and Tegner score*	CT: subchondral bone Recovery; MRI: near-normal cartilagelike tissue regeneration	Regenerated articular cartilage with a smooth surface, but with a slightly	NA

(Continued on following page)

TABLE 2 | (*Continued*) PBSCs in human.

First author	Time	Postoperative treatment	Clinical outcome	Imaging results	Experimental results	Adverse event
					yellowish and shallow morphology	
Turajane et al. (2013)	6 months	Nonweight bearing	Improved WOMAC and KOOS* Succeeded in regenerating articular cartilage	NA	NA	Mild swelling and discomfort
Skowroński and Rutka. (2013)	5 years	Passive and active exercises, nonweight to full-weight bearing	Improved KOOS and Lysholm scales, relief of VAS scale*;	92% of patients with good results MRI: satisfactory reconstruction of the cartilaginous surface and good regenerative integration	NA	NA
Saw et al. (2013)	18 months	NA	No IKDC score difference compared to the control group	Improved MRI morphologic scores	Improved total ICRS II histologic scores	Deep vein thrombosis (1 patient in the control group)
Saw et al. (2013)	10–26 months	crutch assisted partial to full weight-bearing	NA	X-ray: reappearance of medial articulation	generated full-thickness articular hyaline cartilage	Minimal discomfort from PBSCs harvesting and IA injection

* *means statistically different.*

(2020), which did not report the degree of cartilage damage, the rest of the studies reported that cartilage damage and the ICRS grade was greater than grade 3. The evaluation methods include International Knee Documentation Committee score (IKDC), visual analog scale (VAS), and International Cartilage Repair Society morphologic score system (ICRS) for subjective scoring; X-ray and Magnetic Resonance Imaging (MRI) for imaging examination; and tissue biopsy and Immunohistochemistry for laboratory examination. Seven studies used the G-CSF-stimulated peripheral blood stem cells, and two studies used apheresis peripheral blood stem cells. The preparation process uses red blood cell lysis and gradient centrifugation, which has been proven to be effective in isolating PBMSCs (Kim et al., 2012). All studies used the intra-articular injection for cell implantation. Five articles report on postoperative treatment, including drug therapy: acetaminophen, NSAIDs, and Dexmedetomidine, and different types of rehabilitation programs. Seven studies reported clinical outcomes, except Ying, J (Ying et al., 2020), who reported no significant difference in HHSs between the two groups at 36 months followup. However, clinical results of the remaining six studies reported a significant improvement in clinical scores (KOOS, VAS, The Western Ontario, and McMaster Universities Osteoarthritis Index (WOMAC)) after the peripheral blood-derived stem cells were injected into the defect site. Similarly, in the imaging results and laboratory test results, except for Ying, J, all the other reported studies showed a statistically significant improvement after peripheral blood stem cell transplantation. In terms of adverse events, except for a case of deep vein thrombosis reported by Saw, K. Y, which is a high-risk event, all the other adverse events are low-risk events, including fever and joint adhesion (Saw et al., 2013). The detailed information is shown in **Table 2**.

3.3 PBMSC in Animals

Six animal studies were included in our systematic review, including two RCTs, one comparative study, one controlled laboratory study, one preliminary study, and one pilot study (Broeckx et al., 2014a; Fu et al., 2014a; Broeckx et al., 2014b; Broeckx et al., 2019a; Monckeberg et al., 2019; Henson et al., 2021), and subjects included sheep, horses, and rabbits. The lesions are mainly concentrated in the lower extremity joints or the metacarpophalangeal joints. The cartilage defects of the experimental subjects of Fu, W. L (Fu et al., 2014a), Henson, F. (Henson et al., 2021), and Broeckx, S. Y (Broeckx et al., 2019b) were all using experimental modeling, and the cartilage defects of the experimental subjects of other researchers were all caused by degenerative diseases. Grade of cartilage damage was not reported. Two studies used the G-CSF-stimulated peripheral blood stem cells, and four studies used chondrogenic induced PBMSCs. Gradient centrifugation was used for cell isolation in all experiments, and plastic adhesion was also used in some experiments. All studies did not impose strict requirements on the postoperative rehabilitation of experimental animals and did not limit their range and intensity of activities. Only Broeckx, S. Y. in the 2019 experiment gave experimental animals postoperative drug treatment for sedation and analgesia. In experiments where flow cytometry was performed, Henson, F. et al. (2021) detected: *CD34, CD45, CD73, CD90*,and *CD 105*, and Broeckx, S. Y. et al. (2019) detected: *CD45, MHC II, CD29*, *CD44,* and *CD90*, Fu, W. L. et al. (2014) detected: *CD44, CD45, and MHC II*. All studies used intra-articular injection for cell implantation. In the

TABLE 3 | PBSCs *in vitro*.

First author	Species	Number	Character	Type of study	Evaluation method	Injury site(number)	Degree of damage
Frisch, J.(2019)	*in vitro*	NI	4 donors age 42 ± 27	Basic Medical Experiment	Biochemical analyses, Histological and immunohistochemical analyses, Histomorphometry, and Real-time RT-PCR analyses	NI	NA
Hopper, N.(2015)	*in vitro*	NI	12 young (32.9 ± 9.3 years) volunteers	Basic Medical Experiment	Scratch assay, xCELLigence assay, Cell proliferation, Cell proliferation, mRNA expression, PCR array, and Quantitative real-time PCR	NI	NA
Turajane, T.(2014)	*in vitro*	10	10 patients (median age 58 years, range 56–60 years, eight females)	Basic Medical Experiment	Attachment and proliferation assays, Attachment and proliferation assays, Flow cytometry analysis, RT-PCR analysis, Scanning electron microscopy, and Histology	NI	Half ICRS grade = 2 Remainder ICRS grade>3
Kim, J.(2012)	*in vitro*	NI	NA	Basic Medical Experiment	In vitro differentiation, Classification of differentially regulated proteins, western blot, and real-time RT-PCR analysis, and Immunofluorescent-staining	NI	NI
Chong, P. P.(2012)	*in vitro*	NI	NA	Basic Medical Experiment	Biochemical Assays, Morphological Analysis of Chondrogenic, Osteogenic, and Adi-Pyogenic, and Gene Expression Analysis,rt-PCR,	NI	NI
Casado, J. G.(2012)	*in vitro*	NI	Large White pigs aged between 3 and 4 months	Basic Medical Experiment	flow cytometry, adipogenic, chondrogenic and osteogenic differentiation, and Quantitative RT-PCR	NI	NI
Pufe, T.(2008)	*in vitro*	NA	NA	Basic Medical Experiment	Immunohistochemistry, Electron Microscopy, and Enzyme-Linked Immunosorbent Assay,rt-PCR,	NI	NI

First author	Cell source	Cultivation and extraction methods	Cell character markers	Number of cells	Cell implantation method	Surgical approach
Frisch, J.(2019)	rAAV transferred PB MSC	DGC and PA	IGF-I, aggrecan, COL2A1, and SOX9	NA	NA	NA
Hopper, N.(2015)	PBSCs	DGC	C5a, CXCL1, ICAM-1, IL-1β, IL-1ra, IL-6, IL-8, IL-13, IL-16, CXCL10, CXCL11, CCL2, MIF, CCL5, and PAI-1	NA	NA	NA
Turajane, T.(2014)	Autologous G-CSFactivated PB	DGC	*CD34*, *CD29*, *CD44*, *CD45*, *CD90*, *and CD105*	NA	NA	NA
Kim, J.(2012)	PBMSC	NA	*CD34*, *CD45*. *CD133*, *CD73*, *CD90,CD105*,PDGF-B, and HLA-ABC	NA	NI	NI
Chong, P. P.(2012)	PBMSC	NA	*CD105*, *CD166*, *and CD29*	NA	NI	NI
Casado, J. G.(2012)	Peripheral blood mononuclear cells	Erythrocyte lysis, DGC and PA	$CD29^{+}$, $CD44^{+}$, $CD45^{-}$, $CD90^{+}$, and *CD105*+	NA	NI	NI
Pufe, T.(2008)	Peripheral blood mononuclear cells	DGC and PA	NA	NA	NA	NA

First author	Time	Postoperative treatment	Clinical outcome	Imaging results	Experimental results	Adverse event
Frisch, J.(2019)	NA	NI	NI	NI	Enhanced proliferative and chondrogenic activities, Significantly increased cellularity, Enhanced levels of chondrogenic marker expression	NA
Hopper, N.(2015)	NA	NI	NI	NI	The wound closure rate at the 3 h time point was significantly higher* no significant difference between the PBMC-stimulated and non-stimulated test groups in the total DNA amount The mRNA levels for these genes were upregulated by the 24 h PBMC stimulus: SOX9 and COL2A1	NA
Turajane, T.(2014)	7 days	NI	NI	NI	Cell proliferation on day 7 showed statistically significant differences* increase in cell attachment and cell proliferation* Sox9 increased in days 7 and 14, Sox9 increased on days 7, Aggrecan increases were statistically significant on days 7 and 14	NA
Kim, J.(2012)	NA	NI	NA	NI	MSC from PB also shows the differentiation of chondroitin	NA

(Continued on following page)

TABLE 3 | (*Continued*) PBSCs *in vitro*.

First author	Time	Postoperative treatment	Clinical outcome	Imaging results	Experimental results	Adverse event
Chong, P. P.(2012)	NA	NI	NA	NI	MSCs from PB maintain similar characteristics and have similar chondrogenic differentiation potential to those derived from BM while producing comparable s-GAG expressions to chondrocytes	NA
Casado, J. G.(2012)	2 weeks	NI	NA	NI	PBMSC have both chondrogenic and adipogenic potential	NA
Pufe, T.(2008)	6 weeks	NI	NI	NI	A strong accumulation of collagen type II after a 6 weeks found chondrogenic differentiation with a continuous expression of collagen type II mRNA and protein	NA

** means statistically different.*

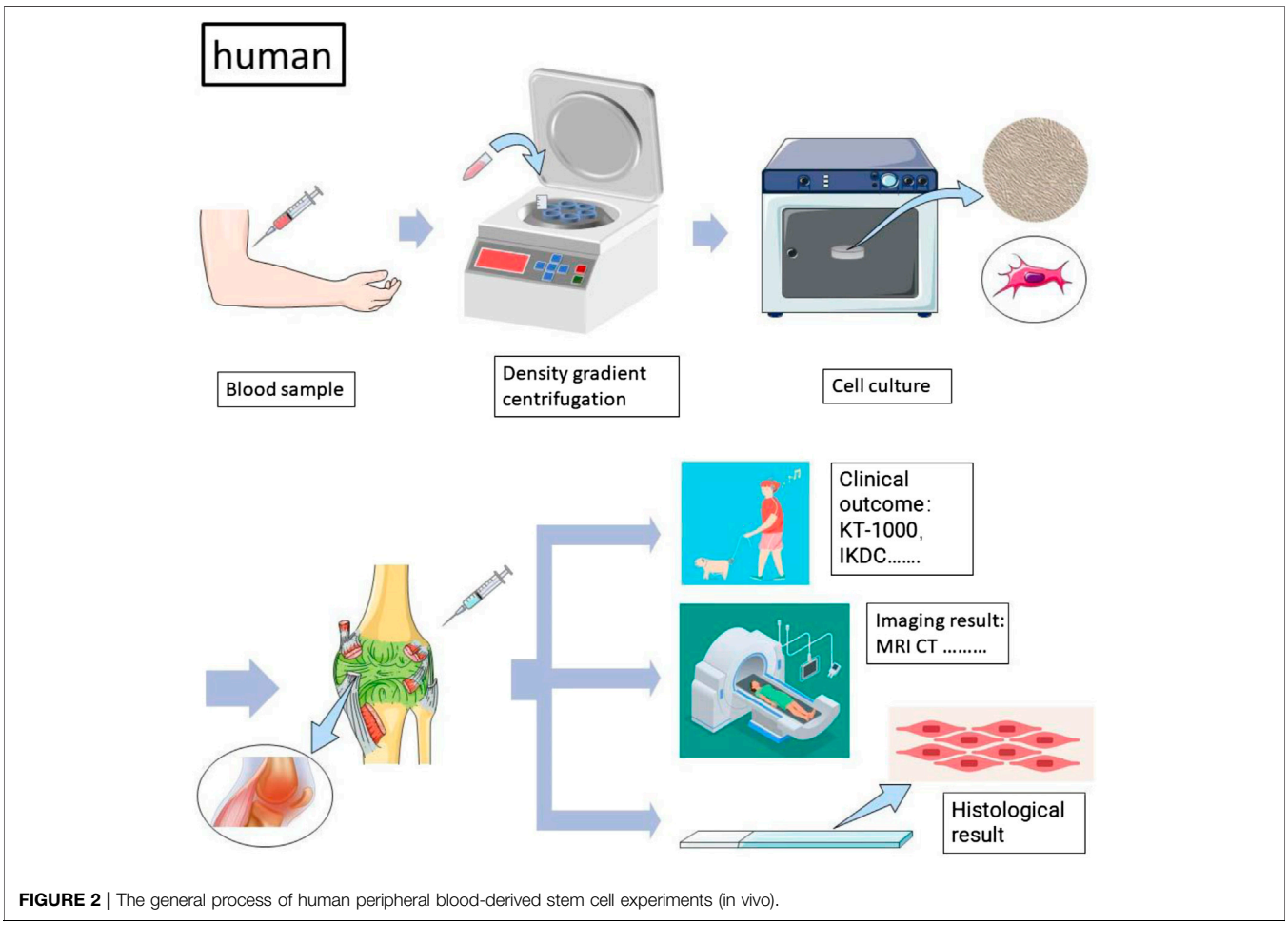

FIGURE 2 | The general process of human peripheral blood-derived stem cell experiments (in vivo).

postoperative results, the clinical results showed a consistent trend of improvement, whether it was objective indicators or subjective scores. In the imaging results, except for the study done by Broeckx, S. Y in 2019, the radiographic changes were not significantly different. The rest showed improvements after the use of peripheral blood-derived stem cells. In the absence of laboratory validation, only three articles showed increased levels of cartilage-related matrix or components around damaged cartilage tissue, such as type II collagen and cartilage oligomeric matrix protein. The detailed information is shown in **Table 1**.

3.4 PBMSC *In Vitro*

In this systematic review, we included a total of seven articles from *in vitro* studies (Pufe et al., 2008; Casado et al., 2012; Chong et al., 2012; Kim et al., 2012; Turajane et al., 2014;

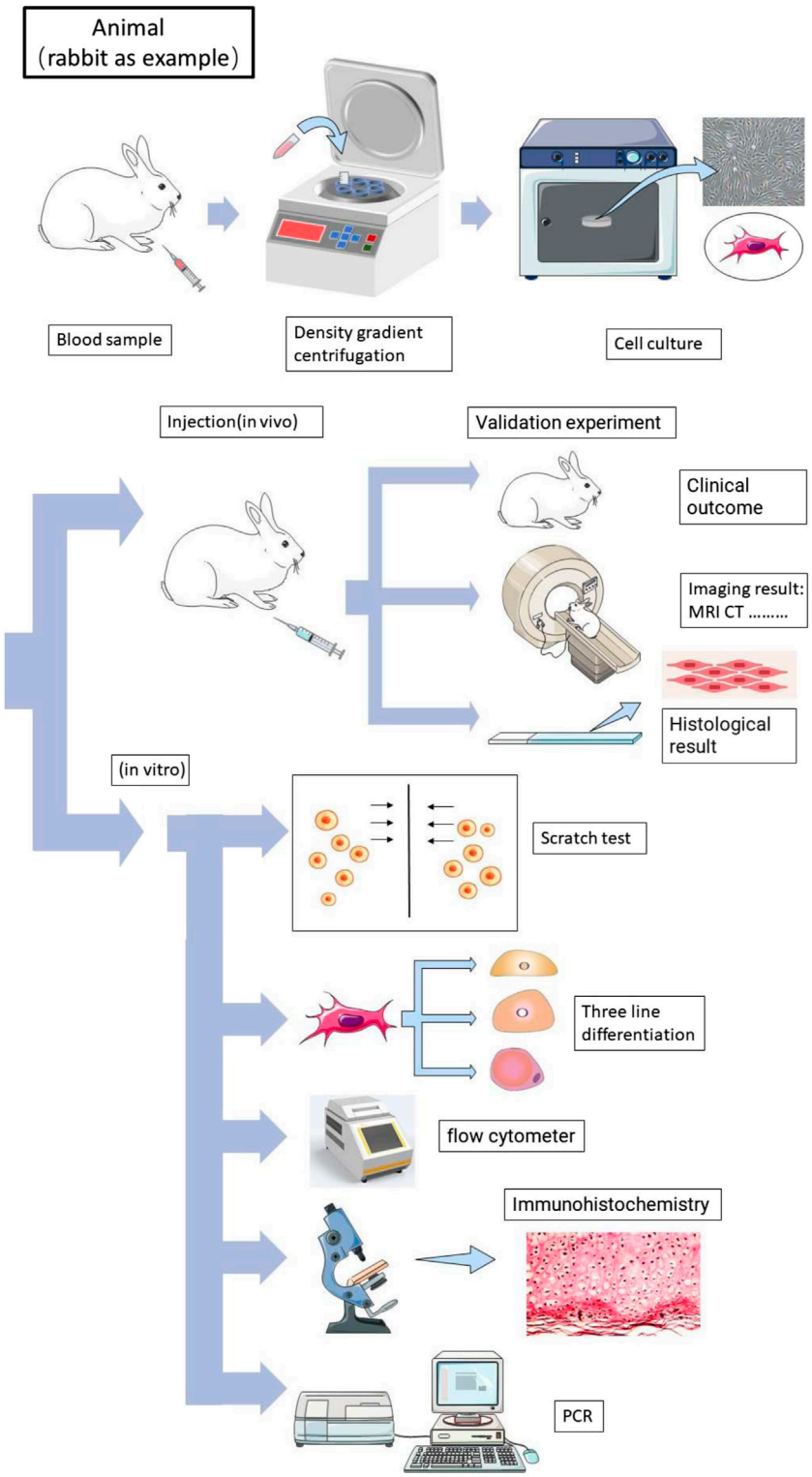

FIGURE 3 | The general process of animal and *in vitro* peripheral blood-derived stem cell experiments (rabbit as an example).

Hopper et al., 2015b; Frisch et al., 2017b). Among them, the donors of three experiments were humans, the donors of one experiment were pigs, and the peripheral blood donors were not specified in the remaining experiments. The validation methods for *in vitro* experiments include scratch experiments, immunohistochemistry, flow cytometry, RT-PCR, and more.

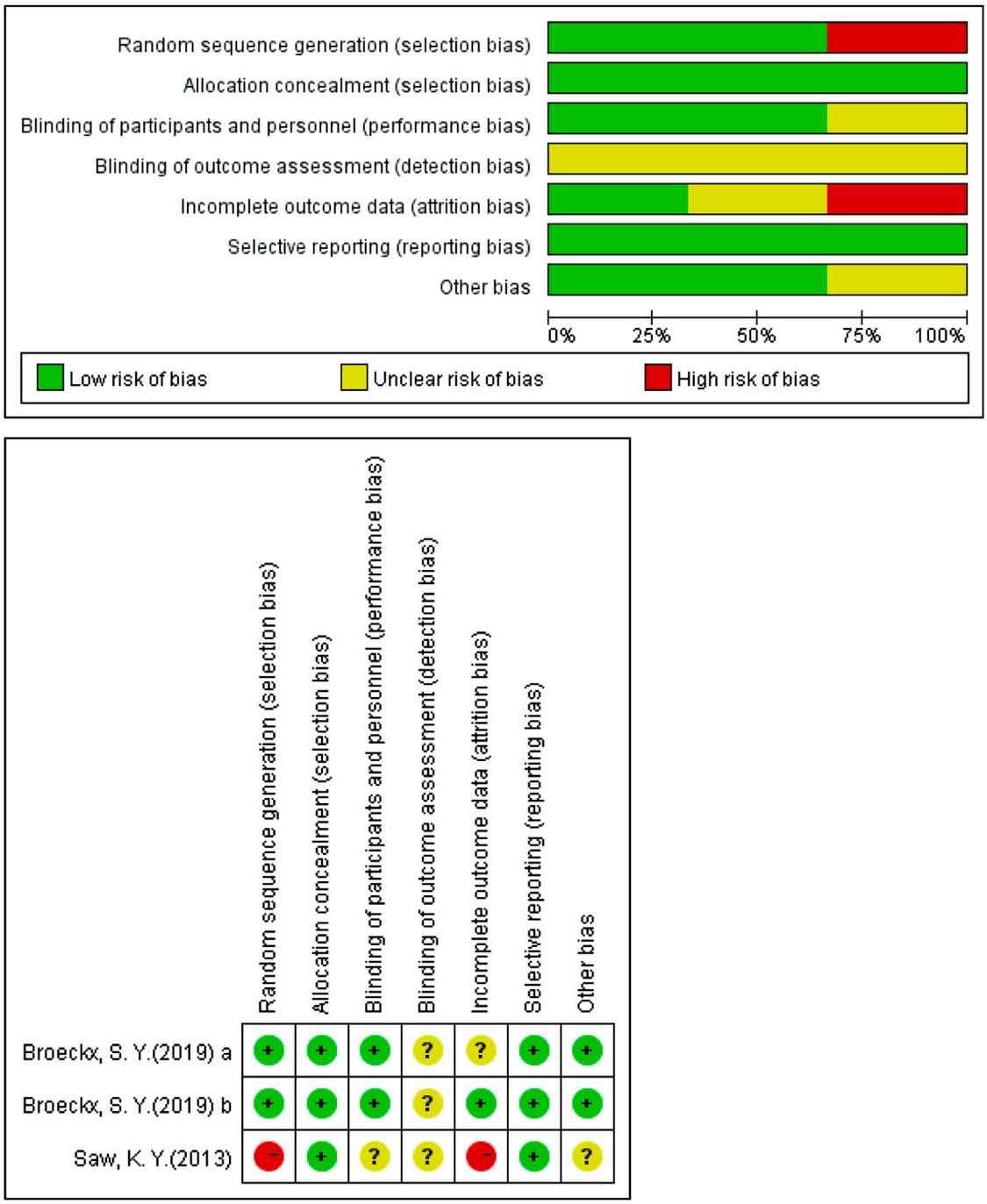

FIGURE 4 | Risk of bias with RCTs.

The authors described the peripheral blood-derived stem cells used in the article, including the peripheral blood mononuclear cells, PBMSC, autologous G-CSF activated PB, and peripheral blood stem cells (PBSCs). CD105+ was found in all experiments with flow cytometry results, but $CD34^{+}$ was found in all experiments by Turajane, T. et al., may indicate that the cells used in the experiments are the nonmesenchymal presence of stem cells. Other experiments uncovered the secretion of many chemokines, which may also be largely involved in the induction of cartilage repair. In terms of results, all studies have proved that the peripheral blood-derived stem cells can differentiate into cartilage and have

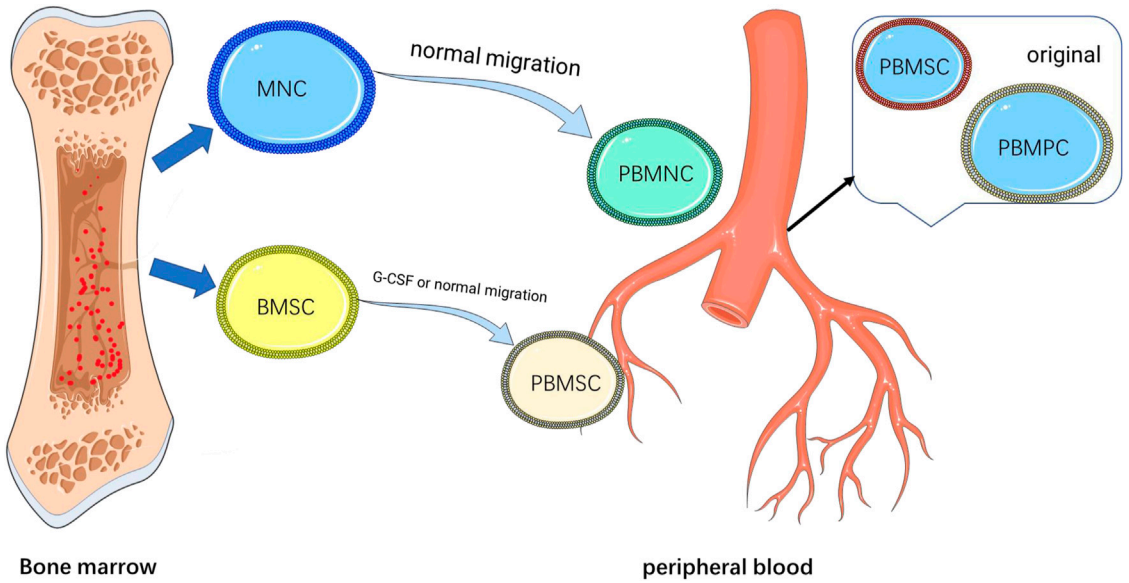

FIGURE 5 | Basic biology of blood-derived stem cells. MNC, mononuclear cells; BMSC, Bone marrow mesenchymal stem cells; PBMSC, peripheral blood mesenchymal stem cells; PBMNC, peripheral blood mononuclear cells; and PBMPC, peripheral blood mesenchymal progenitor cells.

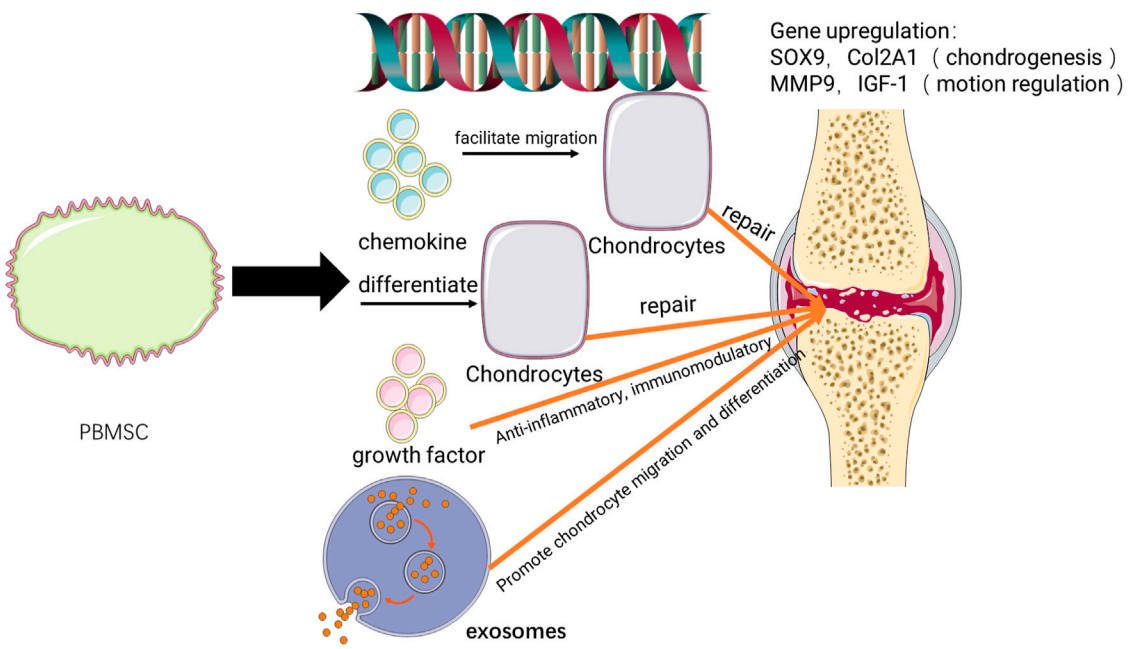

FIGURE 6 | Potential mechanisms of PBMSC in cartilage repair.

the potential to repair cartilage damage. Hopper, N, and Turajane, T. all found the upregulation of SOX-9 in their experiments, indicating that the peripheral blood-derived stem cells have a regulatory effect on cartilage differentiation. The formation of the extrachondral matrix was found in all *in vitro* studies, which is important for cartilage repair. The detailed information is shown in **Table 3**.

4 DISCUSSION

According to the research on stem cells derived from peripheral blood *in vitro*, they have the same or similar chondrogenic differentiation ability as that of the bone marrow mesenchymal stem cells in the process of culture and passage *in vitro*, as Chong, P. P. showed in his research. (Chong et al., 2012; Gong et al., 2021).

TABLE 4 | QUADAS quality assessment of other study(Y =Yes, N=No, and U=Unclear) based on the items that are described in the method section.

items First author	1	2	3	4	5	6	7	8	9	10	11	12	13	14	15	16	17	18
Henson, F. (2021)	Y	Y	Y	Y	U	N	N	N	Y	Y	Y	Y	Y	Y	U	N	N	N
Ying, J.(2020)	Y	Y	Y	U	Y	Y	Y	Y	Y	Y	Y	Y	Y	N	N	Y	Y	U
Monckeberg, J. E. (2019)	Y	Y	Y	Y	Y	Y	Y	Y	N	N	U	Y	Y	Y	Y	Y	Y	Y
Broeckx, S. Y.(2019)	Y	Y	U	N	N	N	Y	Y	Y	Y	Y	N	N	Y	Y	Y	Y	Y
Broeckx, S. Y.(2019)	Y	N	N	U	Y	Y	Y	Y	Y	Y	Y	Y	N	N	Y	N	N	N
Frisch, J.(2019)	Y	Y	Y	Y	N	Y	Y	Y	Y	Y	N	N	U	Y	U	U	U	U
Hopper, N.(2015)	Y	Y	N	Y	Y	Y	N	Y	N	Y	U	Y	Y	U	Y	Y	U	U
Turajane, T.(2014)	N	N	Y	N	N	Y	Y	N	N	U	Y	Y	Y	U	U	Y	U	N
Fu, W. L.(2014)	Y	Y	N	N	Y	Y	N	Y	Y	N	U	Y	Y	Y	Y	N	Y	U
Fu, W. L.(2014)	Y	Y	Y	Y	Y	U	Y	N	N	U	Y	Y	Y	Y	Y	Y	Y	U
Broeckx, S.(2014)	U	Y	N	N	Y	Y	U	Y	Y	Y	Y	Y	Y	U	Y	Y	Y	N
Broeckx, S.(2014)	Y	Y	N	N	Y	Y	N	Y	Y	Y	Y	Y	Y	Y	Y	Y	Y	Y
Turajane, T.(2013)	Y	Y	Y	Y	N	Y	Y	U	Y	N	Y	Y	Y	U	U	Y	Y	Y
Skowroński, J.(2013)	Y	Y	Y	Y	Y	N	Y	Y	U	U	U	N	Y	Y	U	U	U	U
Saw, K. Y.(2013)	Y	N	Y	U	U	U	Y	Y	U	Y	N	Y	N	N	Y	U	Y	U
Skowroński, J.(2012)	N	N	N	Y	U	Y	Y	U	U	U	U	Y	Y	Y	Y	Y	Y	Y
Kim, J.(2012)	N	Y	N	N	U	Y	Y	Y	Y	Y	Y	Y	Y	N	Y	U	U	U
Chong, P. P.(2012)	U	Y	Y	U	Y	Y	Y	U	Y	N	N	Y	Y	U	Y	Y	N	Y
Casado, J. G.(2012)	U	N	Y	Y	N	Y	N	U	U	Y	Y	Y	Y	U	Y	Y	Y	Y
Saw, K. Y.(2012)	Y	Y	Y	N	U	N	Y	Y	U	Y	Y	Y	N	U	Y	Y	N	Y
Pufe, T.(2008)	Y	Y	Y	Y	N	N	Y	U	U	Y	Y	Y	Y	Y	U	U	N	U
Jancewicz, P.(2004)	Y	Y	N	N	Y	U	Y	Y	Y	Y	Y	Y	Y	N	Y	U	Y	N

Combined with the human and animal research reports on its improved *in vivo* results, this systematic review shows that peripheral blood-derived stem cells have chondrogenic differentiation ability and can induce chondrogenic differentiation and repair *in vivo*, and have statistical significance in the clinical and imaging prognosis. There is improvement of academic differences. Compared with bone marrow, the peripheral blood is easier to obtain, widely sourced, and simple to obtain. In the future, peripheral blood will be a more potential cell source for cell therapy in the treatment of cartilage damage.

However, some studies have contrary results. In the study of Ying, J. et al. (Ying et al., 2020), peripheral blood-derived stem cells did not show improvement in the clinical and imaging results in the treatment of femoral head necrosis, and combined treatment in histology. The bone destruction in the group was more severe than that in the control group. But a previous study showed that combination therapy with an intra-arterial infusion of PBSCs showed improved the outcomes in patients with early and mid-stage necrosis of the femoral head (Schmitt-Sody et al., 2008; Mao et al., 2015). Considering the advantages of PBSC in easily harvesting and stimulating neovascularization and osteogenesis in the damaged skeletal tissue, PBSC transplantation is a selective approach for the treatment of ONFH (Zhang et al., 2016). In this study, it was used to treat patients with femoral head necrosis with cartilage cap separation, which has exceeded the early and middle stages and is an advanced stage disease (Xiong et al., 2016). At this stage, the active expression of osteoclasts and the widespread occurrence of inflammatory responses lead to irreversible necrosis of the femoral head, which may require more complex mechanisms to explain (Feng et al., 2010). Femoral head necrosis is a complex pathophysiological process involving cartilage, subchondral bone, bone, and surrounding tissues. The repair mechanism of cartilage damaged by the peripheral blood stem cells alone may not be able to offset the overall damage caused by the inflammatory response. Moreover, in this study conducted by Ying, J. et al., although the injection of PBSCs into the internal circumflex artery did not improve the survival rate of femoral head necrosis, it had a good effect on relieving pain and improving the joint function. This result can also reflect that peripheral blood-derived stem cells have a repairing effect on intra-articular cartilage damage, although it cannot be reflected in the histology of this study (Hopson and Siverhus, 1988). This makes us think that in the treatment of some diseases with more complex mechanisms than simple cartilage damage, the use of stem cells derived from peripheral blood alone may not have a good prognosis, and more combined treatment or surgical treatment is needed. But not being able to cure the disease is not the same as denying its effect on the repair of cartilage damage **Figure 5**.

The cell types and potential repair mechanisms are detailed in **Figure 5**, **6**. At present, the cell source used in most research is G-CSF activated PB or chondrogenic-induced PBMSCs. It has been demonstrated in the previous literature that G-CSF and CXCR4 antagonists can mobilize mesenchymal stem cells into peripheral blood (Pelus, 2008; Kolonin and Simmons, 2009). It can improve the success rate of subsequent mesenchymal stem cell culture, and the density of mesenchymal stem cells is also an important feature to evaluate cartilage repair. Moreover, in the other literature, a simple injection of G-CSF can make bone marrow and peripheral blood mesenchymal stem cells home to the joint cavity and help cartilage regeneration (Sasaki et al., 2017; Turajane et al., 2017). The literature included in this systematic review also showed that G-CSF activated PB has the potential for chondrogenic differentiation and repair and is a good alternative

resource. While chondrogenic-induced PBMSCs secrete more extrachondral matrix including aggrecan, type II collagen, and cartilage oligomeric matrix protein when cultured *in vitro*, which reflects better proliferation ability (Broeckx et al., 2014a) and has been shown in one study to better adhere to cartilage in explant cultures (Spaas et al., 2015). TGF-β, one of the cartilage-stimulating growth factors used in the current study for predifferentiation of chondrocyte differentiation, can reduce the expression of MHC (Berglund et al., 2017). This can reduce the occurrence of inflammatory reactions and reduce the chance of immune rejection (Schnabel et al., 2014). The two preparation methods have their advantages, but there is no research to compare the advantages and disadvantages of the two methods to give guiding opinions. Future research can combine the advantages of the two methods, and it is believed that a more effective new preparation method can be obtained.

Stem cells have many advantages and can effectively treat cartilage damage; for example, they have strong self-renewal capacity, pluripotency, and plasticity. However, the properties of MSCs may be altered by various elements of the local microenvironment that influence differentiation, may cause reduced chondrogenic activity or differentiation into other tissues, so they may suffer from disadvantages such as eventual hypertrophy or tumorigenesis (Chen and Tuan, 2008; Vinatier et al., 2009; Koh et al., 2014; Pandey et al., 2022). However, in the studies we included, adverse events were mild and there was no worsening change in the imaging findings. This may indicate that stem cells derived from peripheral blood have stable differentiation (Chong et al., 2012). This also proves our point that peripheral blood-derived stem cells are an important source of cells to repair cartilage damage.

This article also has certain limitations. In the selection of literature, due to the continuous updating of preparation methods and repair mechanisms, we only included relevant literature after 2008, excluding some studies in older periods, which may make the research results subject to influence. In the statistics of cell phenotype, no further analysis was performed for the events whose cells highly expressed $CD34^{+}$ and some studies did not express the mesenchymal stem cell marker *CD105+*. This means that, in some of the included studies, it is not only mesenchymal stem cells that perform cartilage repair, but may also be mononuclear cells or other stem cells in peripheral blood. Therefore, here, we refer to them as the peripheral blood-derived stem cells and use this fully as a resource for cartilage repair.

5 CONCLUSION

Stem cells derived from peripheral blood have the ability to repair cartilage and are an important resource for the treatment of cartilage damage in the future. The specific mechanism and way of repairing cartilage need further study.

DATA AVAILABILITY STATEMENT

The original contributions presented in the study are included in the article/Supplementary Material. Further inquiries can be directed to the corresponding author.

AUTHOR CONTRIBUTIONS

All authors contributed to the study conception and design. Material preparation, data collection, and analysis were performed by YZ. The first draft of the manuscript was written by YZ and all authors commented on previous versions of the manuscript. All authors read and approved the final manuscript.

REFERENCES

Al Faqeh, H., Nor Hamdan, B. M. Y., Chen, H. C., Aminuddin, B. S., and Ruszymah, B. H. I. (2012). The Potential of Intra-articular Injection of Chondrogenic-Induced Bone Marrow Stem Cells to Retard the Progression of Osteoarthritis in a Sheep Model. *Exp. Gerontol.* 47 (6), 458–464. doi:10.1016/j.exger.2012.03.018

Berglund, A. K., Fisher, M. B., Cameron, K. A., Poole, E. J., and Schnabel, L. V. (2017). Transforming Growth Factor-B2 Downregulates Major Histocompatibility Complex (MHC) I and MHC II Surface Expression on Equine Bone Marrow-Derived Mesenchymal Stem Cells without Altering Other Phenotypic Cell Surface Markers. *Front. Vet. Sci.* 4, 84. doi:10.3389/fvets.2017.00084

Bieback, K., Kern, S., Kocaömer, A., Ferlik, K., and Bugert, P. (2008). Comparing Mesenchymal Stromal Cells from Different Human Tissues: Bone Marrow, Adipose Tissue and Umbilical Cord Blood. *Biomed. Mater Eng.* 18 (1 Suppl. l), S71–S76.

Brittberg, M., Lindahl, A., Nilsson, A., Ohlsson, C., Isaksson, O., and Peterson, L. (1994). Treatment of Deep Cartilage Defects in the Knee with Autologous Chondrocyte Transplantation. *N. Engl. J. Med.* 331 (14), 889–895. doi:10.1056/nejm199410063311401

Broeckx, S., Suls, M., Beerts, C., Vandenberghe, A., Seys, B., Wuertz-Kozak, K., et al. (2014). Allogenic Mesenchymal Stem Cells as a Treatment for Equine Degenerative Joint Disease: a Pilot Study. *Cscr* 9 (6), 497–503. doi:10.2174/1574888x09666140826110601

Broeckx, S. Y., Martens, A. M., Bertone, A. L., Van Brantegem, L., Duchateau, L., Van Hecke, L., et al. (2019). The Use of Equine Chondrogenic-induced Mesenchymal Stem Cells as a Treatment for Osteoarthritis: A Randomised, Double-blinded, Placebo-controlled Proof-of-concept Study. *Equine Vet. J.* 51 (6), 787–794. doi:10.1111/evj.13089

Broeckx, S. Y., Seys, B., Suls, M., Vandenberghe, A., Mariën, T., Adriaensen, E., et al. (2019). Equine Allogeneic Chondrogenic Induced Mesenchymal Stem Cells Are an Effective Treatment for Degenerative Joint Disease in Horses. *Stem cells Dev.* 28 (6), 410–422. doi:10.1089/scd.2018.0061

Broeckx, S., Zimmerman, M., Crocetti, S., Suls, M., Mariën, T., Ferguson, S. J., et al. (2014). Regenerative Therapies for Equine Degenerative Joint Disease: a Preliminary Study. *PloS one* 9 (1), e85917. doi:10.1371/journal.pone.0085917

Casado, J. G., Gomez-Mauricio, G., Alvarez, V., Mijares, J., Tarazona, R., Bernad, A., et al. (2012). Comparative Phenotypic and Molecular Characterization of Porcine Mesenchymal Stem Cells from Different Sources for Translational Studies in a Large Animal Model. *Vet. Immunol. Immunopathol.* 147 (1-2), 104–112. doi:10.1016/j.vetimm.2012.03.015

Chen, F. H., and Tuan, R. S. (2008). Mesenchymal Stem Cells in Arthritic Diseases. *Arthritis Res. Ther.* 10 (5), 223. doi:10.1186/ar2514

Chong, P.-P., Selvaratnam, L., Abbas, A. A., and Kamarul, T. (2012). Human Peripheral Blood Derived Mesenchymal Stem Cells Demonstrate Similar

Characteristics and Chondrogenic Differentiation Potential to Bone Marrow Derived Mesenchymal Stem Cells. *J. Orthop. Res.* 30 (4), 634–642. doi:10.1002/jor.21556

Emadedin, M., Aghdami, N., Taghiyar, L., Fazeli, R., Moghadasali, R., Jahangir, S., et al. (2012). Intra-articular Injection of Autologous Mesenchymal Stem Cells in Six Patients with Knee Osteoarthritis. *Arch. Iran. Med.* 15 (7), 422–428. doi:10.12157/AIM.0010

Feng, Y., Yang, S.-H., Xiao, B.-J., Xu, W.-H., Ye, S.-N., Xia, T., et al. (2010). Decreased in the Number and Function of Circulation Endothelial Progenitor Cells in Patients with Avascular Necrosis of the Femoral Head. *Bone* 46 (1), 32–40. doi:10.1016/j.bone.2009.09.001

Ferris, D. J., Frisbie, D. D., McIlwraith, C. W., and Kawcak, C. E. (2011). Current Joint Therapy Usage in Equine Practice: a Survey of Veterinarians 2009. *Equine veterinary J.* 43 (5), 530–535. doi:10.1111/j.2042-3306.2010.00324.x

Frisbie, D. D., Kisiday, J. D., Kawcak, C. E., Werpy, N. M., and McIlwraith, C. W. (2009). Evaluation of Adipose-Derived Stromal Vascular Fraction or Bone Marrow-Derived Mesenchymal Stem Cells for Treatment of Osteoarthritis. *J. Orthop. Res.* 27 (12), 1675–1680. doi:10.1002/jor.20933

Frisch, J., Orth, P., Rey-Rico, A., Venkatesan, J. K., Schmitt, G., Madry, H., et al. (2017). Peripheral Blood Aspirates Overexpressing IGF-IviarAAV Gene Transfer Undergo Enhanced Chondrogenic Differentiation Processes. *J. Cell. Mol. Med.* 21 (11), 2748–2758. doi:10.1111/jcmm.13190

Frisch, J., Orth, P., Venkatesan, J. K., Rey-Rico, A., Schmitt, G., Kohn, D., et al. (2017). Genetic Modification of Human Peripheral Blood Aspirates Using Recombinant Adeno-Associated Viral Vectors for Articular Cartilage Repair with a Focus on Chondrogenic Transforming Growth Factor-β Gene Delivery. *Stem cells Transl. Med.* 6 (1), 249–260. doi:10.5966/sctm.2016-0149

Fu, W.-L., Ao, Y.-F., Ke, X.-Y., Zheng, Z.-Z., Gong, X., Jiang, D., et al. (2014). Repair of Large Full-Thickness Cartilage Defect by Activating Endogenous Peripheral Blood Stem Cells and Autologous Periosteum Flap Transplantation Combined with Patellofemoral Realignment. *Knee* 21 (2), 609–612. doi:10.1016/j.knee.2013.10.010

Fu, W.-L., Zhou, C.-Y., and Yu, J.-K. (2014). A New Source of Mesenchymal Stem Cells for Articular Cartilage Repair. *Am. J. Sports Med.* 42 (3), 592–601. doi:10.1177/0363546513512778

Gong, J., Fairley, J., Cicuttini, F. M., Hussain, S. M., Vashishtha, R., Chou, L., et al. (2021). Effect of Stem Cell Injections on Osteoarthritis-Related Structural Outcomes: A Systematic Review. *J. Rheumatol.* 48 (4), 585–597. doi:10.3899/jrheum.200021

Henson, F., Lydon, H., Birch, M., Brooks, R., and McCaskie, A. (2021). Using Apheresis-derived Cells to Augment Microdrilling in the Treatment of Chondral Defects in an Ovine Model. *J. Orthop. Res.* 39 (7), 1411–1422. doi:10.1002/jor.24889

Hopper, N., Henson, F., Brooks, R., Ali, E., Rushton, N., and Wardale, J. (2015). Peripheral Blood Derived Mononuclear Cells Enhance Osteoarthritic Human Chondrocyte Migration. *Arthritis Res. Ther.* 17 (1), 199. doi:10.1186/s13075-015-0709-z

Hopper, N., Wardale, J., Brooks, R., Power, J., Rushton, N., and Henson, F. (2015). Peripheral Blood Mononuclear Cells Enhance Cartilage Repair in *In Vivo* Osteochondral Defect Model. *PloS one* 10 (8), e0133937. doi:10.1371/journal.pone.0133937

Hopson, C. N., and Siverhus, S. W. (1988). Ischemic Necrosis of the Femoral Head. Treatment by Core Decompression. *J. Bone & Jt. Surg.* 70 (7), 1048–1051. doi:10.2106/00004623-198870070-00013

Huang, Y.-C., Yang, Z.-M., Chen, X.-H., Tan, M.-Y., Wang, J., Li, X.-Q., et al. (2009). Isolation of Mesenchymal Stem Cells from Human Placental Decidua Basalis and Resistance to Hypoxia and Serum Deprivation. *Stem Cell. Rev Rep* 5 (3), 247–255. doi:10.1007/s12015-009-9069-x

Hunziker, E. B. (2002). Articular Cartilage Repair: Basic Science and Clinical Progress. A Review of the Current Status and Prospects. *Osteoarthr. Cartil.* 10 (6), 432–463. doi:10.1053/joca.2002.0801

Jancewicz, P., Dzienis, W., Pietruczuk, M., Skowroński, J., and Bielecki, M. (1995). Osteochondral Defects of the Talus Treated by Mesenchymal Stem Cell Implantation-Eearly Results. *Rocz. Akad. Med. Bialymst* 49 (Suppl. 1), 25–27.

Jiang, Y., and Tuan, R. S. (2015). Origin and Function of Cartilage Stem/progenitor Cells in Osteoarthritis. *Nat. Rev. Rheumatol.* 11 (4), 206–212. doi:10.1038/nrrheum.2014.200

Kassis, I., Zangi, L., Rivkin, R., Levdansky, L., Samuel, S., Marx, G., et al. (2006). Isolation of Mesenchymal Stem Cells from G-CSF-Mobilized Human Peripheral Blood Using Fibrin Microbeads. *Bone Marrow Transpl.* 37 (10), 967–976. doi:10.1038/sj.bmt.1705358

Kim, J., Shin, J. M., Jeon, Y. J., Chung, H. M., and Chae, J.-I. (2012). Proteomic Validation of Multifunctional Molecules in Mesenchymal Stem Cells Derived from Human Bone Marrow, Umbilical Cord Blood and Peripheral Blood. *PloS one* 7 (5), e32350. doi:10.1371/journal.pone.0032350

Koh, Y. G., Choi, Y. J., Kwon, O. R., and Kim, Y. S. (2014). Second-Look Arthroscopic Evaluation of Cartilage Lesions after Mesenchymal Stem Cell Implantation in Osteoarthritic Knees. *Am. J. Sports Med.* 42 (7), 1628–1637. doi:10.1177/0363546514529641

Kolonin, M. G., and Simmons, P. J. (2009). Combinatorial Stem Cell Mobilization. *Nat. Biotechnol.* 27 (3), 252–253. doi:10.1038/nbt0309-252

Larochelle, A., Krouse, A., Metzger, M., Orlic, D., Donahue, R. E., Fricker, S., et al. (2006). AMD3100 Mobilizes Hematopoietic Stem Cells with Long-Term Repopulating Capacity in Nonhuman Primates. *Blood* 107 (9), 3772–3778. doi:10.1182/blood-2005-09-3592

Madry, H., Grün, U. W., and Knutsen, G. (2011). Cartilage Repair and Joint Preservation. *Dtsch. Arzteblatt Int.* 108 (40), 669–677. doi:10.3238/arztebl.2011.0669

Mao, Q., Wang, W., Xu, T., Zhang, S., Xiao, L., Chen, D., et al. (2015). Combination Treatment of Biomechanical Support and Targeted Intra-arterial Infusion of Peripheral Blood Stem Cells Mobilized by Granulocyte-Colony Stimulating Factor for the Osteonecrosis of the Femoral Head: a Randomized Controlled Clinical Trial. *J. bone mineral Res. official J. Am. Soc. Bone Mineral Res.* 30 (4), 647–656.

Moher, D., Liberati, A., Tetzlaff, J., and Altman, D. G. (2009). Preferred Reporting Items for Systematic Reviews and Meta-Analyses: the PRISMA Statement. *PLoS Med.* 6 (7), e1000097. doi:10.1371/journal.pmed.1000097

Monckeberg, J. E., Rafols, C., Apablaza, F., Gerhard, P., and Rosales, J. (2019). Intra-articular Administration of Peripheral Blood Stem Cells with Platelet-Rich Plasma Regenerated Articular Cartilage and Improved Clinical Outcomes for Knee Chondral Lesions. *Knee* 26 (4), 824–831. doi:10.1016/j.knee.2019.05.008

Orth, P., Rey-Rico, A., Venkatesan, J. K., Madry, H., and Cucchiarini, M. (2014). Current Perspectives in Stem Cell Research for Knee Cartilage Repair. *Stem Cells Cloning* 7, 1–17. doi:10.2147/SCCAA.S42880

Pandey, V., Madi, S., and Gupta, P. (2022). The Promising Role of Autologous and Allogeneic Mesenchymal Stromal Cells in Managing Knee Osteoarthritis. What Is beyond Mesenchymal Stromal Cells? *J. Clin. Orthop. trauma* 26, 101804. doi:10.1016/j.jcot.2022.101804

Pelus, L. M. (2008). Peripheral Blood Stem Cell Mobilization: New Regimens, New Cells, where Do We Stand. *Curr. Opin. Hematol.* 15 (4), 285–292. doi:10.1097/moh.0b013e328302f43a

Pufe, T., Petersen, W., Fändrich, F., Varoga, D., Wruck, C. J., Mentlein, R., et al. (2008). Programmable Cells of Monocytic Origin (PCMO): a Source of Peripheral Blood Stem Cells that Generate Collagen Type II-Producing Chondrocytes. *J. Orthop. Res.* 26 (3), 304–313. doi:10.1002/jor.20516

Rackwitz, L., Djouad, F., Janjanin, S., Nöth, U., and Tuan, R. S. (2014). Functional Cartilage Repair Capacity of De-differentiated, Chondrocyte- and Mesenchymal Stem Cell-Laden Hydrogels *In Vitro*. *Osteoarthr. Cartil.* 22 (8), 1148–1157. doi:10.1016/j.joca.2014.05.019

Raghunath, J., Sutherland, J., Salih, V., Mordan, N., Butler, P. E., and Seifalian, A. M. (2010). Chondrogenic Potential of Blood-Acquired Mesenchymal Progenitor Cells. *J. Plastic, Reconstr. Aesthetic Surg.* 63 (5), 841–847. doi:10.1016/j.bjps.2009.01.063

Reissis, D., Tang, Q. O., Cooper, N. C., Carasco, C. F., Gamie, Z., Mantalaris, A., et al. (2016). Current Clinical Evidence for the Use of Mesenchymal Stem Cells in Articular Cartilage Repair. *Expert Opin. Biol. Ther.* 16 (4), 535–557. doi:10.1517/14712598.2016.1145651

Saris, D. B., Vanlauwe, J., Victor, J., Almqvist, K. F., Verdonk, R., Bellemans, J., et al. (2009). Treatment of Symptomatic Cartilage Defects of the Knee: Characterized Chondrocyte Implantation Results in Better Clinical Outcome at 36 Months in a Randomized Trial Compared to Microfracture. *Am. J. Sports Med.* 37 Suppl 1 (Suppl. 1), 10s–19s. doi:10.1177/0363546509350694

Sasaki, T., Akagi, R., Akatsu, Y., Fukawa, T., Hoshi, H., Yamamoto, Y., et al. (2017). The Effect of Systemic Administration of G-CSF on a Full-Thickness Cartilage

Defect in a Rabbit Model MSC Proliferation as Presumed Mechanism. *Bone & Jt. Res.* 6 (3), 123–131. doi:10.1302/2046-3758.63.bjr-2016-0083

Saw, K.-Y., Anz, A., Merican, S., Tay, Y.-G., Ragavanaidu, K., Jee, C. S. Y., et al. (2011). Articular Cartilage Regeneration with Autologous Peripheral Blood Progenitor Cells and Hyaluronic Acid after Arthroscopic Subchondral Drilling: a Report of 5 Cases with Histology. *Arthrosc. J. Arthrosc. Relat. Surg.* 27 (4), 493–506. doi:10.1016/j.arthro.2010.11.054

Saw, K.-Y., Anz, A., Siew-Yoke Jee, C., Merican, S., Ching-Soong Ng, R., Roohi, S. A., et al. (2013). Articular Cartilage Regeneration with Autologous Peripheral Blood Stem Cells versus Hyaluronic Acid: a Randomized Controlled Trial. *Arthrosc. J. Arthrosc. Relat. Surg.* 29 (4), 684–694. doi:10.1016/j.arthro.2012.12.008

Schmitt-Sody, M., Kirchhoff, C., Mayer, W., Goebel, M., and Jansson, V. (2008). Avascular Necrosis of the Femoral Head: Inter- and Intraobserver Variations of Ficat and ARCO Classifications. *Int. Orthop.* 32 (3), 283–287.

Schnabel, L. V., Pezzanite, L. M., Antczak, D. F., Felippe, M. J. B., and Fortier, L. A. (2014). Equine Bone Marrow-Derived Mesenchymal Stromal Cells Are Heterogeneous in MHC Class II Expression and Capable of Inciting an Immune Response *In Vitro*. *Stem Cell. Res. Ther.* 5 (1), 13. doi:10.1186/scrt402

Seol, D., McCabe, D. J., Choe, H., Zheng, H., Yu, Y., Jang, K., et al. (2012). Chondrogenic Progenitor Cells Respond to Cartilage Injury. *Arthritis & Rheumatism* 64 (11), 3626–3637. doi:10.1002/art.34613

Skowroński, J., and Rutka, M. (2013). Osteochondral Lesions of the Knee Reconstructed with Mesenchymal Stem Cells - Results. *Ortop. Traumatol. Rehabil.* 15 (3), 195–204. doi:10.5604/15093492.1058409

Skowroński, J., Skowroński, R., and Rutka, M. (2012). Cartilage Lesions of the Knee Treated with Blood Mesenchymal Stem Cells - Results. *Ortop. Traumatol. Rehabil.* 14 (6), 569–577. doi:10.5604/15093492.1012404

Spaas, J. H., Broeckx, S. Y., Chiers, K., Ferguson, S. J., Casarosa, M., Van Bruaene, N., et al. (2015). Chondrogenic Priming at Reduced Cell Density Enhances Cartilage Adhesion of Equine Allogeneic MSCs - a Loading Sensitive Phenomenon in an Organ Culture Study with 180 Explants. *Cell. Physiol. Biochem.* 37 (2), 651–665. doi:10.1159/000430384

Turajane, T., Chaveewanakorn, U., Fongsarun, W., Aojanepong, J., and Papadopoulos, K. I. (2017). Avoidance of Total Knee Arthroplasty in Early Osteoarthritis of the Knee with Intra-articular Implantation of Autologous Activated Peripheral Blood Stem Cells versus Hyaluronic Acid: A Randomized Controlled Trial with Differential Effects of Growth Factor Addition. *Stem Cells Int.* 2017, 8925132. doi:10.1155/2017/8925132

Turajane, T., Chaweewannakorn, U., Larbpaiboonpong, V., Aojanepong, J., Thitiset, T., Honsawek, S., et al. (2013). Combination of Intra-articular Autologous Activated Peripheral Blood Stem Cells with Growth Factor Addition/ Preservation and Hyaluronic Acid in Conjunction with Arthroscopic Microdrilling Mesenchymal Cell Stimulation Improves Quality of Life and Regenerates Articular Cartilage in Early Osteoarthritic Knee Disease. *J. Med. Assoc. Thai* 96 (5), 580–588.

Turajane, T., Thitiset, T., Honsawek, S., Chaveewanakorn, U., Aojanepong, J., and Papadopoulos, K. I. (2014). Assessment of Chondrogenic Differentiation Potential of Autologous Activated Peripheral Blood Stem Cells on Human Early Osteoarthritic Cancellous Tibial Bone Scaffold. *Musculoskelet. Surg.* 98 (1), 35–43. doi:10.1007/s12306-013-0303-y

Vinatier, C., Bouffi, C., Merceron, C., Gordeladze, J., Brondello, J.-M., Jorgensen, C., et al. (2009). Cartilage Tissue Engineering: towards a Biomaterial-Assisted Mesenchymal Stem Cell Therapy. *Cscr* 4 (4), 318–329. doi:10.2174/157488809789649205

Xiong, M. Y., Liu, L. Q., Liu, S. Q., Liu, Z. H., and Gao, H. F. (2016). Effects of Osteoprotegerin, RANK and RANKL on Bone Destruction and Collapse in Avascular Necrosis Femoral Head. *Am. J. Transl. Res.* 8 (7), 3133–3140.

Ying, J., Wang, P., Ding, Q., Shen, J., O'Keefe, R. J., Chen, D., et al. (2020). Peripheral Blood Stem Cell Therapy Does Not Improve Outcomes of Femoral Head Osteonecrosis with Cap-Shaped Separated Cartilage Defect. *J. Orthop. Res.* 38 (2), 269–276. doi:10.1002/jor.24471

Zhang, Y., Yin, J., Ding, H., Zhang, C., and Gao, Y.-S. (2016). Vitamin K2 Ameliorates Damage of Blood Vessels by Glucocorticoid: a Potential Mechanism for its Protective Effects in Glucocorticoid-Induced Osteonecrosis of the Femoral Head in a Rat Model. *Int. J. Biol. Sci.* 12 (7), 776–785. doi:10.7150/ijbs.15248

Zvaifler, N. J., Marinova-Mutafchieva, L., Adams, G., Edwards, C. J., Moss, J., Burger, J. A., et al. (2000). Mesenchymal Precursor Cells in the Blood of Normal Individuals. *Arthritis Res. Ther.* 2 (6), 477–488. doi:10.1186/ar130

Conflict of Interest: The authors declare that the research was conducted in the absence of any commercial or financial relationships that could be construed as a potential conflict of interest.

frontiers | Frontiers in Bioengineering and Biotechnology

ORIGINAL RESEARCH
published: 22 July 2022
doi: 10.3389/fbioe.2022.927050

A Structured Scaffold Featuring Biomimetic Heterogeneous Architecture for the Regeneration of Critical-Size Bone Defects

Lingjun Wang[1†], Jiannan Mao[2†], Feng Cai[1†], Jincheng Tang[1], Kun Xi[1], Yu Feng[1], Yichang Xu[1], Xiao Liang[1], Yong Gu[1]* and Liang Chen[1]**

[1]Department of Orthopaedics, The First Affiliated Hospital of Soochow University, Suzhou, China, [2]Department of Orthopaedics, The Affiliated Jiangyin Hospital of Nantong University Medical College, Jiang Yin, China

OPEN ACCESS

Edited by:
Ganjun Feng,
Sichuan University, China

Reviewed by:
Yuzhi Zuo,
Peking Union Medical College Hospital (CAMS), China
Zhenlin Yang,
Chinese Academy of Medical Sciences and Peking Union Medical College, China

***Correspondence:**
Xiao Liang
lxhj1020@126.com
Yong Gu
guyongsuzhou@163.com
Liang Chen
chenliangspine@163.com

[†]These authors have contributed equally to this work and share first authorship

Specialty section:
This article was submitted to Biomaterials, a section of the journal Frontiers in Bioengineering and Biotechnology

Received: 23 April 2022
Accepted: 09 June 2022
Published: 22 July 2022

Citation:
Wang L, Mao J, Cai F, Tang J, Xi K, Feng Y, Xu Y, Liang X, Gu Y and Chen L (2022) A Structured Scaffold Featuring Biomimetic Heterogeneous Architecture for the Regeneration of Critical-Size Bone Defects. Front. Bioeng. Biotechnol. 10:927050. doi: 10.3389/fbioe.2022.927050

The regeneration of critical-size bone defects on long bones has remained a significant challenge because of the complex anatomical structure and vascular network. In such circumstances, current biomaterial forms with homogeneous structure and function can hardly satisfy the need for both osteogenesis and angiogenesis. In the current study, a heterogeneous biomimetic structured scaffold was constructed with the help of a 3D printed mold to simultaneously mimic the outer/inner periosteum and intermediate bone matrix of a natural long bone. Because of the reinforcement *via* modified mesoporous bioactive glass nanoparticles (MBGNs), enhanced structural stability and adequate osteogenic capacity could be achieved for the intermediate layer of this scaffold. Conversely, GelMA incorporated with VEGF-loaded liposome exhibiting controlled release of the angiogenic factor was applied to the inner and outer layers of the scaffold. The resulting heterogeneous structured scaffold was shown to successfully guide bone regeneration and restoration of the natural bone anatomic structure, rendering it a promising candidate for future orthopedic clinical studies.

Keywords: structured scaffold, osteogenesis, angiogenesis, bone defect, biomaterial

INTRODUCTION

As the most common trauma condition, bone fractures have garnered increasing attention over time. Although most fractures heal adequately because of the self-healing capacity of the human body, around 5–10% of fractures suffer from delayed union and nonunion, especially in the presence of diseases such as osteoporosis and diabetes (Zura et al., 2016). The inability to achieve effective fracture healing usually requires multiple surgeries and prolonged hospitalization, which would bring a dramatic burden on patients. Therefore, the treatment of bone defects has been a key area of investigation in orthopedic clinics. From the perspective of anatomy, bone tissue is characterized by its heterogeneous structure composed of outer periosteum, cortical bone, and inner cancellous bone covered by the inner periosteum (Clarke, 2008). Such structures are also responsible for the complex blood supply system in bone tissue which is frequently damaged in trauma conditions (Marenzana and Arnett, 2013). However, current regenerative biomaterials usually focus on reconstructing bone tissue while overlooking the restoration of the normal anatomic structure and blood supply system of a fractured bone (Habibovic and Barralet, 2011; Matassi et al., 2011).

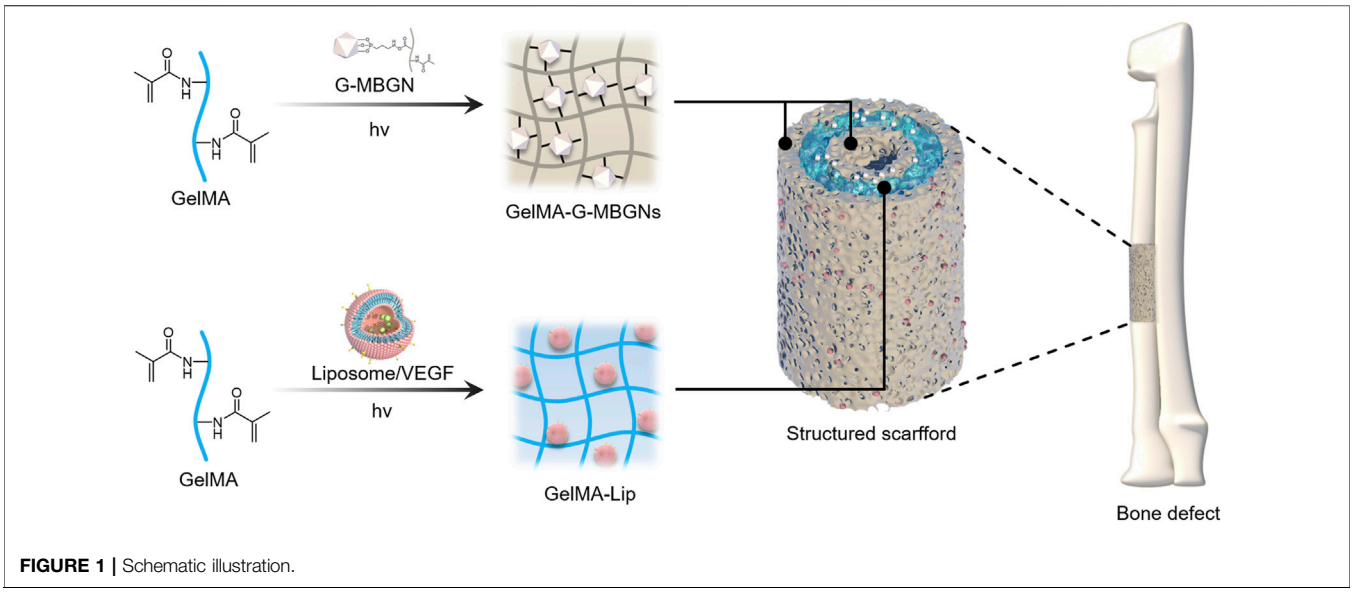

FIGURE 1 | Schematic illustration.

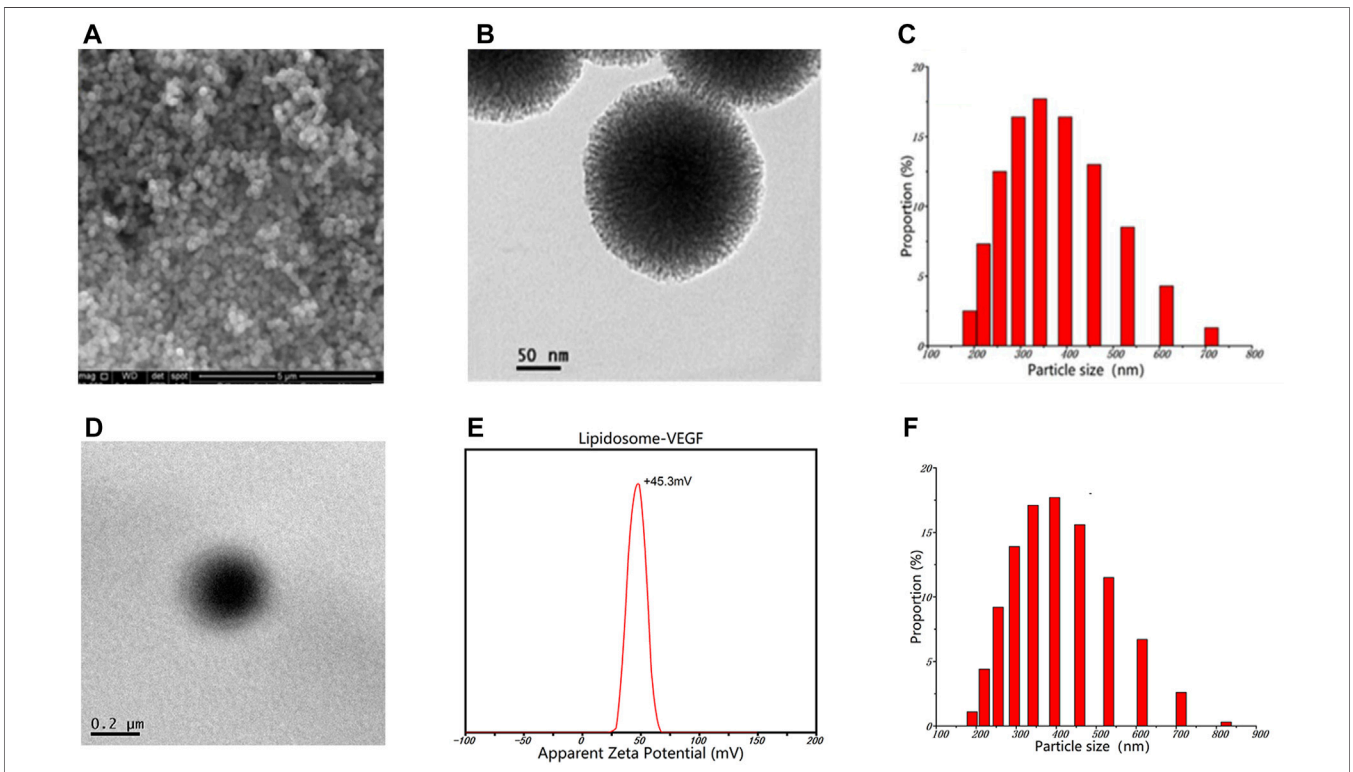

FIGURE 2 | Characterization of G-MBGN and liposomes. **(A)** SEM observation of G-MBGN. Nanoparticles with relatively uniform sizes could be seen under a low magnification view. **(B)** Distinguishable mesopore inside nanoparticles under TEM. **(C)** DLS study on the particle size of G-MBGN and the particle size was around 340 nm. **(D)** TEM observation of the liposome. **(E)** DLS study on the zeta potential of the liposome. **(F)** DLS study on the particle size of the liposome.

The importance of the periosteum in fracture healing has been well recognized (Aro et al., 1990; Neagu et al., 2016). The angiogenic activity guided by the periosteum plays an essential role in the revascularization and reconstruction of damaged bone tissue (Nobuto et al., 2005; Zhang et al., 2008). Numerous attempts have been reported to reconstruct the damaged periosteum at the fracture site using biomedical materials (Li et al., 2016). Electrospun fiber membranes have been reported to

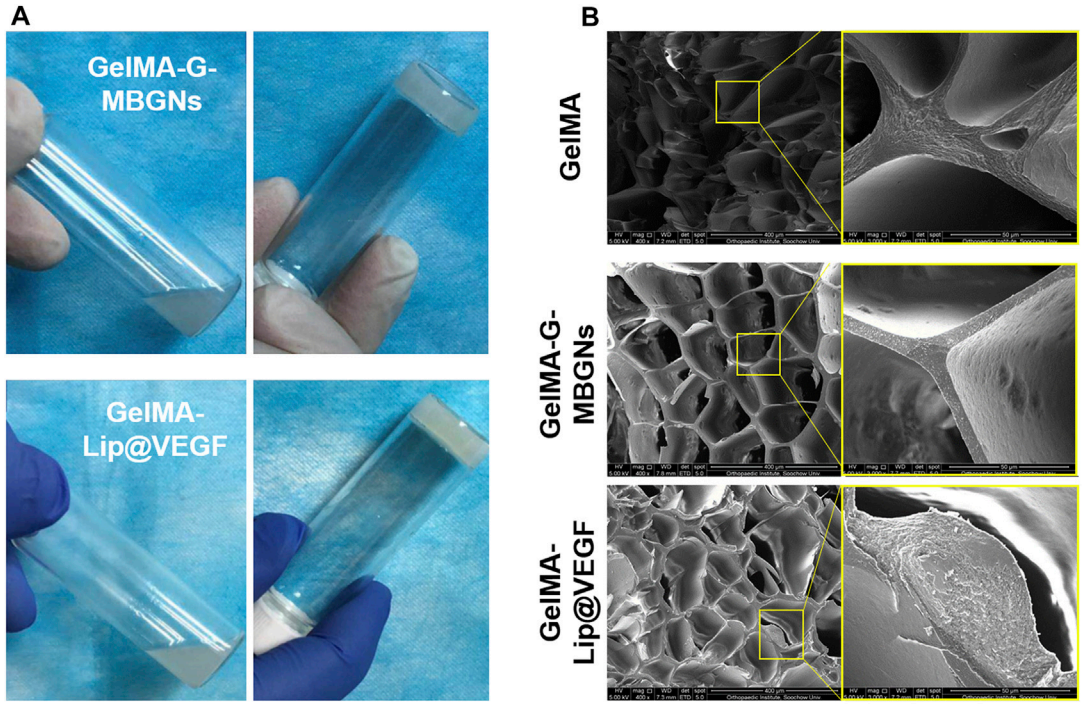

FIGURE 3 | Characterization of the gelation process and microstructure. **(A)** Gelation process of GelMA-G-MBGN and GelMA-Lip were triggered by UV irradiation. **(B)** SEM observation of the microstructure.

act as an artificial periosteum in bone tissue engineering, producing satisfying outcomes in preliminary studies (Gong et al., 2018; Liu et al., 2020). However, the basic form of artificial membrane alone is not adequate for treating critical-size bone defects because of its incapacity to fill defect areas. Combining such membrane-shaped biomaterials with additional bulk materials could be the solution (Zurina et al., 2020). High complexity resulting from the introduction of two distinct forms of materials could still be a persistent problem for its adoption in clinical practice. Designing one scaffold capable of simultaneously acting as an osteogenic matrix and an angiogenic periosteum could represent a potentially ideal solution for this problem.

As a modification of gelatin *via* methacrylic anhydride functionalization, GelMA (gelatin methacryloyl) has been recognized as an excellent platform to mimic the natural extracellular matrix because of the abundance of the RGD (arginine-glycine-aspartate) domain on its molecular chain (Yue et al., 2015). Its potential as a template for osteogenesis and angiogenesis has made GelMA a major topic of interest in tissue engineering (Stratesteffen et al., 2017; Anada et al., 2019). UV light triggers GelMA crosslinking and allows for convenient application in clinical practice. However, the innate nature of the hydrogel material has rendered GelMA with poor mechanical properties, which is unsuitable for the engineering of tough tissue such as bone. Furthermore, because of the loose and water-rich structure of hydrogels, GelMA (as a drug-loading platform) cannot maintain the sustained release of bioactive factors to match the lengthy process of bone regeneration (Lai et al., 2016). Further modification and functionalization would be required to fit the GelMA hydrogel for the mission.

Nanomaterials have garnered increased attention among the various strategies attempting to enhance soft hydrogel's mechanical and biological function because of their high effectiveness and diverse functionalities (Kurian et al., 2022; Sakr et al., 2022). Previously, our group enhanced hydrogels with various nanomaterials. By incorporating hydrogels with surface-modified mesoporous bioactive glass, we have endowed GelMA hydrogel with enhanced mechanical strength and osteogenic potential (Xin et al., 2017). In addition, liposomes were also employed in the modification of GelMA hydrogels and they were found to enhance the structural integrity of GelMA and allow for the loading of multiple drugs for controlled release (Cheng et al., 2018). Because of the strategies mentioned earlier, GelMA enhanced using diverse nanomaterials was adequate to serve as an ECM template and drug reservoir in bone tissue engineering (Gong et al., 2019; Shao et al., 2019). However, mimicking the natural anatomic structure of bone requires much more than tunable mechanical strength and controlled release ability. Recreation of the natural anatomic structure has increased the demand for GelMA hydrogel, which is usually used as a homogeneous bulk material (Klotz et al., 2016). Briefly, GelMA has suffered from its incapacity to construct sophisticated biomimetic structures. This is because the homogeneous architecture of the GelMA scaffolds fails to mimic the heterogeneous structure of natural bone, thus hindering its potential to treat critical-size bone defects (Zhang et al., 2021).

In this study, to address the drawbacks associated with traditional bulk biomaterials in bone regeneration, a hydrogel scaffold with a biomimetic heterogeneous structure was designed to recreate the osteogenic activity of bone matrix and the angiogenic activity of periosteum. GelMA was reinforced with modified MBGN to generate a heterogeneous structured scaffold that mimicked bone matrix with superior structural stability and osteogenic potential. The GelMA was also incorporated with VEGF-loaded liposomes to guide angiogenesis in the inner and outer periosteum. After *in vitro* characterization of these two components individually, the combined heterogeneous structured scaffolds were further applied *in vivo* to treat critical-size bone defects in the rabbit radius (**Figure 1**).

RESULTS AND DISCUSSION

Physicochemical Characterization

As the essential elements incorporated in the outer and inner layer of the scaffold, mesoporous bioactive glass nanoparticles modified with GelMA (G-MBGN) and liposomes were synthesized for structural strengthening and drug loading respectively. Mesoporous bioactive glass nanoparticles modified with GelMA (G-MBGN) and liposomes were synthesized for structural strengthening and drug loading, respectively. The morphology of synthesized MBGN was observed *via* SEM. The synthesized nanoparticles showed relatively uniform size under low magnification (**Figure 2A**). Distinguishable mesopores were seen inside the nanoparticles using TEM (**Figure 2B**). The particle size of G-MBGN was analyzed using DLS. The results showed that the average diameter of the micro-sol particles was 340 nm, and indicated the uniformity of the particles (**Figure 2C**).

Liposome was prepared to load VEGF for controlled release. Before applying for drug loading, the morphology and encapsulating parameters of liposomes were investigated. The morphology of the liposome was observed using TEM. The results showed that liposomes loaded with VEGF exhibited a spherical morphology with a zeta potential of 45.3 mV and a diameter of around 400 nm (**Figures 2D–F**). The encapsulation performance of the liposomes was characterized by the encapsulation rate, which was found to be 62.4% ± 5.7%.

After incorporating the G-MBGN and liposomes into the GelMA hydrogel, the composite hydrogel was also characterized by its morphological performance. The gelation process of GelMA-G-MBGN and GelMA-Lip was triggered after UV irradiation (**Figure 3A**). After gelation, both GelMA-M-MBGN and GelMA-Lip showed a porous structure with a smooth pore wall under SEM (**Figure 3B**). Compared with bare GelMA hydrogel, the addition of G-MBGN resulted in the same porous structure for different pore wall morphologies in the GelMA-G-MBGN hydrogel. White particles could be observed on the surface and section of the pore wall, which could be the incorporated MBGN. However, the particle's appearance could also be observed on the pore wall of the GelMA-Lip porous structure, verifying the successful incorporation of liposome in GelMA-Lip hydrogel.

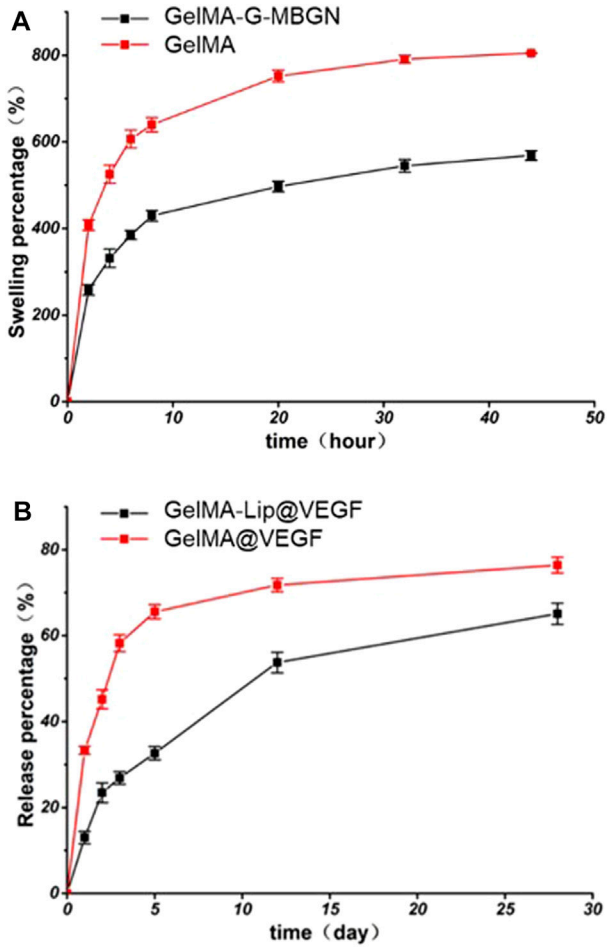

FIGURE 4 | Characterization of the swelling behavior and drug release profile. **(A)** Swelling kinetics of hydrogels. **(B)** VEGF release profile from the hydrogel.

Study on the Swelling Behavior and Drug Releasing Kinetics of GelMA-G-MBGN and GelMA-Lip@VEGF

The swelling behavior plays an important role in maintaining the shape and physical property of hydrogel materials implanted *in vivo*. Due to the high swelling ratio of the unmodified GelMA network, bare GelMA hydrogel could hardly represent a competent candidate as the outer layer of the heterogeneous scaffold. Therefore, based on the previous studies of our group on the mechanical strengthening of GelMA hydrogel, G-MBGN and liposome were respectively employed to improve the swelling performance of GelMA.

The effect of MBGN and liposome addition on the swelling behavior of GelMA hydrogel was studied by testing the swelling ratio on freeze-dried hydrogel samples after soaking them in PBS for a varying amount of time. The introduction of MBGN in the GelMA hydrogel has resulted in relatively lower swelling ratios in the hydrogel samples (**Figure 4A**). Specifically, both GelMA and GelMA-G-MBGN hydrogel samples achieved a stable swelling

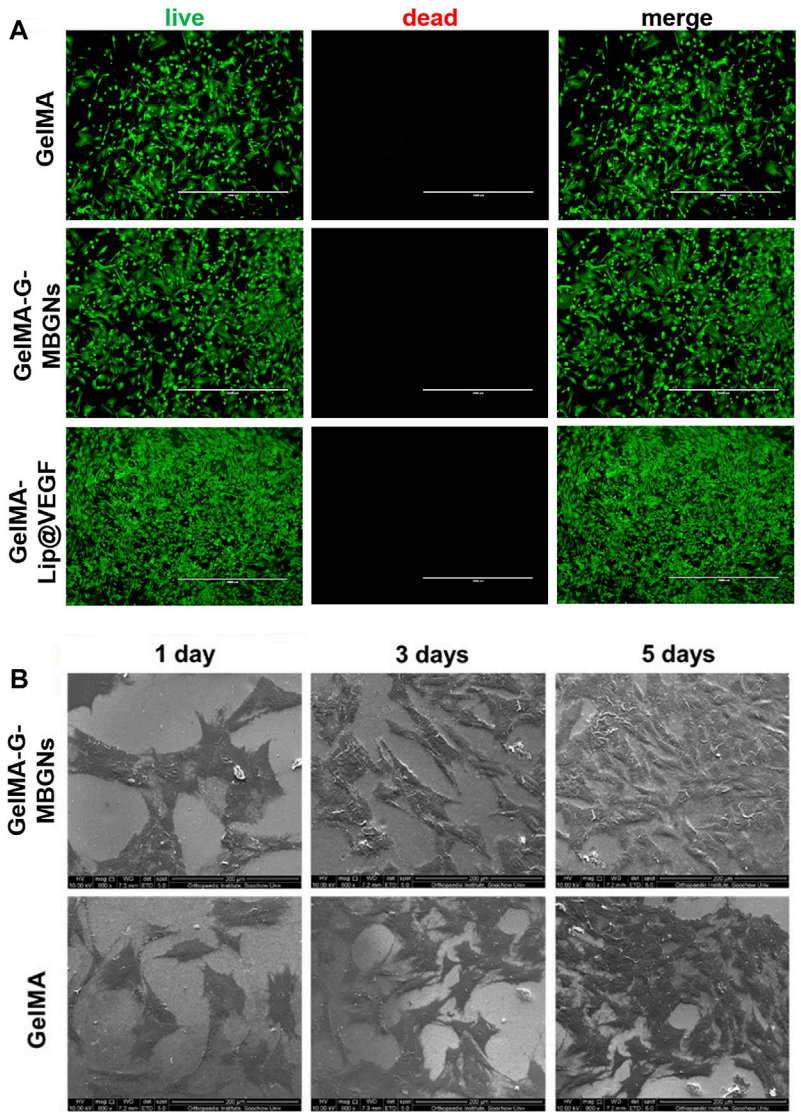

FIGURE 5 | Characterization of biocompatibility. **(A)** Live/Dead staining of BMSCs seeded on hydrogels. **(B)** SEM observation of BMSCs on hydrogels.

state after soaking for 48 h. Among them, the GelMA hydrogel exhibited a higher swelling ratio of 805.2% ± 10.4%, which could be attributed to the loose structure of bare GelMA. The GelMA-G-MBGN exhibited relatively lower swelling ratios, with GelMA-G-MBGN reaching 642.7% ± 9.7% after soaking for 48 h. The relatively lower swelling ratios could be attributed to the structural strengthening effect of G-MBGN on the GelMA hydrogel. Previous studies have verified the strengthening effect of MBGN on the structural integrity of hydrogels. G-MBGN could form covalent integration with the GelMA network, thus achieving a significant enhancement in structural stability as reflected by a lower swelling ratio compared with GelMA.

To endow the inner layer of the scaffold with effective angiogenic capacity, VEGF was loaded into GelMA-Lip hydrogel. However, burst release of VEGF from the loosened hydrogel matrix and the resulting limited half-life of VEGF at the focal area have significantly restricted the performance of VEGF-loaded hydrogel. Therefore, VEGF was loaded in liposomes embedded in GelMA hydrogel to achieve the controlled release kinetic of angiogenic factor. The release kinetics of VEGF from the liposome loaded in the GelMA-Lip@VEGF hydrogel were studied and compared with VEGF physically incorporated in the GelMA@VEGF hydrogel. Directly incorporated VEGF exhibited a burst release of 48.4% ± 4.1% within 5 days (**Figure 4B**). The GelMA@VEGF released 71.2% ± 5.9% of VEGF within 14 days of the release study, showing minor release in the later period. Conversely, VEGF loaded in GelMA-Lip@VEGF exhibited a significantly suppressed burst release activity, with 37.8% ± 4.1% of VEGF released in the first 5 days, and 58.5% ± 5.6% of VEGF released from GelMA-Lip@VEGF within 14 days, thus showing a controlled release profile compared with GelMA@VEGF. As one of the prevailing drug loading vehicles in tissue engineering, liposome has been

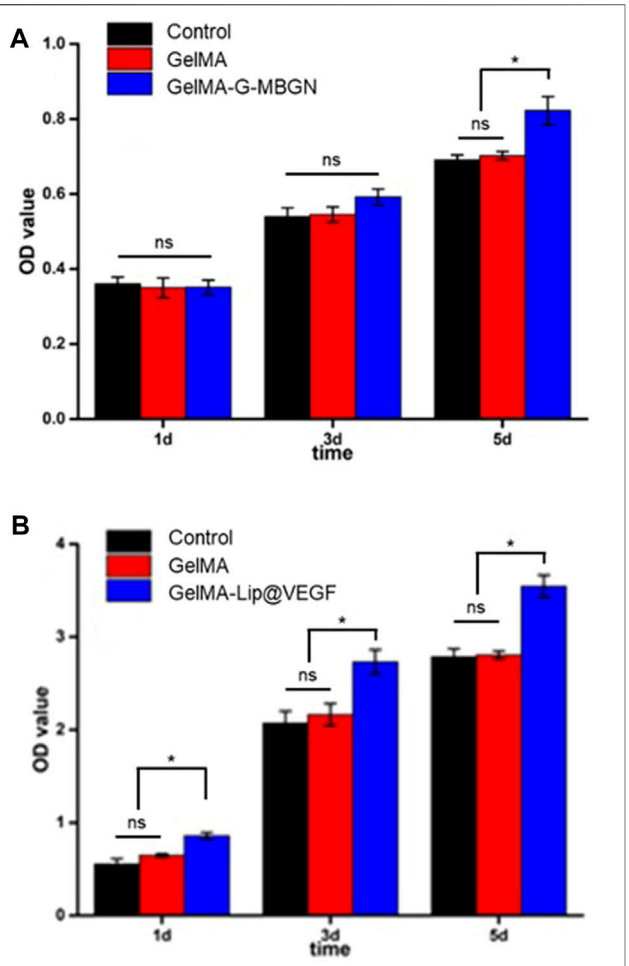

FIGURE 6 | Characterization of the proliferation rate. **(A)** CCK-8 test for BMSCs seeded on the GelMA-G-MBGN hydrogel. **(B)** CCK-8 test for BMSCs seeded on the GelMA-Lip@VEGF hydrogel.

employed for controlled release in various platforms ranging from hydrogel to electrospun scaffold. Under the current scenario, high water content and loosening of the structure of GelMA hydrogel could hardly achieve controlled release of physically incorporated drugs. Hence, liposome was introduced to act as the loading vehicle. Owing to the active interaction between liposome and GelMA molecular network evidenced previously, stable integration of liposome in GelMA-Lip hydrogel could be achieved as well as the lasting release of VEGF. The controlled release of the angiogenesis factor was essential for sustained vascularization in the focal area during bone regeneration (De la Riva et al., 2010; Knaack et al., 2014). GelMA-Lip@VEGF could exert stable angiogenesis activity and serve as the outer and inner periosteum.

In Vitro Characterization of Biocompatibility

The biocompatible performance of hydrogels is one of the decisive factors determining the initial effect after implantation. Although the biocompatibility of GelMA hydrogel has been thoroughly studied previously, the incorporation of G-MBGN and liposome could potentially jeopardize the original performance. Therefore, further investigation would be necessary for evaluation. The biocompatibility and bioactivity of GelMA-G-MBGN and GelMA-Lip hydrogel were assessed using *in vitro* experiments with BMSCs and HUVECs as model cells. The biocompatibility of different hydrogels was studied *via* seeding BMSCs on hydrogel samples. Cell viability and proliferation were investigated using Live/Dead staining and the CCK-8 test. The BMSCs seeded on GelMA, GelMA-G-MBGN, and GelMA-Lip exhibited adequate viability (**Figure 5A**). Adhesion and spread of BMSCs on hydrogels were also observed using SEM. The results showed that BMSCs exhibited a well-spread morphology on both GelMA-G-MBGN and GelMA hydrogels 1 day after seeding (**Figure 5B**). Additionally, significant proliferation of seeded BMSCs was observed as evidenced by a higher density of adhered cells compared with earlier time points (**Figure 5B**).

The result of the CCK-8 test showed the stable proliferation of BMSCs after seeding (**Figure 6A**). When compared with the GelMA and blank control group, the addition of G-MBGN resulted in a significant increase of cells on day 5 after seeding (**Figure 6A**). Moreover, the addition of liposomes loaded with VEGF promoted cell proliferation significantly (**Figure 6B**).

Characterization of *In Vitro* Osteogenic and Angiogenic Potential From GelMA-G-MBGN and GelMA-Lip@VEGF

Apart from serving as the intermediate layer of a structured scaffold to provide mechanical support, GelMA-G-MBGN was also expected to exert biological effects on progenitor cells and guide them towards osteogenic differentiation. The bioactive performance of the GelMA-G-MBGN and GelMA-Lip hydrogel was studied using *in vitro* experiments with BMSCs and HUVECs. BMSCs seeded on GelMA and GelMA-G-MBGN were cultured in an osteogenic medium for 2 weeks. ALP staining was conducted to investigate the early stage osteogenic activity of BMSCs. A higher staining intensity could be observed in BMSCs cultured on GelMA-G-MBGN compared with the GelMA and blank control group (**Figure 7A**). Next, an ALP quantification kit was employed to further investigate the ALP activity in the BMSCs on different hydrogels. A significantly higher quantified ALP value was observed on the GelMA-G-MBGN compared with the GelMA and blank control group 1 week after seeding (**Figure 7B**). The results indicated that GelMA-G-MBGN could induce a higher degree of ALP activity in BMSCs at an early stage of osteogenic induction. On the other hand, in addition to ALP staining and quantification, the formation of calcium nodules in BMSCs was also investigated as a late-stage osteogenic marker *via* Alizarin Red staining. In addition, calcium nodule formation in BMSCs was also observed *via* Alizarin Red staining. Denser calcium nodule staining could be observed on the GelMA-G-MBGN at 2 and 4 weeks after seeding compared with the GelMA and blank control group (**Figure 7C**). This indicates the superior performance of GelMA-G-MBGN in guiding BMSC calcium deposition. The corresponding quantification test revealed a higher OD value in the GelMA-G-MBGN group compared with the GelMA and the blank control group (**Figure 7D**).

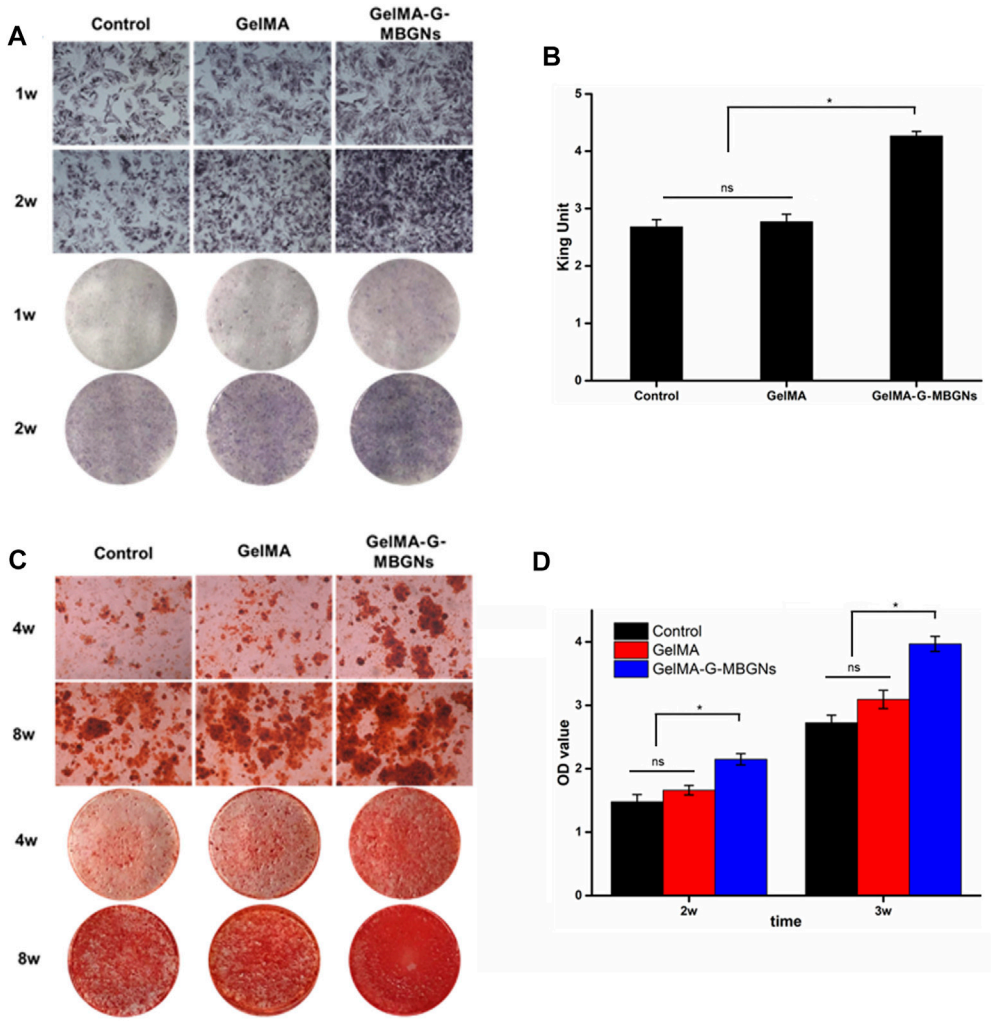

FIGURE 7 | Characterization of the osteogenic activity. **(A)** ALP staining images for the microscopic and gross view. **(B)** ALP quantification test. **(C)** Alizarin red staining images for the microscopic and gross view. **(D)** ARS staining quantification.

In addition to osteogenic activity, angiogenesis was also believed to be a pivotal activity in bone regeneration. In this study, by introducing GelMA-Lip@VEGF as the outer and inner periosteum of structured, enhanced vascular formation was expected to assist the superior bone repair capacity of the scaffold. The angiogenic activity of the GelMA-Lip hydrogel was characterized by seeding HUVECs on hydrogels. Based on the SEM observation, and phalloidin and DAPI staining, the HUVEC adhesion and spreading on GelMA and GelMA-Lip hydrogel was studied comprehensively. Well spread HUVECs could be observed on day 1 after seeding (**Figure 8A**). More HUVECs were observed at later time points, indicating the proliferation of HUVECs on GelMA and GelMA-G-MBGN hydrogels between these time points. Next, after staining with phalloidin and DAPI, HUVECs seeded on hydrogel were observed under a fluorescent microscope for the tube formation assay. Interaction between HUVECs could be seen on hydrogels, and vascular-like networks composed of numerous cell-cell interactions could be observed on the GelMA and GelMA-Lip hydrogels (**Figure 8B**). To quantitatively analyze the *in vitro* angiogenic activity of HUVECs under the influence of different hydrogels, the staining images were quantitatively analyzed using ImageJ software to obtain the angiogenic indexes including the number of tube junctions and tube length at different time points. More junction formations could be observed on the GelMA-Lip compared with the GelMA hydrogel (**Figures 8C,D**). Additionally, a significantly longer tube length could be found on the GelMA-Lip, indicating its superior angiogenic potential *in vitro*.

Construction of a Biomimetic Heterogeneous Structured Scaffold

After thorough characterization of the respective performance of GelMA-G-MBGN and GelMA-Lip hydrogels, the biomimetic structured scaffold with heterogeneous architecture was built

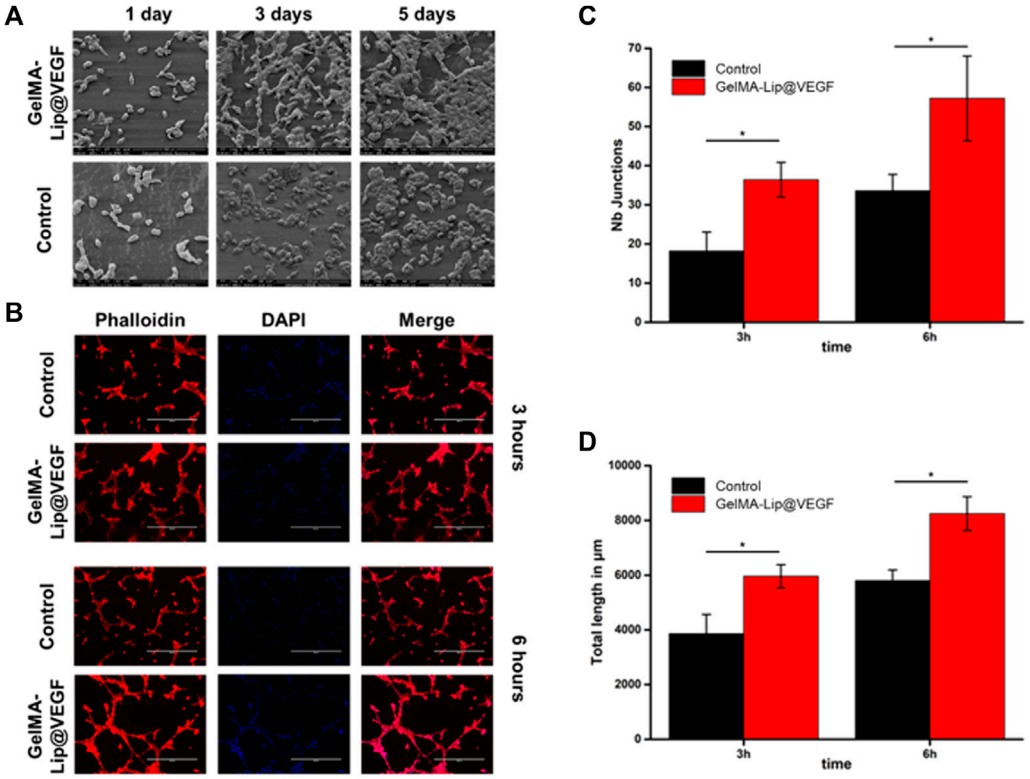

FIGURE 8 | Characterization of the angiogenic activity. **(A)** SEM observation of HUVECs seeded on hydrogels. **(B)** Phalloidin and DAPI staining of HUVECs on hydrogels. **(C)** Quantification of the number of junctions. **(D)** Quantification of the tube length.

with the help of a 3D-print mold (**Figures 9A,B**). Molds with different inner diameters were employed to construct the structured scaffold's inner, intermediate, and outer layers (**Figure 9C**). The constructed structured scaffold was observed under optical microscopy. The structured scaffold had the shape of the bone piece defect of the fractured radius. The cross-section view of the scaffold under optical microscopy also verifies the biomimetic sandwich-like structure consisting of an inner and outer GelMA-Lip layer coupled with an intermediate GelMA-G-MBGN layer. The structured scaffold would be further subjected to *in vivo* study to investigate its performance in promoting repair of bone defects.

In Vivo Characterization of the Structured Scaffold *via* the Rabbit Radius Critical-Size Bone Defect Model

In order to study the *in vivo* performance of biomimetic heterogeneous scaffold in promoting bone regeneration, a rabbit radius critical-size bone defect model was prepared to investigate the *in vivo* performance of a structured scaffold (**Figure 10**). The structured scaffold and bulk hydrogel were implanted in the defect area to guide bone regeneration.

At 4 and 8 weeks after surgery, the rabbits were euthanized to harvest radius-ulna samples subjected to micro-CT scanning. The coronal and axial sections of the radius and ulna were reconstructed to show the details of the bone defect (**Figure 11A**). Varying regeneration activities could be found in all groups. Four weeks after surgery, the blank control group induced negligible regenerated bone because of the critical size of the bone defect. Limited regeneration could be observed at the defect area 8 weeks after surgery and bone marrow cavity closure in the blank control group. Conversely, groups receiving the hydrogel scaffold achieved different healing outcomes. The bone defect treated with the GelMA-Lip bulk hydrogel produced limited new bone, leaving most defect areas filled with undegraded hydrogel 4 weeks after surgery. At 8 weeks after surgery, in spite of the bony connection achieved at the ulnar side of the radius, the bone defect remained at the radial side of the radius which was occupied by the undegraded hydrogel. For the group receiving the GelMA-G-MBGN bulk hydrogel scaffold, active osteogenesis activity was observed at both 4 and 8 weeks after surgery. However, despite abundant bone regeneration in the defect area, bone marrow cavities from two sides of the fracture did not form a connection. In comparison, a structured scaffold composed of GelMA-G-MBGN and GelMA-Lip induced bone regeneration on the radial and

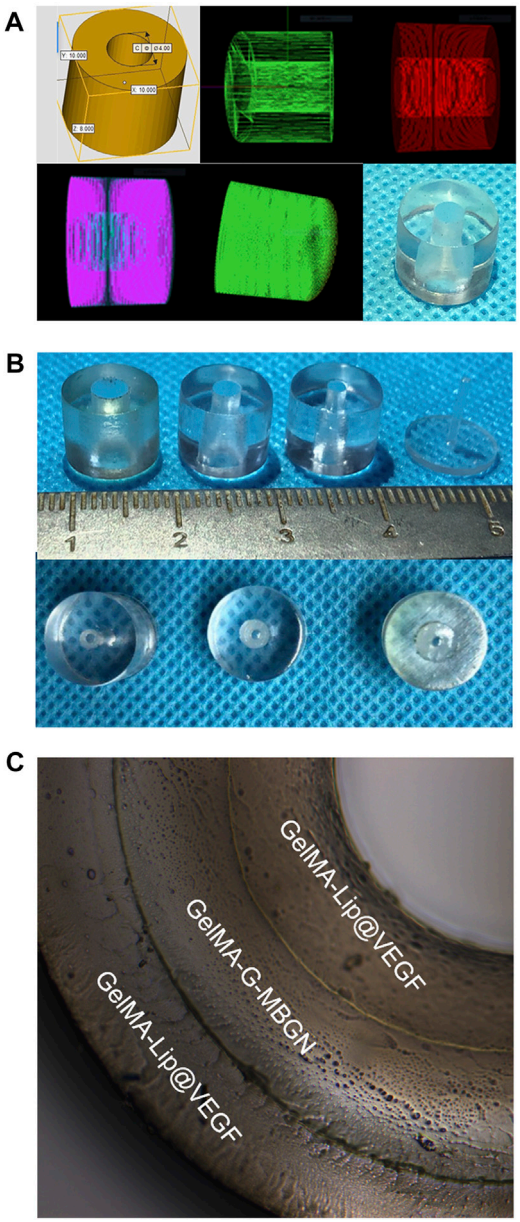

FIGURE 9 | Preparation of the 3D print mold and structured scaffold. **(A)** The digitally programmed shape of the 3D print mold. **(B)** Gross observation of the molds. **(C)** The inner, intermediate, and outer layers of the structured scaffold.

ulnar sides of the defect area. The bone marrow cavity could be reconnected at 8 weeks after surgery with the scaffold wholly degraded in the defect area, thus achieving the natural anatomic structure of the radius. A corresponding quantification study also revealed a similar trend (**Figure 11B**). Although the structured scaffold did not result in a significantly higher BV/TV ratio compared with GelMA-G-MBGN bulk materials, the restoration of the natural anatomic structure still indicated the superior treatment efficiency of the structured scaffold.

The pathological study using H&E staining also revealed similar results to the micro-CT. Although active osteogenesis could be found in GelMA-G-MBGN and GelMA-Lip hydrogels, recanalization of the medullary cavity was not achieved in these two groups (**Figure 11C**). In comparison, owing to the biomimetic heterogeneous architecture of structured scaffolds, the group receiving structured scaffolds exhibited superior regeneration outcomes (**Figure 11C**). The reunion of radius on both ulnar and radial sides as well as the recanalization of radius was achieved at 8 weeks after surgery (**Figure 11C**).

As one of the most difficult tasks in tissue engineering, repair of critical-sized bone defects has remained a tough challenge for most biomaterials. However, due to the increasing demand for healing quality, even more requests have been put forward in treating such conditions. For instance, the healing of bone defect and the reconstruction of normal anatomic structure has been highlighted recently. Both successful healing and recanalization of long bone should be achieved. Traditional bulk materials with homogeneous structures could hardly reproduce the heterogeneous structure of natural bone. In this study, relying on the heterogeneous structured scaffold, the healing and recanalization of critical-sized bone defect were achieved and such design could represent a novel strategy for treating bone defects in the future.

CONCLUSION

This study employed GelMA-G-MBGN to mimic the bone matrix while GelMA-Lip loaded with VEGF was introduced to act as the inner and outer periosteum. A biomimetic, heterogeneous, structured scaffold reproducing the natural bone structure was constructed for the regeneration of the critical-size bone defect. Physiological characterization and *in vitro* experiments demonstrated that GelMA-G-MBGN had stable structural integrity and the potential for promoting osteogenesis. GelMA-Lip loaded with VEGF was also found to exhibit the controlled release of loaded VEGF and exert effective angiogenesis activity *in vitro*. By combining GelMA-G-MBGN and GelMA-Lip@VEGF, the structured scaffold was successfully built with the help of a 3D printing mold. After fitting this scaffold into the critical-size radius bone defect, regeneration of bone defects with recanalization of the medullary cavity could be achieved in a rabbit model, thus verifying the superior performance of the biomimetic heterogeneous structured scaffold.

MATERIALS AND METHODS

Synthesis of Gelatin Methacryloyl

The synthesis of gelatin methacryloyl was conducted according to a previously reported procedure (Hutson et al., 2011). In brief, gelatin (20 g) was dissolved in PBS (200 ml) in a 60°C water bath. Methacrylic anhydrides (16 ml) were then added to the gelatin solution using a syringe pump (speed: 0.25 ml/min). After the injection, the reaction was allowed to continue for 2 h (under

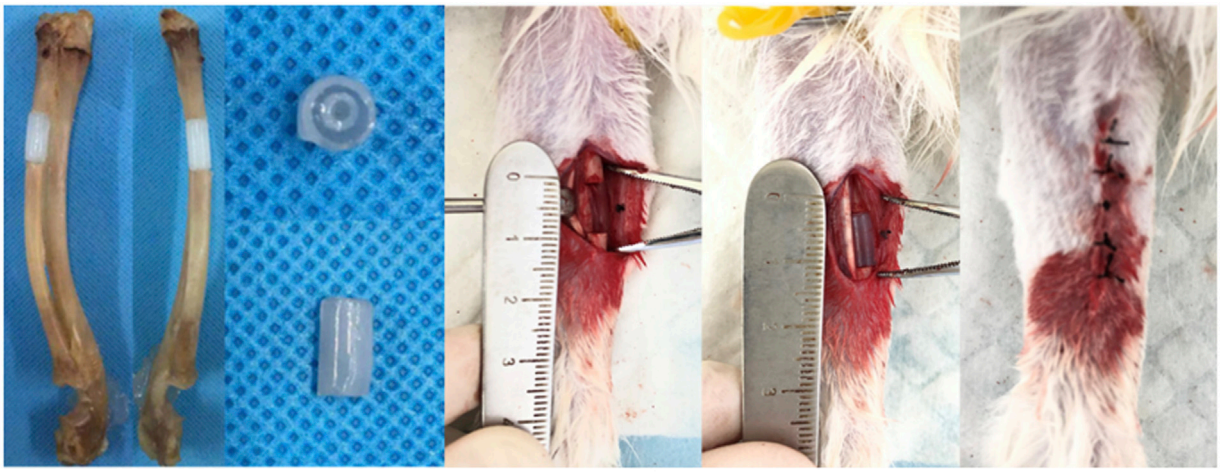

FIGURE 10 | Preparation of the rabbit radius critical-size bone defect model and scaffold implantation.

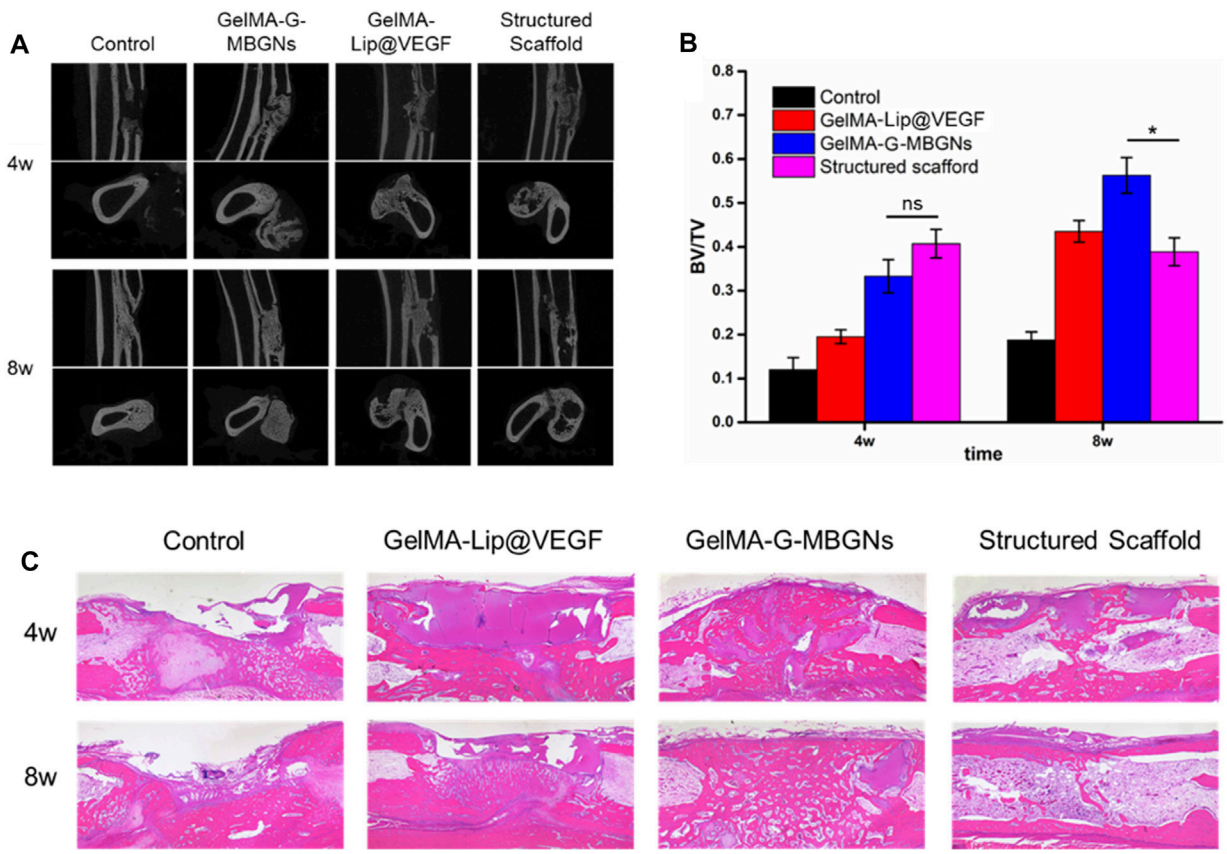

FIGURE 11 | Radiological and pathological assessment of the animal model. **(A)** Micro-CT observation of the bone defect. **(B)** Quantified BV/TV analysis. **(C)** H&E staining of the samples.

stirring conditions). Next, PBS (800 ml), preheated to 50°C, was added to the reaction, followed by a further reaction for 15 min. For 1 week, the resulting mixture was dialyzed against deionized water in a dialysis tube (cut-off MW: 8,000–14,000). After dialysis, the product was filtered to remove precipitates and freeze-dried for future use.

Synthesis of Mesoporous Bioactive Glass Nanoparticles

The mesoporous bioactive glass nanoparticles were synthesized according to previous reports (Xin et al., 2017; Xin et al., 2020). In brief, the reaction was conducted in Tris-HCl buffer solution (pH 8.0) with cetyltrimethylammonium bromide (CTAB) as a templating agent. Then, tetraethyl orthosilicate (TEOS; 16 ml), triethyl phosphate (TEP; 1.22 ml), and calcium nitrate tetrahydrate (CN; 3.39 g) were added sequentially into the buffer solution (and the reaction was completed in a 60°C oil bath). The mixture was allowed to react for 24 h (at 60°C), and the produced nanoparticle was recovered using a centrifuge (at 12000xg). This nanoparticle was further washed (three times) with ethanol and deionized water. The final product containing SiO_2 (80 mol%), CaO (16 mol%), and P_2O_5 (4 mol%) was obtained *via* nanoparticle sintering at 650°C for 3 h.

Synthesis of GelMA-Conjugated MBGN (G-MBGN)

Before synthesizing G-MBGN (Xin et al., 2020), the MBGN was functionalized with amine groups. In brief, MBGN (0.4 g) was dispersed in hexane (100 ml) and aminopropyltriethoxysilane (APTES; 5 ml) for 24 h at 60°C. The amine-functionalized MBGN (A-MBGN) was obtained after washing and drying at 60°C. The GelMA-G-MBGN was synthesized by dispersing MBGN (0.3 g) into deionized water (20 ml) containing GelMA (0.3 g) and reacting with 1-Ethyl-(3-dimethylaminopropyl) carbodiimide hydrochloride (EDC; 0.4 g) and N-Hydroxysuccinimide (NHS; 0.2 g) for 24 h. The GelMA-G-MBGN was obtained after washing and drying the product.

Synthesis of the VEGF-Loaded Liposome

The drug-loaded liposome was prepared *via* phacoemulsification (Cheng et al., 2018). In brief, soy lecithin (160 mg), cholesterol (40 mg), and octadecylamine (5 mg) were added into ether (6 ml). After oscillation to obtain the solution, VEGF (500 μg) was added into deionized water (2 ml) and mixed with the ether-based solution. The resulting mixture was emulsified *via* ultrasonication and then subjected to rotary evaporation under an ice bath. After the evaporation of ether, the VEGF-loaded liposome was obtained through freeze-drying.

Preparation of Gelatin Methacryloyl, GelMA-G-MBGN, and GelMA/Lip Hydrogel

The GelMA hydrogel was prepared by dissolving GelMA (10% w/v) and photoinitiator Irgacure 2959 (1% w/v) in PBS using a 60°C water bath. The solution was cured into the GelMA hydrogel *via* ultraviolet irradiation (10 cm W/cm^2) for 3 min.

The GelMA-G-MBGN hydrogel was prepared using the previously prepared GelMA and G-MBGN. Briefly, GelMA (10% w/v), G-MBGN (3% w/v), and the photoinitiator Irgacure 2959 (1% w/v) were added to the PBS and sonicated at 60°C to dissolve the GelMA and photoinitiator and disperse the G-MBGN. After achieving the stable suspension of G-MBGN in GelMA solution, the mixture was subjected to ultraviolet irradiation (10 cm W/cm^2) to obtain the GelMA-G-MBGN hydrogel.

The GelMA/Lip hydrogel was prepared by dissolving GelMA (10% w/v) and photoinitiator Irgacure 2959 (1% w/v) in PBS at 60°C. The VEGF-loaded liposome was added to the solution and cooled down to room temperature. After full dissolution, the solution was subjected to ultraviolet irradiation (10 cm W/cm^2), and the GelMA/Lip hydrogel was obtained.

Physical Characterization of Nanomaterials and Hydrogels

Scanning electron microscopy (SEM, S-4800, Hitachi, Japan) was employed to observe the microstructure of MBGN and GelMA-based hydrogels. The freeze-dried samples were fixed on the sample stage using conductive tape. The SEM observation was conducted at a voltage of 5 kV after gold coating for 60 s using sputter coating equipment (SC7620, Quorum Technologies, United Kingdom). A transmission electron microscope (TEM) was employed to observe the detailed structure of MBGN and liposome.

A swelling test was applied to study the swelling behavior of hydrogels. In brief, freeze-dried GelMA and GelMA-G-MBGN hydrogel samples were weighed and immersed in PBS and then fixed on a shaker at 37°C. The swelled weights were measured at a specific time to calculate the swelling ratios.

The encapsulation efficiency of liposomes and the release kinetics of VEGF from liposome and hydrogel were studied using an Enzyme-linked immunosorbent assay (ELISA) kit. In brief, the encapsulation rate was studied (using an ELISA kit) by measuring the unencapsulated particles in the supernatant of the liposome-VEGF solution after centrifugation. The release kinetics of VEGF from liposome and hydrogel was studied *via* immersion of the samples in PBS solution. This was performed in a 37°C shaker with a rotating speed of 100 rpm. The released VEGF content was determined by measuring the PBS samples at different time points using an ELISA kit.

In Vitro Characterization of the Hydrogel

The biocompatibility of GelMA, GelMA-G-MBGN, and GelMA-Lip hydrogel was studied by *in vitro* characterization using bone marrow mesenchymal stem cells (BMSCs) and human umbilical vein endothelial cells (HUVEC). The characterization was conducted by seeding BMSCs onto different hydrogels and testing the spreading, viability, and proliferation of cells at different time points using SEM observation, Live/Dead staining kit, and CCK-8 kit. Specifically, SEM observation of the adhesion and spreading conditions was conducted after seeding cells onto hydrogels and culturing for 5 days. The hydrogel-cell samples were fixed using PFA (4%) and further dehydrated *via* a gradient ethanol solution. The sample was subjected to SEM observation with a voltage of 5 kV after gold coating for 75 s. The viability of cells on the hydrogel was studied using a Live/Dead staining kit (Invitrogen, United States) 5 days after seeding. A CCK-8 kit (Beyotime, Shanghai) was employed to

study the BMSC proliferation rate on different hydrogels after culturing for 1, 3, and 5 days.

The *in vitro* bioactivity performance of GelMA-G-MBGN and GelMA-Lip hydrogel on osteogenesis and angiogenesis was investigated. The osteogenic activity of BMSCs cultured on GelMA and GelMA-G-MBGN at an early stage was characterized after seeding BMSCs and culturing in osteogenic media for 7 and 14 days using the ALP staining kit (Beyotime, Shanghai) and ALP quantification kit (Jiancheng, Nanjing). The osteogenic activity of BMSCs at later time points was measured using an Alizarin Red staining kit (Beyotime, Shanghai) after seeding BMSCs on hydrogels and culturing in osteogenic media for 14 and 21 days. A corresponding quantification study was also carried out using perchloric acid to dissolve calcium nodules and further tested for OD value (wavelength: 562 nm).

The angiogenesis of HUVECs on GelMA and GelMA-Lip hydrogels was evaluated by phalloidin and DAPI staining at 3 and 6 h after seeding. The quantification of parameters involved in tube formation based on phalloidin staining of HUVECs was conducted using ImageJ software (United States) to evaluate the angiogenic activity on different hydrogels.

Construction of a Biomimetic Structured Scaffold

A scaffold with a biomimetic heterogeneous structure was constructed with the assistance of three-dimensional (3D)-printed moldings. In brief, the rabbit radius and ulna complex were harvested from male New Zealand rabbits weighing 2.5 kg. A critical-sized radius bone defect with a length of 1.5 cm was prepared using a swing saw on the middle shaft of the radius. The structural parameters of the obtained bone sample were measured for customized 3D printing by the NovaPrint company. A 3D-print mold was prepared for the casting of the biomimetic structured scaffold. The previously prepared GelMA-Lip hydrogel was employed to cast the inner and outer layers of the structured scaffold. Finally, the GelMA-G-MBGN was used to cast the intermediate layer of the scaffold.

Animal Surgery

To characterize the *in vivo* performance, a male New Zealand white rabbit was used to prepare a critical-size bone defect model. All animal experiments conducted in this study, including surgical procedure, perisurgical handling, and postsurgical harvesting, were carried out following the guidelines approved by the Ethics Committee at the First Affiliated Hospital of Soochow University.

The rabbit radius critical-size bone defect model was created according to a previously described procedure (Meinig et al., 1996). In brief, general anesthesia was carried out on rabbits using an intramuscular injection of pentobarbital sodium (60 mg/kg). After skin preparation and disinfection on the forearm, a longitudinal incision was created to expose the radius shaft through blunt separation. A bone defect with a length of 1.0 cm was created using a swing saw. After proper hemostasis, the hydrogel scaffolds were placed in the defect sites, and then the wounds were closed and sutured layer-by-layer. Post-surgery, 8×10^5 U penicillin per day was applied to the rabbits to prevent infection.

Micro-CT Study

The rabbits were euthanized *via* air embolism at 4 and 8 weeks after surgery. The radius-ulna complex was harvested for characterization using micro-CT scanning. The samples were scanned at a resolution of 9 μm with an Al filter (1 mm), and the parameters applied in the examination were 65 kV and 385 mA. The coronal, sagittal, and axial views of the radius-ulna complex were reconstructed to observe bone regeneration in defective areas. The morphological details in the bone defect area was further studied using CTan software (Bruker). The bone volume (BV)/total volume (TV) parameter was calculated in the cylindrical region of interest (ROI) covering a defect area (diameter: 0.5 cm and length: 1 cm).

Pathological Assessment

The pathological details of the defect area were studied using H&E staining. In brief, the radius-ulna sample was decalcified by soaking in an EDTA decalcification solution (Yuanye, Shanghai) for 4 weeks. After decalcification, the sample was further dehydrated and embedded for slicing. Slices (thickness: 8 μm) were prepared for staining using an H&E staining kit (Beyotime, Shanghai). The stained slides were scanned and observed using CaseViewer software.

Statistical Methods

All data in this study were presented in the form of mean ± standard deviation. Statistical analysis was carried out using ImageJ and GraphPad Prism 7. A difference with a p-value less than 0.05 was considered statistically significant.

DATA AVAILABILITY STATEMENT

The original contributions presented in the study are included in the article/Supplementary Material; further inquiries can be directed to the corresponding authors.

ETHICS STATEMENT

The animal study was reviewed and approved by the Department of Animal Science and Ethics Committee, First Affiliated Hospital of Soochow University.

AUTHOR CONTRIBUTIONS

All authors listed have made a substantial, direct, and intellectual contribution to the work and approved it for publication.

FUNDING

This work was supported by the National Natural Science Foundation of China (81772312, 81972059, 81601891,

81702190, and 51873107), Research and Development of Biomedical Materials and Substitution of Tissue and Organ Repair under the National Key R&D Program (2016YFC1101505), Key Talented Man Project of Jiangsu Province (RC2011102), Social Development Project of Jiangsu Province (BE2021646), Jiangsu Provincial Clinical Orthopedic Center, and the Priority Academic Program Development of Jiangsu Higher Education Institutions (PAPD).

REFERENCES

Anada, T., Pan, C.-C., Stahl, A., Mori, S., Fukuda, J., Suzuki, O., et al. (2019). Vascularized Bone-Mimetic Hydrogel Constructs by 3D Bioprinting to Promote Osteogenesis and Angiogenesis. *Ijms* 20 (5), 1096. doi:10.3390/ijms20051096

Aro, H. T., Wippermann, B. W., Hodgson, S. F., and Chao, E. Y. S. (1990). Internal Remodeling of Periosteal New Bone during Fracture Healing. *J. Orthop. Res.* 8 (2), 238–246. doi:10.1002/jor.1100080213

Cheng, R., Yan, Y., Liu, H., Chen, H., Pan, G., Deng, L., et al. (2018). Mechanically Enhanced Lipo-Hydrogel with Controlled Release of Multi-type Drugs for Bone Regeneration. *Appl. Mater. Today* 12, 294–308. doi:10.1016/j.apmt.2018.06.008

Clarke, B. (2008). Normal Bone Anatomy and Physiology. *Clin. J. Am. Soc. Nephrol.* 3 (Suppl. 3), S131–S139. doi:10.2215/CJN.04151206

De la Riva, B., Sánchez, E., Hernández, A., Reyes, R., Tamimi, F., López-Cabarcos, E., et al. (2010). Local Controlled Release of VEGF and PDGF from a Combined Brushite-Chitosan System Enhances Bone Regeneration. *J. Control. Release* 143 (1), 45–52. doi:10.1016/j.jconrel.2009.11.026

Gong, H., Fei, H., Xu, Q., Gou, M., and Chen, H. H. (2019). 3D-engineered GelMA Conduit Filled with ECM Promotes Regeneration of Peripheral Nerve. *J. Biomed. Mater Res.* 108, 805–813. doi:10.1002/jbm.a.36859

Gong, M., Chi, C., Ye, J., Liao, M., Xie, W., Wu, C., et al. (2018). Icariin-loaded Electrospun PCL/gelatin Nanofiber Membrane as Potential Artificial Periosteum. *Colloids Surfaces B Biointerfaces* 170, 201–209. doi:10.1016/j.colsurfb.2018.06.012

Habibovic, P., and Barralet, J. E. (2011). Bioinorganics and Biomaterials: Bone Repair. *Acta Biomater.* 7 (8), 3013–3026. doi:10.1016/j.actbio.2011.03.027

Hutson, C. B., Nichol, J. W., Aubin, H., Bae, H., Yamanlar, S., Al-Haque, S., et al. (2011). Synthesis and Characterization of Tunable Poly(ethylene Glycol): Gelatin Methacrylate Composite Hydrogels. *Tissue Eng. Part A* 17 (13-14), 1713–1723. doi:10.1089/ten.TEA.2010.0666

Klotz, B. J., Gawlitta, D., Rosenberg, A. J. W. P., Malda, J., and Melchels, F. P. W. (2016). Gelatin-Methacryloyl Hydrogels: Towards Biofabrication-Based Tissue Repair. *Trends Biotechnol.* 34 (5), 394–407. doi:10.1016/j.tibtech.2016.01.002

Knaack, S., Lode, A., Hoyer, B., Rösen-Wolff, A., Gabrielyan, A., Roeder, I., et al. (2014). Heparin Modification of a Biomimetic Bone Matrix for Controlled Release of VEGF. *J. Biomed. Mat. Res.* 102 (10), 3500–3511. doi:10.1002/jbm.a.35020

Kurian, A. G., Singh, R. K., Patel, K. D., Lee, J.-H., and Kim, H.-W. (2022). Multifunctional GelMA Platforms with Nanomaterials for Advanced Tissue Therapeutics. *Bioact. Mater.* 8, 267–295. doi:10.1016/j.bioactmat.2021.06.027

Lai, T. C., Yu, J., and Tsai, W. B. (2016). Gelatin Methacrylate/carboxybetaine Methacrylate Hydrogels with Tunable Crosslinking for Controlled Drug Release. *J. Mat. Chem. B* 4 (13), 2304–2313. doi:10.1039/c5tb02518d

Li, N., Song, J., Zhu, G., Li, X., Liu, L., Shi, X., et al. (2016). Periosteum Tissue Engineering-A Review. *Biomater. Sci.* 4 (11), 1554–1561. doi:10.1039/c6bm00481d

Liu, W., Bi, W., Sun, Y., Wang, L., Yu, X., Cheng, R., et al. (2020). Biomimetic Organic-Inorganic Hybrid Hydrogel Electrospinning Periosteum for Accelerating Bone Regeneration. *Mater. Sci. Eng. C* 110, 110670. doi:10.1016/j.msec.2020.110670

Marenzana, M., and Arnett, T. R. (2013). The Key Role of the Blood Supply to Bone. *Bone Res.* 1 (3), 203–215. doi:10.4248/BR201303001

Matassi, F., Nistri, L., Chicon Paez, D., and Innocenti, M. (2011). New Biomaterials for Bone Regeneration. *Clin. Cases Min. Bone Metab.* 8 (1), 21–24.

Meinig, R. P., Rahn, B., Perren, S. M., and Gogolewski, S. (1996). Bone Regeneration with Resorbable Polymeric Membranes: Treatment of Diaphyseal Bone Defects in the Rabbit Radius with poly(L-Lactide) Membrane. A Pilot Study. *J. Orthop. Trauma* 10 (3), 178–190. doi:10.1097/00005131-199604000-00006

Neagu, T. P., Ţigliş, M., Cocoloş, I., and Jecan, C. R. (2016). The Relationship between Periosteum and Fracture Healing. *Rom. J. Morphol. Embryol.* 57 (4), 1215–1220.

Nobuto, T., Suwa, F., Kono, T., Hatakeyama, Y., Honjou, N., Shirai, T., et al. (2005). Microvascular Response in the Periosteum Following Mucoperiosteal Flap Surgery in Dogs: 3-dimensional Observation of an Angiogenic Process. *J. Periodontology* 76 (8), 1339–1345. doi:10.1902/jop.2005.76.8.1339

Sakr, M. A., Sakthivel, K., Hossain, T., Shin, S. R., Siddiqua, S., Kim, J., et al. (2022). Recent Trends in Gelatin Methacryloyl Nanocomposite Hydrogels for Tissue Engineering. *J. Biomed. Mater. Res.* 110 (3), 708–724. doi:10.1002/jbm.a.37310

Shao, Y., You, D., Lou, Y., Li, J., Ying, B., Cheng, K., et al. (2019). Controlled Release of Naringin in GelMA-Incorporated Rutile Nanorod Films to Regulate Osteogenic Differentiation of Mesenchymal Stem Cells. *ACS Omega* 4 (21), 19350–19357. doi:10.1021/acsomega.9b02751

Stratesteffen, H., Köpf, M., Kreimendahl, F., Blaeser, A., Jockenhoevel, S., and Fischer, H. (2017). GelMA-collagen Blends Enable Drop-On-Demand 3D Printablility and Promote Angiogenesis. *Biofabrication* 9 (4), 045002. doi:10.1088/1758-5090/aa857c

Xin, T., Gu, Y., Cheng, R., Tang, J., Sun, Z., Cui, W., et al. (2017). Inorganic Strengthened Hydrogel Membrane as Regenerative Periosteum. *ACS Appl. Mat. Interfaces* 9 (47), 41168–41180. doi:10.1021/acsami.7b13167

Xin, T., Mao, J., Liu, L., Tang, J., Wu, L., Yu, X., et al. (2020). Programmed Sustained Release of Recombinant Human Bone Morphogenetic Protein-2 and Inorganic Ion Composite Hydrogel as Artificial Periosteum. *ACS Appl. Mat. Interfaces* 12 (6), 6840–6851. doi:10.1021/acsami.9b18496

Yue, K., Trujillo-de Santiago, G., Alvarez, M. M., Tamayol, A., Annabi, N., and Khademhosseini, A. (2015). Synthesis, Properties, and Biomedical Applications of Gelatin Methacryloyl (GelMA) Hydrogels. *Biomaterials* 73, 254–271. doi:10.1016/j.biomaterials.2015.08.045

Zhang, L., Fu, L., Zhang, X., Chen, L., Cai, Q., and Yang, X. (2021). Hierarchical and Heterogeneous Hydrogel System as a Promising Strategy for Diversified Interfacial Tissue Regeneration. *Biomater. Sci.* 9 (5), 1547–1573. doi:10.1039/d0bm01595d

Zhang, X., Awad, H. A., O'Keefe, R. J., Guldberg, R. E., and Schwarz, E. M. (2008). A Perspective: Engineering Periosteum for Structural Bone Graft Healing. *Clin. Orthop. Relat. Res.* 466 (8), 1777–1787. doi:10.1007/s11999-008-0312-6

Zura, R., Xiong, Z., Einhorn, T., Watson, J. T., Ostrum, R. F., Prayson, M. J., et al. (2016). Epidemiology of Fracture Nonunion in 18 Human Bones. *JAMA Surg.* 151 (11), e162775. doi:10.1001/jamasurg.2016.2775

Zurina, I. M., Presniakova, V. S., Butnaru, D. V., Svistunov, A. A., Timashev, P. S., and Rochev, Y. A. (2020). Tissue Engineering Using a Combined Cell Sheet Technology and Scaffolding Approach. *Acta Biomater.* 113, 63–83. doi:10.1016/j.actbio.2020.06.016

Conflict of Interest: The authors declare that the research was conducted in the absence of any commercial or financial relationships that could be construed as a potential conflict of interest.

Publisher's Note: All claims expressed in this article are solely those of the authors and do not necessarily represent those of their affiliated organizations, or those of the publisher, the editors, and the reviewers. Any product that may be evaluated in this article, or claim that may be made by its manufacturer, is not guaranteed or endorsed by the publisher.

frontiers | Frontiers in Bioengineering and Biotechnology

TYPE Original Research
PUBLISHED 05 September 2022
DOI 10.3389/fbioe.2022.925339

OPEN ACCESS

EDITED BY
Yusheng Li,
Xiangya Hospital, Central South University, China

REVIEWED BY
Dejian Li,
Fudan University Pudong Medical Center, China
Barbara Blanco-Fernandez,
Institute for Bioengineering of Catalonia (IBEC), Spain
Stanislav Bondarenko,
Academy of Medical Science, Ukraine

*CORRESPONDENCE
Liu Yang,
jointsurgery@163.com
Fuyou Wang,
wfy731023@163.com

SPECIALTY SECTION
This article was submitted to Biomaterials, a section of the journal Frontiers in Bioengineering and Biotechnology

RECEIVED 21 April 2022
ACCEPTED 26 July 2022
PUBLISHED 05 September 2022

CITATION
Ao Y, Guo L, Chen H, He R, Yang P, Fu D, Gu L, Peng Y, Xiong R, Yang L and Wang F (2022), Application of three-dimensional-printed porous tantalum cones in total knee arthroplasty revision to reconstruct bone defects. *Front. Bioeng. Biotechnol.* 10:925339. doi: 10.3389/fbioe.2022.925339

Application of three-dimensional-printed porous tantalum cones in total knee arthroplasty revision to reconstruct bone defects

Yunong Ao, Lin Guo, Hao Chen, Rui He, Pengfei Yang, Dejie Fu, Lingchuan Gu, Yang Peng, Ran Xiong, Liu Yang* and Fuyou Wang*

Center for Joint Surgery, Southwest Hospital, Third Military Medical University (Army Medical University), Chongqing, China

Purpose: Three-dimensional (3D) printing technology has emerged as a new treatment method due to its precision and personalization. This study aims to explore the application of a 3D-printed personalized porous tantalum cone for reconstructing the bone defect in total knee arthroplasty (TKA) revision.

Methods: Between November 2017 and October 2020, six patients underwent bone reconstruction using 3D-printed porous tantalum cones in TKA revision. The knee function was assessed using the Hospital for Special Surgery (HSS) score pre- and postoperatively. The pain was measured by the visual analog scale (VAS) pre- and postoperatively. The quality of life was measured using the 36-Item Short Form Health Survey (SF-36) to pre- and postoperatively evaluate the relief of pain. Operation time, intraoperative blood loss, postoperative drainage volume, and complications were also recorded. At the last follow-up, all patients received X-ray and computed tomography (CT) to confirm the effect of bone reconstruction.

Results: After an average follow-up duration of 26.3 months, no patients developed any operation-related complications. The average intraoperative blood loss and postoperative drainage volumes were 250.1 ± 76.4 ml and 506.7 ± 300.8 ml, respectively. At the last follow-up, the HSS score was significantly higher than that before operation, indicating that the knee function was significantly improved ($p < 0.001$). During the follow-up, the mean VAS score decreased and the mean SF-36 score increased, both of which were significantly improved compared with preoperative conditions ($p < 0.001$). Radiological examination at the final follow-up showed that cones implanted into the joint were stable and bone defects were effectively reconstructed.

Conclusion: This study demonstrated that 3D-printed porous tantalum cones could effectively reconstruct bone defects and offer anatomical support in TKA revision. Further studies are still needed to confirm the long-term effect of 3D-printed tantalum cones for reconstructing bone defects.

KEYWORDS

3D, printed, porous tantalum, bone defect, knee arthroplasty revision, reconstruction

Introduction

Total knee arthroplasty (TKA) is an effective method for the treatment of severe osteoarthritis, rheumatoid arthritis, and various knee deformities, which can effectively relieve joint pain and reconstruct the function of the knee. Since its first clinical application in the 1960s, with the rapid update of the prosthesis design concept and the development of science and technology such as material science and bionics, the process of TKA has also been continuously improved (Fei et al., 2022; Kirschbaum et al., 2022). So far, TKA has solved various symptoms of patients with end-stage knee osteoarthritis. However, with the wide application of TKA in the clinic, the number of TKA revision is also significantly increasing year by year due to periprosthetic joint infection, aseptic loosening, polyethylene wear, osteolysis, instability, stiffness, and periprosthetic fracture, which poses great challenges to joint surgeons. According to the reports of the American Association of Orthopedic Surgeons, by 2030, the number of patients who have undergone TKA revision in the United States will reach 268,000 (Kurtz S. et al., 2007). In knee revision cases, many patients suffer from loosening of the implanted prosthesis due to metaphyseal bone defects caused by various reasons, which seriously affects the joint activity and quality of life of patients (Kurtz S. M. et al., 2007).

At present, the Anderson Orthopedic Research Institute (AORI) system is mainly used to classify metaphyseal bone defects in TKA revision. In detail, Type I has minor local cancellous bone defects which do not affect joint stability. Type II defects are mainly divided into two categories: type IIA only involves one tibial plateau or femoral condyle, while type IIB involves the entire tibial plateau or two femoral condyles (Rossi et al., 2022). Type III defects have severe bone loss and involve a wide range and are often accompanied by collateral ligament injury. The traditional treatment methods for bone defects during TKA revision mainly include bone cement filling, structural allografts, and metal cones (Ritter and Harty, 2004; Tsukada et al., 2013; Lei et al., 2019).

However, the specific bone defect in each patient is extremely complex, and the shape of the bone defect varies widely. The aforementioned treatments cannot effectively reconstruct bone defects, and it is, especially difficult to obtain an ideal therapeutic effect for giant bone defect (Daines and Dennis, 2012; Bloch et al., 2020). Three-dimensional (3D) printing provides a new treatment strategy for bone defects in TKA revision, designing personalized prostheses based on radiographic data. Porous tantalum is an ideal alternative repair material for bone defects because of its excellent biocompatibility and biomechanical properties, which have been previously used in clinical treatment and have achieved good results (Boureau et al., 2015; Hu et al., 2017; You et al., 2019). However, there are few studies on the application of 3D printing combined with porous tantalum materials in repairing bone defects. In this study, 3D printing was used to fabricate a personalized porous tantalum cone to repair bone defects in TKA revision, analyze its early treatment effect, and provide a basis for subsequent wide clinical application.

Materials and methods

Participants

Between November 2017 and October 2020, patients who underwent bone defect reconstruction with a 3D-printed porous tantalum cone during TKA revision were followed up. The inclusion criteria were as follows: 1) age >18; 2) patients suffering AORI II bone defects who received TKA revision; 3) detailed preoperative imaging data; and 4) patient and family signed the informed consent form and agreed to participate in this study. The exclusion criteria were as follows: 1) active infection; 2) severe coagulopathy; 3) poor cardiopulmonary function and unable to tolerate surgery; 4) unable to complete postoperative follow-up; 5) allergic to tantalum; and 6) presence of diseases such as malignant tumor that may affect postoperative follow-up. This study was approved by the Institutional Human Ethics Committee (SWH2016ZDCX2010), and all experimental study protocols conformed to ethical norms.

Study procedures

Main procedures of this study included preoperative imaging examination, prosthesis design and fabrication, surgical operation, and postoperative follow-up. The detailed procedures were as follows: 1) carefully screened the cases that met the inclusion criteria, and obtained the informed consent form; 2) collected the imaging data of the surgical site of the patient, and the professional medical 3D designer

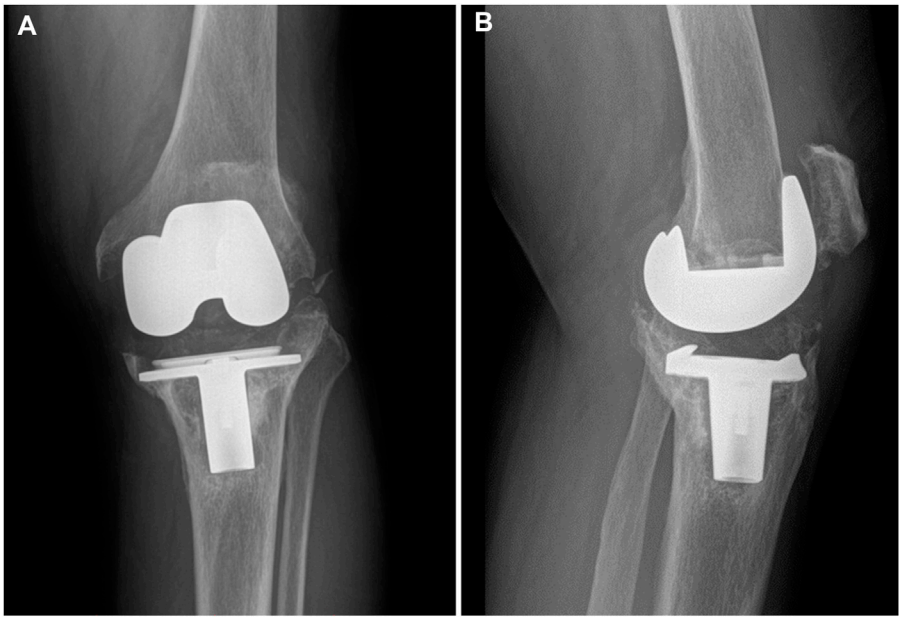

FIGURE 1
Preoperative radiographs of the typical case showing collapse of the tibial plateau. **(A)** Coronal view; **(B)** sagittal view.

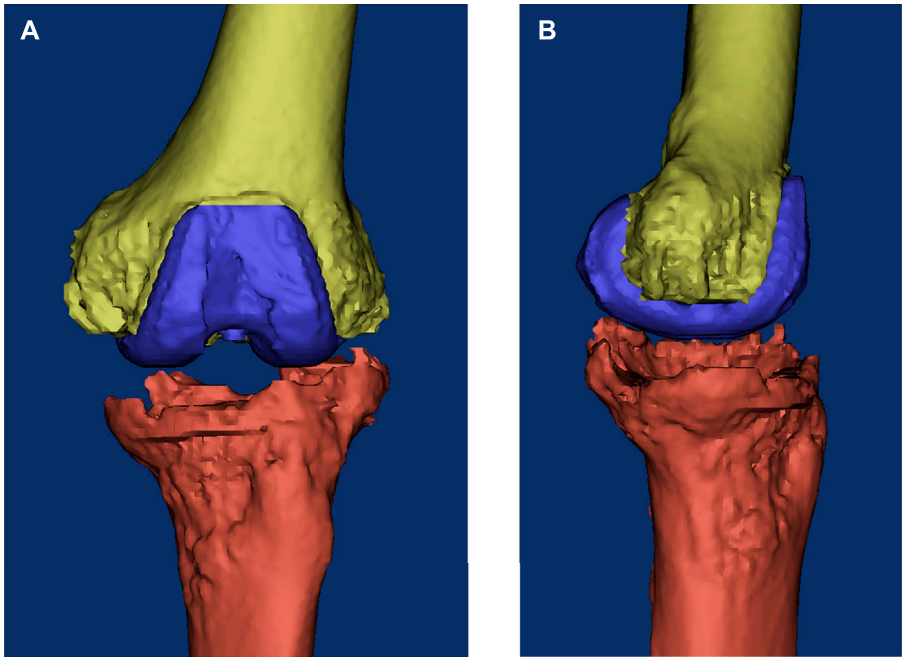

FIGURE 2
Three-dimensional reconstructed image of the knee based on the CT data before surgery. **(A)** Coronal view; **(B)** sagittal view.

performed 3D reconstruction (Figures 1, 2); 3) the designer and the surgeon determined the surgical plan and designed the personalized porous tantalum prosthesis; 4) after determining the prosthesis design, completed the prosthesis printing and sterilization; 5) implanted the personalized porous tantalum prosthesis in TKA revision to repair the bone defect; 6)

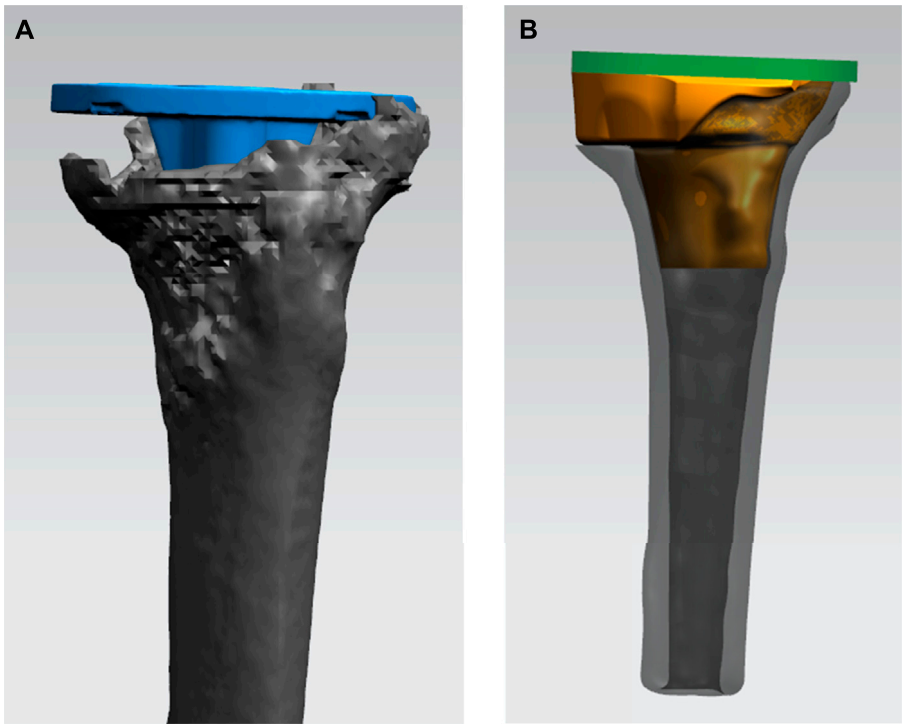

FIGURE 3
Process of designing the 3D-printed porous tantalum cone. **(A)** Simulating the position of the tibial tray (blue) in the tibia in TKA revision. **(B)** Designing the shape and size of the porous tantalum cone (yellow) conforming to the bone defect.

completed the postoperative follow-up and evaluated the patient's joint function and various indicators.

Image data collection

All patients enrolled in this study routinely underwent X-ray and 3D CT scans ranging from the ilium to the ankle, with a scan slice thickness of 1 mm. All digital images were extracted and saved in digital imaging and communications in the medicine (DICOM) format and were uploaded into the Materialise's Interactive Medical Image Control System (MIMICS 17.0 Software, Materialise Corporation, Belgium) for 3D reconstruction and subsequent prosthesis design.

Preoperative planning and prosthesis design

The 3D models of the bone defect and surrounding tissues were established in MIMICS software based on the acquired CT scan DICOM data as described previously, and the process of designing the prosthesis was performed by an experienced engineer (Figure 3). In order to make the prosthesis meet actual clinical demands, engineers and surgeons conducted in-depth communication. The main considerations included the following aspects: 1) most of the patients undergoing knee revision were the elderly with osteoporosis, and the bone debris might be removed during operation; 2) the anatomical shape of the prosthesis should be closely matched with the actual bone defect, so that it would have excellent stability and achieve the therapeutic effect of long-term use; 3) the prosthesis had a feature of porous structure, and its weight and elastic modulus should be considered to avoid stress shielding and other conditions; 4) according to the previous study, the optimal porosity should be designed to promote the subsequent bone ingrowth (Guo et al., 2019).

In the process of designing the porous tantalum cone, the bone defect was simulated according to the preoperative CT images of the patient. The design of the prosthesis mainly included three concepts, namely, anatomical matching,mechanical balance and restoration of function. Based on bone defects, different porous tantalum prostheses were designed. With a few modifications, the porosity was designed to be 75%–80%, so that the autologous bone tissue can be closely combined with the implanted cone as far as possible. After the preliminary design of the prosthesis, a finite element model was established for mechanical analysis

FIGURE 4
Personalized porous tantalum prosthesis printed by pure tantalum.

to ensure that the implanted cone can better disperse the stress without affecting the joint movement.

After the prosthesis design was completed, the data of the designed prosthesis were converted into the STL format and imported into a 3D printer to print a 1:1 plastic model of the prosthesis and surrounding tissues, and the clinician performed a detailed preoperative protocol simulation. Subsequently, porous tantalum prostheses were fabricated and completely sealed and were stored for operation after disinfection (Figure 4).

Surgical procedures

The patient lied in the supine position. After successful anesthesia, a tourniquet was placed on the root of the thigh at a pressure of 280 mmHg. An anteromedial incision was made in the knee, and the skin, subcutaneous tissue, and deep fascia were incised layer by layer to expose the joint cavity. Due to the bone defect, a great number of wear debris were observed in the knee joint, and no secretion was seen in the joint cavity. The hypertrophic synovium and scar tissue in the joint cavity were removed, and the bone debris inside the joint was debrided. In the position of extreme knee flexion, the femoral and tibial prosthesis was taken out, and cement was carefully removed from the bone interface using a curette. After the removal of cement, the medical pulse irrigator was used to flush the surgical field to reduce the risk of infection. Subsequently, medullary reaming of the femur and tibia was conducted, and the excess cortical bone was cut according to the preoperative plan. A customized 3D-printed porous tantalum cone was implanted into the tibia to reconstruct the bone defect; commercial components (Zimmer, tibial component, LCCK femoral component, and LCCK liner) were also used in the revision (Figure 5). After implanting all prostheses, knee flexion and extension were conducted to confirm reliable prosthesis placement. Anticoagulation therapy and intravenous injection of antibiotics were given 6 h after the revision. A silicone drainage tube was maintained until 24 h postoperatively. Functional recovery exercises began after patient's awakening from anesthesia, and ankle flexion and extension were performed to prevent lower limb thrombosis; daily knee flexion and extension were performed on the second postoperative day, and the angle of motion was gradually expanded to 90 degrees.

Indicators

Time of revision, intraoperative blood loss, and postoperative drainage volume were recorded to evaluate the surgical trauma. All patients were followed up at least three times (1, 3, and 6 months after the operation). Preoperative and postoperative visual analog scale (VAS) and Hospital for Special Surgery (HSS) scores were recorded for analysis of improvement in joint function and pain. The 36-Item Short Form Health Survey (SF-36) is an easy measure of reflection in life quality. SF-36 of pre-operation and last follow-up were also recorded to assess the improvement of life quality after revision. At the last follow-up, a CT scan was performed to confirm whether the bone defect was completely reconstructed.

Statistical analysis

All statistical analyses were performed by SPSS software (version 22.0; IBM Corp, United States). The continuous variables were expressed as the mean ± standard deviation. VAS, HSS, and SF-36 scores were compared before and after the operation using the paired *t*-test. The significance level was set at $p < 0.05$.

Results

All patients completed postoperative follow-up, and relevant clinical characteristics such as gender, age, diagnosis classification, and disease course are shown in Table 1. All operations were successfully and smoothly completed, and there were no postoperative complications such as infection, implant loosening, and joint dysfunction. The mean operation time was 189.8 ± 34.1 (range, 139–246) min; intraoperative blood loss was 250.1 ± 76.4 (range, 200–400) ml; mean postoperative drainage volume was 506.7 ± 300.8 (range, 100–1010) ml. The mean preoperative VAS score was 7.2 ± 1.1, the mean VAS score was 3.1 ± 0.9 at the last follow-up ($t = 6.730$, $p < 0.001$), and the

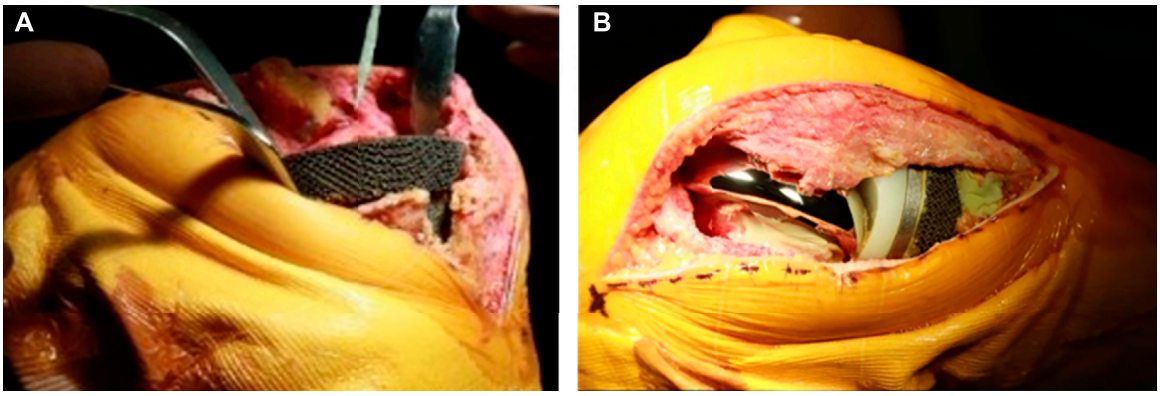

FIGURE 5
Operation of implanting 3D-printed tantalum prosthesis and the TKA revision surgery. **(A)** After trimming the tibial bone defect, the tantalum prosthesis was implanted into the tibia. **(B)** Subsequently, commercial components used in TKA revision were implanted into the knee.

TABLE 1 Demographics of patients.

Patient	Age	Sex	AORI	Symptom	Side of operation	Indication for revision	Duration (year)
1	85	M	Type IIB	Pain and dysfunction	Left	Aseptic loosening	17
2	83	F	Type IIA	Pain and dysfunction	Left	Aseptic loosening	11
3	78	F	Type IIA	Pain and dysfunction	Right	Prosthetic joint infection	3
4	68	F	Type IIB	Pain	Right	Prosthetic joint infection	1.5
5	75	F	Type IIB	Pain and dysfunction	Right	Aseptic loosening	10
6	58	M	Type IIA	Pain	Right	Instability	8

TABLE 2 Relevant data of operation and follow-up.

Variable	Value
Operation time (min)	189.8 ± 34.1 (range, 139–246)
Intraoperative blood loss (ml)	250.1 ± 76.4 (range, 200–400)
Postoperative drainage volume (ml)	506.7 ± 300.8 (range, 100–1010)
Follow-up duration (month)	26.3 ± 12.6 (range, 9–44)
VAS score (pre. vs. post.)	7.2 ± 1.1 vs. 3.1 ± 0.9
HSS score (pre. vs. post.)	31.3 ± 5.7 vs. 64.7 ± 7.2
SF-36 score (pre. vs. post.)	38.8 ± 7.8 vs. 77.8 ± 4.2

VAS score was significantly improved compared with the preoperative score. The mean preoperative HSS score was 31.3 ± 5.7, the mean HSS score was 64.7 ± 7.2 at the last follow-up (t = 8.111, p < 0.001), and there was a significant improvement in joint function compared with the preoperative score. The mean preoperative SF-36 score was 38.8 ± 7.8 and the mean SF-36 score was 77.8 ± 4.2 at the last follow-up (t = 9.836, p < 0.001). Detailed data are shown in Table 2.

Discussion

In this study, we used 3D printing combined with porous tantalum to manufacture a personalized cone for the clinical treatment of metaphyseal bone defects. After multiple postoperative follow-ups, it was confirmed that this technology has a significant clinical therapeutic effect, which can effectively repair the metaphyseal bone defects of the knee joint and improve the joint function of patients (as shown in Figures 6, 7). In TKA revision, most patients are prone to metaphyseal bone defects due to various causes, such as joint prosthesis instability and abnormal lower extremity alignment, affecting normal joint activity and the quality of life (Lotke et al., 2006; Engh and Ammeen, 2007).

In the past, the treatment of metaphyseal bone defect in knee revision was mainly determined according to the patient's underlying disease, the severity of the bone defect, the reason for revision, and the postoperative knee function and activity expectations. AORI type I bone defects, because of their small depth and area, are mainly filled with bone cement; however, the implanted bone cement may decrease in size, resulting in

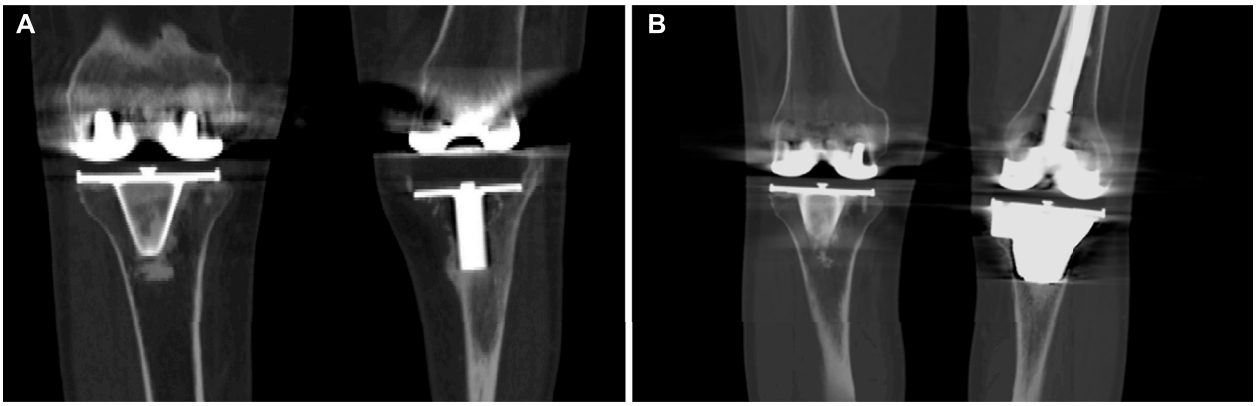

FIGURE 6
CT images of the representative case showed that the tibial bone defect was effectively reconstructed by the porous tantalum cone. **(A)** Preoperative image; **(B)** postoperative image at 3 years after the operation.

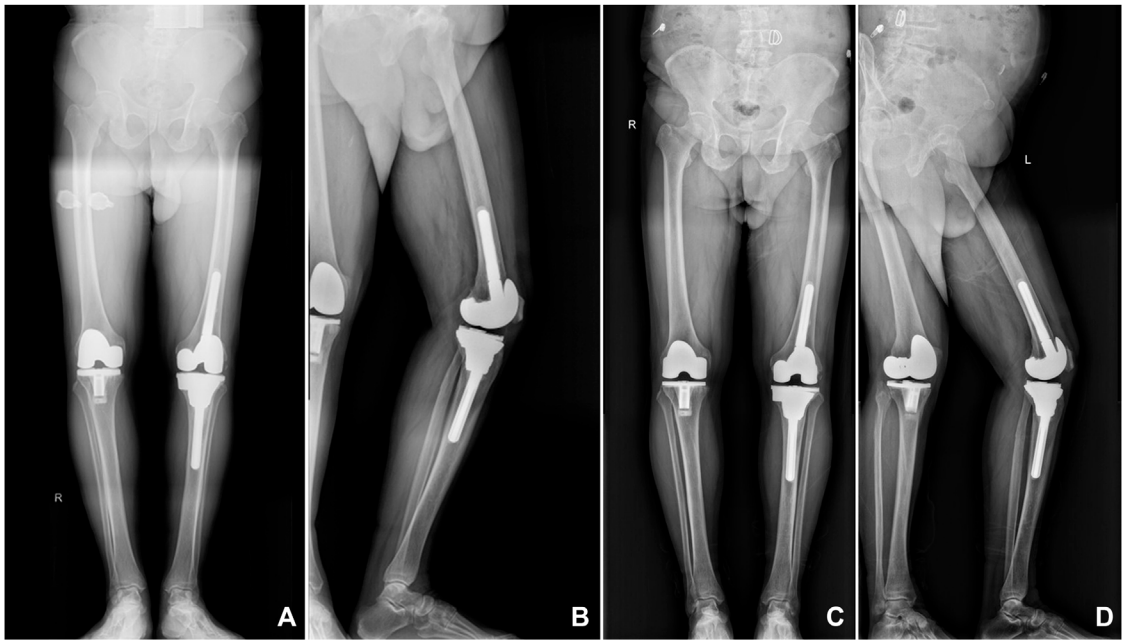

FIGURE 7
X-ray images of a representative patient showed that the 3D-printed porous tantalum cone is stable and tightly integrated with the surrounding bone tissue. **(A,B)** Postoperative radiographs were taken at 6 months after surgery; **(C,D)** postoperative radiographs were taken at 3 years after surgery.

prosthesis loosening during recovery (Toms et al., 2009). For AORI type II bone defects, allogeneic bone transplantation is another treatment strategy. Clatworthy et al. (2001) used this technique to treat 52 patients with tibial plateau bone defect requiring knee revision. After a long-term follow-up, 75% of patients had effective improvement in joint function. However, a large defect area cannot be effectively repaired; there is also a risk of transmitting diseases and bone graft resorption, and its high treatment cost also hinders its wide application in clinical practice (Dennis and Little, 2005; Rudert et al., 2015).

The metal cone is suitable for bone defects with a large area and has a certain therapeutic effect on metaphyseal bone defects. At present, this method is widely used for the treatment of bone defects in clinical practice. This technique can solve the problem of bone

absorption or transmission of diseases (Issack, 2013; Divano et al., 2018). Porous tantalum material has been widely used in many fields of orthopedics because of its excellent biocompatibility, corrosion resistance, and mechanical properties, and the porous structure is conducive to inducing host bone ingrowth and bone adhesion and is the main material of customized metal cone produced by Zimmer (Bencharit et al., 2014; Potter et al., 2016; Huang et al., 2021). Howard et al. (2011) treated patients with bone defects after TKA revision. They used porous tantalum cones to fill femoral metaphyseal bone defects, and after an average follow-up of 33 months, most patients had significant improvement in knee function. Meneghini et al. (2008) also used porous tantalum cones to treat tibial AORI type II and III bone defects in TKA revision and achieved good therapeutic results, but some patients experienced secondary revision. Brown et al. (2015) reported the cases of using porous tantalum cones to fill bone defects and performed joint replacement. After an average follow-up of 40 months, it was found that the treatment effect was good in most patients, with some patients undergoing second operation due to infection and periprosthetic fracture, etc. Lachiewicz et al. (2012) retrospectively analyzed patients treated with porous tantalum cones, and during follow-up, the radiographic findings indicated that the implant augments showed good osseointegration with the host bone. Although the therapeutic effect of the metal cone is better than that of allogeneic bone transplantation, the metal cone is a customized commodity. When the patient's bone defect is large and irregular in shape, it is difficult to completely match. Large and complex bone defects are the main problems surgeons are confronted with.

In recent years, with the development of precision medicine, 3D printing has also become increasingly progressive. With its advantages of precision and individualization, it is, especially suitable for the design and fabrication of personalized prostheses in orthopedics (Duan et al., 2019; Sun M. et al., 2020). The rise of 3D printing has provided a new and accurate solution for the treatment of various osteoarticular diseases (Duan et al., 2018). England et al. (2021) used 3D printing to manufacture a porous titanium prosthesis for the repair of bone defects during TKA revision. The follow-up results showed that the porous titanium prosthesis had better integration and stability with the host bone and had a better therapeutic effect on bone defects. Sun M. L. et al. (2020) used 3D printing to manufacture personalized surgical guides to assist in TKA, which could make the surgical operation more accurate. Compared with titanium, tantalum has good physical and chemical properties and is more suitable for the repair of bone defects. Balla et al. (2010) used 3D printing to prepare porous tantalum and porous titanium and found that porous tantalum has better biocompatibility than porous tantalum. When osteoblasts were cultured on the surface of porous tantalum, the expression level of alkaline phosphatase was increased, indicating that porous tantalum has a better bone-promoting ability. Guo et al. (2019) found through experimental studies that porous tantalum could promote stem cell proliferation, adhesion, and differentiation more than porous titanium and had better osteointegration performance, which was more suitable for utility as a bone substitute product. For metaphyseal bone defects after TKA, 3D-printed personalized prostheses can better match the shape of the defect and help make a detailed preoperative plan and enable a smoother operation. The porous structure can make the implanted metal more tightly integrated with the host bone, ensure the stability of the implanted augment and the stability of the joint prosthesis, and avoid the occurrence of re-revision (Small et al., 2022).

To the best of our knowledge, it is rare to use 3D printing to manufacture personalized porous tantalum prostheses for repairing metaphyseal bone defects in TKA revision. In this study, 3D printing was used to fabricate a personalized porous tantalum cone for repairing the metaphyseal bone defect, achieving an ideal repair effect, effectively relieving patient's pain symptoms and improving joint range of motion and the patient's quality of life. This study also has some limitations: first, due to the small number of patients included in the study, it lacks a control group; second, this study mainly observes the mid-term clinical efficacy, the follow-up time is relatively short, and it still needs a longer follow-up to observe its long-term therapeutic effects; third, a simple radio imaging follow-up was performed after the operation to observe the stability of the prosthesis, but the relevant osseointegration is not analyzed in detail.

Conclusion

This study reported the mid-term clinical outcome of the 3D-printed porous tantalum prosthesis for reconstructing bone defects during TKA revision. In this study, a porous tantalum prosthesis manufactured by 3D printing presented favorable effects on the treatment of bone defects in revision, including relieving pain and improvement of knee function and quality of life. Great reconstruction of bone defect was achieved by anatomically conforming the design and excellent osseointegration of tantalum prosthesis. Despite these beneficial outcomes, future multicenter case–control studies are still needed to be conducted to research the long-term effect.

Data availability statement

The original contributions presented in the study are included in the article/Supplementary Material; further inquiries can be directed to the corresponding authors.

Ethics statement

The studies involving human participants were reviewed and approved by the Institutional Human Ethics Committee of Southwest Hospital, Army Medical University. The patients/participants provided their written informed consent to

participate in this study. Written informed consent was obtained from the individual(s) for the publication of any potentially identifiable images or data included in this article.

Author contributions

Conception and design: FW and LY; surgical operation: LG, HC, and RH; provision of materials: PY and DF; collection of data: LG and YP; data analysis: RX and YA; and manuscript writing: YA. All authors read and agreed to the published version of the manuscript.

Funding

The authors acknowledge the funding provided by the Personalized Cultivation Program for Excellent Talent of Army Medical University (No. XZ-2019-505-038) and Chongqing Graduate Scientific Research Innovation Project (No. CYB21230).

Acknowledgments

The authors would like to thank Xin Chen from the Center for Joint Surgery, Southwest Hospital, Third Military Medical University, for the language support for this article.

Conflict of interest

The authors declare that the research was conducted in the absence of any commercial or financial relationships that could be construed as a potential conflict of interest.

Publisher's note

All claims expressed in this article are solely those of the authors and do not necessarily represent those of their affiliated organizations, or those of the publisher, the editors, and the reviewers. Any product that may be evaluated in this article, or claim that may be made by its manufacturer, is not guaranteed or endorsed by the publisher.

References

Balla, V. K., Bodhak, S., Bose, S., and Bandyopadhyay, A. (2010). Porous tantalum structures for bone implants: fabrication, mechanical and *in vitro* biological properties. *Acta Biomater.* 6, 3349–3359. doi:10.1016/j.actbio.2010.01.046

Bencharit, S., Byrd, W. C., Altarawneh, S., Hosseini, B., Leong, A., Reside, G., et al. (2014). Development and applications of porous tantalum trabecular metal-enhanced titanium dental implants. *Clin. Implant Dent. Relat. Res.* 16, 817–826. doi:10.1111/cid.12059

Bloch, B. V., Shannak, O. A., Palan, J., Phillips, J. R. A., and James, P. J. (2020). Metaphyseal sleeves in revision total knee arthroplasty provide reliable fixation and excellent medium to long-term implant survivorship. *J. Arthroplasty* 35, 495–499. doi:10.1016/j.arth.2019.09.027

Boureau, F., Putman, S., Arnould, A., Dereudre, G., Migaud, H., and Pasquier, G. (2015). Tantalum cones and bone defects in revision total knee arthroplasty. *Orthop. Traumatol. Surg. Res.* 101, 251–255. doi:10.1016/j.otsr.2014.11.020

Brown, N. M., Bell, J. A., Jung, E. K., Sporer, S. M., Paprosky, W. G., and Levine, B. R. (2015). The use of trabecular metal cones in complex primary and revision total knee arthroplasty. *J. Arthroplasty* 30, 90–93. doi:10.1016/j.arth.2015.02.048

Clatworthy, M. G., Ballance, J., Brick, G. W., Chandler, H. P., and Gross, A. E. (2001). The use of structural allograft for uncontained defects in revision total knee arthroplasty. A minimum five-year review. *J. Bone Jt. Surg. Am.* 83, 404–411. doi:10.2106/00004623-200103000-00013

Daines, B. K., and Dennis, D. A. (2012). Management of bone defects in revision total knee arthroplasty. *J. Bone Jt. Surg.* 94, 1131–1139. doi:10.2106/jbjs.l00143

Dennis, D. A., and Little, L. R. (2005). The structural allograft composite in revision total knee arthroplasty. *Orthopedics* 28, 1005–1007. doi:10.3928/0147-7447-20050901-45

Divano, S., Cavagnaro, L., Zanirato, A., Basso, M., Felli, L., and Formica, M. (2018). Porous metal cones: gold standard for massive bone loss in complex revision knee arthroplasty? A systematic review of current literature. *Arch. Orthop. Trauma Surg.* 138, 851–863. doi:10.1007/s00402-018-2936-7

Duan, X., He, P., Fan, H., Zhang, C., Wang, F., and Yang, L. (2018). Application of 3D-printed personalized guide in arthroscopic ankle arthrodesis. *Biomed. Res. Int.* 2018, 3531293. doi:10.1155/2018/3531293

Duan, X. J., Fan, H. Q., Wang, F. Y., He, P., and Yang, L. (2019). Application of 3D-printed customized guides in subtalar joint arthrodesis. *Orthop. Surg.* 11, 405–413. doi:10.1111/os.12464

Engh, G. A., and Ammeen, D. J. (2007). Use of structural allograft in revision total knee arthroplasty in knees with severe tibial bone loss. *J. Bone Jt. Surg. Am.* 89, 2640–2647. doi:10.2106/jbjs.f.00865

England, T., Pagkalos, J., Jeys, L., Botchu, R., and Carey Smith, R. (2021). Additive manufacturing of porous titanium metaphyseal components: early osseointegration and implant stability in revision knee arthroplasty. *Materials (Basel)* 15, 60–64. doi:10.3390/ma14102647

Fei, Z., Zhang, Z., Wang, Y., Zhang, H., and Xiang, S. (2022). Comparing the efficacy of articulating spacers in two-stage revision for periprosthetic joint infection following total knee arthroplasty: all-cement spacers vs sterilized replanted metal-polyethylene spacers. *Int. J. Gen. Med.* 15, 3293–3301. doi:10.2147/IJGM.S354808

Guo, Y., Xie, K., Jiang, W., Wang, L., Li, G., Zhao, S., et al. (2019). *In vitro* and *in vivo* study of 3D-printed porous tantalum scaffolds for repairing bone defects. *Orthop. Surg.* 5, 1123–1133. doi:10.1111/os.12425

Howard, J. L., Kudera, J., Lewallen, D. G., and Hanssen, A. D. (2011). Early results of the use of tantalum femoral cones for revision total knee arthroplasty. *J. Bone Jt. Surg.* 93, 478–484. doi:10.2106/jbjs.i.01322

Hu, B., Chen, Y., Zhu, H., Wu, H., and Yan, S. (2017). Cementless porous tantalum monoblock tibia vs cemented modular tibia in primary total knee arthroplasty: a meta-analysis. *J. Arthroplasty* 32, 666–674. doi:10.1016/j.arth.2016.09.011

Huang, G., Pan, S. T., and Qiu, J. X. (2021). The clinical application of porous tantalum and its new development for bone tissue engineering. *Materials (Basel)* 14, 2647. doi:10.3390/ma14102647

Issack, P. S. (2013). Use of porous tantalum for acetabular reconstruction in revision hip arthroplasty. *J. Bone Jt. Surg.* 95, 1981–1987. doi:10.2106/jbjs.l.01313

Kirschbaum, S., Weynandt, C., Fuchs, M., Perka, C., and Gwinner, C. (2022). Major shortening of the patellar tendon during septic two-stage knee arthroplasty revision using static spacers. *J. Arthroplasty* S0883-5403 (22), 00384–00389. doi:10.1016/j.arth.2022.03.082

Kurtz, S. M., Ong, K. L., Schmier, J., Mowat, F., Saleh, K., Dybvik, E., et al. (2007b). Future clinical and economic impact of revision total hip and knee arthroplasty. *J. Bone Jt. Surg.* 89 (3), 144–151. doi:10.2106/jbjs.g.00587

Kurtz, S., Ong, K., Lau, E., Mowat, F., and Halpern, M. (2007a). Projections of primary and revision hip and knee arthroplasty in the United States from 2005 to 2030. *J. Bone Jt. Surg.* 89, 780–785. doi:10.2106/jbjs.f.00222

Lachiewicz, P. F., Bolognesi, M. P., Henderson, R. A., Soileau, E. S., and Vail, T. P. (2012). Can tantalum cones provide fixation in complex revision knee arthroplasty? *Clin. Orthop. Relat. Res.* 470, 199–204. doi:10.1007/s11999-011-1888-9

Lei, P. F., Hu, R. Y., and Hu, Y. H. (2019). Bone defects in revision total knee arthroplasty and management. *Orthop. Surg.* 11, 15–24. doi:10.1111/os.12425

Lotke, P. A., Carolan, G. F., and Puri, N. (2006). Technique for impaction bone grafting of large bone defects in revision total knee arthroplasty. *J. Arthroplasty* 21, 57–60. doi:10.1016/j.arth.2006.01.019

Meneghini, R. M., Lewallen, D. G., and Hanssen, A. D. (2008). Use of porous tantalum metaphyseal cones for severe tibial bone loss during revision total knee replacement. *J. Bone Jt. Surg. Am.* 90, 78–84. doi:10.2106/jbjs.f.01495

Potter, G. D., 3rd, Abdel, M. P., Lewallen, D. G., and Hanssen, A. D. (2016). Midterm results of porous tantalum femoral cones in revision total knee arthroplasty. *J. Bone Jt. Surg.* 98, 1286–1291. doi:10.2106/jbjs.15.00874

Ritter, M. A., and Harty, L. D. (2004). Medial screws and cement: a possible mechanical augmentation in total knee arthroplasty. *J. Arthroplasty* 19, 587–589. doi:10.1016/j.arth.2003.11.009

Rossi, S. M. P., Perticarini, L., Ghiara, M., Jannelli, E., Cortesi, L., and Benazzo, F. (2022). High survival rate at mid-term follow up of porous tantalum cones for bone defects in revision total knee replacement: a 3-11 years follow up report. *Knee* 35, 175–182. doi:10.1016/j.knee.2022.03.007

Rudert, M., Holzapfel, B. M., Von Rottkay, E., Holzapfel, D. E., and Noeth, U. (2015). Impaction bone grafting for the reconstruction of large bone defects in revision knee arthroplasty. *Oper. Orthop. Traumatol.* 27, 35–46. doi:10.1007/s00064-014-0330-3

Small, I., Meghpara, M., Stein, J., Goh, G., Banerjee, S., and Courtney, P. M. (2022). Intermediate-term survivorship of metaphyseal cones and sleeves in revision total knee arthroplasty. *J. Arthroplasty* S0883-5403 (22), 00387–394. doi:10.1016/j.arth.2022.03.085

Sun, M. L., Zhang, Y., Peng, Y., Fu, D. J., Fan, H. Q., and He, R. (2020). Accuracy of a novel 3D-printed patient-specific intramedullary guide to control femoral component rotation in total knee arthroplasty. *Orthop. Surg.* 12, 429–441. doi:10.1111/os.12619

Sun, M., Zhang, Y., Peng, Y., Fu, D., Fan, H., and He, R. (2020). Gait analysis after total knee arthroplasty assisted by 3D-printed personalized guide. *Biomed. Res. Int.* 2020, 6485178. doi:10.1155/2020/6485178

Toms, A. D., Barker, R. L., Mcclelland, D., Chua, L., Spencer-Jones, R., and Kuiper, J. H. (2009). Repair of defects and containment in revision total knee replacement: a comparative biomechanical analysis. *J. Bone Jt. Surg. Br.* 91, 271–277. doi:10.1302/0301-620x.91b2.21415

Tsukada, S., Wakui, M., and Matsueda, M. (2013). Metal block augmentation for bone defects of the medial tibia during primary total knee arthroplasty. *J. Orthop. Surg. Res.* 8, 36. doi:10.1186/1749-799x-8-36

You, J. S., Wright, A. R., Hasegawa, I., Kobayashi, B., Kawahara, M., Wang, J., et al. (2019). Addressing large tibial osseous defects in primary total knee arthroplasty using porous tantalum cones. *Knee* 26, 228–239. doi:10.1016/j.knee.2018.11.001

frontiers | Frontiers in Bioengineering and Biotechnology

TYPE Original Research
PUBLISHED 19 September 2022
DOI 10.3389/fbioe.2022.976706

OPEN ACCESS

EDITED BY
Jun Lin,
First Affiliated Hospital of Soochow University, China

REVIEWED BY
Yong-Can Huang,
Peking University, China
Lu Cao,
Fudan University, China

*CORRESPONDENCE
Liming Liu,
liulimin_spine@163.com

†These authors have contributed equally to this work

SPECIALTY SECTION
This article was submitted to Biomaterials, a section of the journal Frontiers in Bioengineering and Biotechnology

RECEIVED 23 June 2022
ACCEPTED 05 September 2022
PUBLISHED 19 September 2022

CITATION
Chen Q, Wang J, Xia Q, Wu L, Chen F, Li L, Zhu C, He M, Jiang Y, Huang Y, Ding H, Wu R, Zhang L, Song Y and Liu L (2022), Treatment outcomes of injectable thermosensitive hydrogel containing bevacizumab in intervertebral disc degeneration. *Front. Bioeng. Biotechnol.* 10:976706. doi: 10.3389/fbioe.2022.976706

Treatment outcomes of injectable thermosensitive hydrogel containing bevacizumab in intervertebral disc degeneration

Qian Chen[1,2†], Juehan Wang[1†], Qinghong Xia[3†], Lei Wu[4], Fei Chen[5], Li Li[5], Ce Zhu[1], Miaomiao He[6], Yulin Jiang[6], Yong Huang[1], Hong Ding[1], Ruibang Wu[1], Li Zhang[6], Yueming Song[1] and Liming Liu[1*]

[1]Department of Orthopedic Surgery and Orthopedic Research Institute, West China Hospital, Sichuan University, Chengdu, Sichuan, China, [2]Department of Orthopaedics, Affiliated Hospital of North Sichuan Medical College, Nanchong, Sichuan, China, [3]Operating Room of Anesthesia Surgery Center, West China Hospital, Sichuan University, West China School of Nursing, Sichuan University, Chengdu, Sichuan, China, [4]Histology and Imaging Platform, Core Facilities of West China Hospital, Sichuan University, Chengdu, Sichuan, China, [5]The Institute of Clinic Pathology, Sichuan University, Chengdu, China, [6]Analytical and Testing Center, Sichuan University, Chengdu, Sichuan, China

Intervertebral disc (IVD) degeneration (IDD) is a common musculoskeletal disease and its treatment remains a clinical challenge. It is characterised by reduced cell numbers and degeneration of the extracellular matrix (ECM). Nucleus pulposus (NP) cells play a crucial role in this process. The purpose of this study is to explore the role of bevacizumab, a vascular endothelial growth factor (VEGF) inhibitor, in the treatment of IDD through local drug delivery. High expression of VEGF was observed in degenerating human and rat IVDs. We demonstrated that MMP3 expression was decreased and COL II synthesis was promoted, when VEGF expression was inhibited by bevacizumab, thereby improving the degree of disc degeneration. Thus, these findings provide strong evidence that inhibition of VEGF expression by local delivery of bevacizumab is safe and effective in ameliorating disc degeneration in rats. The injectable thermosensitive PLGA-PEG-PLGA hydrogels loaded with bevacizumab is a potential therapeutic option for disc degeneration.

KEYWORDS

bevacizumab, intervertebral disc degeneration, VEGF, thermosensitive injectable hydrogel, biomaterial

Introduction

Intervertebral disc degeneration (IDD) is the main cause of low back pain, especially in the elderly population, and brings huge economic and social burden (Francisco et al., 2022). More than 40% of patients with low back pain are caused by IDD. In severe cases it can cause nerve dysfunction in the lower limbs and even incontinence. Therefore, IDD is considered to be the main pathological basis (Barber et al., 2015). Intervertebral disc (IVD) is colloids composed of nucleus pulposus (NP) and annulus fibrous (AF) cells. IDD is characterized by the progressive deterioration of the NP microenvironment, which maintains important biological functions through the production of extracellular matrix (ECM), including type II collagen (COL II), proteoglycan and aggrecan (Xu et al., 2020; Wang et al., 2022). NP requires a hypoxic and avascular microenvironment to maintain normal function. Due to the lack of a complete understanding of the mechanism of IDD, there is still a lack of effective prevention and treatment methods for disc degeneration. (Pan et al., 2018; Wang et al., 2021a).

Currently, drug analgesia is the main conservative treatment for patients with IDD. In severe cases, surgery is necessary. However, these treatment methods are still unsatisfactory due to their side effects and limitations. Hence, researchers have never stopped searching for effective treatment approaches for IDD, particularly the application of regenerative medicine strategies to repair and reconstruct IVD. (Pan et al., 2018; Liao et al., 2021).

Vascular endothelial growth factor (VEGF) plays an important role in tissue homeostasis (Kim et al., 2017). VEGF was found to be highly expressed in degenerating disc tissue, altering the NP microenvironment and accelerating disc degeneration through neovascularization and infiltration. (Lu et al., 2013). In addition, several studies have illustrated that VEGF signaling pathway plays a pivotal role in IDD (Zhang Y et al., 2019; He et al., 2020; Hwang et al., 2020; Wang et al., 2021b; Chen and Jiang, 2021; Ye et al., 2021). VEGF may represent a therapeutic target for IVD degeneration. Bevacizumab is an FDA-approved recombinant humanised monoclonal antibody that is widely used to treat tumours. It works by binding to human vascular endothelial growth factor (VEGF) and blocks its biological activity to inhibit tumour angiogenesis (Garcia et al., 2020; Haunschild and Tewari, 2020; Nakai and Matsumura, 2022). Numerous clinical cases have already proven its efficacy and safety in human patients, which making it easier to translate into clinical applications in other diseases (Garcia et al., 2020).

Nowadays, this anti-tumour drug has been reported to cause serious side effects when systemic administration. To improve the effectiveness of bevacizumab treatment and reduce its side effects. A thermosensitive injectable poly (lactide-co-glycolide)-block-poly (ethyleneglycol)-block-poly (lactide-co-glycolide) (PLGA-PEG-PLGA) hydrogel was utilized for the local controlled-release of bevacizumab to restore degenerative IVDs. The injectable hydrogel has been shown good biocompatibility and degradability and is easily to mix with drugs. It has been used for topical delivery of targeted therapies (Gao et al., 2020; López-Cano et al., 2021). The gel-like characteristic of the injectable hydrogel facilitates injection into the Degenerated area entirely (Pan et al., 2018; Wei et al., 2021). The aim of this study was to explore the Treatment potential of bevacizumab, a VEGF inhibitor, in improving IVD degeneration through local delivery.

Materials and methods

Collection of degenerated disc samples

All human degenerated disc samples in this research were obtained from the West China Hospital of Sichuan University, and all trials were approved by the Ethics Committee of Sichuan University. Degenerative IVD samples (n = 10, 5 males and 5 females, aged 48–69 years) were obtained from patients requiring surgical treatment for degenerative spine disease, while non-degenerative controls (n = 5, 2 males and 3 females, aged 42–59 years) were obtained from patients with lumbar fracture requiring surgery. Degenerated IVDs were identified by MRI and histological staining.

Animal experiments were approved by our Animal Protection and Utilisation Committee. Sprague Dawley rats (female, 8 weeks old, 440 g) were obtained from the West China Hospital Animal Centre. The surgical procedure was performed using a previously described method (Han et al., 2008). Briefly, 1% sodium pentobarbital (Sigma Aldrich, St. Louis, MO) was administered intraperitoneally to 48 rats at a dose of 0.3 mg/kg body weight. Pre-puncture radiographs were taken to determine the position of the caudal intervertebral disc (Co7/8) by digital palpation and confirmed by counting the vertebrae from the sacral region in the trial film (Han et al., 2008). After imaging, 48 rats were randomly allocated into four groups: a non-degenerative group (without puncture and without any injection, n = 12), and a degenerative group (with puncture and PBS injection only, n = 12), and a PLGA-PEG-PLGA hydrogel group (with puncture and hydrogel injection, n = 12), a PLGA-PEG-PLGA-Bevacizumab hydrogel group (with puncture and bevacizumab-loaded hydrogel injection, n = 12) for follow-up MRI, histological analysis and immunochemistry at week 8.

Fixation and histological examination of intervertebral disc tissues

The IVD samples were first fixed with 4% (v/v) paraformaldehyde solution for 1 day and then decalcified with

neutral 10% (w/v) ethylenediaminetetraacetic acid solution for 4 weeks. Following this, the samples were dehydrated with gradient alcohol and then embedded in paraffin for tissue entire continuous section. At last, sections of each sample were stained with hematoxylin and eosin (H&E), Safranin O-Fast Green (SO) staining and immunohistochemical analysis.

Histological score of degenerative intervertebral discs

These sections (7 μm) of IVD were gathered (approximately five slides per sample) for H&E staining and SO staining. Two experienced histological pathologists observed the morphology and number of NP, AF, and endplate (EP) cells through a microscope and evaluated using previously described grading criteria (Kawchuk et al., 2001; Norcross et al., 2003). A normal disc histology score was 5 points; the moderate degenerative disc histology score was 6–11 points, and the severe degenerative disc histology score was 12–14 points.

Primary culture of rat NP cells

NP tissue was rinsed twice using a PBS containing 1% penicillin/streptomycin and then cut into small pieces. (2–3 mm^3). The cells were obtained using a type II collagenase (Invitrogen, Carlsbad, CA, USA) digestion method, overnight at 37°C, and the NP cells were suspended in Dulbecco's modified Eagle's medium (DMEM). The NP cells cultured in DMEM containing 10% fetal bovine serum (Gibco) and 1% penicillin/streptomycin (Invitrogen) were placed in a 5% CO2 incubator at 37°C. The medium was replaced every 2 days. Cells of the second passage were used for subsequent experiments.

Bevacizumab and TNF-α treatment *in vitro*

After 24 h of 10 ng/ml TNF-α treatment, rat NP cells were treated with 1 mg/ml bevacizumab for 30 min, and then RNA and protein were extracted for subsequent experiments.

Immunofluorescence

After being seeded in 24-well plates, cells were treated with different regimens overnight. After incubation, the cells were washed three times with PBS and then fixed with 4% paraformaldehyde for 20 min, then permeabilised with 0.25% Triton X-100 and blocked with 5% bovine serum albumin for 30 min. Next, the cells were incubated with anti-VEGF (1:300; Abcam, ab69479) and anti- COL II antibodies (ab34712, 1:200, Abcam, UK) at 4°C overnight. Subsequently, the cells were washed with PBS followed by incubation with the secondary antibody IgG-rhodamine (1:500 dilution, SAB3700860) (Sigma-Aldrich) and antibody IgG-FITC (1:200 dilution) (Sigma-Aldrich, F0257) for 1 h at ambient temperature, respectively. Nuclei were dyed with 4,6-diamidino-2-phenylindole (DAPI; Beyotime, China). Fluorescence images were observed with a fluorescent microscope (Zeiss Axioplan microscope, Carl Zeiss Microscopy, Thornwood, NY, USA).

Western blotting

Western blot test was carried out according to standard methods. In brief, the proteins were transferred to the polyvinylidene fluoride (PVDF) membranes (Amersham, Buckinghamshire, UK) immediately after separation through 10% SDS-PAGE gel. Then, the membranes were blocked with 5% nonfat dried milk for 2 h and incubated overnight at 4°C with anti-COL II (ab34712, 1:200; Abcam, UK), anti-VEGF (1:200; Abcam, ab69479), or anti-MMP3 antibody (ab52915, 1:200; Abcam). The membranes were incubated with the secondary antibody at room temperature for 2 h after being rinsed with Tris-buffered saline. The proteins were measured by enhanced chemiluminescence using Bio-Rad Image Lab Software 5.2 (Bio-Rad Laboratories, Hercules, CA, USA).

RT-qPCR

RNA from rat cells was lysed with TRIzol (Invitrogen, Carlsbad, California, USA) and then reversely transcribed. PCR was implemented with Brilliant SYBR Green QPCR Master Mix (TakaRa) and a Light Cycler instrument (ABI 7900HT). The expression of the compared genes was quantified by verifying the amplification efficiency of the primer pairs. The following primer sequences were used: COL II
Sense5′-GAGTGGAAGAGCGGAGACTACTG-3′,
antisense5′-CTCCATGTTGCAGAAGACTTTCA-3'; MMP3
Sense 5′-TTTGGCCGTCTCTTCCATCC-3′,
antisense 5′-TTTGGCCGTCTCTTCCATCC-3'; VEGF
Sense 5′-GCACCCATGGCAGAAGGAG-3′,
antisense 5′-ACACAGGATGGCTTGAAGATGT-3'.

Each experiment was repeated at least three times on different experimental samples.

PLGA-PEG-PLGA-bevacizumab hydrogel synthesis

Poly (*D,L*-lactic acid-*co*-glycolic acid)-*b*-poly (ethylene glycol)-*b*-poly (*D,L*-lactic acid-*co*-glycolic acid) (PLGA–PEG–PLGA) triblock copolymers were synthesized by ring-opening polymerization of lactide (LA) and glycolide (GA) in

the presence of PEG (M_n 1,500 Da), and stannous octoate was used as catalyst. PLGA–PEG–PLGA triblock copolymers were prepared for subsequent procedure. Concentrations were reported in wt/vol percentages. polymer was weighed about 3 mg and placed in a 4 ml glass bottle, then 10 ml phosphate-buffered saline (PBS) buffer (pH 7.4) was added to make a 30% solution. Then, at 4°C, the mixtures were stirred continuously overnight to ensure that complete dissolution of the polymer. At 4°C, 20% were prepared for stocking by further dilution by adding appropriate volumes of PBS. 0.25 ml of polymer solution was added to the glass vial to prepare the hydrogel. Subsequently, the vial was incubated in a 37°C incubator to trigger the gelation process.

Hydrogels loaded with bevacizumab were prepared by swelling-diffusion method. Bevacizumab (1 mg/ml) was added to PBS containing D-a-Tocopherol polyethylene glycol 1,000 succinate (TPGS), and then, by ultrasonic dispersion and free swelling in continuous contact with 20% (w/v) lyophilized PLGA-PEG-PLGA copolymer at 4°C for 24 h. Finally, at 37°C, the unloaded PLGA–PEG–PLGA hydrogel was eluted by PBS to obtain PLGA–PEG–PLGA- bevacizumab hydrogel.

Fourier-transform infrared spectroscopy spectra acquisition

Infrared spectra of lyophilized PLGA-PEG-PLGA hydrogels and PLGA-PEG-PLGA-Bevacizumab hydrogels were obtained through using a TGS detector and a ZnO crystal sampling accessory by a Jasco FT-IR-4100 spectrometer (Tokyo, Japan) in cross-task mode. The spectrometer has a detection range of 400-4000cm^{-1} and a resolution of 4cm^{-1}. After 100 times scan of each sample, the average spectrum was used for analysis.

Rheological analysis

Rheological analysis of PLGA-PEG-PLGA hydrogels was carried out at 4°C by using a rheometer (MCR-92; Anton Paar, Graz, Austria). The heating rate was set to 0.5°C/min, the angular frequency (ω) was set to 1 rad/s and the temperature range tested was 10–50°C.

In vivo and *in vitro* evaluation of the biocompatibility of hydrogel

According to the manufacturer's method, rat NP cells were co-cultured with hydrogel for 1,3,7 days and then tested for live/dead cell activity and CCK-8 cytotoxicity, respectively. (Thermo Fisher; Solarbio, China). After the PLGA-PEG-PLGA-Bevacizumab hydrogel was prepared, the skin was cut in the middle of the dorsum (length 2 cm) and the hydrogel polymer was implanted subcutaneously under aseptic conditions, followed by wound closure. On days 7, 14 and 20 after implantation, the rats were euthanised by inhaling carbon dioxide and the hydrogels was then collected together with the surrounding tissue. These tissue samples were then further used for histological analysis and degradation study.

In vitro release of bevacizumab

PLGA–PEG–PLGA and PLGA–PEG–PLGA-bevacizumab hydrogels were placed in 20 ml of PBS (pH = 7.4) respectively, followed by a water bath at 37°C. Then 3 ml of the supernatant was taken from each solution at different time points for testing and then 3 ml of fresh PBS was added to the original solution. The absorption value of each sample at 260 nm was measured with a UV–Vis spectrophotometer. The concentration of Bevacizumab in the sample solution was calculated via the standard curve and the cumulative release was counted to identify the bevacizumab release profile of this hydrogel delivery system. The measurement wavelength was determined by full-spectrum measurements.

Treatment effect of the PLGA–PEG–PLGA-bevacizumab hydrogel in a rat model of IDD

To assess the effect of bevacizumab *in vivo*, 8-week-old Sprague Dawley rats from the Sichuan University Animal Center were acquired for animal experiments. In total, rats were randomly divided into four groups: the non-degenerative (NC) group, the degenerative control (DC) group, the PLGA-PEG-PLGA hydrogel group, and the PLGA-PEG-PLGA-Bevacizumab hydrogel group. The rat IDD model was then created in accordance with previous methods. At week 8, the degree of disc degeneration was first assessed by micro-computed tomography (micro-CT) and MRI. All photos were analyzed using ImageJ software. The disc height index (DHI) was measured in accordance with previously described method (Masuda et al., 2005). Next, the rats were euthanised and the IVDs were then extracted for subsequent experiments. Such as: HEstaining, SO staining, immunohistochemistry.

Statistics analysis

Data were analyzed using SPSS 20.0 (SPSS, Chicago, IL, USA) and presented as the mean ± SD. Analysis of variance or Student's t-test with the Student–Newman–Keuls (SNK) posthoctest were performed to determine the statistical significance between differences; $p < 0.05$ indicated statistical significance.

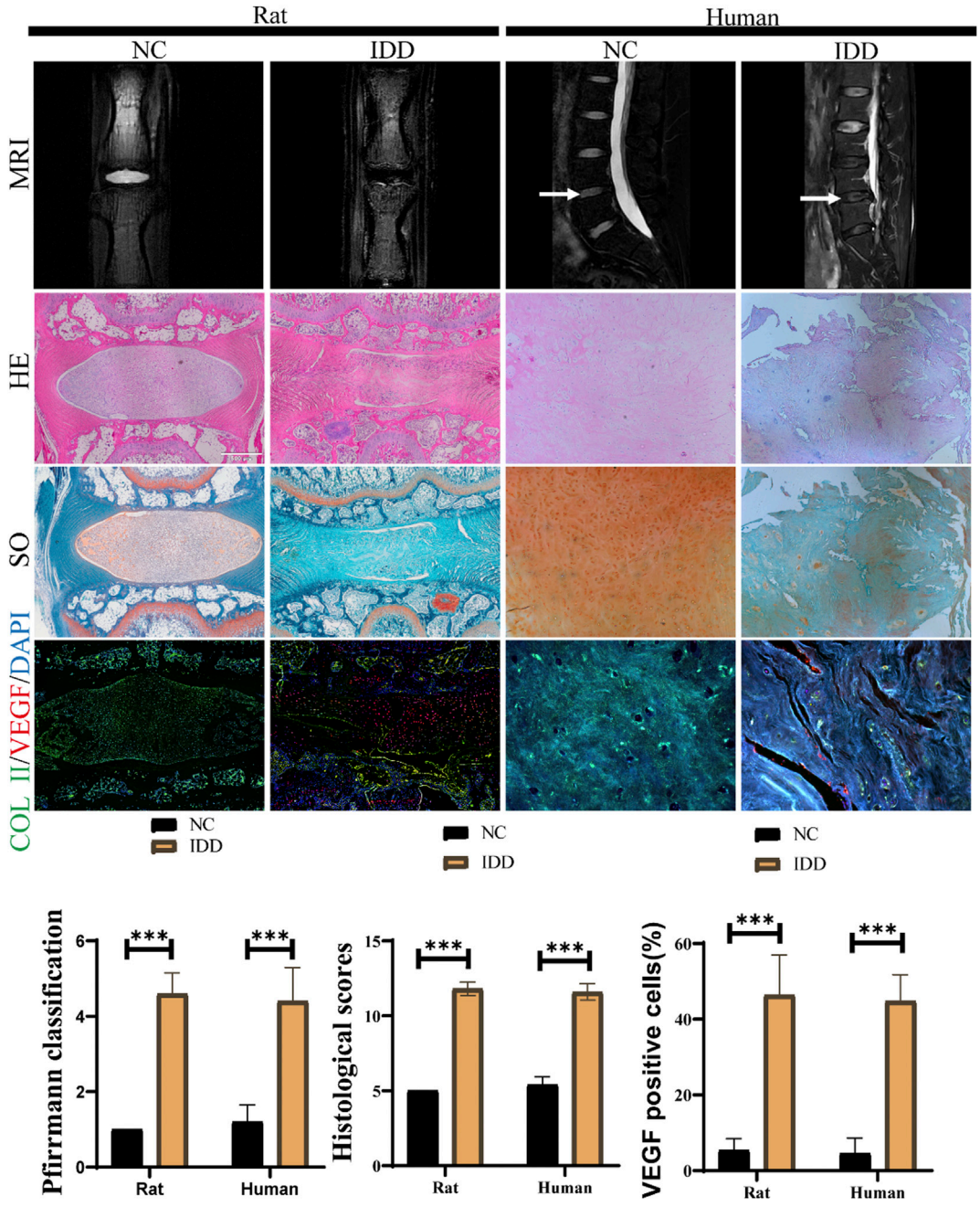

FIGURE 1
Aberrant VEGF expression in IVDs in rats and humans. **(A)**MRI, H&E staining, SO staining for observation of disc degeneration, and immunofluorescent staining for measurement of VEGF (red) and COL II (green) expression in human and rat IVDs. **(B,C)** The histological scores and MRI grading scores in human and rat IVDs. **(D)** Ratio of VEGF positive NP cell numbers to total NP cells in IVDs of human and rat. data are expressed as mean ± SD (n = 5). *$p < 0.05$; ***$p < 0.01$. Scale bar = 500 um.

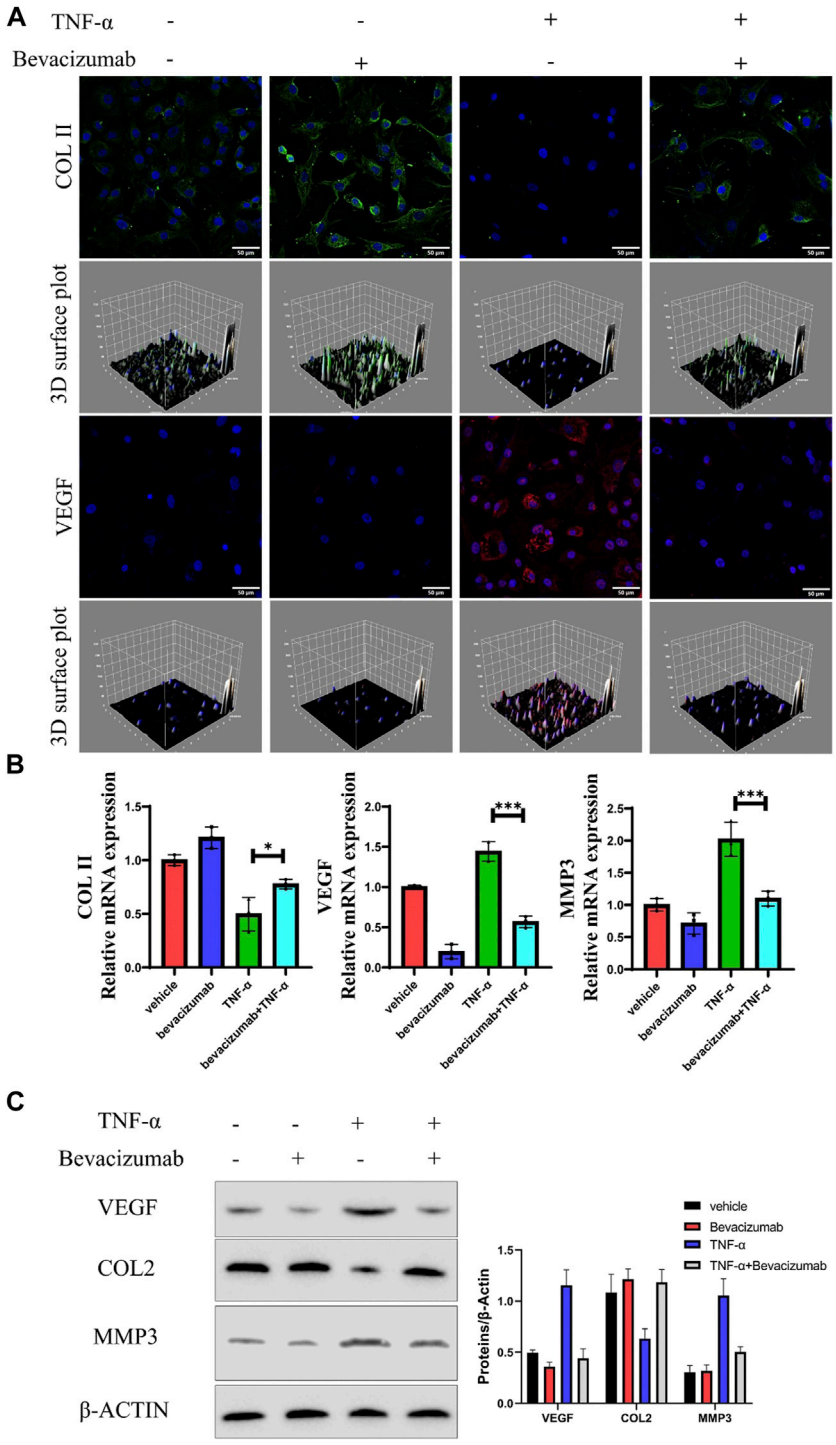

FIGURE 2
Bevacizumab promotes NP cells anabolism by inhibiting VEGF expression. **(A)** Immunofluorescence analysis of COL II (green) and VEGF (red) production of rat NP cells in 4 groups. Scale = 50 μm. **(B)** The relative expression levels of mRNA in the 4 groups were assessed by RT-qPCR. **(C)** Western blot analysis of VEGF, COL II and MMP13 proteins are displayed in 4 groups. data are presented as mean ± SD (n = 5). *$p < 0.05$; ***$p < 0.01$. Scale bar = 50 um.

Results

VEGF is highly expressed in rat and human degenerative intervertebral discs

Safranin O-Fast Green, histological staining and MRI were undertaken to determine the degeneration of rat and human IVDs. In contrast to non-degenerative IVDs, The MRI T2-weighted signal intensity was significantly lower in degenerative IVDs (Figure 1A). By H&E staining, a few chondrocyte-like cells and disordered, hypocellular fibrocartilaginous tissue was observed in IDD of rats. The NP tissue of degenerative IVDs was a loss of structural integrity and lacked extracellular matrix (Figure 1A). In SO staining, the extracellular matrix of normal NPs was cartilaginous and appears orange in colour. However, the degenerating NPs matrix was green in colour because it was fibrous. (Figure 1A). The pfirrmann MRI grading of rat and human degenerative discs was markedly higher than that of the non-degenerative group (Figure 1B). As well as the histological score of rat and human degenerative IVDs above non-degenerative controls (Figure 1C).

The expression levels of VEGF and ECM component COL II in NP cells was observed by immunohistochemistry (Figure 1A). The proportion of positive cells showed that VEGF was notably upregulated in degenerating IVDs in rats and humans and COL II expression was significantly inhibited. (Figure 1D). This indicated that the catabolism was more active in degenerated discs.

Bevacizumab inhibited the expression of vascular endothelial growth factor and prevented the degeneration of NP cells *in vitro*

After confirming that high expression of VEGF may be a potential contributor to IDD, we assessed whether bevacizumab, a specific small molecule inhibitor of VEGF, could inhibit or repair degeneration in NP cells by inhibiting VEGF expression. COL II expression was significantly reduced in degenerating NP cells by Immunofluorescence. Meanwhile, COL expression was partially restored in degenerating NP cells treated with Bevacizumab (Figure 2A). RT-PCR results showed that the results of PCR showed that COL II mRNA expression levels were significantly restored after inhibition of VEGF expression, while the expression levels of MMP3 mRNA were significantly inhibited (Figure 2B). Similar to RT-PCR results, after VEGF expression was inhibited, Western blot results showed that COL II protein expression was significantly increased and MMP3 expression was decreased in TNF-α treated NP cells (Figure 2C). These results suggest that bevacizumab inhibited the degeneration of NP cells by suppressing the expression of VEGF.

Controlled release of bevacizumab injectable thermosensitive hydrogel with proven biocompatibility

To achieve a safe and effective therapeutic effect, we need to work on the development of a drug delivery system for locally controlled release of bevacizumab. PLGA-PEG-PLGA polymers have been successfully used as drug delivery vehicles due to their excellent biocompatibility and thermosensitive as well as their ability to form hydrogels *in situ*. Therefore, it was chosen for local delivery of bevacizumab (Figure 3A). FTIR analysis confirmed the successful synthesis of PLGA-PEG-PLGA-bevacizumab (Figure 3B). The 20% concentration copolymer is liquid below room temperature and forms a gel as the temperature rises. Similar results for the sol-gel transition temperature were obtained by rheology (Figure 3C). We examined the composition and structure of the copolymers by ^{1}H NMR spectroscopy (Figure 3D). The signals of −CH3 and −CH in the LA segment appeared at 1.57 and 5.16 ppm; −CH2 of the GA and EG fractions were observed at 4.29 and 3.65ppm, respectively. At 37°C, release profile of bevacizumab from PLGA-PEG-PLGA hydrogel shows a long drug duration of action (Figure 3E).

To observe the impact of bevacizumab-encapsulated hydrogels on cellular activity at different time points, a live/dead cell assay was performed. After 1, 3 or 7 days of incubation respectively, the cell viability or cell numbers of each group were tested and the results were not significantly different. (Figure 3F). In order to further investigate its biocompatibility, PLGA-PEG-PLGA-Bevacizumab hydrogels were implanted subcutaneously in rats to evaluate degradation rates and local responses with animal tissues, as well as immune reactions with the host. At days 14, 28, and 56, improvements in biocompatibility and integration of the hydrogel *in vivo* were observed (Figure 3G). These results suggest that thermosensitive hydrogel containing bevacizumab is safe and effective for the treatment of IDD.

Treatment effect of injected bevacizumab-loaded thermosensitive hydrogel in a puncture-induced rat model of IDD

Puncture-induced rat IDD model was established to assessment the therapeutic effect of PLGA-PEG-PLGA-Bevacizumab hydrogels *in vivo*. At 8 weeks following puncture injury, a significant increase in the number and size of osteophytes was observed in the degenerative control (DC) group. In contrast, less bone formation was detected in the

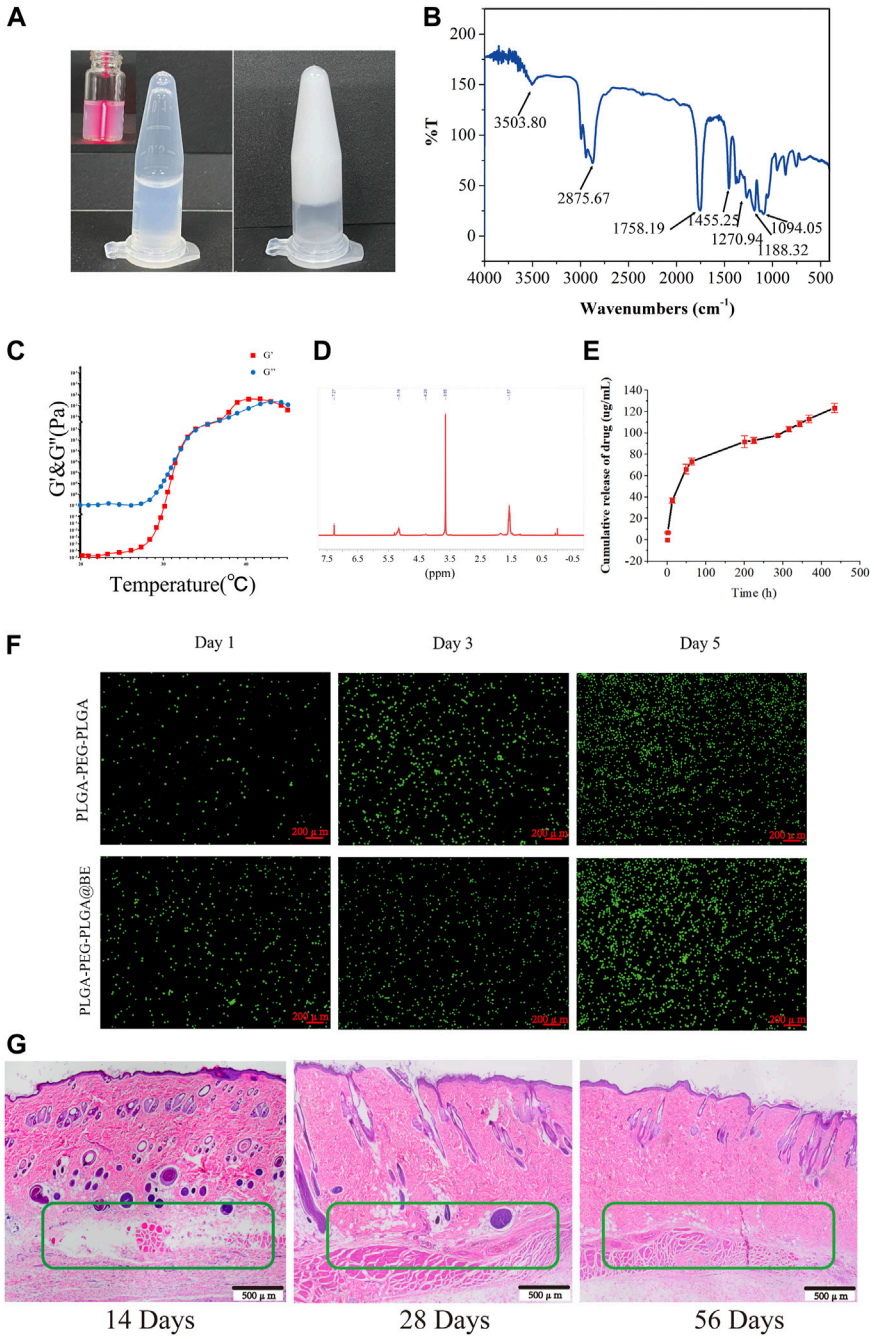

FIGURE 3
Controlled release of bevacizumab from thermosensitive injectable hydrogels with biocompatibility. **(A)** Sol-gel phase transfer measurement of PLGA-PEG-PLGA copolymers at 37°C using the vial inversion test. **(B)** FTIR transmission spectra of PLGA-PEG-PLGA-bevacizumab hydrogel. **(C)** Storage modulus G′ and loss modulus G″ of the PLGA-PEG-PLGA in PBS (20%). **(D)**The ^{1}H NMR spectrum of the PLGA-PEG-PLGA triblock copolymer. **(E)** Release curve of bevacizumab releasing from PLGA-PEG-PLGA hydrogel at 37°C. **(F)** Live/dead dyeing of NP cells in rats incubated on PLGA-PEG-PLGA hydrogels and PLGA-PEG-PLGA-bevacizumab hydrogels on day 1, 3 and 5, respectively. Red fluorescent cells indicate dead cells and green fluorescent cells are surviving. Scale bar = 200 um. **(G)** H&E staining of subcutaneously implanted PLGA-PEG-PLGA-bevacizumab hydrogels on postoperative days 14, 28, and 56. The green box indicates subcutaneous hydrogel. Scale bar = 500 um. data are expressed as mean ± SD (n = 5).

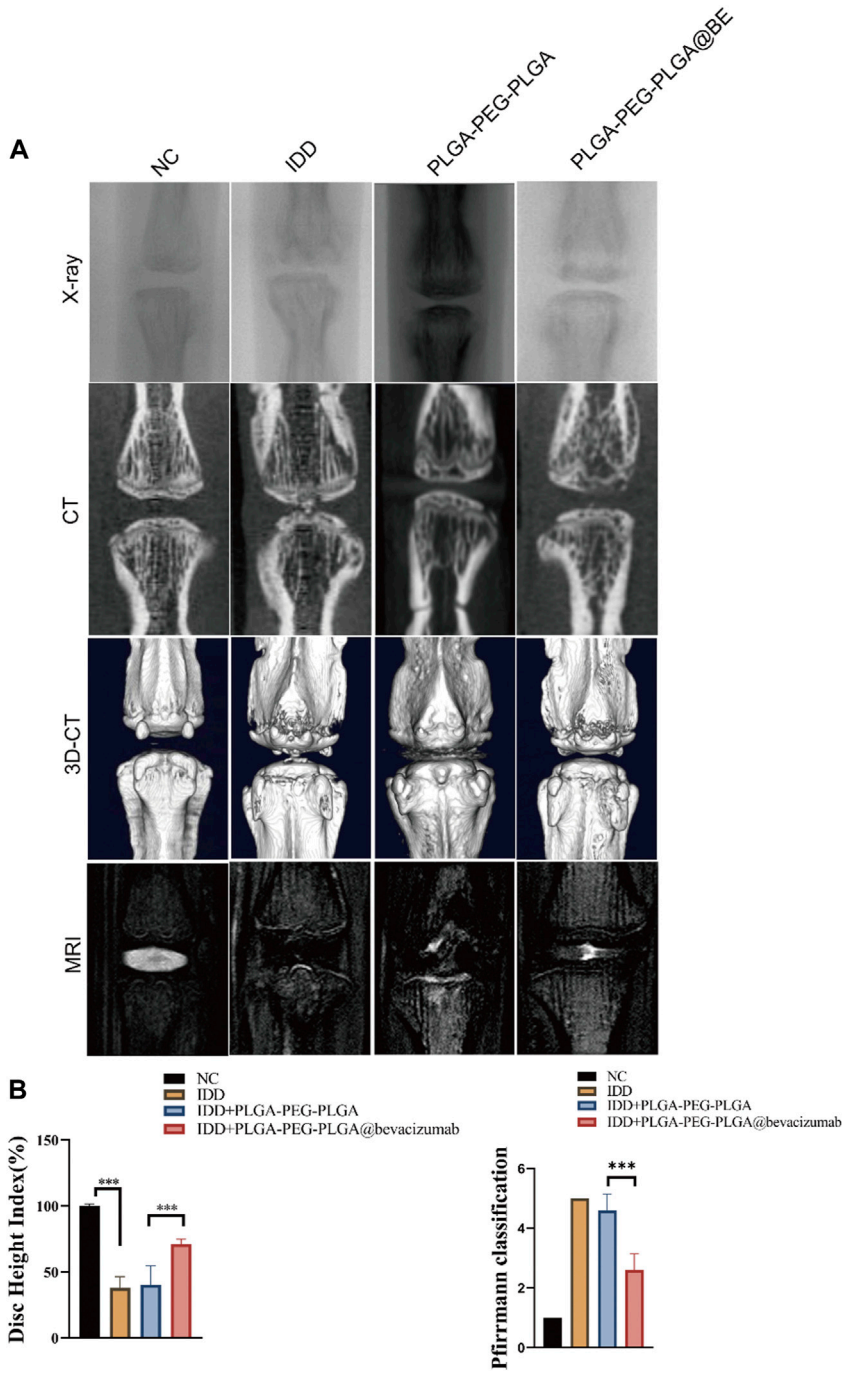

FIGURE 4
Radiological data of animal experiments by imaging system. **(A)** Representative X-ray, CT and MRI images of the rat's caudal vertebrae at 8 weeks. **(B)** The change of DHI% in 4 groups at 8 weeks. (C) MRI grading changes in each group at 8 weeks. data are expressed as mean ± SD (n = 5). *$p < 0.05$; ***$p < 0.01$.

intervertebral space in the non-degenerative (NC) group and the bevacizumab-loaded hydrogel group compared to the DC group (Figure 4A). Changes in the water content of the nucleus pulposus, assessed by MRI T2-weighted signals, can also reliably reflect disc regeneration. At 8 weeks, compared with the DC group, the MRI T2-weighted signal in nucleus pulposus was significantly restored in the bevacizumab-loaded hydrogel group. (Figure 4A). The DHI% (disc height index %)

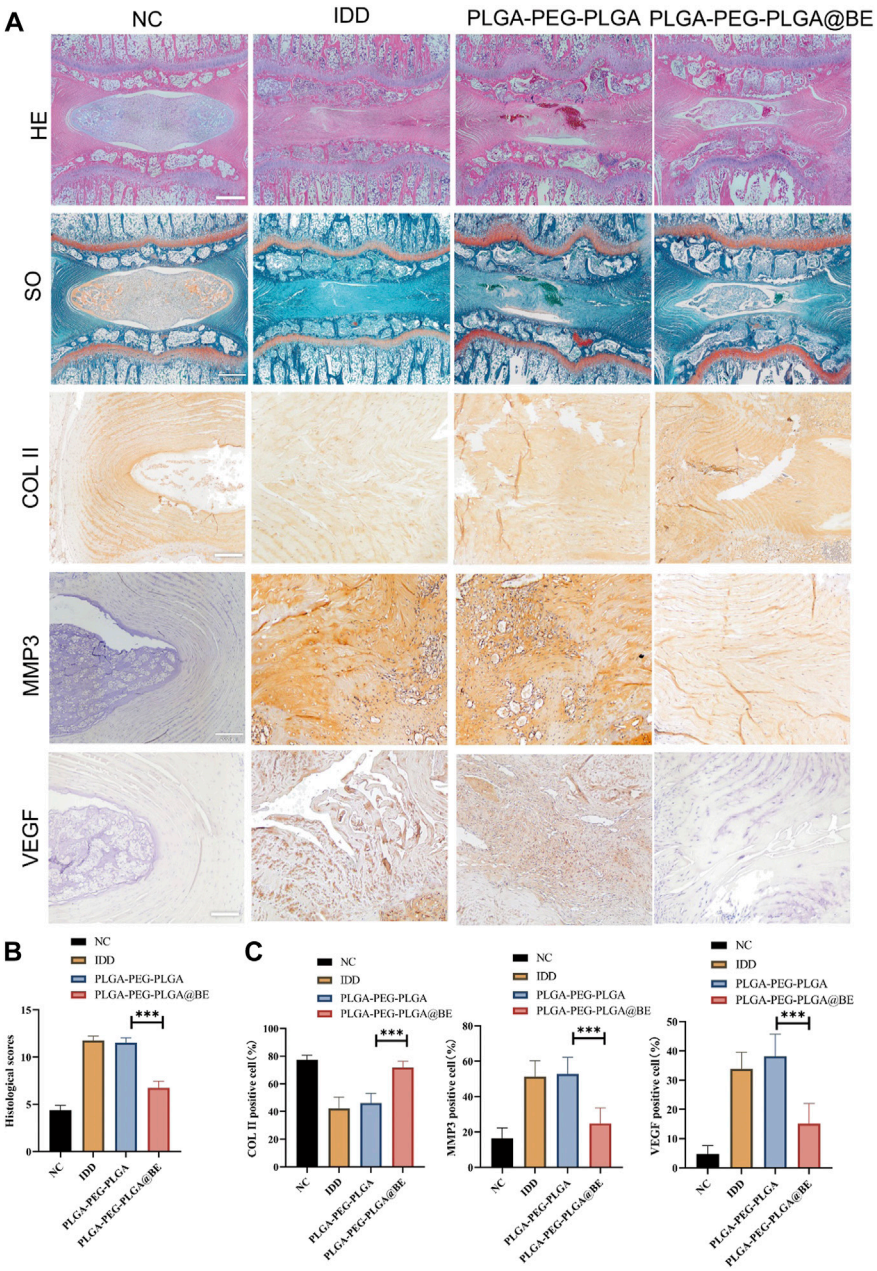

FIGURE 5
Histological assessment of rat IDD model. **(A)** H&E staining, SO staining, and Immunohistochemistry staining of COL II, MMP3, VEGF. **(B)** Histological grades in week 8 in each group. **(C)**Ratio of COL II, MMP3, VEGF positive NP cell numbers to total NP cells in 4 groups. data are presented as mean ± SD (n = 5). *$p < 0.05$; ***$p < 0.01$. Scale bar = 200 um.

values and MRI grading score were significantly higher in the bevacizumab-loaded hydrogel group than in the DC group (Figure 4B). Thus, the bevacizumab-loaded hydrogel group showed the best protection against IVD, while the hydrogel treatment alone did not have a significant protective effect.

H&E staining confirmed that bevacizumab-loaded hydrogel played a protective role in NP degeneration and deterioration of IVD structure. In DC group and hydrogel-only group, NP structure was obviously lost, and there was no visible demarcation between AF and NP. However, in the bevacizumab-loaded hydrogel group, the NP cells were slightly degenerated, and although the intact structure of the NP tissue was somewhat disrupted (Figure 5A). With SO staining, the normal extracellular matrix was orange, but the severely

degenerated fibrous tissue stained green. In the bevacizumab-loaded hydrogel group, plenty of orange extracellular matrix was found in the NP tissue with only Mild degeneration (Figure 5A). Immunochemical staining revealed an upregulation of COL II and a downregulation of VEGF, MMP3 in the bevacizumab-loaded hydrogel group, compared to what was observed in the DC group and hydrogel-only group (Figure 5A). The histological score in the bevacizumab-loaded hydrogel group was obviously lower than in DC group and hydrogel-only group, with a relatively mild degree of IDD (Figure 5B). The ratio of positive cells revealed that COL II was upregulated in the bevacizumab-loaded hydrogel group, whereas VEGF, MMP3 was downregulated, compared to DC group and hydrogel-only group (Figure 5C). Combined with the results of our *in vitro* study, these findings suggest that PLGA-PEG-PLGA hydrogels loaded with bevacizumab improve IDD by modulating the expression of VEGF and MMP3 in a rat model of IVD degeneration through local delivery of the drug.

Discussion

IDD is one of the leading causes of impaired movement and low back pain. Because the underlying molecular mechanism of IDD is still unclear, the clinical treatment mainly aims to relieve the symptom instead of targeting IDD directly (Francisco et al., 2022; Wang et al., 2022). In this study, a new strategy was established to treat IDD by the controlled release of bevacizumab from thermosensitive hydrogels, which was shown not only to inhibit the degradation of cartilage matrix, but also to promote the synthesis of COL II. These findings suggest the local administration of bevacizumab for the treatment of disc degeneration has potential clinical application.

Some studies have observed a relationship between VEGF and chondrocytes in terms of physiology and pathology (Chen et al., 2019; Qian et al., 2021; Xiao et al., 2021; Xiaoshi et al., 2021), but there was a lack of relevant studies in IVD. We found that VEGF is highly expressed in IDD of humans and rats. VEGF is an important factor in promoting angiogenesis in both physiological and pathological conditions. High expression of VEGF was associated with vascular infiltration in tissues. Some studies have found that High expression of VEGF is a major factor contributing to angiogenesis in NP tissue (David et al., 2010; Lee et al., 2011; Lu et al., 2013; Binch et al., 2015). Angiogenesis during disc degeneration is thought to be the main cause of low back pain (Pohl et al., 2016; Melincovici et al., 2018; Azarpira et al., 2021). In addition, our study also found that MMP3 expression was significantly reduced following inhibition of VEGF with bevacizumab. Sahin et al. (Sahin et al., 2012) found that VEGF promotes angiogenesis through the induction of matrix metalloproteinase-3 (MMP3) expression, which in turn attenuates tendon biomechanical properties in degenerative tendon disease. It has also been shown that MMP3 promotes the catabolism of extracellular matrix during IDD (Zhang B et al., 2019; Zhao et al., 2020; Song et al., 2021).

Bevacizumab specifically binds VEGF and impedes blood vessel growth and formation. It has been widely used in oncology patients (Garcia et al., 2020; Haunschild and Tewari, 2020; Nakai and Matsumura, 2022). There have been a number of studies applying it to age-related macular degenerative diseases (Gil-Martínez et al., 2020; Weinstein et al., 2020). Our results revealed that inhibition of VEGF with bevacizumab protects IVDs from degeneration. To reduce the side effects associated with the systemic administration of Bevacizumab, such as gastrointestinal perforation, wound healing complications, congestive heart failure, bleeding, the injectable thermosensitive PLGA-PEG-PLGA hydrogel is used as a vehicle for local release of the drug in the treatment of IDD. As a well-established thermosensitive hydrogel, PLGA-PEG-PLGA hydrogel has been used in previous study for the treatment of IDD (Zou et al., 2013). In addition, unique structure of the hydrogel has been shown to be a good carrier for small molecule drugs (Bakhaidar et al., 2019; Chan et al., 2019). When mixed with bevacizumab, the hydrogel can be injected into the NP tissue through a small diameter needle, thus reducing the chance of annulus fibrous damage.

Due to its temperature sensitivity, it forms gel within a few seconds after injection into IVD, thus reducing the risk of drug leakage. Moreover, the characteristics and excellent biocompatibility of the PLGA-PEG-PLGA hydrogel render it an effective and safe drug delivery system (Yu et al., 2013; Dimchevska et al., 2017). The results of our animal experiments showed that the PLGA-PEG-PLGA hydrogels containing bevacizumab had a remarkable effect on the maintenance of the disc height, synthesis of the COL II, and integrity of the disc structure. Nevertheless, without the help of the drug carrier, small molecule drugs are prone to leakage. It was difficult to maintain adequate drug concentrations in lesion areas of the IVD and may cause adverse events. When PLGA-PEG-PLGA hydrogel was used alone, it did not produce a therapeutic effect in the degenerated discs due to insufficient biological effect. Our results, which are identical to those of previous studies, confirm this again (Zou et al., 2013; Frauchiger et al., 2017). The therapeutic effect of bevacizumab alone or hydrogel alone was not ideal, which also confirmed the necessity and effectiveness of demonstrating the necessity of using the PLGA-PEG-PLGA hydrogels drug delivery system in IDD treatment. The degenerative disc did not recover completely after treatment with bevacizumab-encapsulated hydrogels, which may be due to the complex microenvironment of the degenerative disc. Inhibition of VEGF alone is not sufficient to address all issues. The molecular basis and targeting factors of IDD need to be further explored.

There are some limitations to our work, for example, the rat IDD model established by caudal disc puncture, which differs from human IDD. Not only that, the main limitation is the biological

differences between rat and human IVD. Compared with human NP cells, rat NP cells were more spinal cord cells than chondrocytes; thus, rat NP cells may have differential response to treatments (Bang et al., 2018; Dudli et al., 2018). Moreover, because rats are reptiles, unlike humans, their intervertebral discs do not bear the longitudinal load of their body weight. Therefore, more studies are needed on bipeds that are biologically and biomechanically similar to humans IVDs, so that the results can be applied to humans.

Conclusion

In conclusion, our findings provide evidence that bevacizumab, an FDA-approved drug, plays a protective role in disc degeneration by inhibiting VEGF expression and promoting extracellular matrix synthesis. These results believe that bevacizumab, administered topically through the injectable thermosensitive PLGA-PEG-PLGA hydrogel drug delivery system, has a potential therapeutic effect on IDD.

Data availability statement

The original contributions presented in the study are included in the article/Supplementary Material, further inquiries can be directed to the corresponding author.

Ethics statement

The animal study was reviewed and approved by Animal Ethics Committee of West China Hospital of Sichuan University. Written informed consent was obtained from the individual(s) for the publication of any potentially identifiable images or data included in this article.

Author contributions

LW, FC, LL, CZ, YH, HD, and RW helped in methods and analysis. MH, YJ, and LZ provides support for material synthesis. Work on this study was carried out under the guidance of YS and LML. All authors viewed and ratified the manuscript.

Funding

This study was supported by grants from the Projects of the Science and Technology Department of Sichuan Province (2022ZDZX0029,2021YFS0218),the National Natural Science Foundation of China (81871772, 82172495, 82072434), the 1·3·5 project for disciplines of excellence–Clinical Research Incubation Project, West China Hospital, Sichuan University (2021HXFH003), Research Projects of Affiliated Hospital of North Sichuan Medical College (2022JC020).

Acknowledgments

We are appreciated to Yan Wang, Xiangyi Ren, Li Fu, and Hongying Chen from the Core Research Facility of West China Hospital, Sichuan University, for their kind assistance with the cell/molecular experiments. We also thanks Chunjuan Bao of the Institute of Clinic Pathology, Sichuan University, for dealing with histology staining.

Conflict of interest

The authors declare that the research was conducted in the absence of any commercial or financial relationships that could be construed as a potential conflict of interest.

Publisher's note

All claims expressed in this article are solely those of the authors and do not necessarily represent those of their affiliated organizations, or those of the publisher, the editors and the reviewers. Any product that may be evaluated in this article, or claim that may be made by its manufacturer, is not guaranteed or endorsed by the publisher.

References

Azarpira, N., Kaviani, M., and Sarvestani, F. S. (2021). Incorporation of VEGF- and bFGF-loaded alginate oxide particles in acellular collagen-alginate composite hydrogel to promote angiogenesis. *Tissue Cell.* 72, 101539. doi:10.1016/j.tice.2021.101539

Bakhaidar, R., Green, J., Alfahad, K., Samanani, S., Moollan, N., O'Neill, S., et al. (2019). Effect of size and concentration of PLGA-PEG nanoparticles on activation and aggregation of washed human platelets. *Pharmaceutics* 11 (10), 514. doi:10.3390/pharmaceutics11100514

Bang, W. S., Lee, D. H., Kim, K. T., Cho, D. C., Sung, J. K., Han, I. B., et al. (2018). Relationships between vitamin D and paraspinal muscle: Human data and experimental rat model analysis. *Spine J.* 18 (6), 1053–1061. doi:10.1016/j.spinee.2018.01.007

Barber, R. M., Bell, B., Bertozzi-Villa, A., Biryukov, S., Bolliger, I., Charlson, F., et al. (2015). Global, regional, and national incidence, prevalence, and years lived with disability for 301 acute and chronic diseases and injuries in 188 countries, 1990-2013: A systematic analysis for the global burden of disease study 2013. *Lancet* 386 (9995), 743–800. doi:10.1016/S0140-6736(15)60692-4

Binch, A. L., Cole, A. A., Breakwell, L. M., Michael, A. L., Chiverton, N., Creemers, L. B., et al. (2015). Class 3 semaphorins expression and association with innervation and angiogenesis within the degenerate human intervertebral disc. *Oncotarget* 6 (21), 18338–18354. doi:10.18632/oncotarget.4274

Chan, P. S., Xian, J. W., Li, Q., Chan, C. W., Leung, S., and To, K. (2019). Biodegradable thermosensitive PLGA-PEG-PLGA polymer for non-irritating and

sustained ophthalmic drug delivery. *AAPS J.* 21 (4), 59. doi:10.1208/s12248-019-0326-x

Chen, D., and Jiang, X. (2021). Correlation between proteolytic enzymes and microangiogenesis in degenerative intervertebral disc nucleus. *J. Invest. Surg.* 34 (6), 679–684. doi:10.1080/08941939.2019.1679921

Chen, Y., Zhao, B., Zhu, Y., Zhao, H., and Ma, C. (2019). HIF-1-VEGF-Notch mediates angiogenesis in temporomandibular joint osteoarthritis. *Am. J. Transl. Res.* 11 (5), 2969–2982.

David, G., Ciurea, A. V., Iencean, S. M., and Mohan, A. (2010). Angiogenesis in the degeneration of the lumbar intervertebral disc. *J. Med. Life* 3 (2), 154–161.

Dimchevska, S., Geskovski, N., Koliqi, R., Matevska-Geskovska, N., Gomez Vallejo, V., Szczupak, B., et al. (2017). Efficacy assessment of self-assembled PLGA-PEG-PLGA nanoparticles: Correlation of nano-bio interface interactions, biodistribution, internalization and gene expression studies. *Int. J. Pharm.* 533 (2), 389–401. doi:10.1016/j.ijpharm.2017.05.054

Dudli, S., Liebenberg, E., Magnitsky, S., Lu, B., Lauricella, M., and Lotz, J. C. (2018). Modic type 1 change is an autoimmune response that requires a proinflammatory milieu provided by the 'Modic disc. *Spine J.* 18 (5), 831–844. doi:10.1016/j.spinee.2017.12.004

Francisco, V., Pino, J., González-Gay, M. Á., Lago, F., Karppinen, J., Tervonen, O., et al. (2022). A new immunometabolic perspective of intervertebral disc degeneration. *Nat. Rev. Rheumatol.* 18 (1), 47–60. doi:10.1038/s41584-021-00713-z

Frauchiger, D. A., Tekari, A., Wöltje, M., Fortunato, G., Benneker, L. M., and Gantenbein, B. (2017). A review of the application of reinforced hydrogels and silk as biomaterials for intervertebral disc repair. *Eur. Cell. Mat.* 34, 271–290. doi:10.22203/eCM.v034a17

Gao, Y., Ji, H., Peng, L., Gao, X., and Jiang, S. (2020). Development of PLGA-PEG-PLGA hydrogel delivery system for enhanced immunoreaction and efficacy of newcastle disease virus DNA vaccine. *Mol. (Basel, Switz.* 25 (11), 2505. doi:10.3390/molecules25112505

Garcia, J., Hurwitz, H. I., Sandler, A. B., Miles, D., Coleman, R. L., Deurloo, R., et al. (2020). Bevacizumab (Avastin®) in cancer treatment: A review of 15 years of clinical experience and future outlook. *Cancer Treat. Rev.* 86, 102017. doi:10.1016/j.ctrv.2020.102017

Gil-Martínez, M., Santos-Ramos, P., Fernández-Rodríguez, M., Abraldes, M. J., Rodríguez-Cid, M. J., Santiago-Varela, M., et al. (2020). Pharmacological advances in the treatment of age-related macular degeneration. *Curr. Med. Chem.* 27 (4), 583–598. doi:10.2174/0929867326666190726121711

Han, B., Zhu, K., Li, F. C., Xiao, Y. X., Feng, J., Shi, Z. L., et al. (2008). A simple disc degeneration model induced by percutaneous needle puncture in the rat tail. *Spine* 33 (18), 1925–1934. doi:10.1097/brs.0b013e31817c64a9

Haunschild, C. E., and Tewari, K. S. (2020). Bevacizumab use in the frontline, maintenance and recurrent settings for ovarian cancer. *Future Oncol. Lond. Engl.* 16 (7), 225–246. doi:10.2217/fon-2019-0042

He, M., Pang, J., Sun, H., Zheng, G., Lin, Y., and Ge, W. (2020). P14ARF inhibits regional inflammation and vascularization in intervertebral disc degeneration by upregulating TIMP3. *Am. J. Physiology-Cell Physiology* 318 (4), C751–C761. doi:10.1152/ajpcell.00271.2019

Hwang, M. H., Son, H. G., Kim, J., and Choi, H. (2020). *In vitro* model of distinct catabolic and inflammatory response patterns of endothelial cells to intervertebral disc cell degeneration. *Sci. Rep.* 10 (1), 20596. doi:10.1038/s41598-020-77785-6

Kawchuk, G. N., Kaigle, A. M., Holm, S. H., Rod Fauvel, O., Ekström, L., and Hansson, T. (2001). The diagnostic performance of vertebral displacement measurements derived from ultrasonic indentation in an *in vivo* model of degenerative disc disease. *Spine* 26 (12), 1348–1355. doi:10.1097/00007632-200106150-00018

Kim, K. H., Kim, Y. H., Son, J. E., Lee, J. H., Kim, S., Choe, M. S., et al. (2017). Intermittent fasting promotes adipose thermogenesis and metabolic homeostasis via VEGF-mediated alternative activation of macrophage. *Cell. Res.* 27 (11), 1309–1326. doi:10.1038/cr.2017.126

Lee, J. M., Song, J. Y., Baek, M., Jung, H. Y., Kang, H., Han, I. B., et al. (2011). Interleukin-1β induces angiogenesis and innervation in human intervertebral disc degeneration. *J. Orthop. Res.* 29 (2), 265–269. doi:10.1002/jor.21210

Liao, Z., Li, S., Lu, S., Liu, H., Li, G., Ma, L., et al. (2021). Metformin facilitates mesenchymal stem cell-derived extracellular nanovesicles release and optimizes therapeutic efficacy in intervertebral disc degeneration. *Biomaterials* 274, 120850. doi:10.1016/j.biomaterials.2021.120850

López-Cano, J. J., Sigen, A., Andrés-Guerrero, V., Tai, H., Bravo-Osuna, I., Molina-Martínez, I. T., et al. (2021). Thermo-Responsive PLGA-PEG-PLGA hydrogels as novel injectable platforms for neuroprotective combined therapies in the treatment of retinal degenerative diseases. *Pharmaceutics* 13 (2), 234. doi:10.3390/pharmaceutics13020234

Lu, X. Y., Ding, X. H., Zhong, L. J., Chen, X. D., and Huang, H. (2013). Expression and significance of VEGF and p53 in degenerate intervertebral disc tissue. *Asian Pac. J. Trop. Med.* 6 (1), 79–81. doi:10.1016/S1995-7645(12)60206-5

Masuda, K., Aota, Y., Muehleman, C., Imai, Y., Okuma, M., Thonar, E. J., et al. (2005). A novel rabbit model of mild, reproducible disc degeneration by an anulus needle puncture: Correlation between the degree of disc injury and radiological and histological appearances of disc degeneration. *Spine* 30 (1), 5–14. doi:10.1097/01.brs.0000148152.04401.20

Melincovici, C. S., Boşca, A. B., Şuşman, S., Mărginean, M., Mihu, C., Istrate, M., et al. (2018). Vascular endothelial growth factor (VEGF) - key factor in normal and pathological angiogenesis. *Romanian J. Morphol. embryology = Revue roumaine de Morphol. embryologie* 59 (2), 455–467.

Nakai, H., and Matsumura, N. (2022). The roles and limitations of bevacizumab in the treatment of ovarian cancer. *Int. J. Clin. Oncol.* 27, 1120–1126. doi:10.1007/s10147-022-02169-x

Norcross, J. P., Lester, G. E., Weinhold, P., and Dahners, L. E. (2003). An *in vivo* model of degenerative disc disease. *J. Orthop. Res.* 21 (1), 183–188. doi:10.1016/S0736-0266(02)00098-0

Pan, Z., Sun, H., Xie, B., Xia, D., Zhang, X., Yu, D., et al. (2018). Therapeutic effects of gefitinib-encapsulated thermosensitive injectable hydrogel in intervertebral disc degeneration. *Biomaterials* 160, 56–68. doi:10.1016/j.biomaterials.2018.01.016

Pohl, P. H., Lozito, T. P., Cuperman, T., Yurube, T., Moon, H. J., Ngo, K., et al. (2016). Catabolic effects of endothelial cell-derived microparticles on disc cells: Implications in intervertebral disc neovascularization and degeneration. *J. Orthop. Res.* 34 (8), 1466–1474. doi:10.1002/jor.23298

Qian, J. J., Xu, Q., Xu, W. M., Cai, R., and Huang, G. C. (2021). Expression of VEGF-A signaling pathway in cartilage of ACLT-induced osteoarthritis mouse model. *J. Orthop. Surg. Res.* 16 (1), 379. doi:10.1186/s13018-021-02528-w

Sahin, H., Tholema, N., Petersen, W., Raschke, M. J., and Stange, R. (2012). Impaired biomechanical properties correlate with neoangiogenesis as well as VEGF and MMP-3 expression during rat patellar tendon healing. *J. Orthop. Res.* 30 (12), 1952–1957. doi:10.1002/jor.22147

Song, Q., Zhang, F., Wang, K., Chen, Z., Li, Q., Liu, Z., et al. (2021). MiR-874-3p plays a protective role in intervertebral disc degeneration by suppressing MMP2 and MMP3. *Eur. J. Pharmacol.* 895, 173891. doi:10.1016/j.ejphar.2021.173891

Wang, J., Huang, L., Huang, Y., Jiang, Y., Zhang, L., Feng, G., et al. (2021a). Therapeutic effect of the injectable thermosensitive hydrogel loaded with SHP099 on intervertebral disc degeneration. *Life Sci.* 266, 118891. doi:10.1016/j.lfs.2020.118891

Wang, J., Huang, L., Yang, X., Zhu, C., Huang, Y., Feng, G., et al. (2021b). The regulatory effect of MicroRNA-101-3p on disc degeneration by the STC1/VEGF/MAPK pathway. *Oxidative Med. Cell. Longev.* 2021, 1–16. doi:10.1155/2021/1073458

Wang, Y., Deng, M., Wu, Y., Hu, C., Zhang, B., Guo, C., et al. (2022). Sustained gene deliverfrom inflammation-responsive anti-inflammatory hydrogels promotes extracellular matrix metabolism balance in degenerative nucleus pulposus. *Compos. Part B Eng.* 236, 109806. doi:10.1016/j.compositesb.2022.109806

Wei, P. S., Chen, Y. J., Lin, S. Y., Chuang, K. H., Sheu, M. T., and Ho, H. O. (2021). *In situ* subcutaneously injectable thermosensitive PEG-PLGA diblock and PLGA-PEG-PLGA triblock copolymer composite as sustained delivery of bispecific anti-CD3 scFv T-cell/anti-EGFR Fab Engager (BiTEE). *Biomaterials* 278, 121166. doi:10.1016/j.biomaterials.2021.121166

Weinstein, O., Abu Tailakh, M., Lifshitz, T., Novack, V., and Levy, J. (2020). Intravitreal bevacizumab treatment for neovascular age-related macular degeneration and thromboembolic events. *Eur. J. Ophthalmol.* 30 (1), 66–71. doi:10.1177/1120672118823128

Xiao, P., Zhu, X., Sun, J., Zhang, Y., Qiu, W., Li, J., et al. (2021). Cartilage tissue miR-214-3p regulates the TrkB/ShcB pathway paracrine VEGF to promote endothelial cell migration and angiogenesis. *Bone* 151, 116034. doi:10.1016/j.bone.2021.116034

Xiaoshi, J., Maoquan, L., Jiwei, W., Jinqiu, N., and Ke, Z. (2021). SETD7 mediates the vascular invasion in articular cartilage and chondrocytes apoptosis in osteoarthriis. *FASEB J.* 35 (3), e21283. doi:10.1096/fj.202000373RRRR

Xu, Y., Gu, Y., Cai, F., Xi, K., Xin, T., Tang, J., et al. (2020). Metabolism balance regulation via antagonist-functionalized injectable microsphere for

nucleus pulposus regeneration. *Adv. Funct. Mater.* 30 (52), 2006333. doi:10.1002/adfm.202006333

Ye, Z., Zhao, S., and Liu, Z. (2021). Prevention of lumbar disc degeneration through co-manipulation of insulin-like growth factor 1 and vascular endothelial growth factor. *Ann. Transl. Med.* 9 (20), 1572. doi:10.21037/atm-21-4977

Yu, L., Ci, T., Zhou, S., Zeng, W., and Ding, J. (2013). The thermogelling PLGA-PEG-PLGA block copolymer as a sustained release matrix of doxorubicin. *Biomater. Sci.* 1 (4), 411–420. doi:10.1039/c2bm00159d

Zhang, B., Zhao, Q., Li, Y., and Zhang, J. (2019). Moxibustion alleviates intervertebral disc degeneration *via* activation of the HIF-1α/VEGF pathway in a rat model. *Am. J. Transl. Res.* 11 (9), 6221–6231.

Zhang, Y., He, F., Chen, Z., Su, Q., Yan, M., Zhang, Q., et al. (2019). Melatonin modulates IL-1β-induced extracellular matrix remodeling in human nucleus pulposus cells and attenuates rat intervertebral disc degeneration and inflammation. *Aging* 11 (22), 10499–10512. doi:10.18632/aging.102472

Zhao, Z., Li, S., Huang, H., Fang, J., Wei, H., and Xi, Y. (2020). *In vivo* delivery of MMP3-shRNA and Sox9 lentivirus cocktail enhances matrix synthesis to prevent lumbar disc degeneration. *Adv. Clin. Exp. Med.* 29 (6), 639–647. doi:10.17219/acem/121509

Zou, F., Jiang, J., Lu, F., Ma, X., Xia, X., Wang, L., et al. (2013). Efficacy of intradiscal hepatocyte growth factor injection for the treatment of intervertebral disc degeneration. *Mol. Med. Rep.* 8 (1), 118–122. doi:10.3892/mmr.2013.1450

Frontiers in
Bioengineering and Biotechnology

Accelerates the development of therapies, devices, and technologies to improve our lives

A multidisciplinary journal that accelerates the development of biological therapies, devices, processes and technologies to improve our lives by bridging the gap between discoveries and their application.

Discover the latest Research Topics

See more →

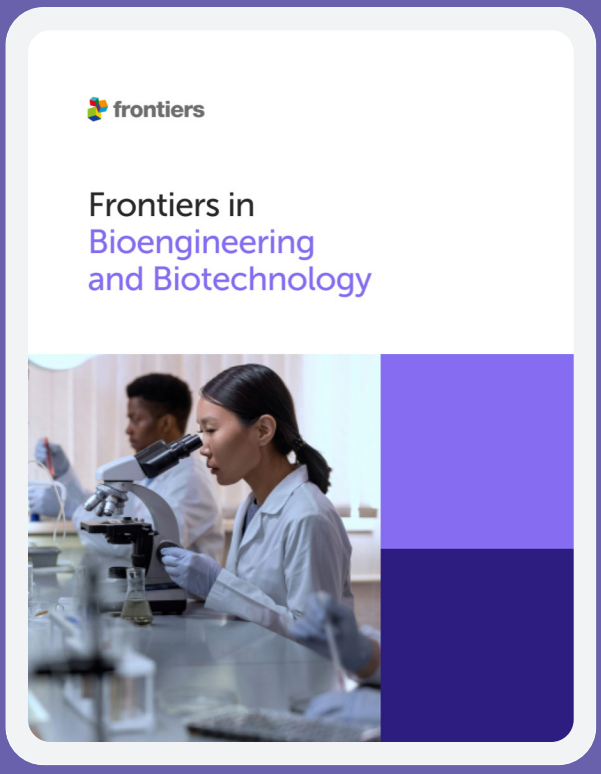

Frontiers

Avenue du Tribunal-Fédéral 34
1005 Lausanne, Switzerland
frontiersin.org

Contact us

+41 (0)21 510 17 00
frontiersin.org/about/contact